pennsylvania
DEPARTMENT OF TRANSPORTATION

Development of a Fatigue Testing Protocol for Supporting Integrated Design of Asphalt Pavement

FINAL REPORT

July 28, 2023

By Mansour Solaimanian, Ali Sahraei Joubani, Shihui Shen, Scott Milander, and Cheng Zhang

PENNSTATE 1855

Pennsylvania State University

COMMONWEALTH OF PENNSYLVANIA
DEPARTMENT OF TRANSPORTATION

CONTRACT # PSUCIAMTIS2019
WORK ORDER # 01

Technical Report Documentation Page

1. Report No.	2. Government Accession No.	3. Recipient's Catalog No.
FHWA-PA-2024-002-CIAMTIS WO 01		

4. Title and Subtitle	5. Report Date
Development of a Fatigue Testing Protocol for Supporting Integrated Design of Asphalt Pavement	7-28-2023
	6. Performing Organization Code

7. Author(s)	8. Performing Organization Report No.
Mansour Solaimanian, Ali Sahraei Joubani, Shihui Shen, Scott Milander, and Cheng Zhang	LTI 2024-02

9. Performing Organization Name and Address	10. Work Unit No. (TRAIS)
The Thomas D. Larson Pennsylvania Transportation Institute The Pennsylvania State University 201 Transportation Research Building University Park, PA 16802	11. Contract or Grant No. **PSUCIAMTIS2019/WO 01**

12. Sponsoring Agency Name and Address	13. Type of Report and Period Covered
The Pennsylvania Department of Transportation Bureau of Planning and Research Commonwealth Keystone Building 400 North Street, 6th Floor Harrisburg, PA 17120-0064	Final Report 6/8/2021 – 7/28/2023
	14. Sponsoring Agency Code

15. Supplementary Notes

Tim Ramirez, PennDOT Engineer of Tests, and Jay Sengoz, PennDOT Asphalt Lab Unit Manager served as the project technical advisors. Heather Source of PennDOT Bureau of Planning and Research served as the project contract manager.

16. Abstract

This research study was sponsored by PennDOT and US DOT Transportation Research Center to evaluate the potential of the Hamburg wheel tracking device (HWTD) in determining the mix quality in terms of fatigue cracking resistance. The research work included applying changes to HWTD, developing the test setup and the experimental plan, conducting the tests and analysis, and finally developing a test protocol.

The test setup included the HWTD, a data acquisition system and foil strain gauges to capture the strain response under repeated wheel tracking. The tests were conducted under two different temperatures and various support conditions. Various types of asphalt mixtures were included in the study. Specimens were in the form of rectangular slabs and were prepared from loose asphalt mixes through compaction. Based on the numerical analysis, a width of 6 inches was used for the majority of the slabs tested in this work. However, the experiment also included the 4-inch width for comparison. The thickness of the slab was also selected at three levels: 1, 1.5, and 2 inches, with the 1.5-inch thickness being the core thickness applied to most of the slabs. The experiment showed that as the width and the thickness become smaller, the strain amplitude and its corresponding growth rate become larger, exhibiting a higher rate of fatigue damage. It was also found that the rate of growth in strain amplitude during the test considerably increased when the binder content in the mix was decreased. The mix with 35% RAP content and a softer binder delivered lower growth in strain amplitude compared with the mix with no RAP. At the conclusion of the work, a test protocol in the AASHTO format was developed.

17. Key Words	18. Distribution Statement
Asphalt, binder, fatigue, slabs, strain, strain gauge, Hamburg, wheel tracking	No restrictions. This document is available from the National Technical Information Service, Springfield, VA 22161

19. Security Classif. (of this report)	20. Security Classif. (of this page)	21. No. of Pages	22. Price
Unclassified	Unclassified	205	$70,081.88

Development of a Fatigue Protocol for Supporting Integrated Design of Asphalt Pavements

PennDOT/PSU/CIAMTIS

Work Order No. 1

Final Report

Mansour Solaimanian
Ali Sahraei
Shihui Shen
Scott Milander
Cheng Zhang

Larson Transportation Institute

Pennsylvania State University

July 28, 2023

Table of Contents

List of Figures

List of Tables

Acknowledgements

The authors greatly appreciate the financial support for this research project that was provided by the Pennsylvania Department of Transportation and U.S. Department of Transportation's University Transportation Centers Program. Mr. Tim Ramirez and Jay. Sengoz acted as the project technical advisors and Ms. Heather Sorce oversaw the execution of the project as the contract administrator. The support and their guidance was necessary for the success of the project and is sincerely appreciated. Thanks are also extended to Dr. Zhanping You and his students at Michigan Technological University because of their excellent contribution to the project through compaction of asphalt concrete slabs, an integral part of this research. Finally, we are grateful to Mr. Michael Casper for editing the final report, and to other staff of the Larson Transportation Institute at Penn State for their support.

Disclaimer

The contents of this report reflect the views of the authors who are responsible for the facts and the accuracy of the data presented herein. The contents do not necessarily reflect the official views or policies of the Federal Highway Administration or the Commonwealth of Pennsylvania at the time of publication. This report does not constitute a standard, specification, or regulation.

CHAPTER 1

Review of Laboratory Fatigue Tests

Background

Asphalt pavement is the most widely used pavement type and is used in almost 90% of road networks in the United States (NAPA, 2009). Asphalt mixture is a viscoelastic composite and highly dependent on the loading rate and temperature. An integral part of constructing high-quality asphalt pavement is designing the asphalt mix formulation in the laboratory. The laboratory asphalt mix design is used to establish a combination of aggregates, asphalt binder, recycling materials, and additives that provides a long-lasting pavement structure (Asphalt Institute., 2014). After designing the asphalt mixture and placing it in the field, the quality and performance of the pavement should be monitored during the service life. A large portion of state and federal funding is spent on the maintenance of roads to improve performance, serviceability, and functionality. Three major distresses in asphalt mixture include fatigue cracking, thermal cracking, and rutting. These distresses can be reduced by using a suitable mix and structural design.

Fatigue cracking pertains to interconnected or independent cracks and is considered among the primary distresses in asphalt pavements. This type of distress is mainly associated with repeated traffic loads and may occur in both transverse and longitudinal directions. Initiation and propagation of fatigue-induced cracking is complicated and depends on many influencing factors. Numerous numerical and experimental studies have been undertaken through decades to understand the fatigue cracking mechanism and to develop proper methods of increasing pavement fatigue resistance. In many cases, researchers have resorted to empirical equations to establish the relationship between asphalt mixture characteristics and pavement performance in terms of resistance to fatigue cracking. For example, in the AASHTOWare® Pavement ME, a set of transfer functions is utilized to connect the mixture engineering properties to fatigue cracking in a pavement structure under specific climatic and traffic conditions. These models require calibration mainly due to the fact that the main

ingredients making asphalt mixtures (i.e., the asphalt binder and the aggregates), as well as the climatic regions where asphalt pavements are placed, are so diverse.

Several laboratory tests have been developed at various times to characterize the asphalt mixture behavior in terms of fatigue cracking resistance. These tests fall into two general categories: cyclic (repeated) loading tests and monotonic (single-cycle) fracture loading tests. Among the former group, one can name four-point bending beam, uniaxial tension-compression, and repeated load indirect tensile fatigue. For the latter, indirect tensile strength, semi-circular bend (SCB) test, and indirect tensile asphalt cracking index (IDEAL-CT) test can be named. A single-cycle loading to capture fatigue properties is much simpler but does not truly capture the mix characteristics in terms of crack propagation. It may be more appropriate to refer to such tests as index tests or performance-related tests rather than performance tests.

Four approaches are used to characterize the fatigue resistance of asphalt mixtures, which include the phenomenological approach, the viscoelastic continuum damage approach, the fracture mechanics approach, and the dissipated energy-based approach. In the phenomenological approach, the number of load repetitions to failure is related to the stiffness and strain or stress responses of asphalt mixtures. The viscoelastic continuum damage approach was introduced by Kim (1988), and it showed great potential to characterize the fatigue performance of asphalt. This method applies Schapery's viscoelastic constitutive theory for materials with distributed damage to describe the behavior of sand asphalt under controlled strain cyclic loading. One obvious benefit of this method is that one can use test results from a single set of conditions to predict the behavior of that material under any variety of alternate conditions, making the experimental characterization of the damage resistance properties of a material far more efficient to perform. The fracture mechanics approach is based on the initiation and propagation of the crack. In the dissipated energy-based approach, the assumption is that the fatigue life of asphalt mixtures is dependent on the dissipated energy of each loading cycle. In this study, the phenomenological approach was used to investigate the fatigue performance of asphalt mixtures.

While most state highway agencies have adopted specific test protocols to address asphalt pavement rutting, few have adopted test protocols to deal with the problem of fatigue cracking. The dilemma that has existed with state highway agencies to finalize their decision in the selection of the fatigue

test protocol is mainly due to the complexity of the problem, variability in test results, and difficulty in establishing mix design criteria.

The main objective of this study was to develop a new fatigue test that was simple to conduct and analyze for evaluation of different types of mixtures. The Hamburg wheel tracking test (HWTT) has been widely accepted as a reasonable and reliable test to evaluate the rutting and moisture damage performance of asphalt mixtures. Hence, its use as a fatigue resistance test was new and subjected to exploration under this research. The standardized protocol for HWTT has been around under AASHTO Test Method T 324 for almost two decades. Several state DOTs and industries are now adopting this testing method as part of their routine testing protocols to verify asphalt mix designs and to perform mixture performance evaluations. Some are also considering this testing protocol as part of their approach to a balanced mix design. However, for fatigue performance evaluation, there is still no standard testing method that has been widely accepted by state DOTs as a routine testing method. Under this study, a new standardized fatigue test protocol was developed that can evaluate the fatigue cracking resistance of the asphalt mixture in the Hamburg wheel tracking device (HWTD), with specific supporting conditions, so that an integrated design of material and structure can be achieved for use by the pavement industry. Before delving into the specifics of the newly developed fatigue test concept, it is critical to understand the context of current fatigue performance tests and their capabilities.

Laboratory Tests To Determine Fatigue Performance of Asphalt Mixtures

Various tests have been developed and used to evaluate the fatigue resistance of asphalt mixtures in the laboratory. As mentioned previously, these tests are either performed in the form of a single load cycle or through repeated loading of the asphalt concrete specimens. In the case of the latter, the tests can be performed either in displacement (or strain) controlled mode or in load (or stress) controlled mode. Repeated load tests are better indicators of the asphalt mixture fatigue performance, as they capture both initiation and propagation of the cracks developed in the mixtures. However, they are more complicated to run. The single-cycle loading test protocols are considerably simpler and faster to run, but they lack the robustness of the repeated load tests. At the time of drafting this report, it

appeared that many state highway agencies were tending toward the test standards that are based on the single-cycle loading because of its simplicity.

Four of the laboratory tests associated with characterizing the fatigue resistance of asphalt concrete mixtures are presented below. The first two cover two of the standards for monotonic loading most commonly used today: the semi-circular bend test and the IDEAL-CT test. The third and fourth test protocols are examples of the repeated loading type testing: the tension compression test and the Texas overlay test. It should be noted that there are many other fatigue-related test protocols, and the four test standards discussed here are just examples of those currently in use by some state highway agencies.

Semi-Circular Bend (SCB) Test

To simplify fracture testing in rock materials, a semi-circular bend was developed by Chong and Kuruppu (1984). A fracture notch in the bottom of the test specimen is created, and the load is applied from the top at a given rate until the failure point. This test has been adopted for asphalt mixtures (Figure 1) because of its practicality, repeatability, and simplicity. The fracture-related parameters, such as cracking resistance index, fracture energy, and flexibility index (FI), are calculated to interpret the test results (Nsengiyumva and Kim, 2019; Nsengiyumva et al., 2020).

Among the pioneers to introduce SCB into asphalt testing were Krans et al. (1996) and Molenaar et al. (2002). Later, the test was further investigated by the Louisiana Transportation Research Center (LTRC) to relate the mixture fracture properties to cracking potential (Mohammad et al., 2004). The test protocol developed by LTRC became part of Louisiana DOT specifications and was published as a provisional standard under AASHTO TP 105. Further work on SCB was conducted by the University of Illinois at Urbana-Champaign (UIUC), and their efforts resulted in the development of a test protocol in 2015 known as the I-FIT or Illinois Flexibility Index Test (Al-Qadi et al., 2019). This test protocol was first published by AASHTO as TP 124 in 2016 and was later adopted as a full standard, T 393, in 2021. This test takes advantage of the fracture work and post-peak slope from the test to evaluate the cracking potential of the mix. Al-Qadi et al. (2019) reported a good correlation between the I-FIT test results and observed field cracking. Evaluation of the asphalt mixture cracking resistance using SCB is also covered under ASTM Standard Test Method D8044. The SCB test has

been the subject of many research studies, and some have used it as a tool for balanced mix design (BMD). As an example, Xuan Chen et al. (2019) used the test to optimize the rejuvenator content in a BMD approach.

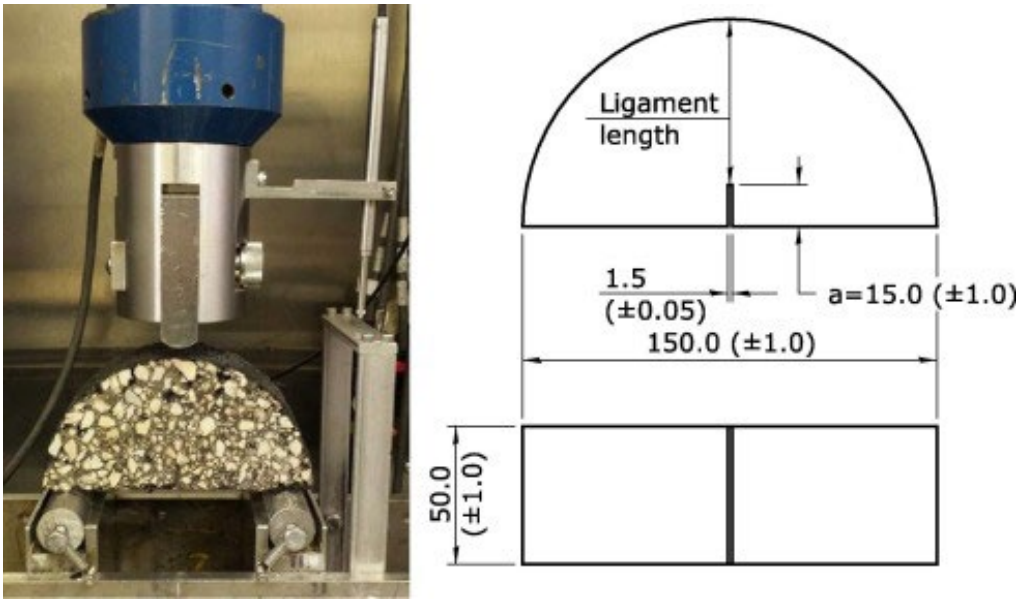

Figure 1. SCB test setup and sample dimensions.

Researchers have used SCB test geometry to produce alternative indices other than FI. For example, Kaseer et al. (2018) used the SCB test setup and introduced the cracking resistance index (CRI), which was defined as G_f/P_{max}, where P_{max}=maximum load, and G_f=fracture energy. Nemati et al. (2019) proposed a rate-dependent cracking index (RDCI) parameter using the SCB-type geometry. Majidifard et al. (2021) used the same geometry and produced a balanced cracking index (BCI) that was defined as BCI= 0.01 × Gf × L75. The objective of all these alternative solutions was to improve the repeatability of the SCB test output and introduce a parameter that can distinguish the mixtures in terms of cracking resistance more accurately.

An important consideration in utilizing any performance related or performance-based test protocol is the condition of the specimen in terms of duration of exposure to hot temperature and radiation. As such exposure gets prolonged, more aging and brittleness of the asphalt mixture occurs. At the initial

stages of pavement performance when the asphalt is not yet highly aged and tends to be more flexible, rutting is the distress type of the most concern. Hence, the performance tests that capture rutting are best suited to be conducted on short-term aged asphalt mixtures. On the other hand, long-term aged asphalt is overly sensitive to cracking, and therefore, the results from the tests to assess cracking resistance are more reliable when conducted on long-term conditioned specimens. The importance of considering the aging effect in SCB testing and any other fatigue-related test protocol discussed in this document cannot be overemphasized. Similarly, one cannot ignore the especially important effect of the loading rate and the test temperature. Chen and Solaimanian conducted extensive research on the impact of long-term aging, loading rate, and test temperature on the SCB test results and demonstrated that the test results vary significantly depending on the testing conditions (Chen and Solaimanian, 2019; Xuan Chen et al., 2019).

Indirect Tensile Asphalt Cracking Test (IDEAL-CT)

Zhou et al. (2017) developed the indirect tensile asphalt cracking test (IDEAL-CT) to simplify the fracture testing of asphalt mixtures. This test is similar to the indirect tension test (IDT), and it is known as a simple, practical, and quick test to examine the fracture resistance of asphalt mixtures. The IDEAL-CT test specimens have a thickness of approximately 62 mm, and the load is applied at the rate of 50 mm/min to generate indirect tension at 25 °C (ASTM D8225, 2019). The parameters such as fracture energy and flexibility index are used to analyze the fracture properties of the asphalt mixture. After conditioning, the specimens are placed in the test equipment. A seating load of 0.1 kN is applied to make appropriate contact between the loading head and the specimen. The specimen is then loaded under a displacement rate of 50 mm/min while the loading level is measured by the machine. The cracking parameter for the IDEAL-CT is derived from the load vs. displacement curve (Figure 2). It is believed that a larger CT index is an indication of better cracking resistance of the mixture. The CT index equation is as follows.

$$CT_{index} = \frac{G_f}{|m_{75}|} \times \left(\frac{l_{75}}{D}\right) \times \left(\frac{t}{62}\right) \qquad \text{Eq. 1}$$

where G_f = fracture energy (area under the curve normalized by the area fractured), m_{75} = slope parameter (absolute value of the slope at 75% of peak load), l_{75} = vertical displacement when the

load is reduced to 75% of peak load, l_{75}/D = strain tolerance parameter (when the load is reduced to 75% of peak load), D = diameter of the specimen, and t = specimen thickness.

(a)

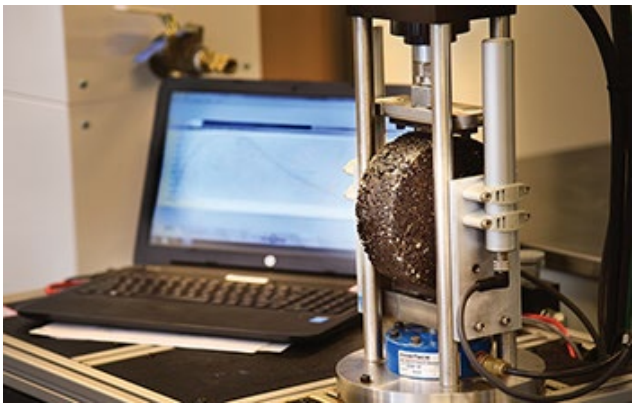

(b)

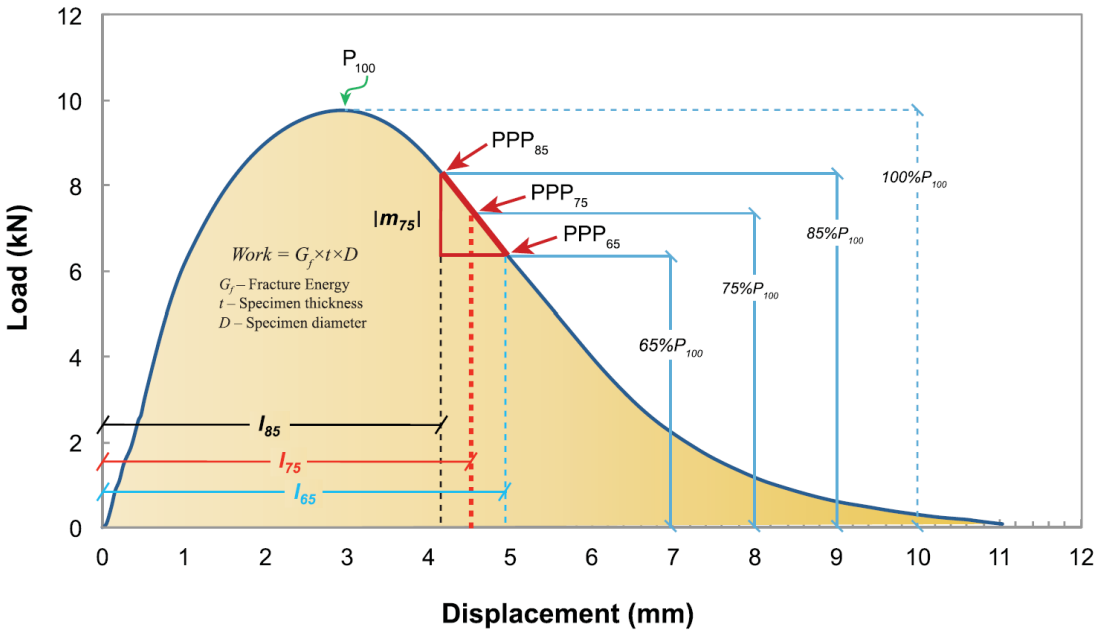

Figure 2. a) IDEAL-CT test setup, b) illustration of the PPP75 point and its slope |m75| (Zhou et al., 2017).

Zhou et al. (2018) conducted the IDEAL-CT test on asphalt mixtures with two types of rejuvenators and reported that the IDEAL-CT test could effectively differentiate between the two types of mixtures. Chen et al. (2021) tried to validate the capability of the IDEAL-CT test to characterize the fatigue performance of asphalt mixtures. To this end, the correlation between the fatigue-related binder tests (e.g., linear amplitude sweep [LAS] and Binder Yield Energy Test [BYET]) with the

IDEAL-CT test was examined. Based on the experimental observation, the role of the binder system, including virgin binder and recycling contents of RAP and RAS, in fatigue damage could be captured in the asphalt mixture using the IDEAL-CT test. Also, a good correlation between the fatigue life of the binder obtained from the LAS test and the CT index was developed. Alfalah et al. (2021) implemented the IDEAL-CT test to study the effect of fiber type and content along with binder grade on the cracking performance of asphalt mixtures. The authors used basalt, fiberglass, and carbon fibers at dosage rates of 0.15 and 0.30% by the weight of the mixture and changed the binder content (Pb) from 5.0% to 6.2% with 0.2% increments. The CT index revealed that fiberglass does not have any significant impact on the cracking performance, while 0.3% of carbon and basalt fibers were shown to have the potential to improve the durability of the carbon-reinforced and basalt-reinforced mixtures, respectively. Yan et al. (2020) compared three testing geometries, including SCB-IFIT with a notch, SCB-IFIT without a notch, and IDEAL-CT, using six different plant-produced asphalt mixtures. They reported that the lowest coefficient of variation (COV) was recorded by IDEAL-CT. In addition, IDEAL-CT was found to be highly correlated with the I-FIT test. This is while IDEAL-CT sample fabrication was the simplest among the three tested geometries.

Tension-Compression (Push-pull) Fatigue Test

The uniaxial push-pull fatigue test (also known as the uniaxial compression-tension test) was first introduced in the United States by Soltani and Anderson (2005) at the Pennsylvania State University. Based on the developed test protocol, the test is conducted in the strain control mode. There are alternatives to how the strain is induced into the specimen. In the simplest form, the test can be conducted under one continuous strain level higher than the material endurance limit until the mix goes through micro and macro damage levels. As an alternative to capture the “true” damage level or to determine the endurance limit, the test can be conducted at multiple strain levels. For example, Soltani et al,. (2006) reported on conducting the test in three stages of loading. In the first and third stages of loading, the strain level is maintained extremely small (to ensure it is lower than the endurance limit), while during the middle stage, the strain level is significantly increased to induce damage. Figure 3 illustrates the schematics of the three stages of the loading. Figure 4 shows the fixtures, thermocouples, and transducers along with the asphalt mixture test specimen. The asphalt mixture specimen has a height of 4.7 in. and a diameter of 3 in. The gauge length for measuring displacement is 3 inches and a sinusoidal load is applied at a 10-Hz frequency at 10 °C.

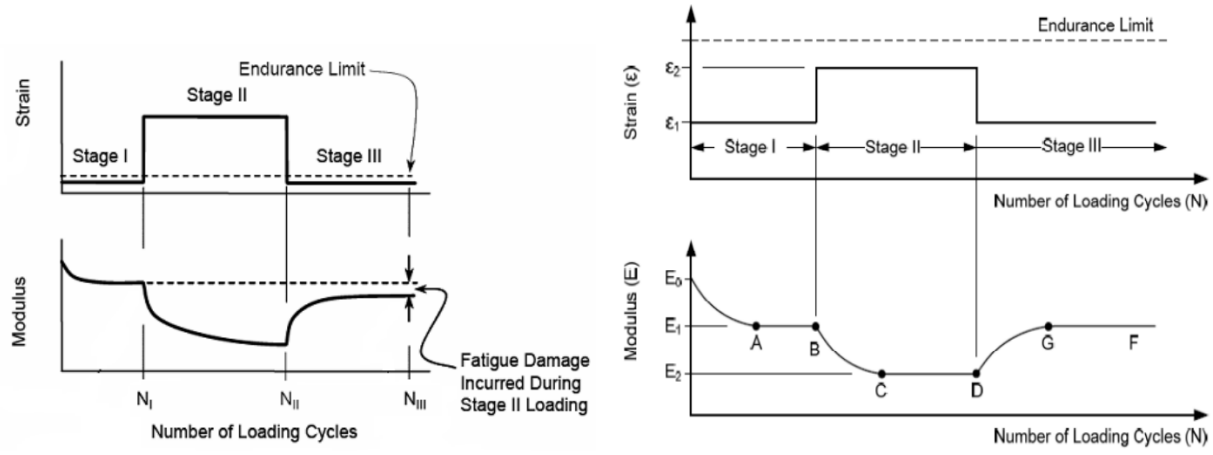

Figure 3. Loading in Stages I, II, and III (Soltani A et al., 2006).

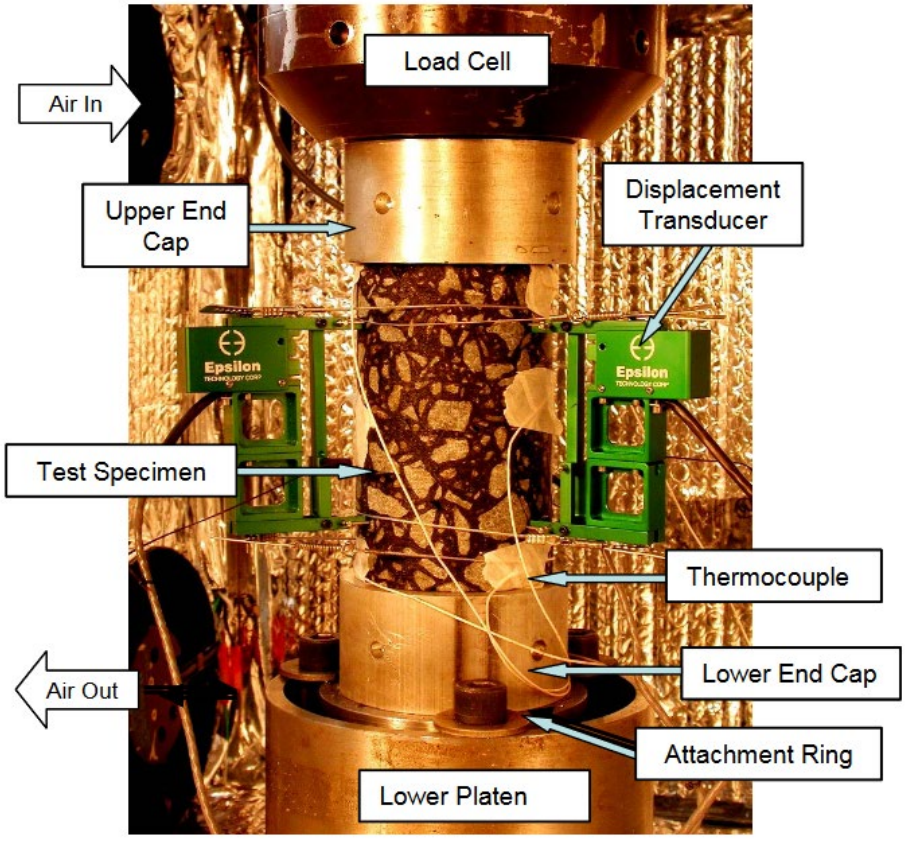

Figure 4. Test specimen with transducers and thermocouples (Soltani & Anderson, 2005).

Underwood, et al. (2012) developed a viscoelastic continuum damage model (S-VECD) for fatigue analysis, and one of the main test protocols used to capture properties for the model is based on the push-pull uniaxial fatigue test. In their protocol, they established specific requirements on the loading and sampling rates during the test to collect the required data for the damage model.

Texas Overlay Test

Germann and Lytton (1979) developed the Texas overlay test (OT) in the 1970s to examine the reflective cracking of asphalt mixtures using two steel plates, one of which is fixed and the other horizontally moves, to simulate the opening and closing of the joints underneath the surface layer (Ma et al., 2014). This test has been further developed and verified by Zhou et al. (2007) to capture the fatigue properties of the asphalt mixture using prismatic test specimens that are 6 in. long, 4 in. wide, and typically 1.5 in. thick that are glued to the metal plates using epoxy (Figure 5). The test measures the number of cycles that led to failure, defined as a 93% reduction in the load carried by the specimen during the first cycle, and the obtained data can be used to find the crack initiation and the potential for propagation. It is performed according to the Tex-248-F standard. Mogawer et al. (2011) fabricated eight types of mixtures including control, 40% RAP, 5% RAS, and 35% RAP+5% RAS with and without warm-mix additive (WMA). The OT test was implemented to measure the reflective cracking resistance at 15 ℃ (59 °F) with a 6-mm (0.025-in.) gap between the plates. The results indicated that increasing the asphalt binder replacement (ABR) results in lower reflective cracking resistance. Also, adding 1% of WMA was able to decrease the negative effect of recycled material on the cracking resistance.

Gu et al. (2015) obtained field cores 1, 9, and 15 months after the construction of three projects including control hot mix asphalt, Evotherm™ and foamed asphalt warm mixtures. These field cores were tested using the (OT) test at 25 ℃. Although the standard OT test applies 0.64-mm (0.025-in.) displacement at each cycle until the specimen fails, the authors modified the test protocol such that 10 non-destructive load cycles with 0.05-mm opening displacement were applied followed by 15 minutes of rest. Then, the samples underwent 200 destructive load cycles with 0.32-mm displacement. This modified test protocol was proposed to determine the fracture properties (A and n parameters)

based on Paris law. Paris' Law, named after Paul Paris, is a fundamental principle in fracture mechanics that describes the growth rate of cracks in a material due to repeated or cyclic loading. This law uses the concept of a stress intensity factor to gauge the distribution of stress around a crack, which helps in understanding how a crack propagates with each cycle of applied stress. A variant of Paris' Law employs a metric known as the J-integral, which quantifies the energy dissipation per unit area of crack growth. This variant is especially useful in scenarios involving non-linearly elastic materials. Moreover, for viscoelastic materials, an adapted form of the J-integral, known as the Jr-integral, is used. This form varies with the time of loading. Overall, Paris' Law and its variants provide essential insights into predicting and understanding the propagation of cracks in different materials under various loading conditions (Lytton et al., 1993). Comparing the n-parameter obtained from the test, it was shown that the OT test could detect the effect of aging. Also, the Evotherm warm mix showed better cracking resistance (lower n) compared to the control and foamed asphalt warm mix after one month of construction. However, HMA and two warm mixes did not show a significant difference in cracking resistance after 9 months of field aging.

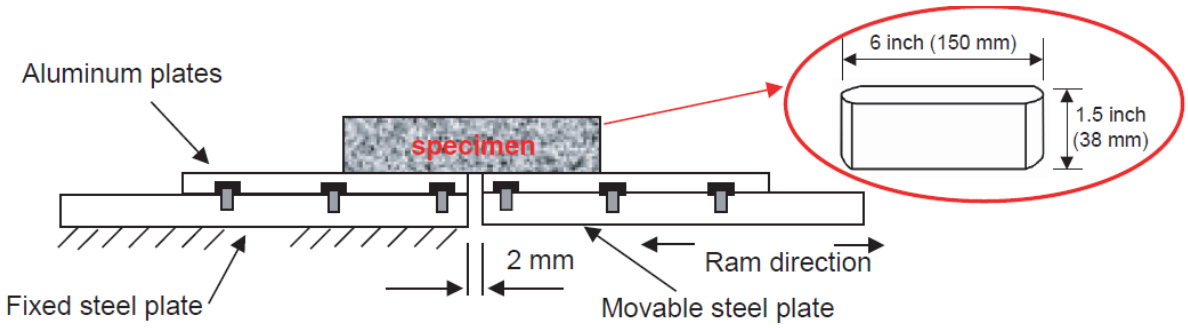

Figure 5. Texas overlay test setup and sample (Zhou et al., 2007).

The principal shortcoming of these existing tests is their failure to adequately consider the structure of asphalt pavement in real-world scenarios. Often, a singular load is applied to the test specimen, a situation that diverges significantly from actual field conditions that lead to fatigue damage. Consequently, there was a clear necessity to develop a new test capable of addressing both of these issues effectively.

Using HWTD to Predict the Fatigue Performance

It should be noted that throughout this document, two abbreviated terms related to the Hamburg tracking test are frequently used. One is HWTT, and that is the abbreviation for the Hamburg wheel

tracking test, covering the testing protocol. The other is HWTD, which is the abbreviation of the Hamburg wheel tracking device, i.e., the equipment itself.

The fatigue characteristic of an asphalt mixture is one of the most crucial factors to determine the service a of the flexible pavement. As stated earlier, a lot of fatigue tests have been introduced to examine the fatigue performance of an asphalt mixture using different methods and approaches. Some of these tests have already been presented in this chapter. Even though all tests significantly contribute to a better understanding of the fatigue performance of an asphalt mixture, there are various limitations for each of these tests that cannot be ignored. These tests have been used to characterize the fatigue behavior of the asphalt materials. The main drawback of these tests is ignoring the pavement structure, and none of the test methods are even close to the pavement structure in the real world. Numerous studies indicated that fatigue performance of an asphalt pavement is impacted by two main criteria: the structure and materials characteristics (Sabouri & Kim, 2014; Wang et al., 2018). Therefore, the structure can dominate the impact of the materials characteristic on the fatigue life of the asphalt pavement, which can lead to differences between laboratory results and field performance. It should be noted that the small-scale accelerated pavement testing like mobile load simulator 3 (MMLS3) and accelerated pavement testing (APT) can consider the structure for predicting the fatigue life; however, these two tests are expensive, time consuming, and require a lot of materials for a single test (Füssl et al., 2015). The second drawback is ignoring the real loading condition in the field. Most of the tests use a single load or repeated non-moving loads, which cannot simulate the real pavement loading condition. A moving load results in creating stress and strain in two directions (Figure 6). Longitudinal stress is the combination of compression and tension. When the wheel is exactly in the same position of the target point (with different height) the tensile is expected, but when the wheel is moving forward or backward, compression stress is expected in the target point. On the other hand, the pure tensile stress is expected during the loading period at the bottom of the asphalt pavement (Zhang, Kohlmeier, et al., 2021). By considering these drawbacks and overcoming these challenges, the concept of measuring the fatigue life using HWTD has been introduced in this study. Both loading condition and structure would be very close to the real pavement.

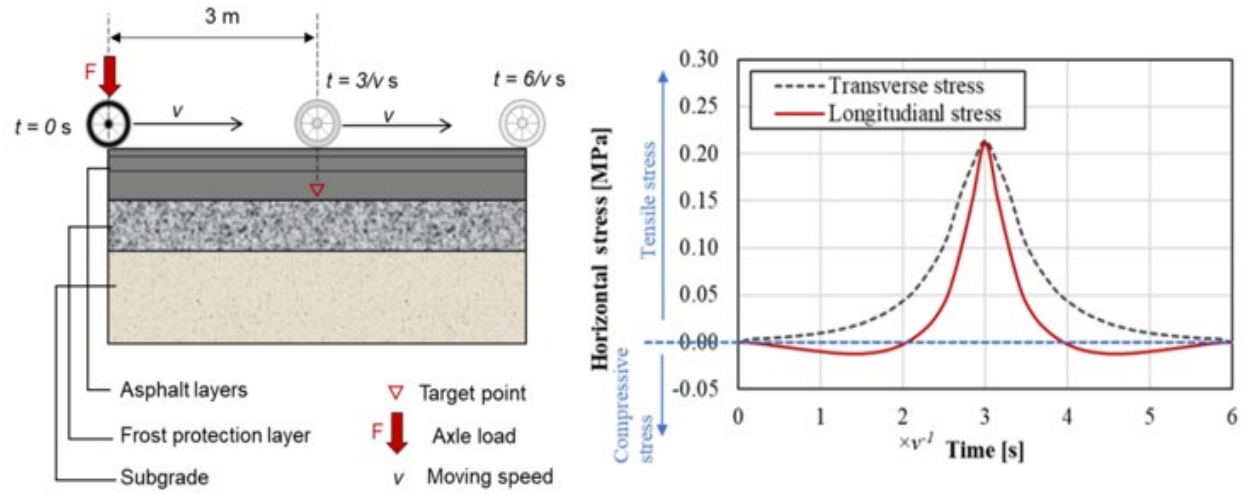

Figure 6. Transverse and longitudinal stress at the target point under moving load (Zhang, Kohlmeier, et al., 2021).

asphalt pavement analyzer (APA) and HWTT have been widely used to evaluate the rutting and moisture sensitivity performance of asphalt mixture for decades. Because of moving loading and with some modifications in the test procedures, the equipment of these two tests can be used to detect the fatigue performance of an asphalt mixture. There has been a very limited number of studies considering the moving loads in a laboratory environment for evaluating the fatigue damage resistance of asphalt mixtures.

Wu et al. (2012) used the APA machine to evaluate the fatigue performance of asphalt mixtures. The asphalt beams were prepared and tested under moving load. Figure 7 shows the specimens, extensometers, linear variable differential transformers (LVDTs) and loading wheel for the proposed test. Before starting the test, the extensometers were glued to the bottom of the specimens to measure the deformation. The LVDT was used to record the moving position of the wheels. After acquiring the moving position, the stress was calculated at the bottom of the specimens. Various loading frequencies of 0.1, 0.2, 0.5, 1, and 2 Hz were used. All samples were tested at three different temperatures (10, 25 and 40 °C). Finally, by using various equations, the creep compliance, phase angle, and dynamic modulus were calculated. The results indicated that the proposed test could detect the viscoelastic properties of the asphalt mixture using several types of binder, aggregates, and various binder contents. With all progress in simulating the real world loading condition, this test could not simulate the field condition because of the different support condition compared to the field.

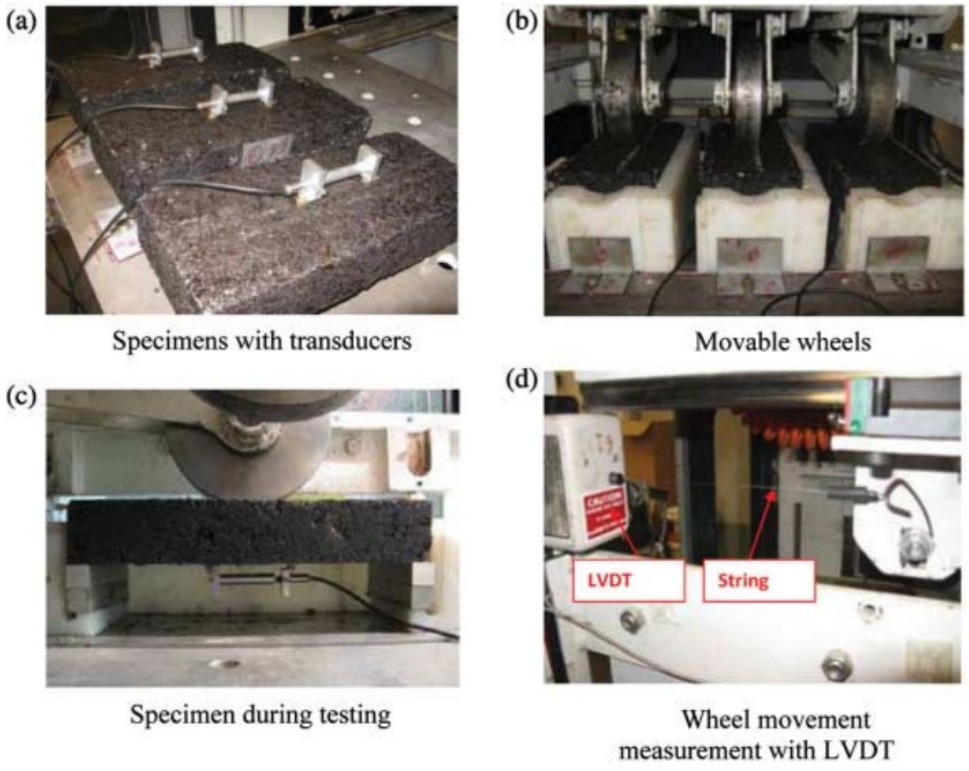

Figure 7. Specimens, extensometers, LVDTs and loading wheel for the proposed fatigue test using APA (Wu et al., 2012).

Zhang et al. (2021) used HWTT to simulate the fatigue properties of an asphalt mixture. In that study, three different mixtures (two slabs from each) with a known fatigue performance were prepared and compacted to be tested under moving loading. A neoprene base was used as a second layer for providing the full support condition similar to the field. Various strain gauges along with pressure cells were utilized to obtain the strain and stress at the bottom of the specimens in two different directions. Two different methods, including the ratio of dissipated energy change and phenomenological fatigue life analysis approach, were used to examine the fatigue performance of the asphalt mixtures. Based on the results, it was found that the results obtained from the HWT machine on the slabs are consistent with results obtained from the SCB test with the same mixture. Therefore, it was concluded that the HWT machine has the potential to simulate the fatigue performance of the asphalt mixture.

While the work of Wu et al. (2012) and Zhang et al. (2021) offered valuable insights into the fatigue performance of asphalt mixtures, their scope was quite limited. Their findings, though valuable, highlight the necessity for a more comprehensive examination of asphalt mixture fatigue performance, underscoring the relevance and need for the present research.

CHAPTER 2

Setup of the Testing Equipment

Introduction

Several activities were undertaken to develop a working test setup for fatigue test using the Hamburg wheel tracking device. One was conducting a numerical analysis to determine the optimum width of the test slab for use in the test considering the constraints existing with the HWTD. The second activity evolved around finding a suitable technique in the production of test slabs. Parallel to these two was the activity associated with finding the appropriate transducer for recording the deformations or strains during the test.

Numerical Analysis

Theoretical work was undertaken to assist the research team with selection of a suitable width for the asphalt concrete specimens to be tested in HWTD. The device tracking wheel has a width of 50 mm (≈ 2 inches). The objective was to find the slab width beyond which no considerable change in the strain response would be noticed. A 3-D finite element modeling (FEM) analysis was performed using commercial ABAQUS software to determine the strain distribution within the slab specimens and to decide on the desired slab width for the experimental work.

Assumptions and Basic Model Setup

Considering the objective sought under this portion of the work, the analysis was simplified to include solely finite element linear elastic analysis. Reasonable values were assumed regarding engineering properties of the asphalt concrete specimen and the underlying supporting layer. Factors considered in the analysis included specimen width and thickness and stiffness of supporting condition. A static linear load of 158 lbs with a width of 2 inches was applied at the center of the specimen to simulate the weight and width of the HWTD wheel.

Figure 8 shows the meshed model for the mold and the specimen. The asphalt mixture slab was placed inside the stainless-steel mold, with or without supporting layers. Other assumptions and model parameters included: (a) the asphalt mixture was considered as an elastic material with an elastic modulus of 500 ksi; (b) the mold was considered as a rigid material with an elastic modulus of 29,000 ksi; (c) the coefficient of friction between the asphalt mixture and steel (mold) was set as 0.7; and (d) the mold was considered fixed with no movement or rotation in any direction. The assumption of elasticity was made because the material are to be tested at 25 °C and at this temperature the material tends to exhibit less time-dependent viscoelastic behavior compared to high-temperature testing. The main reason the assumption of elastic behavior is reasonable is that the purpose of this part of the study was not to investigate the viscoelastic material behavior under moving load, but rather to decide on the appropriate width of the slab to be used with the experimental part. However, testing at this lower temperature in no way implies that the viscoelastic creep response can be ignored for slow-moving loads.

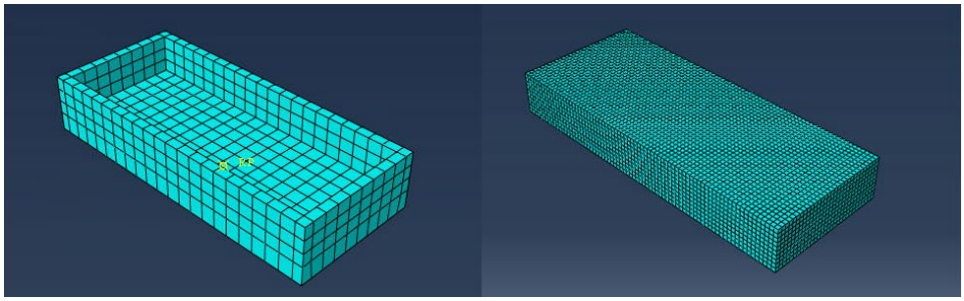

Figure 8. Mesh models for the mold and the specimen.

Analysis Factors

Using the basic FEM model setup, a parametric analysis was conducted to evaluate how the change of asphalt specimen geometry and supporting conditions might affect the stress/strain distribution within the specimens. Results from this analysis were used as a guide to decide on the configuration of the experimental setup. Table 1 shows a total of 18 cases that were considered in the parametric analysis, with 4 levels of slab thickness (1, 1.5, 2.0, and 2.5 inches), 4 levels of slab width (2, 4, 6, and 8 inches), and 2 levels of supporting conditions (rigid base with steel and flexible base support). The thickness of the flexible base was considered to be 1 inch for all cases. It was assumed that the

specimen resided inside the stainless-steel mold for all cases and the coefficient of friction between the asphalt mixture specimen and the underlying support was 0.7. This friction coefficient was selected based on past research exploring the friction at the contact surface between asphalt concrete and steel (Mihora et al., 2012).

Table 1. Cases Evaluated in the Numerical Experiment.

Configuration (Case No.)	Asphalt Thickness (inches)	Asphalt Width (inches)	Underlying Support Type
1	1.0	2	Steel
2	1.0	4	Steel
3	1.0	6	Steel
4	1.0	8	Steel
5	1.5	2	Steel
6	1.5	4	Steel
7	1.5	6	Steel
8	1.5	8	Steel
9	2.0	2	Steel
10	2.0	4	Steel
11	2.0	6	Steel
12	2.0	8	Steel
13	2.5	2	Steel
14	2.5	4	Steel
15	2.5	6	Steel
16	2.5	8	Steel
17	1.0	4	Flex base, no bond with slab
18	1.0	4	Flex base, full bond with slab

Discussion of Results for Different Cases

Slab on Rigid Base

The numerical analysis for cases 1 to 16 presented in Table 1 provides information on the effect of slab geometry (width and thickness) on strain distribution when the slab is placed directly on the rigid base. Output examples are presented in Figures 9 and 10 when the load is applied at the center of the

slab and is distributed linearly for 2 inches across the 4-inch-wide slab. Figure 9 presents maximum compressive strain at the surface of the specimen. Figure 10 demonstrates an example of the tensile strain contour at the bottom of the asphalt concrete slab specimen.

Analysis was repeated for various configurations; a summary of the tensile strain at the bottom of the specimen as a function of the specimen width and height is presented in Figure 11. As shown, with the increase of the specimen thickness, the tensile strain at the bottom of the specimen is reduced. The strain decreases significantly when the width increases from 2 to 4 inches. However, the rate of strain change is reduced when the width increases from 4 to 6 and from 6 to 8 inches. The results are also summarized in Table 2. The idea of varying the width was to determine at what width the tensile strain begins to stabilize and not be affected by the slab width. Based on these results, the width of slab for the main and reference slabs was selected to be 6 inches.

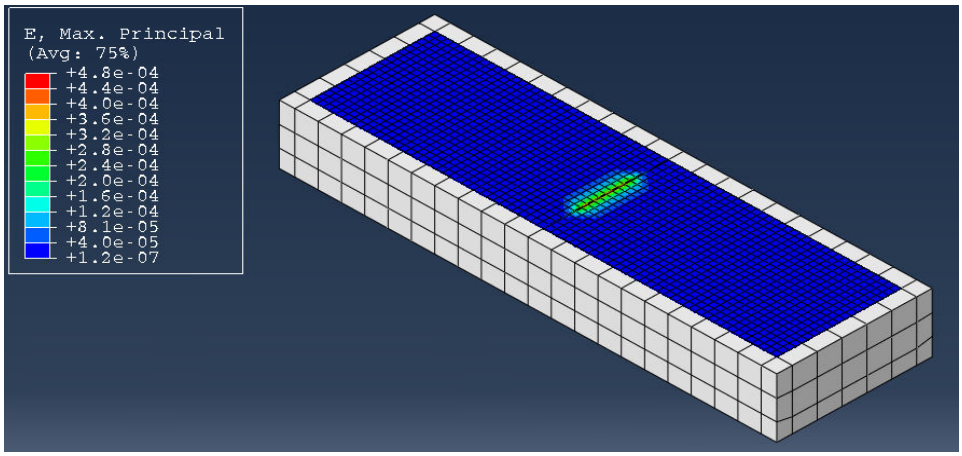

Figure 9. Setup and compressive strain at the top of asphalt concrete slab under static load (15×4×1.5 inch).

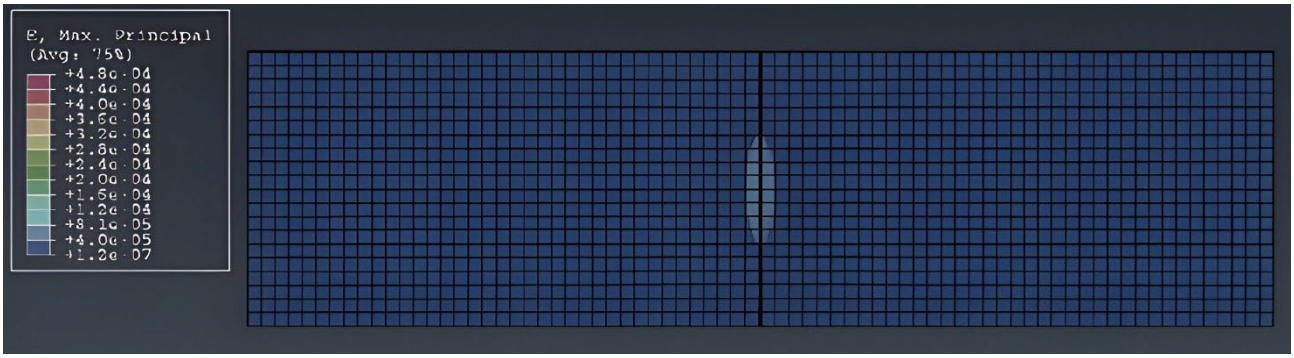

Figure 10. Tensile strain at the bottom of the slab under static load (15×4×1.5 inch, and deformation scale factor of 1).

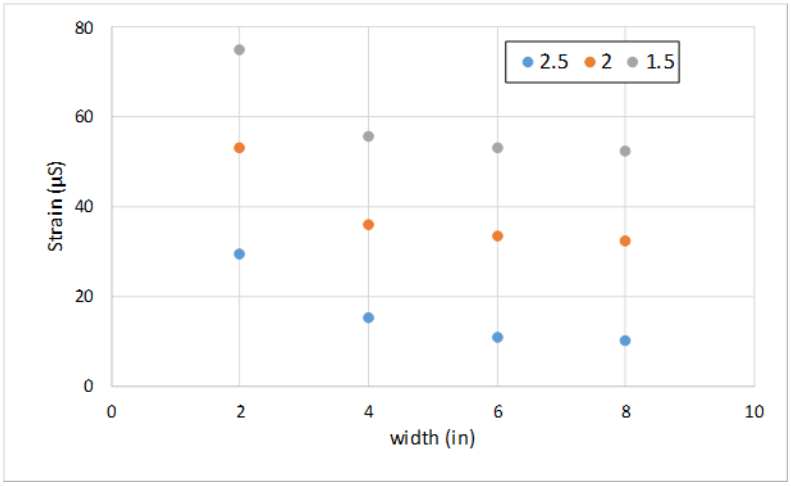

Figure 11. Tensile strain at center and bottom of the specimen with rigid base.

Table 2. Tensile strain at the center and the bottom of the specimen with rigid base (microstrain).

Width (in) / **Thickness (in)**	2	4	6	8
2.5	29.4	15.1	10.7	10.2
2.0	53.2	36.0	33.3	32.5
1.5	75.2	55.7	53.2	52.5

Slab on Flexible Base with No Bonding at Interface

Following the first numerical trial using the slab residing on a rigid base, a second set of analyses were performed using a flexible base underlying the asphalt concrete slab, delivering a three-layer system (asphalt slab + base) residing on the underlying support foundation (treated as half-space). The elastic modulus of the asphalt slab and the flexible base were assumed to be 30 ksi. Assumptions made in the numerical exercise with the rigid base were also applied in the flexible three-layer system. Furthermore, the contact surface of the flexible base with the asphalt slab was considered to be frictionless (no bond). Two scenarios were considered for the bond between the base and the underlying support foundation: no bonding and full bonding.

Figure 12 shows the strain on the surface of the flexible base under the load, while Figure 13 illustrates the strain at the bottom of the 1.5-inch asphalt mixture layer residing over the flexible base layer. In this three-layer system, for the 1.5-inch slab thickness, the tensile strain at the center of the bottom of the asphalt specimen was 83.1 microstrain. This is almost 46 percent higher than the tensile strain at the bottom of a 1.5-inch asphalt specimen without the flexible base layer (55.7 microstrain).

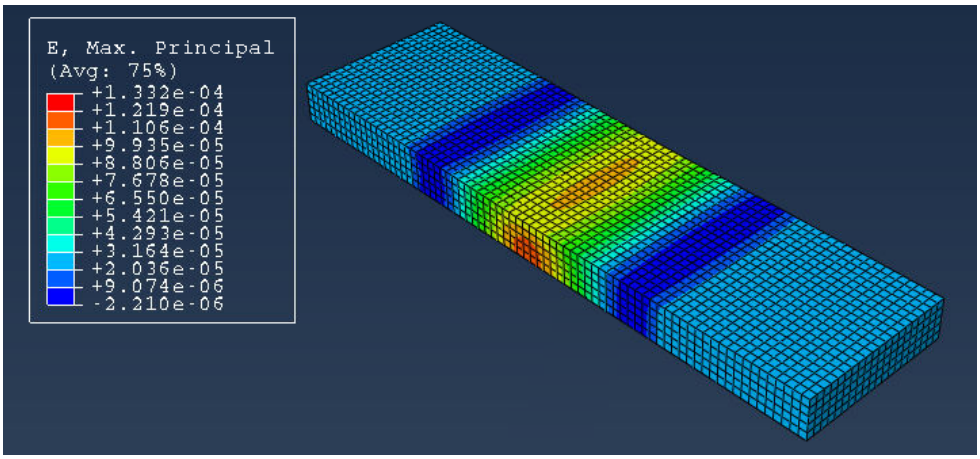

Figure 12. Compressive strain at flexible base surface (1.5-inch asphalt, 1-inch base, and deformation scale factor of 1).

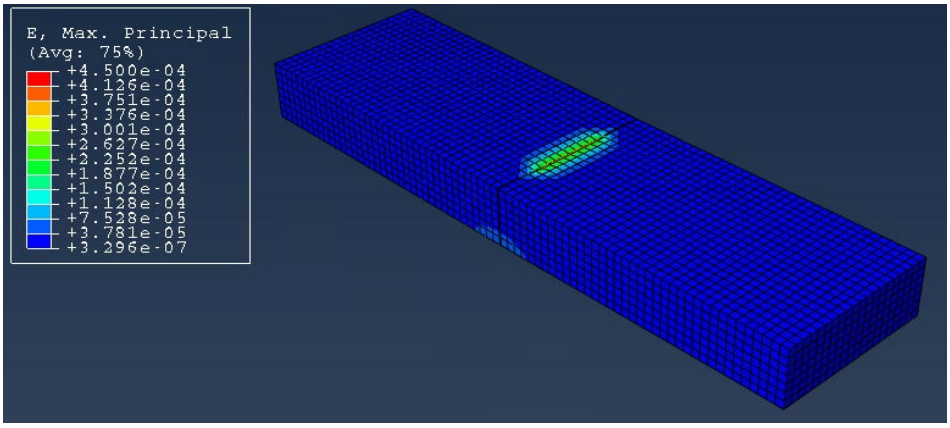

Figure 13. Tensile strain at specimen bottom (1.5-inch asphalt, 1-inch base, and deformation scale factor of 100).

Slab on Flexible Base with Full Bonding at Interface and Comparison with No Bonding

Following the numerical analysis on the three-layer system with free movement between the slab and base, linear elastic analysis was conducted on the three-layer system with full bonding between the slab and the base for comparison. To expedite analysis for this part of the work, the Kenlayer application package was used. This application package is used for pavement design and analysis using multi-layered elastic analysis. The results from Kenlayer are not directly comparable with those from the FE analysis, since the results discussed above were found using the FE analysis applied to small-dimensioned slabs as used in the HWTD, whereas analysis with the Kenlayer system is for a full-scale pavement, and its application for this part of the work was for the sole purpose of comparison of strains between bonded and unbonded layers. Table 3 provides strains at the bottom of the slab and surface of the flex base with four conditions, free movement between the asphalt slab and the base, and complete bonding between the asphalt slab and the base. The results are based on the Kenlayer elastic analysis package. For this analysis, the moduli of layers were assumed as 500 ksi for the asphalt layer, 30 ksi for the base, and 29,000 ksi for the bottom support.

In the three-layer system with full bonding, for the 1.5-inch-thick slab, the strain at the center of the bottom of the asphalt slab was 83 microstrain. This strain is approximately 9% lower than the strain at the bottom of the slab in the three-layer system with free movement between the slab and base. For the no-bond condition, the reduction is almost 12%. It can also be seen that, as expected for the case of bonding between the asphalt slab and the base, the tensile strain at the bottom of the asphalt slab and top of the base are almost the same. Finally, one can see that when no bond exists between the

asphalt slab and the base, whether tensile or compressive strain develops at the base surface depends on the bond between the base and the underlying support (negative sign indicates compression).

Table 3. Strains at the bottom of the slab and surface of the flex base (1.5-in asphalt slab and 1-in base).

	Strain at the bottom of the asphalt slab (μs)	Strain at the surface of the base (μs)
Bond Condition	Full bond between the base and underlying support	
Free movement between the slab and base	91.4	-8.1
Complete bonding between the slab and base	83.0	84.0
	No bond between the base and underlying support	
Free movement between the slab and base	94.0	24.4
Complete bonding between the slab and base	88.3	89.7

Tensile Strain Response due to Changes to the Base Modulus

To establish a reference for experimental work in terms of the effect of base modulus on strain response, a numerical analysis was conducted for three different base moduli: 3,000 psi, 30,000 psi, and 300,000 psi. All the preceding results reported from numerical analysis were for the base modulus of 30,000 assuming a typical value for crushed stone base. The neoprene used in the experimental work has a significantly lower modulus. Hence, it is important to understand the effect of significant increase or decrease in the base modulus on the tensile strain response. The analysis was conducted for a 1.5-inch-thick slab residing on a 1-inch-thick base layer and with full bonding at the interface of these two layers. In an ideal situation when full bonding exists, the tensile strain at the bottom of the slab and the tensile strain at the surface of the base must be equal. Table 4 indicates that these two types of strain are very close. In terms of the base modulus effect, Table 4 indicates that using 30-ksi modulus as reference, the tensile strain at the bottom of the slab increases almost 45 to 50% when the modulus changes to 3 ksi. Similarly, there is almost a 60% decrease in strain when the modulus increases from 30 ksi to 300 ksi.

Table 4. Effect of Base Modulus on Tensile Strain (Full Bonding, 1.5-in Slab over 1-in Base).

	Strain at the bottom of the slab (με)	% strain change from strain for 30-ksi base modulus	Strain at the surface of the base (με)	% strain change from strain for 30-ksi base modulus
Flex Base modulus (psi)	Full bond between the base and underlying support			
3,000	125.0	50.6%	126.9	51.1%
30,000	83.0	0.0%	84.0	0.0%
300,000	31.9	61.6%	31.6	62.4%
	No bond between the base and underlying support			
3,000	128.2	45.3%	131.1	46.2%
30,000	88.2	0.0%	89.7	0.0%
300,000	35.6	59.6%	35.4	60.5%

Slab Preparation

Work with ENERPAC

During the initial trials of compacting specimens in the laboratory, a hydraulic hand pump and hydraulic cylinder were used. An ENERPAC model P-392 hydraulic hand pump and RSM500 hydraulic cylinder were used to compact the specimens. The P-392 hand pump and RSM500 cylinder have an operating pressure of 10,000 psi and capacity of 50 tons.

The asphalt concrete specimens were compacted in rectangular concrete molds of 4 inches in width, 16 inches in length, and 4 inches in height, as seen in Figure 14. Even though the numerical work indicated that the 6-inch-wide slab is more suitable than the 4-inch-wide slab, this compaction experiment was initiated with a 4-inch-wide slab to check the feasibility of the process. If the target air void could not be achieved with the 4-inch-wide slab, one would expect that achieving density would be an even larger challenge with the 6-inch-width slab.

Three slabs were compacted at a width of 4 inches. For all, the same amount of asphalt mixture was used (4,500 g), targeting 7.0% air voids. The molds were lined with non-stick paper on the bottom and on top of the asphalt during compaction to help with the removal of the slab from the mold after compaction.

Figure 14. Concrete Mold and Compaction Plate (I-Beam).

For the initial slab, only the loose asphalt mixture was heated to 158 °C for compaction. During the production of the second and third slabs, the asphalt mixture was heated to 158 °C along with the mold and the compaction plate prior to compaction. When the asphalt was at compaction temperature, it was placed in the mold and a compaction plate was placed on the asphalt mixture in the mold, and the entire setup was placed inside a strong steel frame for compaction (Figure 15). The hydraulic cylinder would allow vertical movement of only 0.6; therefore, several pieces of steel plate were used to fill in the gap between the frame and mold during compaction. Each time the cylinder was at the maximum displacement and the compaction plate was pressed down, the cylinder was released, and an additional piece of flat steel plate was inserted between the compaction plate and frame. This procedure was repeated several times until it was not possible to compact the asphalt mixture any further.

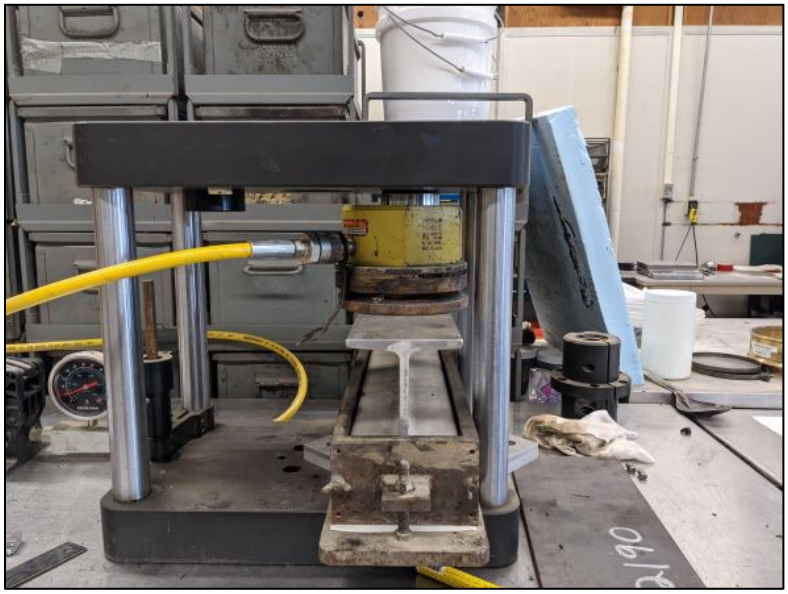

Figure 15. Compaction Mold with ENERPAC and Frame.

The slabs that were compacted in the lab had high air void content: 14.1% for the first slab, 14.2% for the second slab, and 12.2% for the third slab. The air voids were measured according to AASHTO T 166. In addition to the high air voids, these slabs were slightly tapered on the top after compaction, with one side being a few millimeters higher than the other side. The process also proved to be energy intensive.

Work with the Plate Compactor

Since it was not possible to achieve the desired air voids level with the ENERPAC compactor, an alternative was sought. For the next set of slabs, it was decided to compact them using a plate compactor. A large mold was used, with the bottom of the mold being a steel plate and the sides of the mold being wood. Inside of the mold, a piece of 1-inch thick neoprene rubber was inserted, and a piece of non-stick paper was placed on top of the neoprene before compaction (Figure 16). An Ingersoll Rand gasoline-powered plate compactor, model BX-6, was used to compact the slab. The plate compactor has a plate size of 16 inches in width and 21 inches in length and a weight of 150 lb. The maximum centrifugal force is 2,650 lb, and the vibration frequency is 5,500 vibrations per minute.

Figure 16. Plate Compactor and Wooden Mold.

The mold used was 25.5” in width and 24” in length. Several buckets of asphalt mixture were heated in the oven and then split into trays for ease of transferring to the mold. A total of 77 lb (≈35kg) of asphalt mixture was used to compact the slab to a thickness of 1.5”. The trays containing loose asphalt mixture were inserted in the oven at 162 °C, the trays were in the oven for 6 hours and the final temperature before compaction was 152 °C. Hot, loose asphalt was placed in the mold and was evenly spread inside the mold. The plate compactor was then used to compact the asphalt mixture inside the mold by moving the plate compactor around the surface several times in multiple directions. During compaction, the asphalt mixture was shoving and some of the asphalt mixture was pushed out of the mold.

The cooled slab was then trimmed from 25.5” by 24” to a size of 14” by 16” using a gasoline-powered concrete cut saw. The outside area of the slab was uneven and was not very well compacted, as the plate compactor could not properly get close to the edges of the mold to compact the asphalt mixture. Therefore, only the middle portion of the slab was used after initial trimming. The 14” by 16” slab was then further trimmed to the test size of 6” in width and 12.5” in length using a MK diamond tile saw. Only two test size slabs were produced from the original trimmed slab (Figure 17).

Figure 17. Test slabs cut from larger compacted slab.

Due to the possibility of high air voids, the AASHTO T 331 method was used to measure air voids, which uses the CoreLok device and a plastic bag to seal the specimen. The two slabs compacted with the plate compactor also had high air voids, with slab #1 having 11.5% and slab #2 having 11.2% air voids.

Slabs from Michigan Technological University

Neither the ENERPAC compactor nor the plate compactor produced slabs within the desired range of air voids. A request was made to Michigan Technological University (MTU) to produce slabs for this research, as MTU is equipped with a capable slab compactor. The loose mix was prepared in the laboratory and shipped to MTU. Figure 18a shows the loose mix that was prepared in the lab. In MTU, the loose mix was placed in the oven for 4 hours at 135 °C for conditioning and 1 hour at the compaction temperature. The loose mix was compacted by MTU and shipped to Penn State. The slabs were trimmed to a test size of interest, 6” or 4” in width and 12.5” in length. Figure 18b illustrates the compacted specimens after trimming. The air voids of the slab after trimming was determined using the CoreLok device and according to AASHTO T 331. The air voids for the slabs from MTU were mostly in the acceptable range of 6 to 8%.

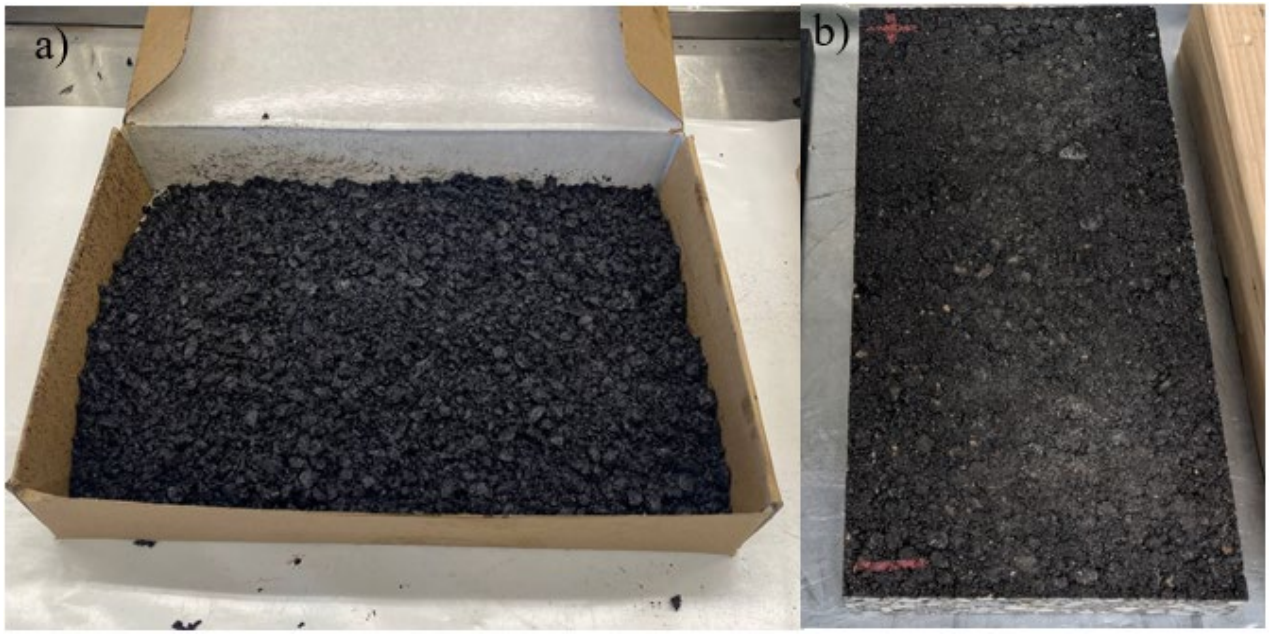

Figure 18. a) Loose mix that was prepared in the lab and b) compacted specimens after trimming.

Instrumentation for Measuring and Collecting the Strain Data

A quantitative analysis of fatigue behavior of an asphalt mixture should be based on an accurate measurement of the change of stress/strain responses of the specimen during the repetitive loading. The method of measuring the tensile strain at the bottom of the asphalt specimen using foil strain gauges was explored. Strain gauges were attached to the bottom of the asphalt slab specimen and the data acquisition (DAQ) from the National Instruments Corp (NI PXIe-1078) was used to collect the strain level at the bottom of the slabs.

Strain Gauges

The use of strain gauges in the field to capture pavement dynamic response in tension and compression in the horizontal direction has been around for decades. There are numerous cases of such instrumentation for pavements. For example, during the PennDOT-sponsored research project titled "Superpave In-Situ Strain/Stress Investigation (SISSI)," numerous H-type strain gauges were installed in several pavement sections, and data are captured for several years from dynamic loading of pavement under controlled loading conditions (Solaimanian et al., 2006). A more recent example

is the effort by Huang et al. (2017) to measure the dynamic strain response of asphalt pavement under moving loads. An example of placing the H-type strain gauge for one of the SISSI project sites is shown in Figure 19. A comprehensive layout of such gauges is presented in Figure 20.

Figure 19. H-type Strain Gauge installed on the top of base course (Solaimanian et al., 2006).

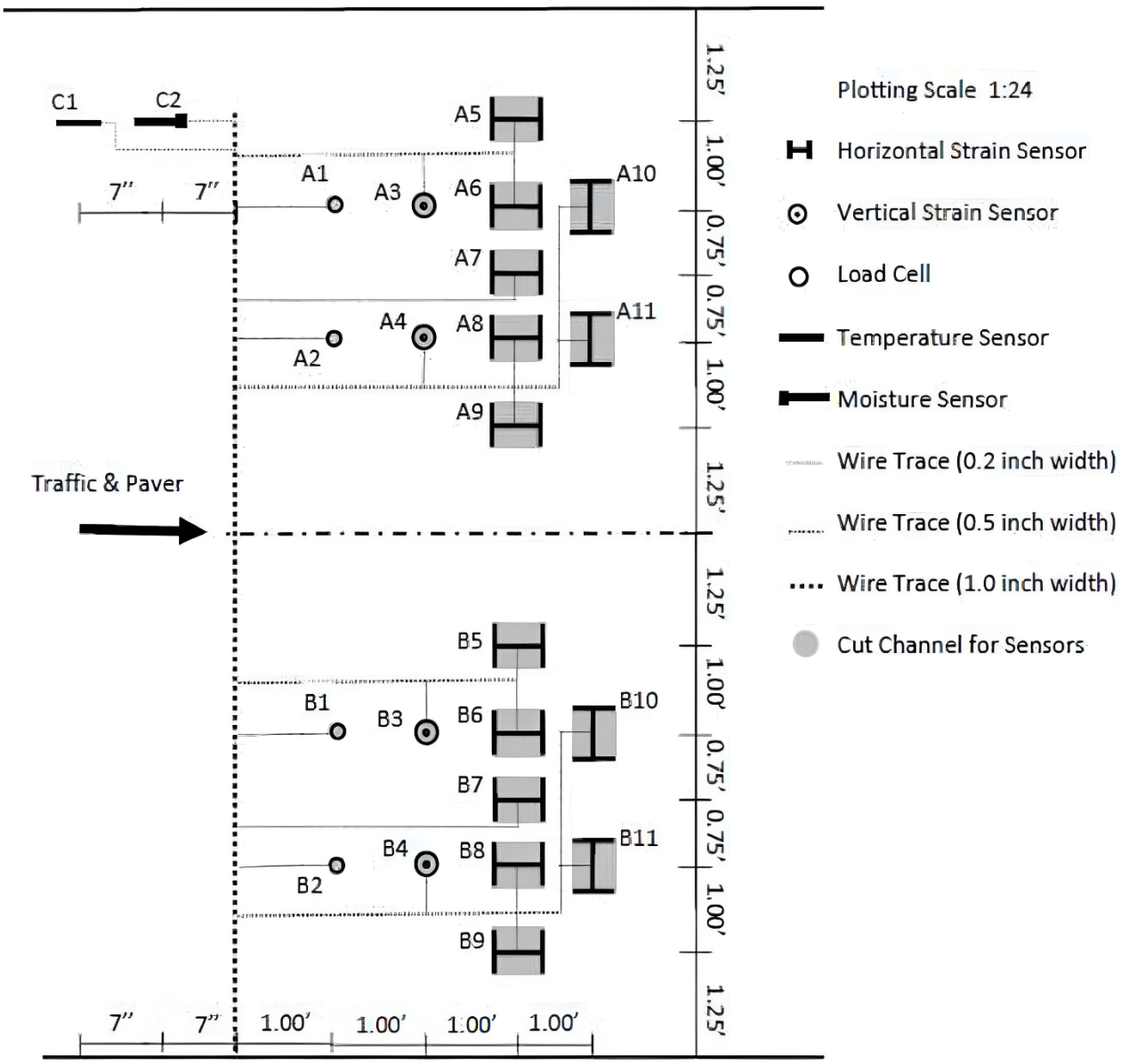

Figure 20. Sensor Distribution and Layout in a VDOT overlay project (Wang et al., 2012).

Figure 21 shows the dimensions of H-type strain gauges. The scale of laboratory testing to measure material strain is significantly smaller compared to that of field measurements, making the use of H-type strain gauges impossible. For laboratory measurement of deformations and displacements, the use of linear variable transducers, extensometers, and foil strain gauges is common. For measuring horizontal strain in asphalt concrete slabs when tested under wheel loading of Hamburg wheel

tracking, the use of foil strain gauges is the most direct option. In this study, these strain gauges were chosen as strain-measuring devices. Figure 22 shows the schematic of the selected gauges as manufactured by Omega (model number: SGD-30/350-LY40). Selection was made considering the type of strain measurement (static, dynamic, etc.), the gauge resistance, gauge length, availability, and delivery speed. The specification and key parameters of the strain gauge are shown in Table 5.

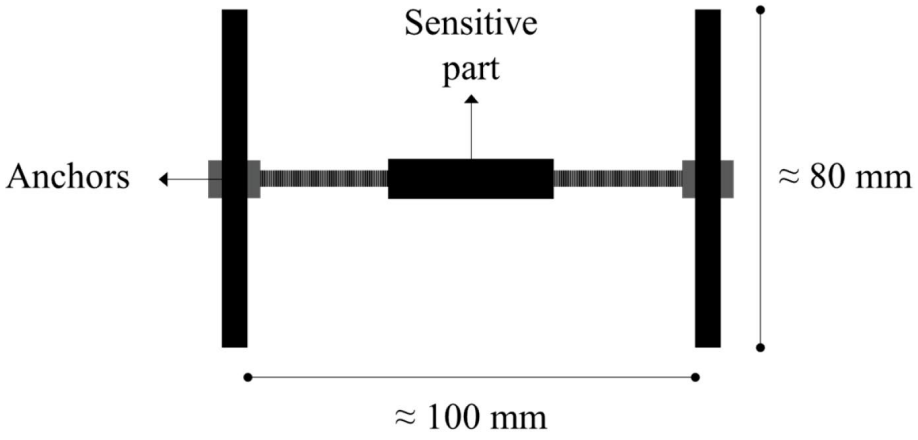

Figure 21. Schematics of an H-gauge (Barriera et al., 2020).

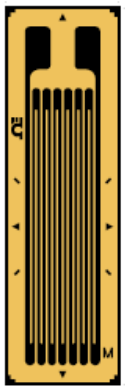

Figure 22. Picture of the foil strain gauge (SGD-30/350-LY40).

Table 5. Parameters of the Foil Strain Gauge (SGD-30/350-LY40).

Resistance	350 Ω
Strain Range	± 3%
Maximum permitted bridge energizing voltage (Vrms)	14
Gauge Factor	2.09

The selected strain gauge is a general-purpose static and dynamic strain gauge. The gauge resistance is 350 ohms. A higher resistance gauge (350 ohms over 120 ohms) was selected because it reduces the heat generation rate. In addition, a high-resistance gauge increases the signal-to-noise ratio by decreasing the effects of random resistance change, such as lead wire resistance changes caused by temperature fluctuations. The 3-cm strain gauge was selected in this project to ensure that the gauge length could be at least three times the nominal maximum aggregate size of the asphalt mixture. The unwired strain gauges with a length of 3 cm were bought and wired.

Data Acquisition System

The DAQ is the hardware system used to sample the electric signals generated from the physical response of a loaded system. It converts analog signals from the sensors into digital signals that can be recognized by the application software installed on a computer. In this project, the National Instruments DAQ (NI PXIe-1078) was connected to the strain gauges and the computer (Figure 23). This DAQ can amplify the measured voltage changes caused by strain gauges and convert voltage signals to digital signals.

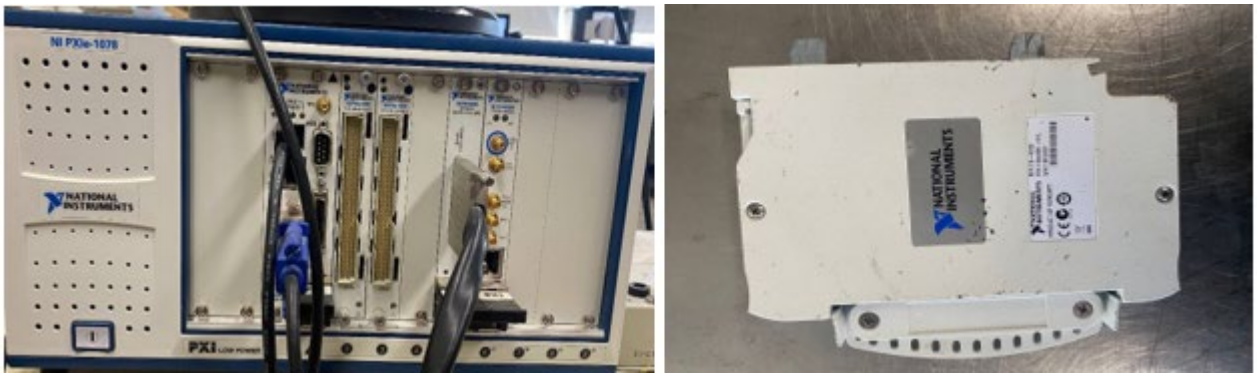

Figure 23. The NI DAQ system (NI PXIe-1078) and Data Acquisition Junction Box (NI TB-4330).

This DAQ system can collect data from 8 channels simultaneously. The collected data can be saved for further analysis. Three types of strain gauge configurations, quarter-, half-, and full-bridge, can be selected according to the type of strain to be measured and the sensitivity requirements (Figure 24). Generally, full-bridge configurations are the most sensitive to strain, but this requires more strain gauges. Besides, these full-bridge and half-bridge configurations are more suitable for homogeneous materials. Therefore, a quarter-bridge configuration was used in this experiment.

The regular test duration was roughly 16.6 hours, which is equal to 51,740 passes of the HWTD wheel. The data are collected at different frequencies, including 10, 20, and 40 Hz. Table 6 shows the frequency of the data collection. This scheme of data collection was followed for a large number of slabs that were tested. Later in the experiment, it was decided to modify this schedule to better suit the experiment because of lower tracking speed. Appendix A provides the data collection information for the second half of the project and the low-speed test slabs.

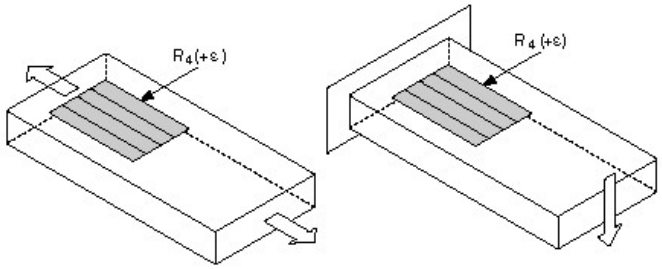

(a) Quarter-Bridge Strain Gauge Configurations (ni.com)

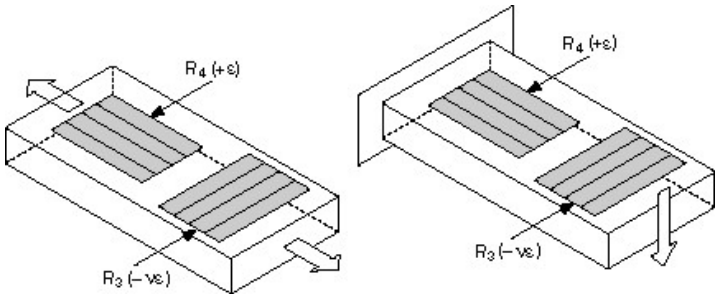

(b) Half-bridge Strain Gauge Configurations (ni.com)

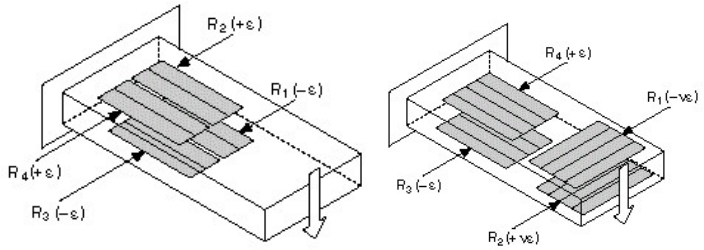

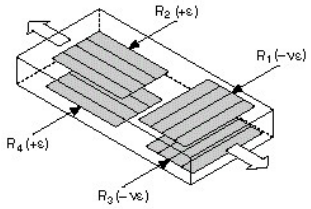

(c) Full-Bridge Strain Gauge Configurations (adapted from ni.com)

Figure 24. Strain Gauge Configurations.

Table 6. Data Collection Times and Sampling Rates.

Time from start of tracking, hrs.	Interval for data collection, minutes[1]	Duration of sampling, minutes[2]	Sampling Freq, Hz (data points per second)	Cumulative # of wheel passes from the start of tracking
0.000	2[3]	2.00[4]	40	0
0.033	2	1.00	20	104
0.083	3	2.00	10	260
0.583	30	5.00	20	1,820
1.083	30	0.50	20	3,380
1.583	30	0.50	20	4,940
2.083	30	0.50	20	6,500
2.583	30	0.50	20	8,060
3.083	30	0.50	20	9,620
3.583	30	0.50	20	11,180
4.083	30	0.50	20	12,740
4.583	30	0.50	20	14,300
5.083	30	0.50	20	15,860
5.583	30	0.50	20	17,420
6.083	30	0.50	20	18,980
6.583	30	0.50	20	20,540
7.083	30	0.50	20	22,100
7.583	30	0.50	20	23,660
8.083	30	0.50	20	25,220
8.583	30	0.50	20	26,780
9.083	30	0.50	20	28,340
9.583	30	0.50	20	29,900
10.083	30	0.50	20	31,460
10.583	30	0.50	20	33,020
11.083	30	0.50	20	34,580
11.583	30	0.50	20	36,140
12.083	30	0.50	20	37,700
12.583	30	0.50	20	39,260
13.083	30	0.50	20	40,820
13.583	30	0.50	20	42,380
14.083	30	0.50	20	43,940
14.583	30	0.50	20	45,500

(1) The time interval selected for data collection.
(2) Duration of data collection within the corresponding time interval.
(3) This first 2-minute time interval was before the start of tracking.
(4) This 2-minute duration of data sampling at 0 time indicates the data collected for 2 minutes before the tracking started.

Table 6. Data Collection Times and Sampling Rates (Continued).

Time from start of tracking, hrs.	Interval for data collection, minutes	Duration of sampling, minutes	Sampling Freq, Hz (data points per second)	Cumulative # of wheel passes from the start of tracking
15.083	30	0.50	20	47,060
15.583	30	0.50	20	48,620
16.083	30	0.50	20	50,180
16.583	30	0.50	20	51,740

Final Test Setup

The tests were conducted on a two-layer structure with the asphalt concrete slab as the top layer and the neoprene or PennDOT No. 2A aggregate as the underlying layer.

Base Layer

Neoprene elastomer exhibits excellent resiliency, making it a popular choice for load-bearing bases in civil engineering applications. In order to conduct tests on flexible bases with varying moduli, neoprene sheets were procured with two distinct levels of shore hardness: 40A and 60A. Shore hardness is measured using a durometer, which measures the penetration of an indenter into the material on a scale ranging from 10A to 95A, with higher numbers indicating stiffer rubber. Additionally, a different type of underlying material, PennDOT No. 2A, aggregate was selected to evaluate the effect of the underlying support on the strain response. PennDOT uses PennDOT No. 2A aggregate as their pavement aggregate subbase material and it is a minus 50 mm (2 in.), slightly gap-graded, aggregate material with a maximum 10 percent passing the 75 µm (No. 200) sieve. Throughout the project, the neoprene shore 60A rating was used as the reference base layer, and it was the support used for most of the slabs tested in this research.

Preparation of the Slab

The asphalt concrete slab specimens received from MTU had dimensions of roughly 15 inches in length, 8 inches in width, and 1, 1.5, or 2 inches in thickness. The slabs were trimmed to approximately 12.5 inches in length and 6 or 4 inches in width. Before placing the slab inside the HWTD test mold, either five, four, or three strain gauges were glued to the specimen and base layer

at various stages of the project. During the early stages of the project, two strain gauges were glued to the bottom of the specimen, one to the surface of the specimen and two to the surface of the neoprene. Based on the initial results, it was decided to use only strain gauges that were glued to the bottom of the asphalt specimen. In the first half of the project, two transverse and one longitudinal strain gauge were glued to the bottom of the slabs. Based on the initial results obtained from those gauges, in the second half of the project two longitudinal and one transverse strain gauges were used. Figure 25 shows the strain gauges glued to the bottom of the specimens. Gorilla^{TM} superglue was used to attach the strain gauges to the specimens. For the purpose of this study, two sets of testing conditions were considered: the bonded condition, where an emulsified asphalt CSS-1h was applied as a tack coat between the surfaces, and the unbonded condition, where no emulsified asphalt was applied. It should be noted that the majority of the tests conducted were in the bonded condition. The emulsified asphalt CSS-1h was applied as a tack coat to the surface of the neoprene at a rate of 0.045 gal/yd^2. After allowing the tack coat to break and set, the asphalt mixture slab was placed on top of the Neoprene.

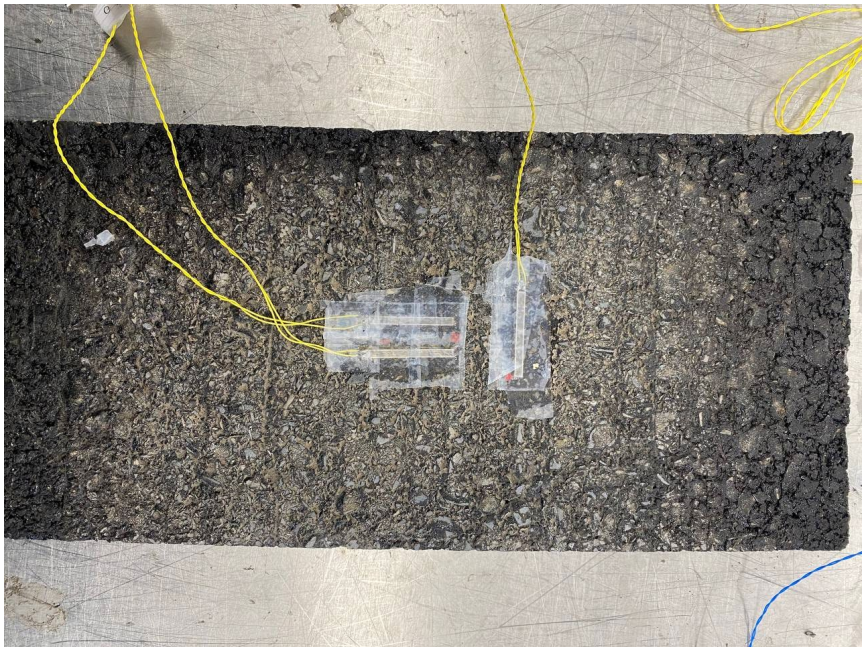

Figure 25. Strain gauges glued to the bottom of the specimens.

Assembly

The thickness of the underlying neoprene rubber with a Shore hardness of 60A was roughly 1.5, 1, or 0.5” based on the slab thickness, giving the total thickness of the specimen assembly to be approximately 2.5 inches. The slab and the underlying support were placed inside the standard HWTD mold, with internal dimensions of 12.5 inches in length and 10.4 inches in width. The gap between the specimen and the mold was filled with wood blocks to ensure the slab specimen was secured inside the mold (Figure 26). In the next step, the sample was placed inside the machine. The hood and fan were used to keep the temperature constant during the test.

Figure 26. Test setup for the first trial test.

CHAPTER 3

Experimental Plan

Introduction

This chapter provides a detailed overview of the experimental factors, the selection of mixtures, the sources of materials, and the specific performance tests employed.

Selection of Experimental Factors

For this research, with the focus being on equipment capabilities, factors presented in Table 7 were considered to assess the capability of the HWTD for evaluation of fatigue resistance characteristics of asphalt mixtures.

Table 7. Factors Considered in This Research.

Type of Variable (Factor)	**Levels**	**Purpose**
Slab Geometry (Thickness)	1 inch, 1.5 inches, and 2 inches	to evaluate the effect of thickness on the response
Support Condition	Neoprene with shore hardness of 40 and 60 and base aggregate (PennDOT No. 2A)	to evaluate the effect of the underlying support on the response
Mix Type	9.5-mm dense graded Superpave mix (reference mix), SMA, reference mix with RAP, reference mix with change in binder grade, reference mix with RAP and change in binder content.	to evaluate the equipment capability in distinguishing among different mixtures
Test Temperature	25°C and 30°C	to determine the effect of temperature effect on the response
Loading Rate	52-wheel passes per minute (standard tracking speed) and 20 wheel passes per minute (low speed)	to evaluate the effect of loading rate on the response
Bonding condition	Bonded with tack coat, and no bonding	to evaluate the effect of the bond between the test slab layer and the supporting layer on the response

Selection of Mixtures

Six different mixtures were selected with the goal of establishing their differences in performance levels in terms of fatigue resistance. These mixes included a conventional dense-graded Superpave mix with nominal maximum aggregate size (NMAS) of 9.5 mm and made with PG 64S-22 (Mix 1, the reference mix). There are two 9.5-mm mixtures containing 35% reclaimed asphalt pavement (RAP), with one containing PG 58S-28 and the other containing PG 64S-22 binder (Mixes 2 and 4). Mix 3 was a stone mastic asphalt mixture made with 9.5-mm NMAS aggregate size and PG 64E-22. Slabs were made with Mix 1 at an asphalt binder content 0.5% above the optimum and 0.5% below the optimum (Mixes 5 and 6). All six mixes are presented in Table 8.

Table 8. Asphalt Mixtures Considered in the Experiment

Mixture ID	Mix Type	Virgin Binder Grade	NMAS mm	RAP Content %
Mix #1	SP Dense Graded	PG 64S-22	9.5	0
Mix #2	SP Dense Graded	PG 58S-28	9.5	35
Mix #3	SMA	PG 64E-22	9.5	0
Mix #4	SP Dense Graded	PG 64S-22	9.5	35
Mix #5	Mix 1 + 0.5% binder	PG 64S-22	9.5	0
Mix #6	Mix 1 – 0.5% binder	PG 64S-22	9.5	0

Materials

Virgin Binder Source

Three different performance-grade binders from an approved source (PennDOT Publication 35, Bulletin 15) were used for this study: a standard PG 64S-22 binder, a standard PG 64E-22 binder, and a standard PG 58S-28 binder, all meeting the requirements of AASHTO M 332.

Aggregate Source

The aggregate for this research was a limestone aggregate from a PennDOT-approved source (PennDOT Publication 34, Bulletin 14) located in central Pennsylvania.

RAP

Material from a single RAP source was used in the study. The RAP recovered binder was graded as PG 90-18.

Performance-Related Tests

Table 9 presents the testing protocol (conditions) for the experiments. The standard protocol and condition in this study was a slab geometry of 6" in width and 1.5" in thickness, neoprene supporting hardness 60A, and testing temperature of 25 °C. Mixes 2 through 6 were tested following these standard conditions, with two replicates for each mix (in total 10 slab specimens). Mix 1 was used as the control mix to study the factors of support condition (three levels: PennDOT No. 2A, neoprene of 60A and 40A hardness), slab thickness (three levels: 1.0", 1.5", and 2.0"), slab width (two levels: 4" versus 6"), temperature (two levels: 25 °C and 30 °C), and speed effect (two levels: standard and a lower speed). Performance testing also included IDEAL-CT testing of Superpave gyratory compacted (SGC) specimens according to ASTM D8225.

Table 9. Mixture Testing Protocol for This Experiment.

Mix Performance Test	Response	Mixes tested	Number of replicate slabs or SGC specimens	Slab or SGC Specimen Thickness inches
Hamburg Wheel Tracking for Fatigue at 25°C and 30°C, dry condition	Number of cycles to cracking or number of cycles to a specified mix modulus	1, 2, 3, 4, 5, 6	21 slabs successfully tested for Mix 1 and two slabs for all other mixes	1.5" for all mixes. 1.0 and 2.0" also for mix 1.
IDEAL-CT test at 25ºC, 50 mm/minute loading	IDEAL-CT index, fracture energy, strength, initial and post peak modulus	1, 2, 3, 4, 5, 6,	four	≈ 2.5"

Table 10 provides information for different slabs with different dimensions and mix designs. The air voids for some of the slabs were outside of the acceptable range. Although investigating the effect of the air voids on response was not part of the experimental plan, these high-void slabs were also tested under moving load and the strain response was recorded.

Table 10. Mixtures Information.

Mix code	Slab ID	Width (in)	Binder	Thicknesses (in)	AC, %	RAP, %	Air Voids After Trim, %
Mix #1	1-1	6	64S-22	2	5.7	0	5.3
Mix #1	1-2	6	64S-22	2	5.7	0	5.6
Mix #1	1-3	6	64S-22	1.5	5.7	0	7.0
Mix #1	1-4	6	64S-22	1.5	5.7	0	6.5
Mix #1	1-5	6	64S-22	1.0	5.7	0	11.8
Mix #1	1-6	6	64S-22	1.0	5.7	0	11.7
Mix #1	1-7	6	64S-22	1.0	5.7	0	6.3
Mix #1	1-8	6	64S-22	1.0	5.7	0	6.5
Mix #1	1-9	6	64S-22	1.5	5.7	0	10.5
Mix #1	1-10	6	64S-22	1.5	5.7	0	10.7
Mix #1	1-11	6	64S-22	1.5	5.7	0	7.6
Mix #1	1-12	6	64S-22	1.5	5.7	0	7.5
Mix #1	1-13	6	64S-22	1.5	5.7	0	6.0
Mix #1	1-14	6	64S-22	1.5	5.7	0	7.8
Mix #1	1-15	4	64S-22	1.5	5.7	0	7.6
Mix #1	1-16	4	64S-22	1.5	5.7	0	7.6
Mix #5	5-1	6	64S-22	1.5	6.2	0	6.7
Mix #5	5-2	6	64S-22	1.5	6.2	0	5.1
Mix #6	6-1	6	64S-22	1.5	5.2	0	7.1
Mix #6	6-2	6	64S-22	1.5	5.2	0	7.5
Mix #4	4-1	6	64S-22	1.5	3.8	35	6.6
Mix #4	4-2	6	64S-22	1.5	3.8	35	6.4
Mix #2	2-1	6	58S-28	1.5	3.8	35	7.8
Mix #2	2-2	6	58S-28	1.5	3.8	35	7.9
Mix #3 SMA	3-1	6	64E-22	1.5	6.8	0	7.0
Mix #3 SMA	3-2	6	64E-22	1.5	6.8	0	6.4
Mix #1	1-17	6	64S-22	1.5	5.7	0	7.8
Mix #1	1-18	6	64S-22	1.5	5.7	0	7.1
Mix #1	1-19	6	64S-22	1.5	5.7	0	8.1
Mix #1	1-20	6	64S-22	1.5	5.7	0	5.6
Mix #1	1-22	6	64S-22	1.5	5.7	0	7.6
Mix #1	1-23	6	64S-22	2.0	5.7	0	7.5
Mix #1	1-24	6	64S-22	2.0	5.7	0	7.3
Mix #1	1-25	6	64S-22	1.5	5.7	0	7.0
Mix #1	1-26	6	64S-22	1.5	5.7	0	6.3
Mix #1	1-27	6	64S-22	1.5	5.7	0	7.1

The IDEAL-CT was included in the testing plan to generate CT-index data for comparison with damage response from testing the slabs in the HWTD. This test was performed in accordance with ASTM D8225-19, at a displacement rate of 50 mm per minute and a test temperature of 25 °C. The test setup and the corresponding response were presented in Chapter 1: however, they are further illustrated in Figures 27 and 28. Based on the load-displacement curve obtained, several engineering parameters are calculated, such as pre-peak and post-peak modulus, peak load, and fracture energy. To determine the cracking index (Equations 2 and 3), the energy of fracture is divided by the slope of the post-peak curve at 75% of the peak load, and the resulting value is multiplied by the extension at 75% of the peak load.

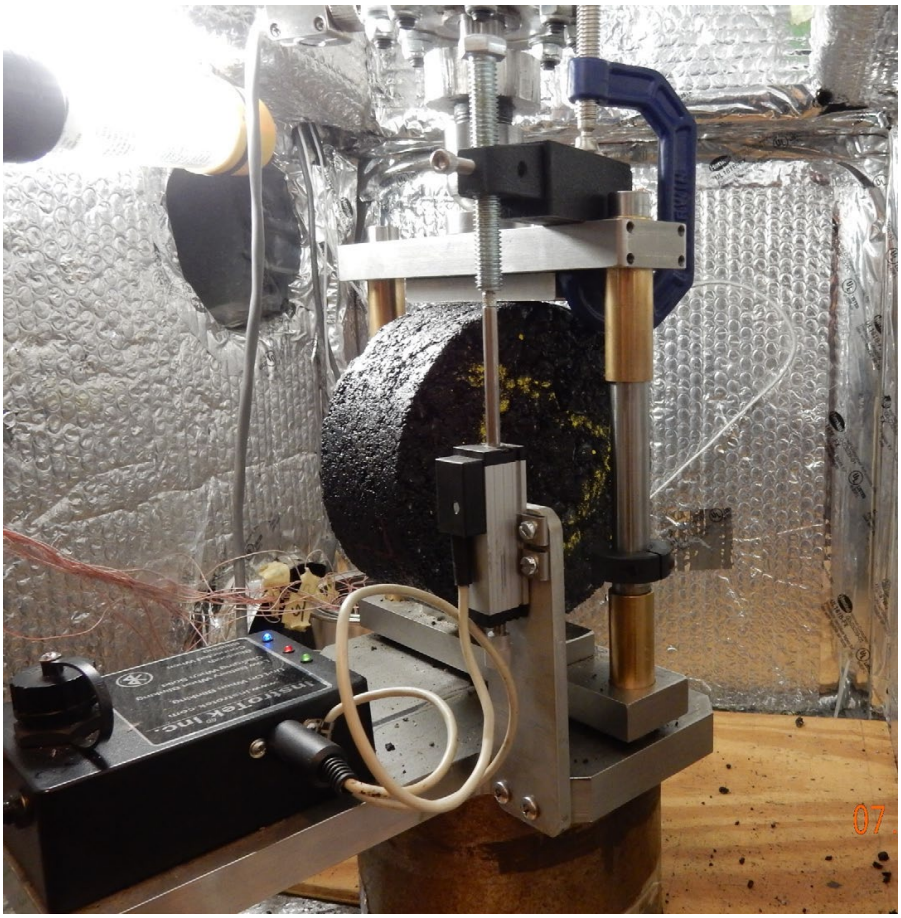

Figure 27. A picture of the IDEAL-CT test setup.

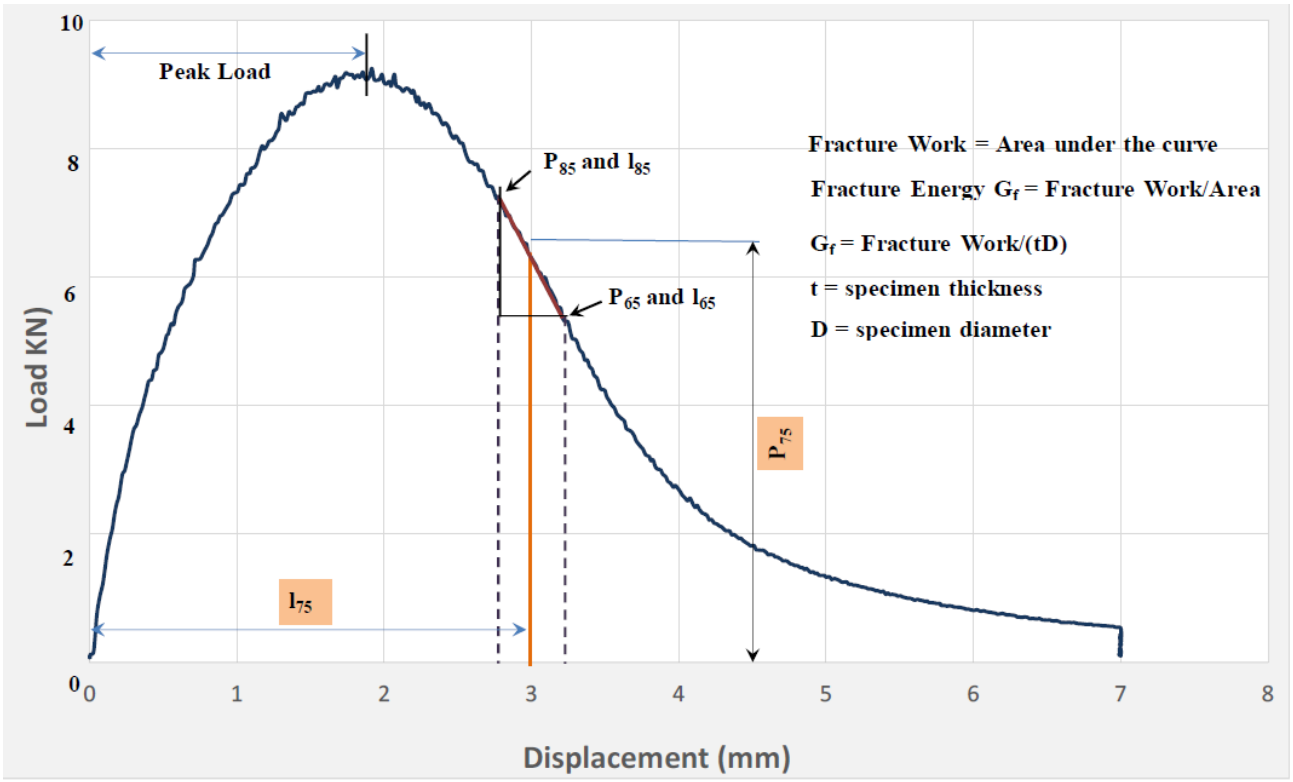

Figure 28. Load-displacement curve from a typical IDEAL-CT test.

$$CT_{index} = \frac{G_f}{\frac{P}{l}} \times \left(\frac{l_{75}}{D}\right) \quad (2)$$

$$\frac{p}{l} = |m_{75}| = \frac{p_{85-}\, p_{65}}{l_{85-}\, l_{65}} \quad (3)$$

CHAPTER 4

Data Analysis and Interpretation

Introduction

This chapter delves into the intricacies of the strain response as observed during the HWTD fatigue testing, examining the influence of various parameters on these responses. Factors such as slab thickness, support type, slab width, test temperature, loading speed, and mix binder content were thoroughly investigated. Attention is then directed toward understanding the impact of different mixture types under these conditions. Lastly, the IDEAL-CT test results are brought into focus, offering a comparative analysis with the previous findings.

Air Voids of Compacted Slabs

An important consideration in the research was to achieve a similar air void content for all the slabs with a target value of 7%. Reaching this target for all the slabs proved to be challenging, considering the intensive level of work needed in preparing each slab and limitations in the reproduction phase. However, for the most part, one could say that the air void content was within 7±1%. For Mix 1, in one case the air void content was roughly around 12% and required reproduction of the slabs. Table 11 presents the air voids data for all the compacted slabs after trimming the slab to the testing size. It should be noted that the first number refers to mixture ID number from Table 7 and the second number indicates the replicate number of the mix. One can see that 26 slabs were prepared for Mix 1, out of which 21 were successfully tested, which was the main mix studied in this research to capture the effect of different parameters on the results.

Table 11. Air Void Content of Slabs after Trimming.

Slab ID	Air Void After Trimming, %	Slab ID	Air Void After Trimming, %	Slab ID	Air Void After Trimming, %	Slab ID	Air Void After Trimming, %
1-1	5.3	1-10	10.7	1-19	8.1	2-2	7.9
1-2	5.6	1-11	7.6	1-20	5.6	3-1	7.0
1-3	7.0	1-12	7.5	1-22	7.6	3-2	6.4
1-4	6.5	1-13	6.0	1-23	7.5	4-1	6.6
1-5	11.8	1-14	7.8	1-24	7.3	4-2	6.4
1-6	11.7	1-15	7.6	1-25	7.0	5-1	6.7
1-7	6.3	1-16	7.6	1-26	6.3	5-2	5.1
1-8	6.5	1-17	7.8	1-27	7.1	6-1	7.1
1-9	10.5	1-18	7.1	2-1	7.8	6-2	7.5

Review and Discussion of Results

Strain Response from HWTD Fatigue Testing at Various Times

In general, in a laboratory environment, repeated loading of the asphalt concrete specimen is conducted to determine the magnitude and growth rate of the tensile strain at various stages of loading. The idea is that the growth of the strain within the specimen as a result of the increase in the load repetitions is an indication of the level of fatigue-induced damage into the material. In other words, under the same loading conditions, the material which manifests larger growth of strain is believed to be more prone to fatigue cracking. One simplified approach in characterizing the quality of an asphalt mixture in resisting fatigue cracking is to find the number of cycles needed to double the strain level compared to the initial strain. Another simplified approach is to consider the growth of the strain to a level where sudden increase in strain is observed beyond this level, resulting in macrocracking. It was also the approach taken in this research to consider how the tensile strain changed during the test as the number of load repetitions increased.

The testing conducted under this research is similar to other laboratory tests in which repeated loading of the specimen at intermediate temperature is used to investigate fatigue resistance properties of the asphalt mixture. In this research, the response of the slab to the moving load was captured by various strain gauges installed on the slab. The strain data were collected at various times during the tracking

of the asphalt concrete slab. Three distinct stages were defined during the test to make determination of the strain growth rate easier. These stages are referred to as early stage, middle stage, and late stage. The longitudinal strain amplitude has been investigated at these three stages. Table 12 provides the time of data collection from the beginning of the test for various stages. The first number in the interval shows the time from the beginning of the test when data collection started. The second number shows the end of time for data collection. For example, the interval 200 to 215 indicates that data collection started 200 seconds after starting the test and continued for 15 seconds. One can see some differences in the data collection intervals between what is referred to as the first and the second half of the project data. For most of the specimens, the time intervals used for the first half of project were applied. However, as the project progressed further and evaluation of the tracking speed was brought into consideration, adjustments were made to the frequency and time of data collection, as reflected in the second half of project data collection of Table 12. It should be noted that the duration of the test was almost 16.6 hours, which is equal to 51,740 wheel passes.

Table 12. Range of Time for Data Collection Corresponding to Early, Middle, and Late Stages.

Stage During the Test	Time Interval for First Half of Project (seconds)	Time Interval for Second Half of Project (seconds)
Early stage	200-215	200-215
Middle Stage	29200-29215	29210-29225
Late stage	59800-59815	59810-59825

Figure 29 illustrates the typical response of the longitudinal strain gauge. The strain amplitude, as shown in the graph, indicates the difference between the peak and the valley of the strain response.

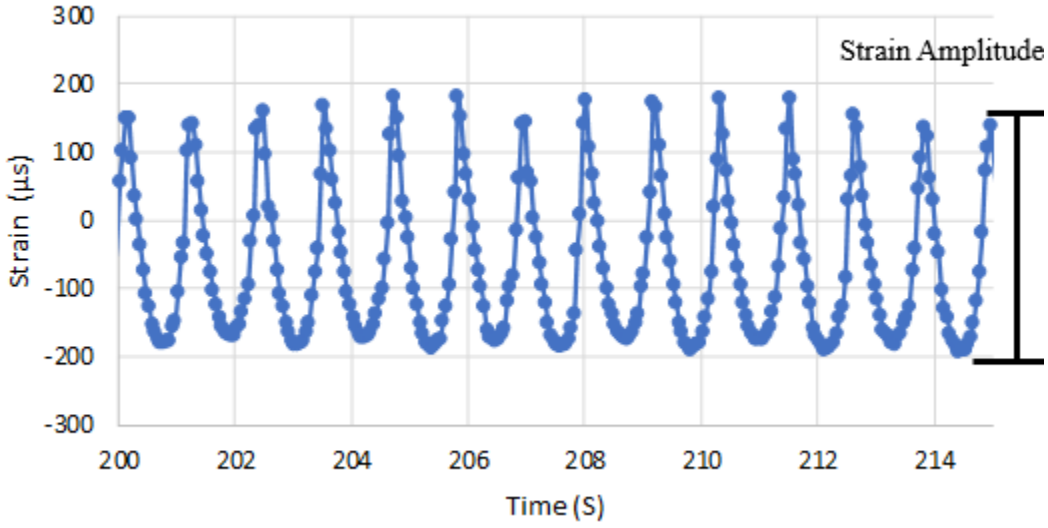

Figure 29. Typical response of the longitudinal strain gauge.

The variations in strain amplitude were deemed a critical factor throughout the entire testing period. Figure 30 illustrates the strain amplitude changes for a slab with a thickness of 1.5 inches, tested using neoprene shore 40A as a base layer during the whole period of testing. Two longitudinal strain gauges were used to monitor the changes in strain during the test. As evident, there was a substantial increase in strain amplitude during the initial 2 hours of the test, followed by a gradual decline in the rate of increase in strain amplitude until the end of the test. This observation indicates that the tested asphalt concrete slab was successfully tested. Appendix B includes graphs of strain amplitude versus tracking time for all the slabs tested in this study, providing a comprehensive overview of the strain amplitude and corresponding changes for various slabs. A comprehensive set of tables (part 1, 2, and 3) containing a summary of all the test results and the parameters and dimensions of the mixtures is presented in Appendix C.

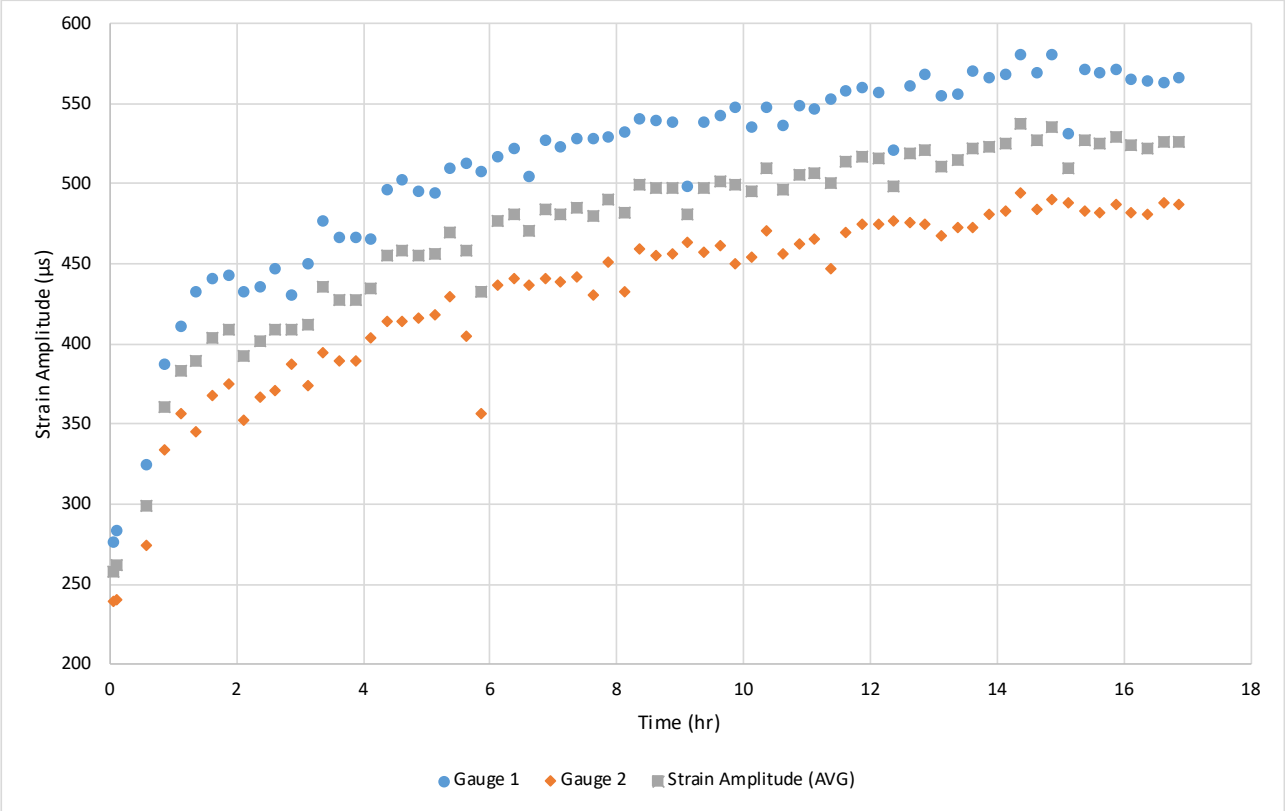

Figure 30. Longitudinal strain amplitude at the bottom of the slab during the period of the test for a slab with a thickness of 1.5 inches, tested on Neoprene shore 40A.

Sensitivity of the Strain Response to Various Test and Mixture Parameters

The study included investigating the strain response as a result of changes in various experimental factors. These factors can be classified into three categories: (1) geometry of slab, (2) loading parameters, and (3) mix parameters. In the case of geometry, the thickness and the width of the slab varied. For the load, the effect of temperature and speed of tracking were investigated. Finally, in regard to the mix, the effect of the changes in the asphalt mix parameters such as the binder content or the change in the RAP content were considered. In the following section, results from this sensitivity analysis are presented based on the data obtained from the longitudinal strain gauges. Results of testing based on the data from the transverse strain gauges are provided in Appendix D.

Effect of the slab thickness

The asphalt concrete slab specimens were made and tested at three different thicknesses: 1, 1.5, and 2 inches. Neoprene rubber 60A was used as the support layer under the slab. Emulsion tack coat was applied to the neoprene before placement of the slab to bond the two layers together. The longitudinal strain gauges for the 1-inch, 1.5-inch and 2-inch specimens maintained their functionality and continued responding during the whole duration of the test. Therefore, the comparison is provided between 1-inch, 1.5-inch, and 2-inch specimens, as seen in Figure 31. As expected, results indicate that the strain amplitude kept growing with time for both 1-inch and 1.5-inch specimens. Only the 2-inch specimen showed a decrease from the middle to the late stage. As expected, the rate of increase in the thinner slab was considerably higher than the increase rate in the thickest slab. For the 1.5-inch-thick specimen, the strain amplitude increased by almost 38% from early to the middle stage of testing, while for the 1-inch-thick specimen this rate is roughly 141%. This observation is an indication of a significantly higher rate of fatigue damage as the slab gets thinner. Despite the fact that higher levels of damage can be achieved with thinner slabs, it was decided to not use this thickness as the main thickness for testing the slabs in this research because of the aggregate size used in the mixture. The mixes tested were 9.5-mm nominal maximum aggregate size (NMAS). It is recommended that at least a ratio of 3 to 1 be maintained between the test slab layer thickness and the NMAS of the asphalt mixture. Testing the 9.5-mm mixture at 1-inch thickness does not satisfy this requirement. Therefore, the decision was made to select the 1.5” slab as the reference thickness for this study. Furthermore, while asphalt mixes are made at thin layers such as 1-inch thick (e.g., Superpave 6.3-mm asphalt mixture), such thin mixes are not intended to provide structural enhancement, but rather are considered as pavement preservation tools.

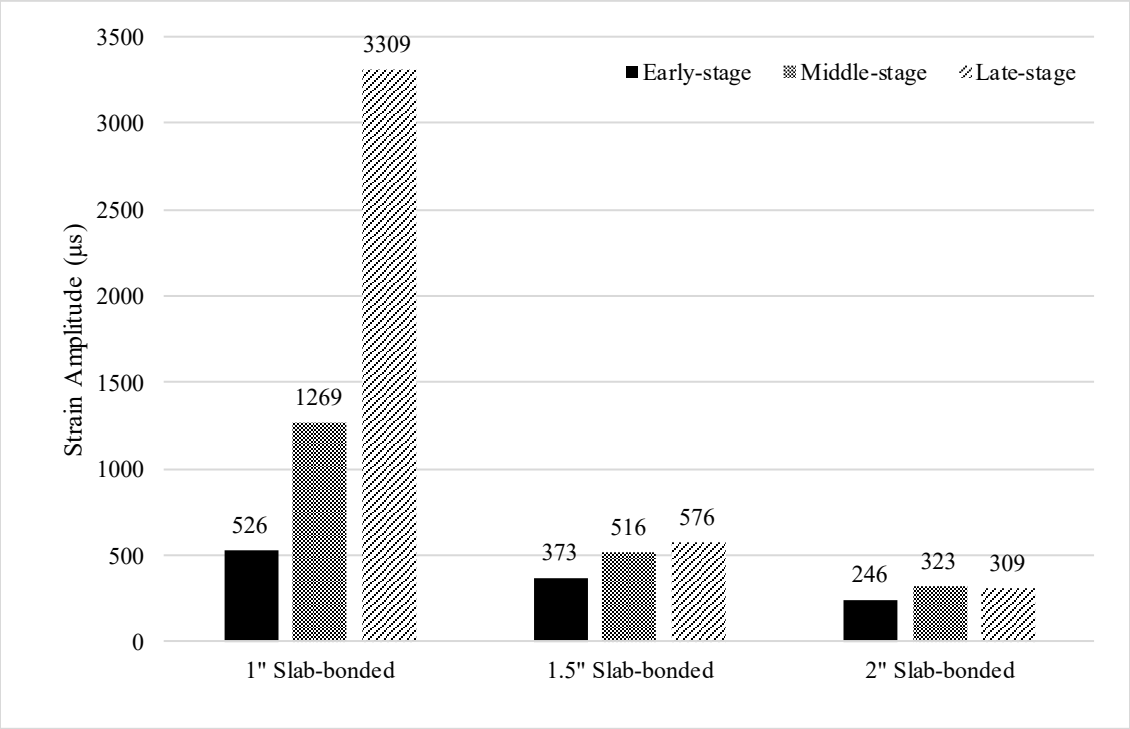

Figure 31. Longitudinal strain amplitude at the bottom of the slab at different thicknesses.

Effect of the support type

To investigate the effect of underlying support material (base layer), an aggregate support layer, with gradation satisfying PennDOT No. 2A aggregate designation, was also included in the study. In addition, the study included a neoprene with a shore hardness of 40A, i.e., a support softer than the neoprene with the shore hardness of 60A that was frequently used in this research as the reference support. The PennDOT No. 2A aggregate is typically used as base or subbase in field applications. In this study, all material larger than 9.5 mm are removed from the original PennDOT No. 2A to make it possible to produce a smooth and even surface as the base layer under the asphalt concrete slabs.

Figure 32 shows the results for the 1.5-inch-thick slabs placed on the neoprene (60A and 40A) and the PennDOT No. 2A material. For each slab, one longitudinal strain gauge was glued to the slab and the slab was bonded to the underlying neoprene. The data provided in the figure is the average longitudinal strain from two slabs. For the slabs placed on the PennDOT No. 2A base, two longitudinal strain gauges for each slab were glued to the slab. No bonding material was applied between the slab and the PennDOT No. 2A base. Only a very thin layer of rubber was used to protect

the strain gauges from damage induced by the aggregate. The results provided in this graph for the aggregate base are the average of three strain gauges from two slab specimens, as the results for one of the strain gauges was considered an outlier.

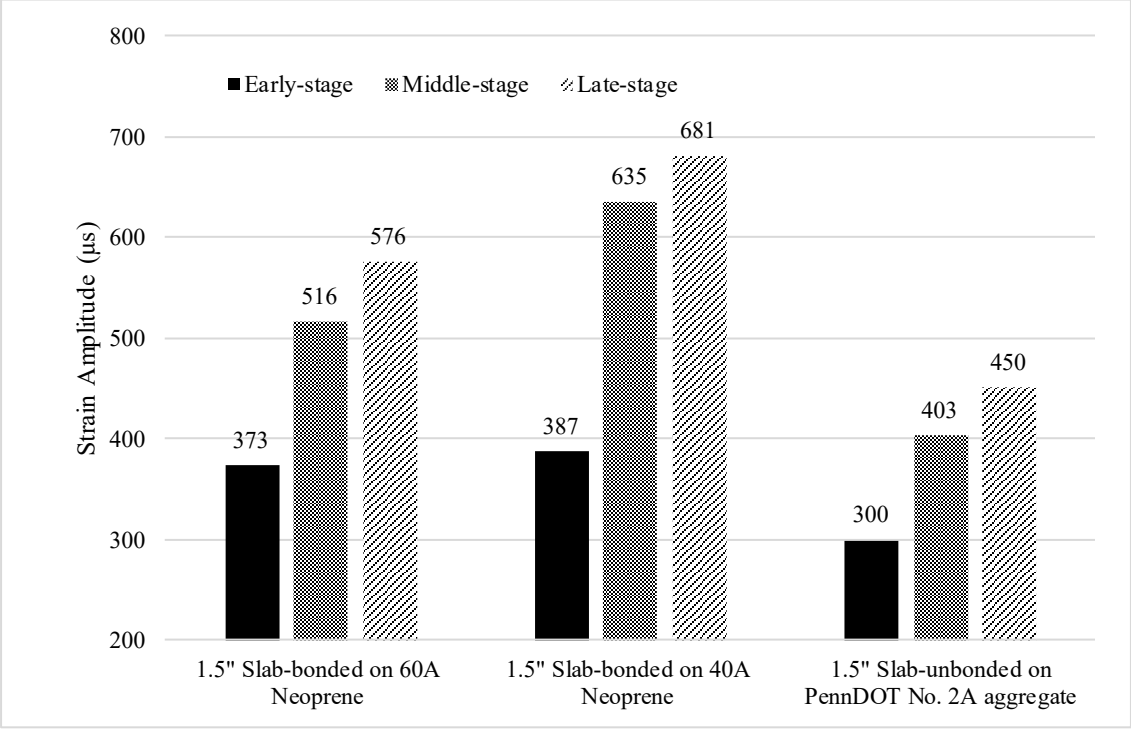

Figure 32. Longitudinal strain amplitude at the bottom of the slab placed on the neoprene (60A and 40A) and PennDOT No. 2A.

The strain increased by almost 38%, 64%, and 34% from early to the middle stage for the specimens placed on the neoprene 60A, neoprene 40A, and PennDOT No. 2A aggregate base, respectively (Figure 33). The changes in strain from the early to the late stages were almost 54%, 76%, and 50% for the specimens placed on these three supports, respectively. From the middle to the late stage, the slabs on the 60A neoprene base and the PennDOT No. 2A base showed approximately the same enhancement in the strain amplitude. The slab on the 40A neoprene base showed a slightly lower increase compared to the other two from the middle to the late stage. In general, the slab on the PennDOT No. 2A base showed the smallest strain increase to the late stage but very comparable to the slab on the 60A neoprene. The slab on the 40A base showed not only the highest initial strains but also the highest change in strain amplitude, considering the results to the final stage of loading.

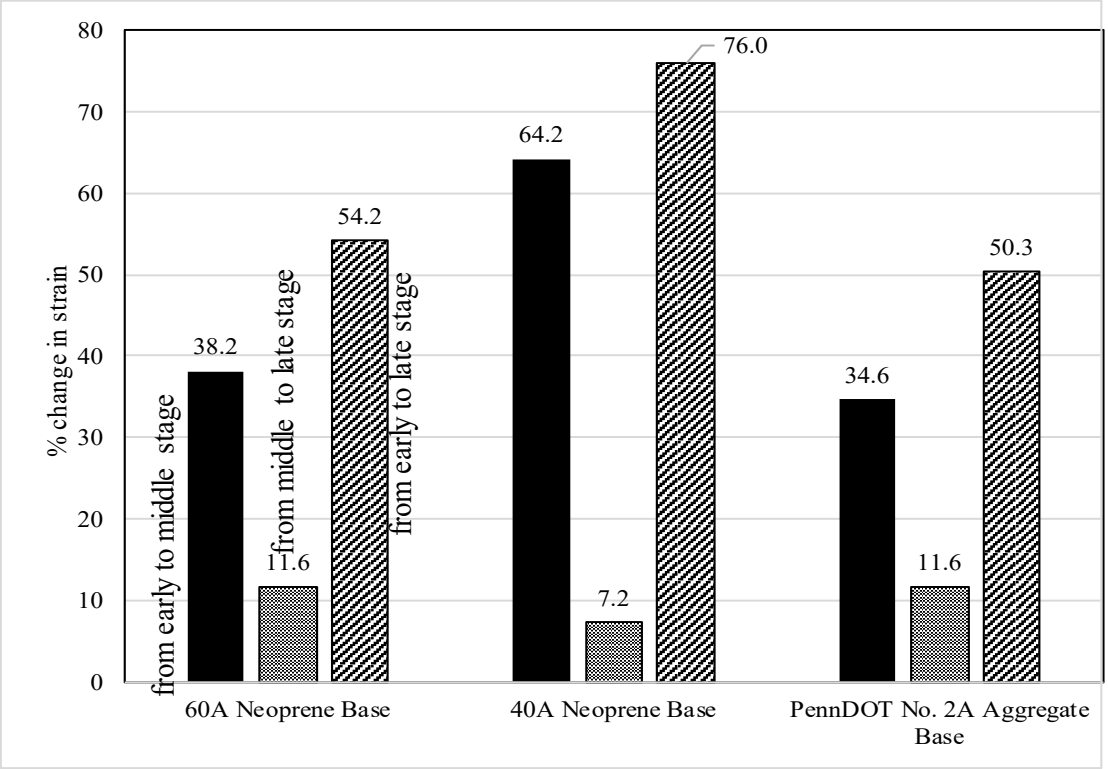

Figure 33. Rate of change in strain level from early stage to middle and late stages, 1.5"-thick slabs (Mix 1).

Figure 34 demonstrates the strain amplitude for the slabs with 10.5% and 10.70% air voids placed on the neoprene and PennDOT No. 2A base, respectively. The slab on the PennDOT No. 2A shows a significant increase in the strain from the early to the late stage for high-void slabs (Figure 35). This response is different from the case shown in Figures 32 and 33 and could be due to the uneven surface of the PennDOT No. 2A base. The unevenness of the base surface could intensify the development of the strain at the bottom of the slab. In conclusion, based on the results obtained from testing the specimens with the acceptable range of air voids (Figure 32) and the practical difficulty of using PennDOT No. 2A as a base material for this work, the decision was made to use the neoprene as the main base layer for all remaining slabs tested in this study. An exception to this rule was the study of the temperature effect for which both the PennDOT No. 2A base and the neoprene base were used.

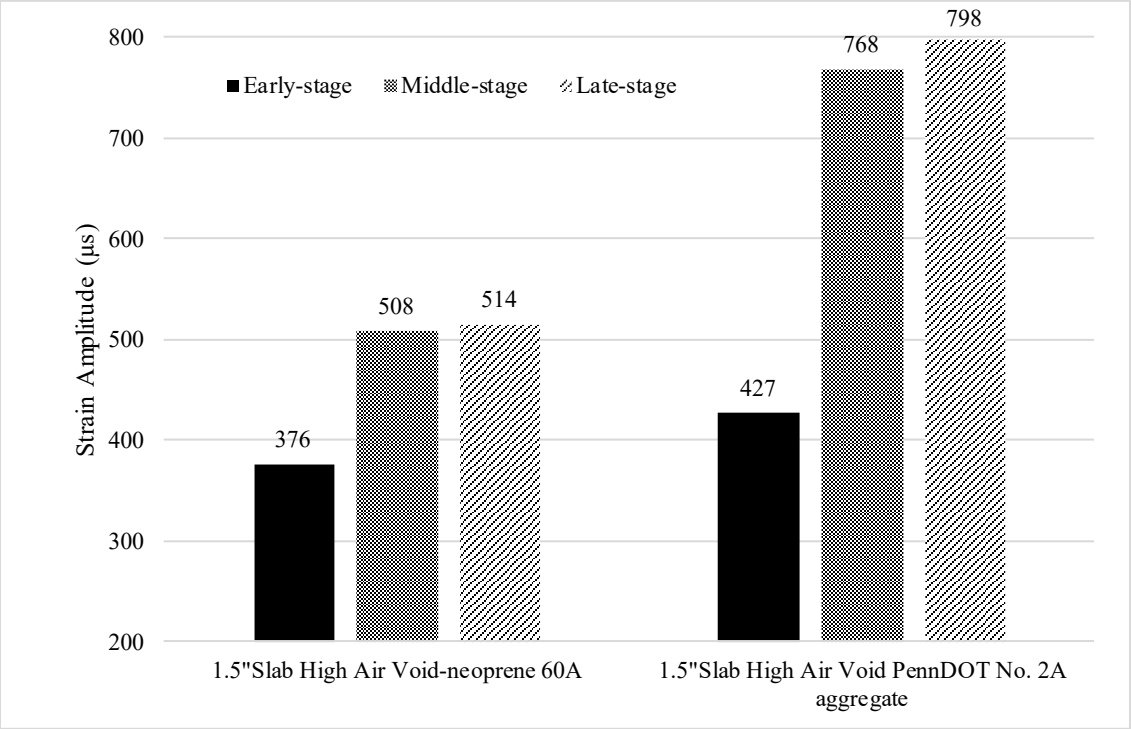

Figure 34. Longitudinal strain amplitude at the bottom of the high air void slabs placed on the neoprene (60A) and base PennDOT No. 2A.

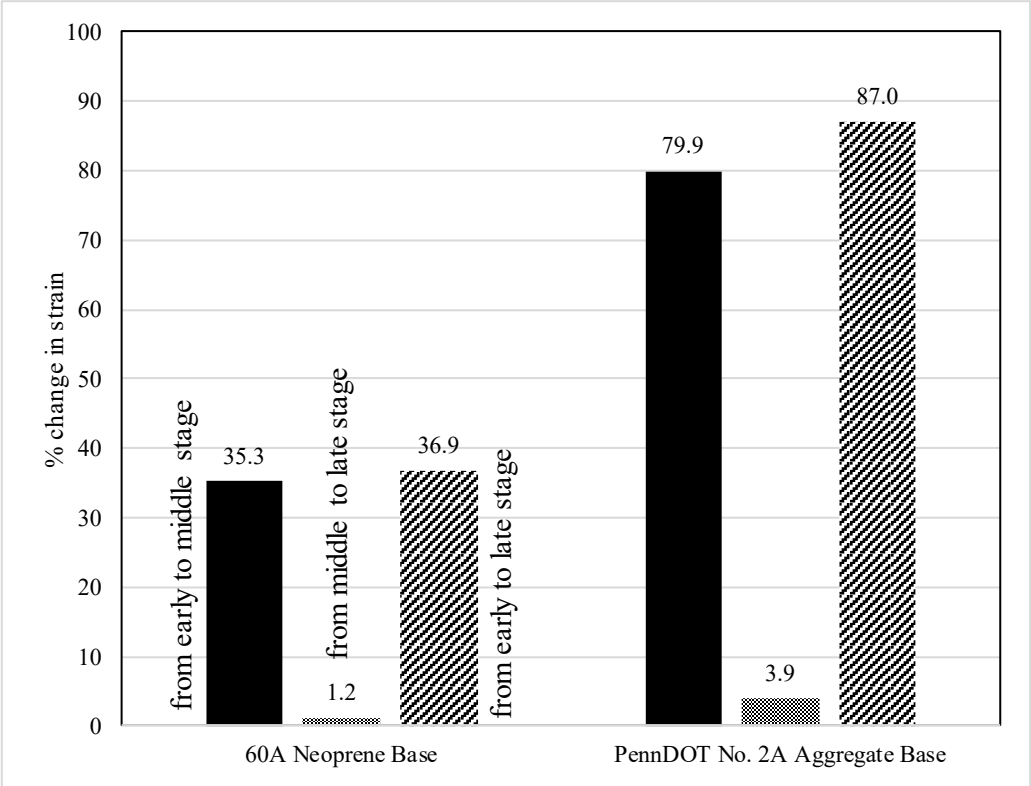

Figure 35. Rate of change in strain level from early stage to middle and late stages, 1.5"-thick high voids slabs (Mix 1).

Effect of the slab width

Four slabs, prepared 4 and 6 inches wide, were tested to investigate the effect of the slab width on the development of the tensile strain at the bottom of the slabs. The strain was recorded for the two slabs with the width of 6 inches, using two strain gauges (one longitudinal strain gauge for each slab). The average of the strain amplitudes from these two strain gauges represents the strain magnitude for different stages of the test. Two slabs with a width of 4 inches were tested using four strain gauges (two strain gauges per slab) to record the strain amplitude at the bottom of the slabs. The average of these four strain gauges was utilized to monitor the strain development. Figure 36 shows the strain amplitude for the samples with the width of 4 and 6 inches at three distinct stages. All slabs had air voids in the range of 7±1%, and all were placed on neoprene. Furthermore, emulsified asphalt was applied to the surface of the neoprene to create a bond between the base and the slab. The results demonstrate that reduction in the width of the slabs led to an increase in strain amplitude during the test. Moreover, the development of the strain at the bottom of the slabs for the 4-inch-wide slab is faster than that for the 6-inch-wide slab. The strain increased 51% and 38%, respectively, from the early to the middle stage for the 4-inch-wide and 6-inch-wide slabs. One would expect that if this faster development of the strain continued, the fatigue life would have been achieved in a shorter period of time for the 4-inch-wide slabs. However, in this case, the increase from the middle to the late stage are roughly 6% and 12% for the 4-inch-wide and 6-inch-wude slabs, respectively. It is not exactly clear why the strain growth rate was higher for the 4-inch-wide slab in the range from the early stage to the middle stage but then it reversed the trend from the middle stage to the late stage. It could have been associated with debonding of the gauges after the middle stage of loading or other factors unknown at this point.

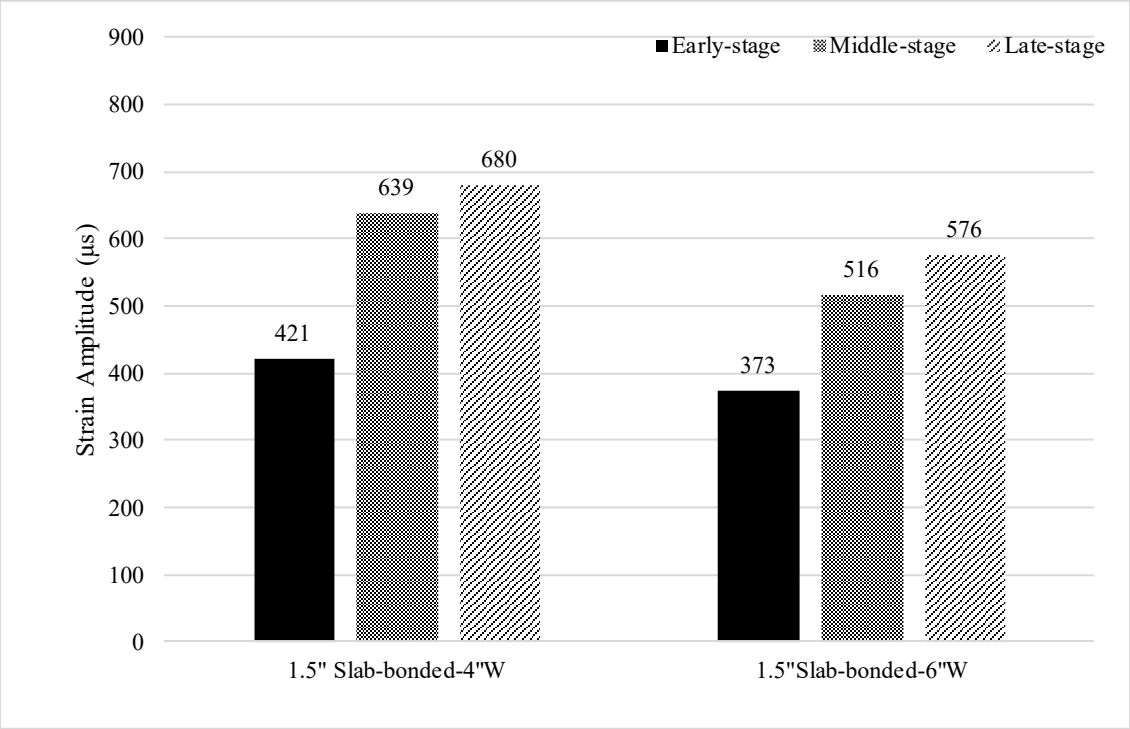

Figure 36. Longitudinal strain amplitude for the samples with the width of 4 and 6 inches at three different stages.

Effect of the test temperature

Four slabs were placed on the PennDOT No. 2A aggregate base and tested at 25 °C and 30 °C to investigate the effect of the test temperature on the strain amplitude and growth during the test. Four strain gauges (two strain gauges per slab) were used to record the longitudinal strain during the test at 25 °C and all strain gauges remained functional throughout the whole test period. The average of these four strain gauges was used to examine the strain development during the test. However, out of the four strain gauges used on the slab at 30 °C, only one strain gauge survived until the end of the test. For this test, the PennDOT No. 2A material was used as the base, and no bonding were applied between the asphalt concrete slab and the base. It should be noted that a thin rubber layer was used to protect the strain gauges from potential damage induced by the PennDOT No. 2A particles. In spite of taking this measure, some of the gauges did not survive the whole loading period. Figure 37 illustrates the results of the strain amplitude in three different stages of the test at 25 °C and 30 °C. As expected, the higher temperature led to a higher magnitude of the strain amplitude at the bottom of the slab. In other words, the higher temperature led to a reduction in the slab's stiffness. However,

the rate of increase in the strain amplitude for the sample at 30 °C is less than the one at 25 °C. From the early stage to the middle stage, the strain amplitude increased by almost 35%, and 23% for the slabs tested at 25 °C and 30 °C, respectively. The enhancement of the strain amplitude from the early to the late stages for the slabs tested at 25 °C and 30 °C were 50% and 29%, respectively.

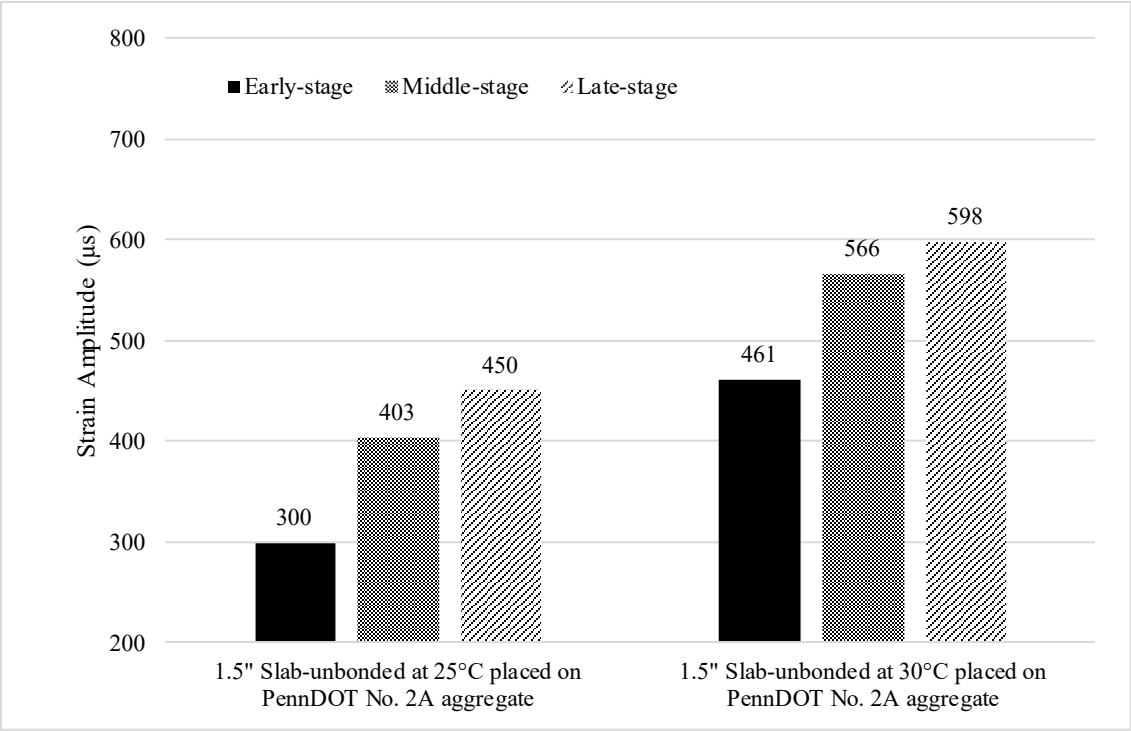

Figure 37. Longitudinal strain amplitude at two different temperatures for the slab placed on PennDOT No. 2A aggregate base.

As a follow-up to studying the temperature effect using the PennDOT No. 2A aggregate base as the supporting layer, a similar study was conducted using the 60A hardness neoprene as the supporting layer. The results of this study, i.e., using two different temperatures but with the neoprene base, are presented in Figure 38. It can be seen that the starting strain levels (early-stage strain levels) are somewhat higher for the neoprene base compared with the PennDOT No. 2A aggregate base at similar test temperatures. However, the more important observation is that the strain growth rate is considerably higher when the neoprene base is used compared with the PennDOT No. 2A aggregate base. When the neoprene was used and for the slabs tested at 25 °C and 30 °C, the strain amplitude increased respectively by almost 38% and 106%, from the early to the middle stage (Figure 39).

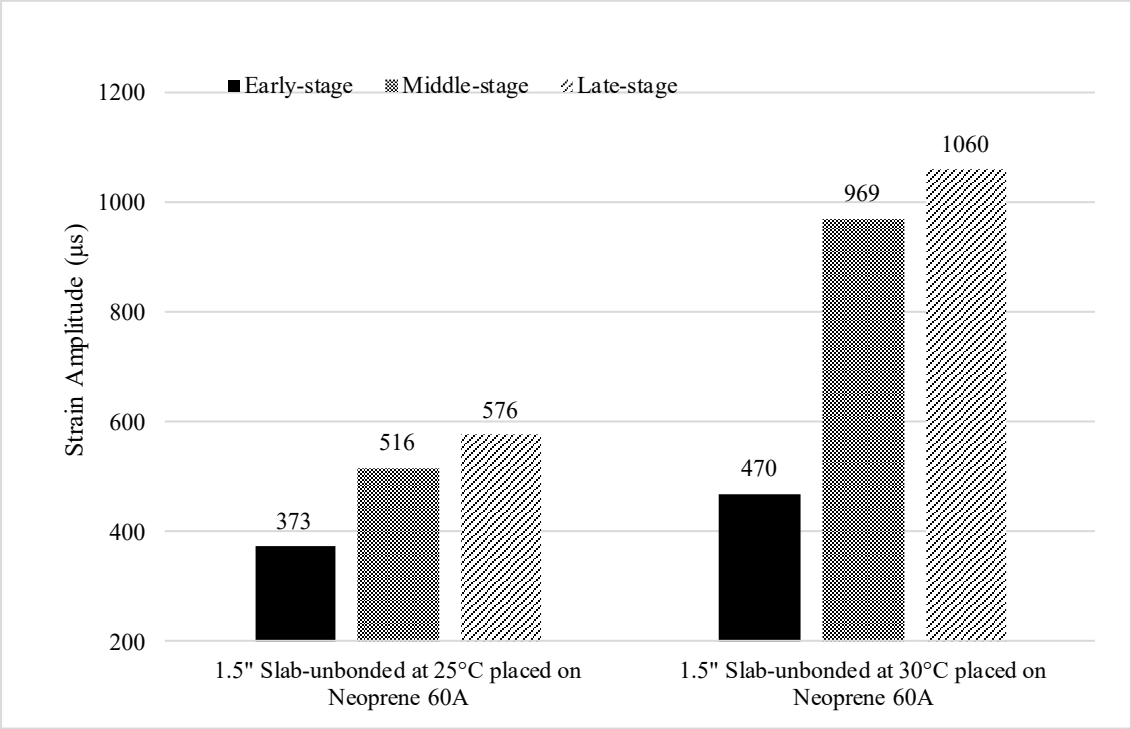

Figure 38. Longitudinal strain amplitude at two different temperatures for the sample placed on Neoprene 60A.

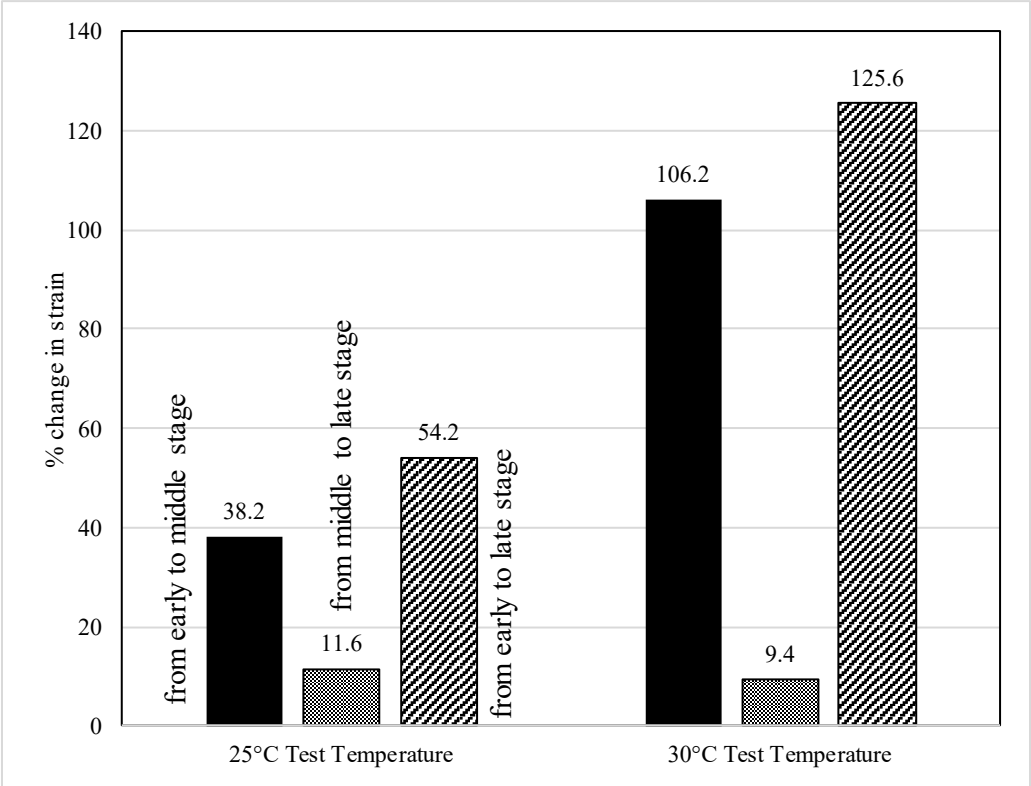

Figure 39. Rate of change in strain level from early stage to middle and late stages, 1.5"-thick slabs (Mix 1).

Effect of the loading speed

It was discussed previously that one of the crucial factors to be investigated in this research was the tracking speed. The conventional tracking in HWTD delivers almost 52 passes (26 load cycles) of the wheel per minute. It is expected that a lower speed will produce higher strain levels and a higher rate of strain amplitude growth, and hence, expediting the test time. The lowest possible speed in the HWTD model used at Northeast Regional Superpave Center (NECEPT) delivers 20 passes (10 load cycles) per minute. Therefore, testing was conducted at this low speed and results were compared with those from testing at normal speed.

Figure 40 presents the longitudinal strain amplitude of mix 1 subjected to both regular and low-speed conditions, with the speeds corresponding to 26 and 10 cycles per minute, respectively. Longitudinal strain measurements were obtained at approximately 220 seconds, 8.1 hours (29215 S), and 16.6 hours (59815 S) for both mixtures. Data were collected using two longitudinal strain gauges located at the bottom of each slab tested under a low-speed moving load. The graph displays the average longitudinal strain values derived from two slabs.

As evident from the graph, the overall strain amplitude is higher under the low speed (Figure 40). In other words, the lower tracking speed induces higher tensile strain at the bottom of the asphalt layer. The strain increased by approximately 38% and 73% from the initial to the middle stage for specimens tested at regular and low speeds, respectively (Figure 41). Although the strain amplitude for samples tested under low-speed conditions did not double, a significant increase in strain amplitude was observed in comparison to the regular-speed samples. This indicates a significant increase in the rate of damage growth in the slab as a result of speed reduction. In other words, at equivalent points in the experiment, greater damage can be observed in low-speed test specimens. Consequently, the low-speed condition appears to be more suitable for the objectives of this study in terms of expediting the damage growth and reducing the testing time.

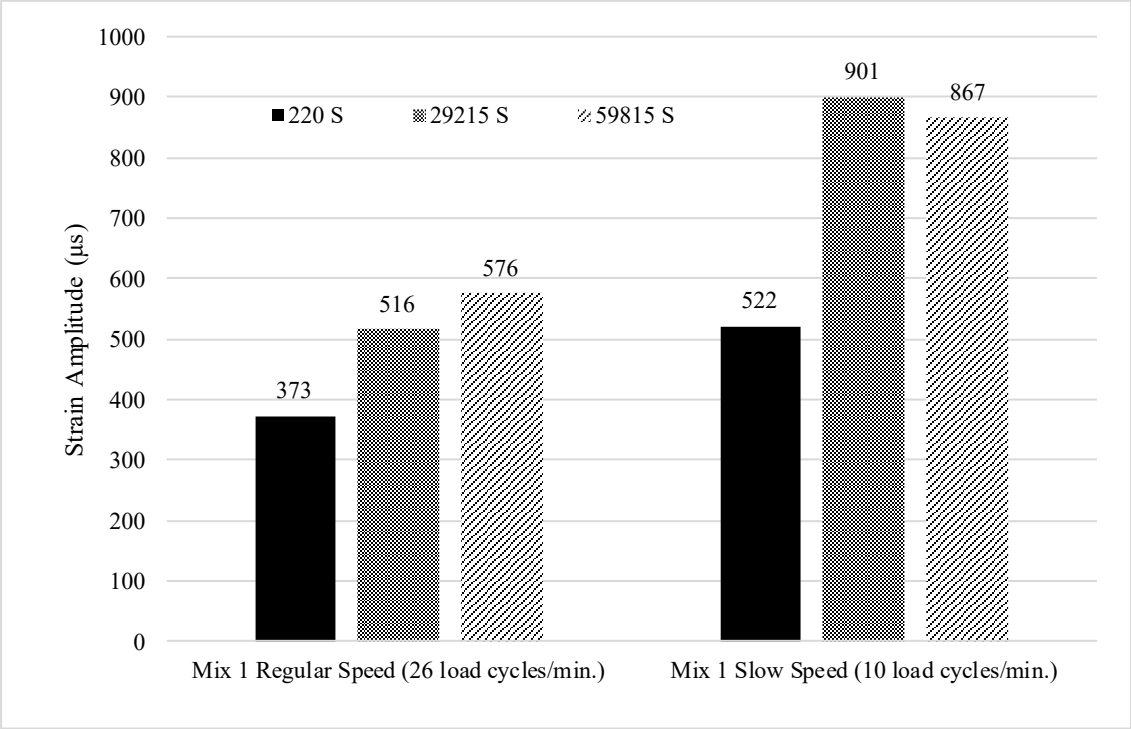

Figure 40. Strain amplitude for mix 1 under moving load at regular and low speeds.

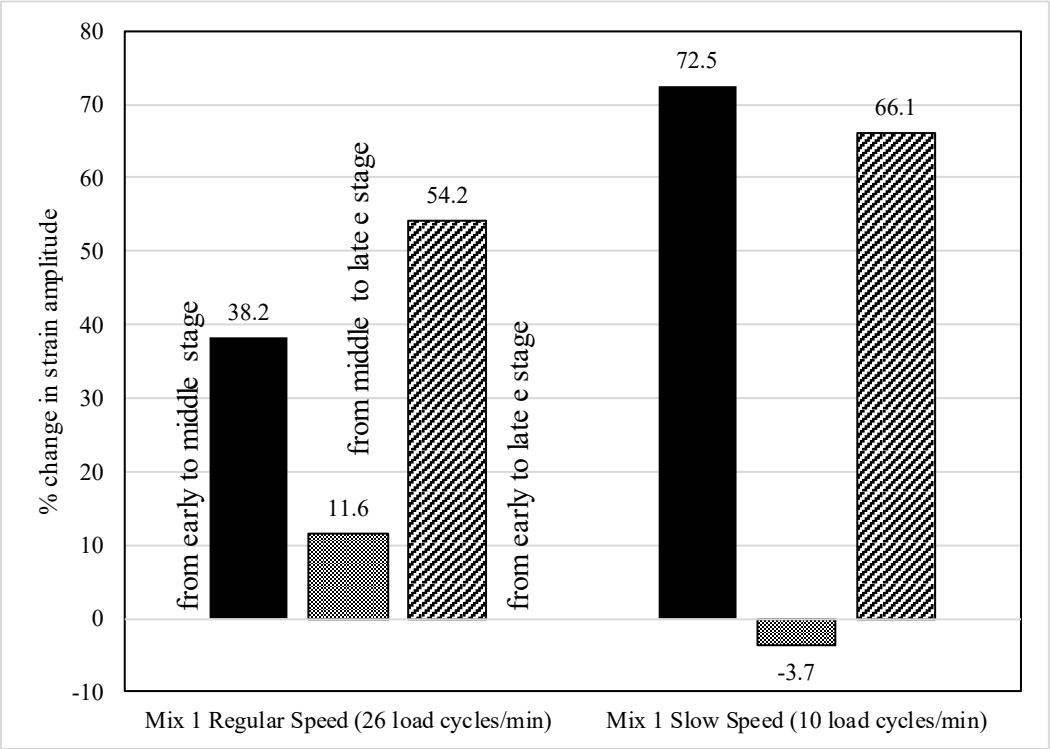

Figure 41. Rate of change in strain level from early stage to middle and late stages, 1.5"-thick slabs (Mix 1).

Effect of the mix binder content

To examine the effect of the binder content on the strain amplitude and its growth during the test, six slabs with three different binder contents were tested under the moving load. The design binder content for the core mixture (i.e., Mix 1, the reference mixture) tested in this research was 5.7%. This optimum binder content was selected based on the PennDOT Superpave design criteria at 75 gyrations. Two slabs were prepared at 5.2% binder content (0.5% lower than optimum) and two at 6.2% (0.5% higher than optimum). These four slabs were tested at 25 °C, and four strain gauges (two per slab) were used to monitor and record the longitudinal strain. In comparison, each of the two slabs that were previously tested at optimum binder content of 5.7% had only one longitudinal strain gauge to record the strain at the bottom of the slab.

Figure 42 illustrates the strain amplitude for the slabs with low, optimum, and high binder contents. Based on the data presented, one can generally conclude that the binder content significantly affects the rate of damage and strain growth in an asphalt mixture. It can be seen that when the binder content was decreased from the optimum, the strain grew at a considerably faster rate. In general, lower binder content can reduce the flexibility of the asphalt mixture, which can lead to lower fatigue life. The rate of increase in the strain amplitude for the specimens with 5.2% binder content from the early to the middle stage and from the early stage to the late stage was almost 79% and 128%, respectively. This enhancement in the strain amplitude clearly shows that based on the phenomenal approach of considering the fatigue life at a point where the strain is doubled, the fatigue life for this lower binder content slab was achieved sometime between the middle and late stage of testing.

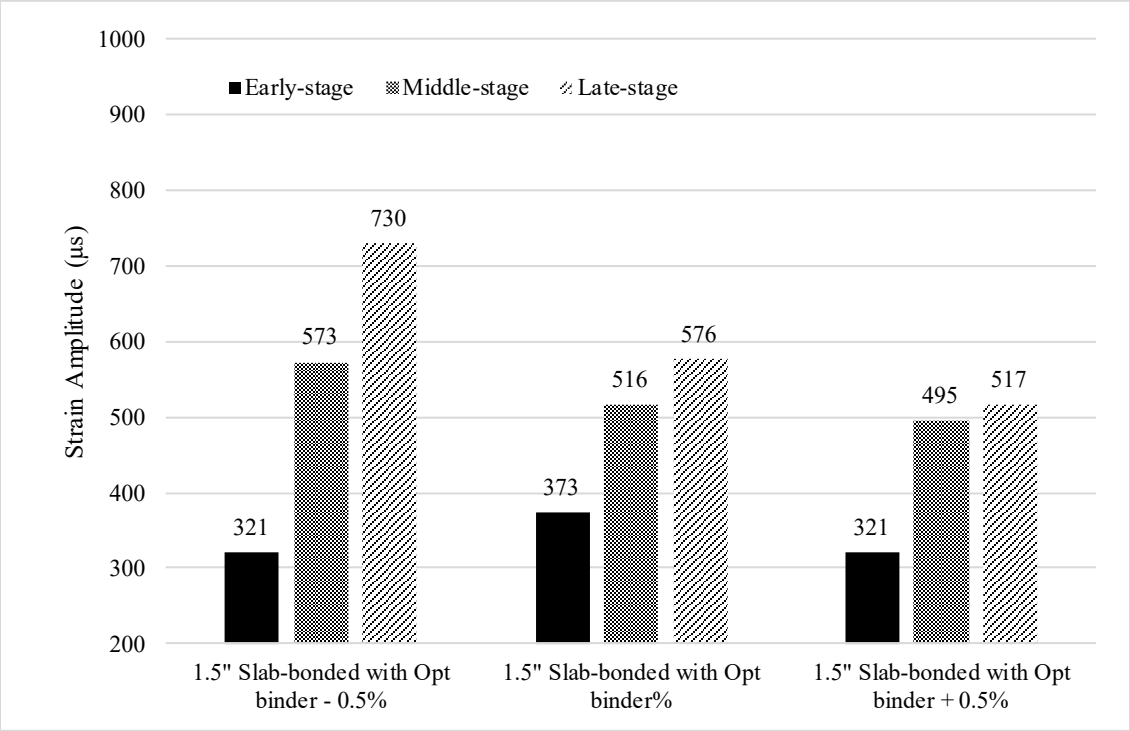

Figure 42. Longitudinal strain amplitude for high and low binder mixes.

For the slab with higher binder content, the early-stage strain level was to some extent lower than the strain level of the slab made at optimum binder content. This reduction was not expected, but the difference is not that significant. The high binder content slab demonstrated a higher rate of increase (54%) in strain amplitude compared to the optimum binder slab (38%) up to the middle stage, but then, from the middle stage to the late stage, the rate of increase in strain amplitude was lower for the high binder content slab (4%) compared with the optimum binder content slab (12%). The final strain amplitude was lower for the slab with high binder content compared to the slab with optimum binder content (517 microstrain compared with 576 microstrain). However, the rate of strain growth was higher for the slab with higher binder content (61% versus 54%). This higher level of change in strain is because the initial strain was lower for the high binder slab. Considering the data from both the low and high binder contents, one may conclude that for the specific test configuration used in this study, the reduction of binder content from the optimum level significantly reduces the fatigue life, while increasing the asphalt content from optimum may or may not improve the fatigue life. Figures 43 through 45 present a visual presentation of how the strain amplitude grows for the mix with different

binder contents. The considerable damage due to the low binder content is obvious from Figure 43 due to magnitude of strain growing rapidly.

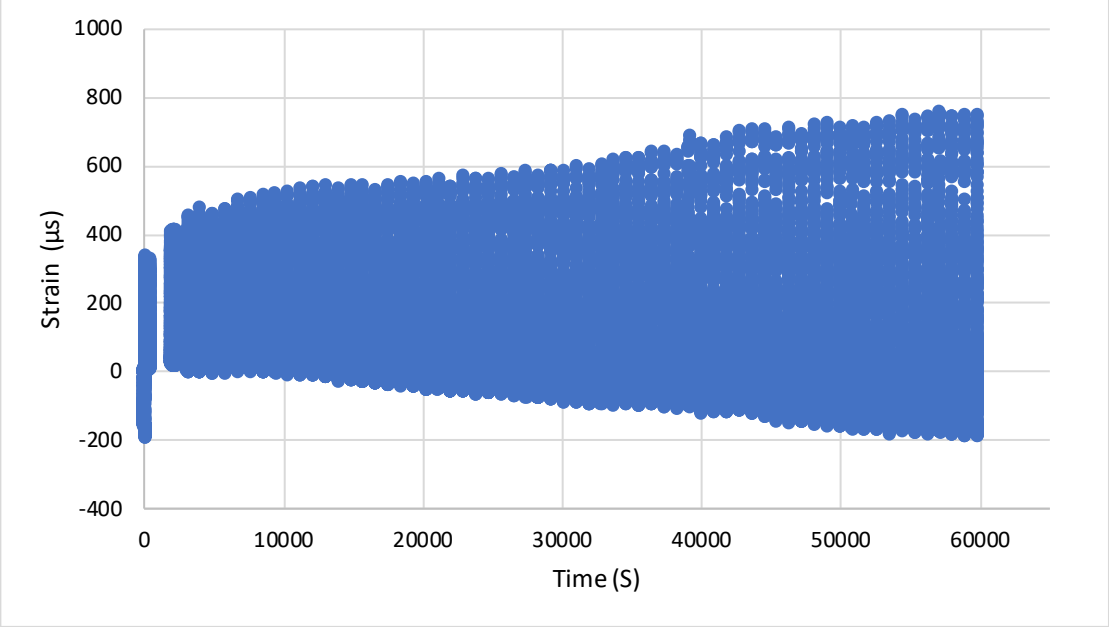

Figure 43. Strain amplitudes at the bottom of the slabs with lower binder content during the test.

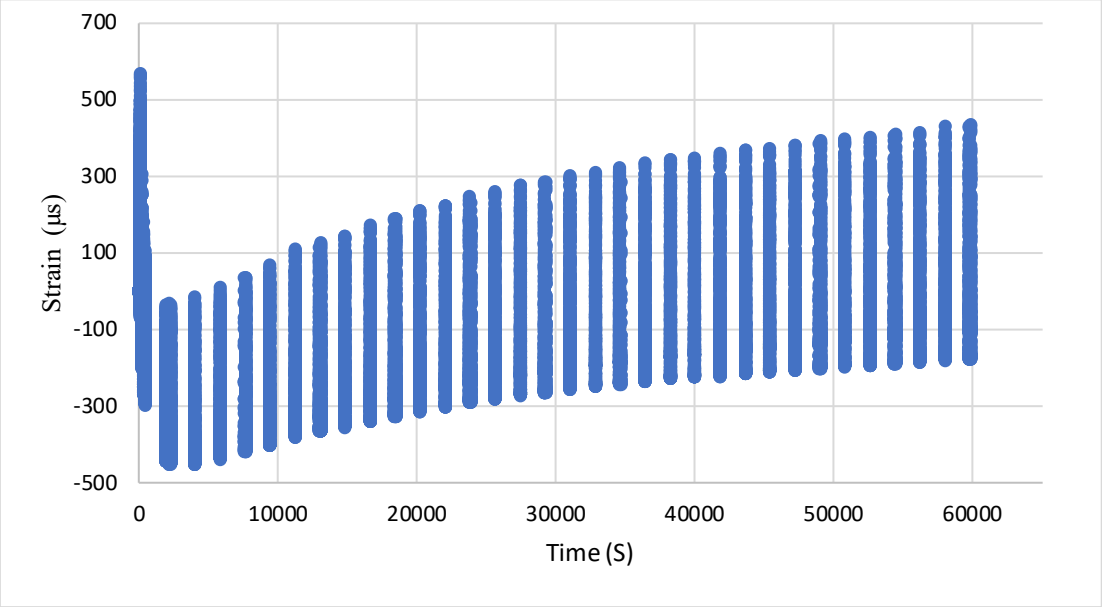

Figure 44. Strain amplitudes at the bottom of the slabs with optimum binder content during the test.

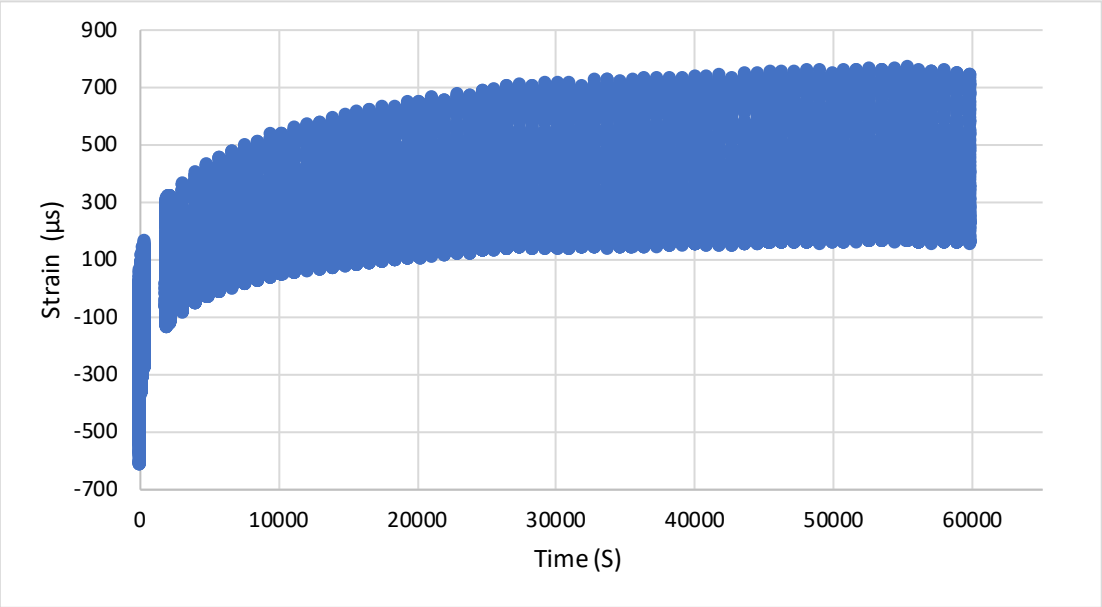

Figure 45. Strain amplitudes at the bottom of the slabs with higher binder content during the test.

Effect of mixture types

Six different mixtures were tested under the moving load. Mixes 5 and 6 were investigated for the effect of binder content and were compared to Mix 1, as discussed previously. In this section the results for Mixes 2, 3, and 4 are provided and compared to the reference mix (Mix 1). As a reminder, Mixes 2 and 4 contain 35% RAP, with the difference that the former is made with PG 58S-28 and the latter with PG 64S-22. Mix 3 is a 9.5-mm SMA mix. The results for Mixes 2 and 3 are the average response of the four longitudinal strain gauges. The results for Mix 4 are the average of the two longitudinal strain gauges, since two strain gauges did not survive and were lost during the test. The longitudinal strains from early to late stages were increased by 54%, 67%, 104% and 3% for Mixes 1, 2, 3, and 4, respectively (Figure 46 and Figure 47).

Based on the results, the SMA had the highest development of the longitudinal strain during the test, and the asphalt concrete slab with 35% RAP and 64S-22 binder had the lowest development of the strain. The high growth rate of the SMA mix was not expected and further investigation is needed to determine the cause. The study was limited to only one SMA mixture, and it was difficult to draw solid conclusions regarding the behavior of this mixture.

It is also interesting to see that the mix with PG 64S-22 and 35% RAP had not only the smallest level of initial strain but also the smallest rate of strain growth (Figure 47). This is an indication of a stiff mix, but it did not exhibit significant strain amplitude growth, nor did it show any cracking in the test. The fact that the strain did not grow much is an indication of good performance of this mix under the loading conditions used in this study. However, adjustments to the testing system may be needed for better evaluation of this mix, such as higher temperature and using a slab at a smaller width. Increasing the load to expedite crack growth is not an option in the existing HWTD, as the load is constant.

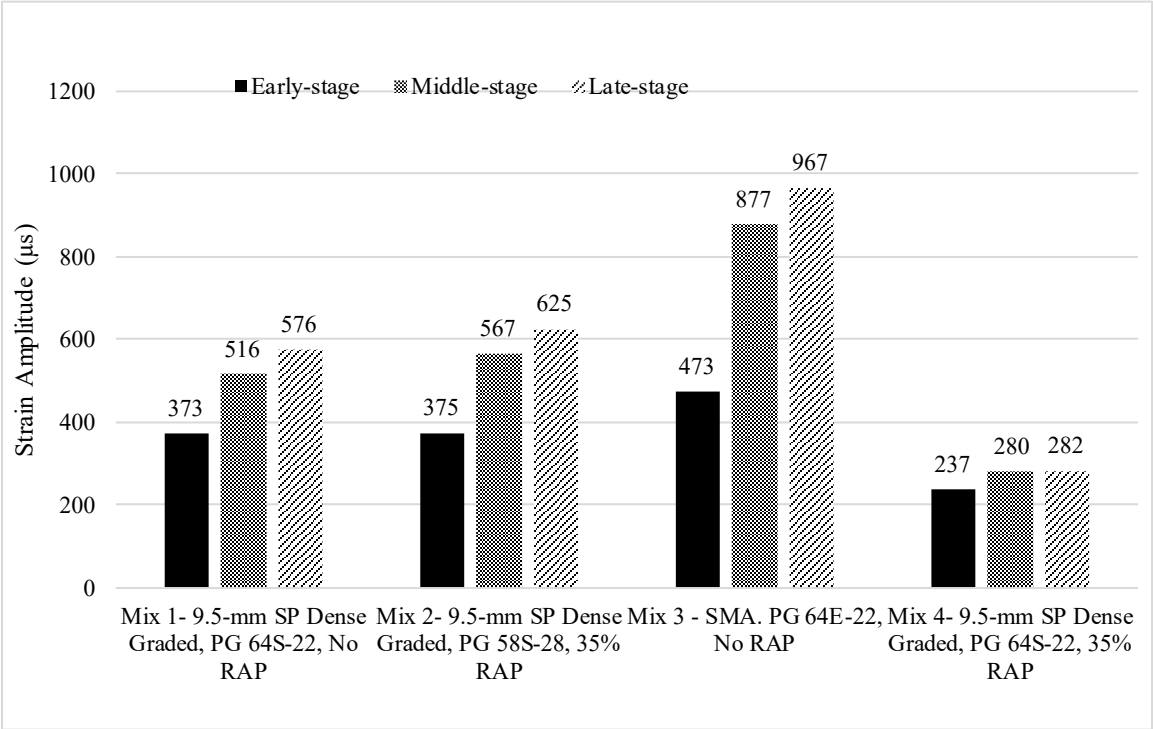

Figure 46. Longitudinal strain amplitude for different mixes.

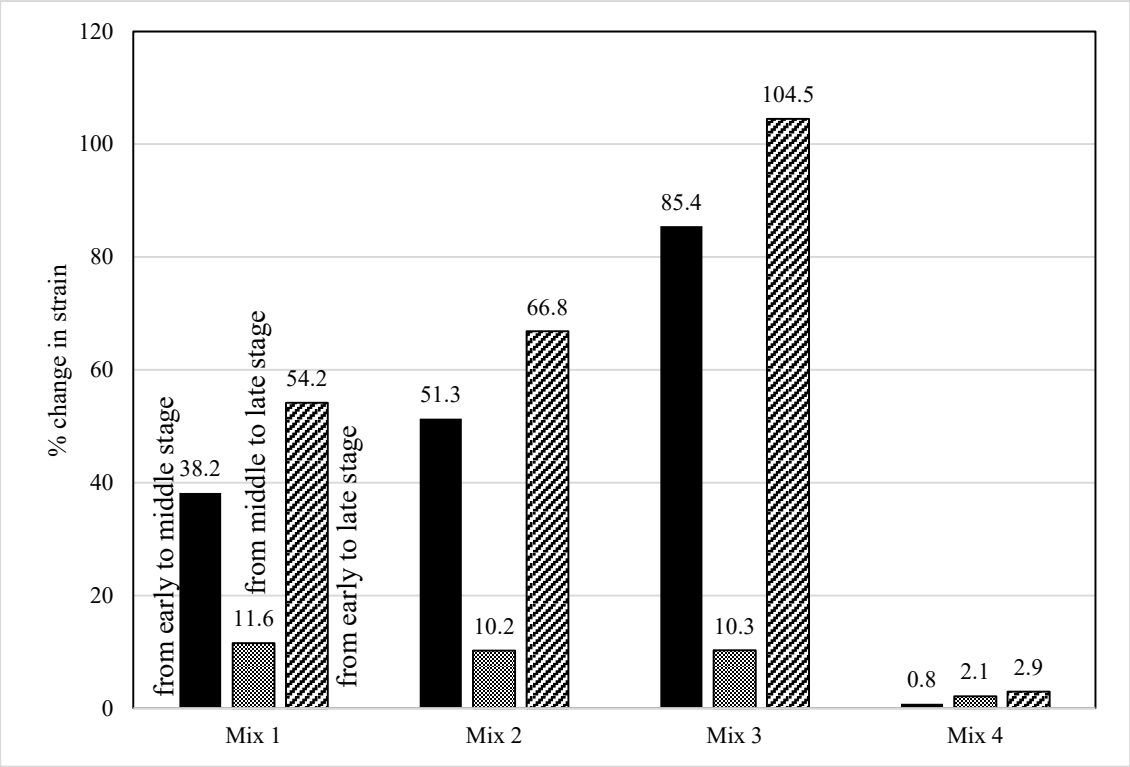

Figure 47. Rate of change in strain level from early stage to middle and late stages for different mixes.

IDEAL-CT Test Results

The IDEAL-CT was conducted on four replicates for all the mixtures. Through extensive testing and inclusion of numerous mixtures at NECEPT, it became clear that the IDEAL-CT test, like other cracking tests, is sometimes associated with high variability, due to the effect of post-peak slope of the load-displacement curve. Using four replicates assists with identification of outliers and reducing variability, offers superior management of data accuracy, and creates a more dependable circumstance for eliminating any anomalies. Examples of load-displacement curves associated with Mixes 1 and 2 are presented in Figures 48 and 49, respectively. Graphs for all six mixtures are presented in Appendix E.

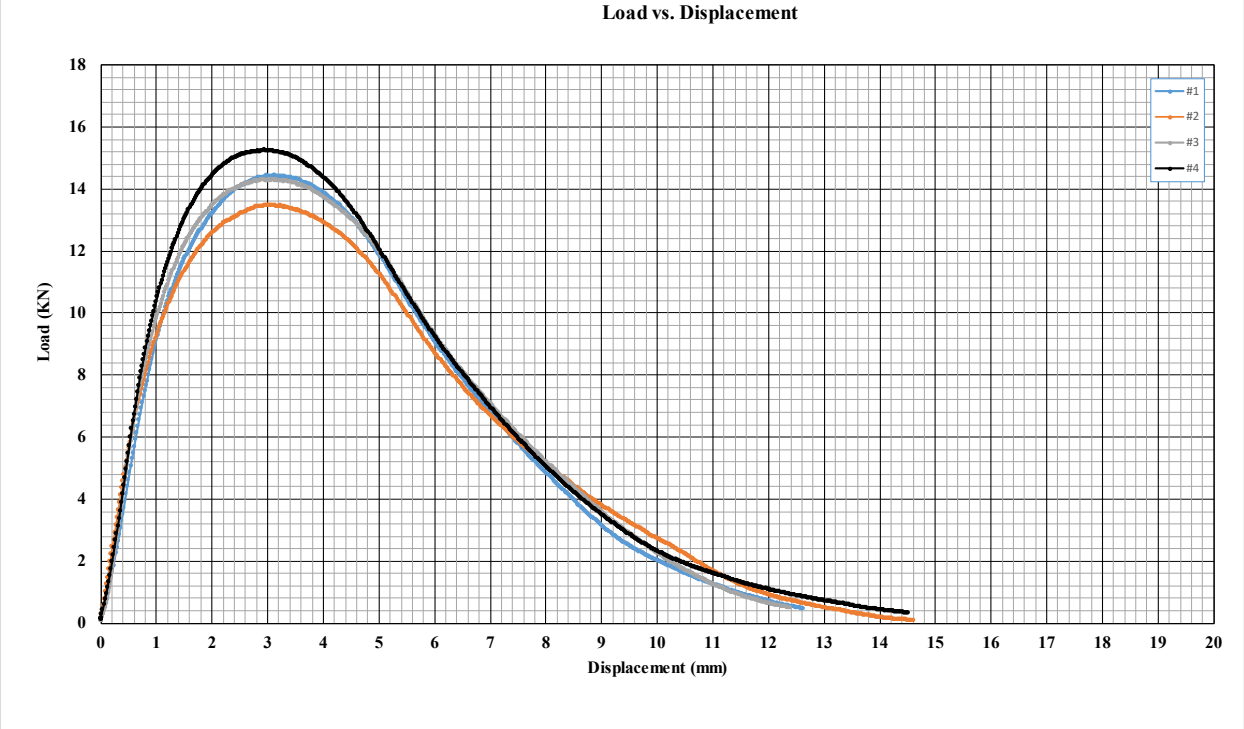

Figure 48. Load-displacement curve for Mix 1 (SP-DG, 9.5 mm, PG 64S-22, 0% RAP).

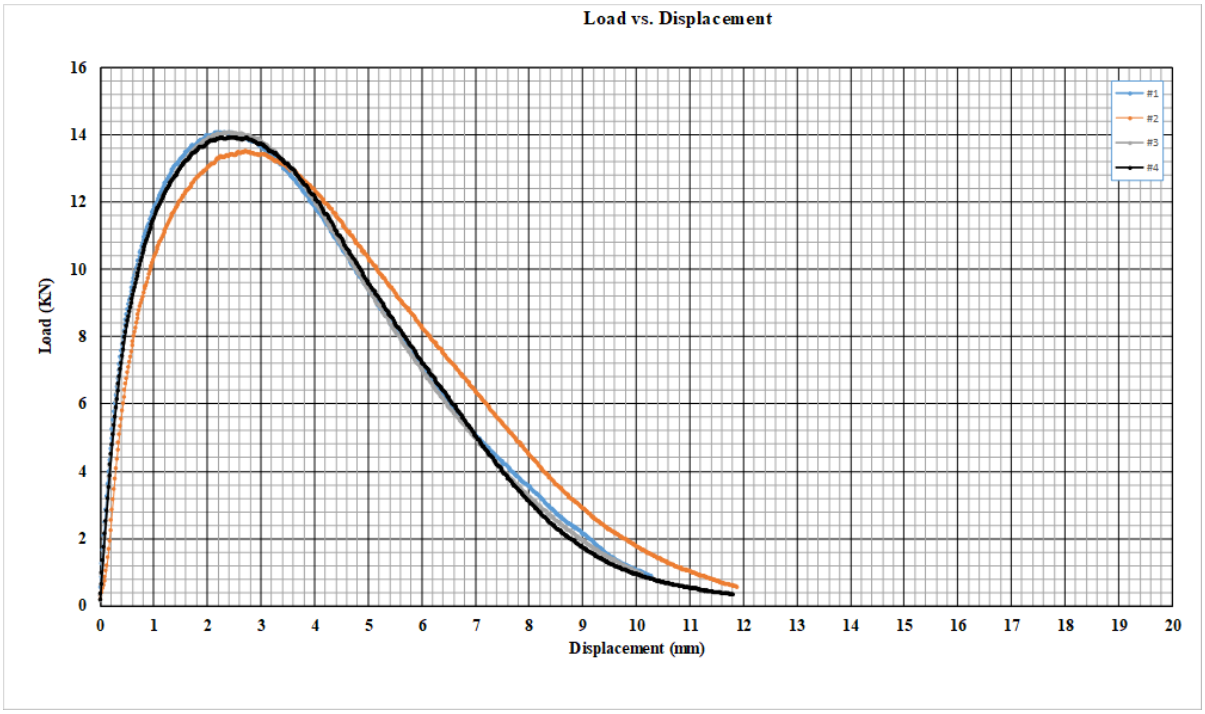

Figure 49. Load-displacement curve for Mix 2 (SP-DG, 9.5 mm, PG 58S-28, 35% RAP).

Detailed results for all the mixtures are presented in Table 13. The IDEAL-CT index varied in the range of almost 81 to 354 for the mixtures tested for this research project. All of the mixtures except mix 4 satisfy the existing criteria as given in PennDOT Bulletin 27. The criteria included in Bulletin 27 are based on the strike-off letter 481-22-01 issued on 1/21/2022. Minimum IDEAL-CT values as specified in Bulletin 27 are 90, 80, and 70 for traffic levels of >10, between 3 and 10, and less than 3 million ESALS, respectively.

It can be seen that the coefficient of variation (COV) for the IDEAL-CT index is between 4.7% and 20.4%. Although there is currently no defined level of acceptable precision for this test, the authors of the report suggest that the COV does not exceed 25%. It was found that all the asphalt mixes of this study met this requirement.

Table 13. Detailed Results of IDEAL-CT for All the Mixtures.

Mix Code	Peak Load (kN)	Work of Fracture (J)	Fracture Energy (J/m2)	IDEAL-CT Index	Peak Strength (KPa)	Displ. at Peak Load (mm)	Post Peak Displ. at 75% Peak Load (mm)	Post Peak Tangential Slope at 75% Peak Load (kN/mm)
1 - HV	11.268	99.43	10,682	354.4	770.7	4.3	7.7	-1.58
1	14.371	93.95	10,127	134.1	986.2	3.0	5.4	-2.70
2	13.899	83.21	8,929	118.6	949.5	2.5	4.7	-2.40
3	16.073	124.29	13,322	247.4	1,096.7	3.2	6.0	-2.19
4	16.978	93.1	9,981	80.8	1,158.9	2.3	4.4	-3.67
5	12.490	97.23	10,421	244.4	852.2	3.1	6.2	-1.78
6	14.719	90.90	9,774	108.6	1,007.5	2.3	4.6	-2.78
Coefficient of Variation (COV)								
1 - HV	4.6	7.5	7.5	20.4	4.6	7.7	4.7	8.93
1	5.1	3.6	3.8	4.7	5.2	2.9	2.2	4.72
2	1.9	2.8	2.8	19.0	2.0	7.7	5.6	9.19
3	2.1	3.6	3.6	10.0	2.1	5.5	3.7	5.50
4	3.5	3.9	4.0	20.2	3.4	13.3	8.2	10.1
5	5.8	4.5	4.5	12.9	5.8	3.9	5.4	13.28
6	8.7	7.2	7.3	10.0	8.7	7.5	5.3	10.24

There are several findings from the results obtained from the IDEAL-CT testing. For one, Mix 1 (1-HV) at an average air void content of 10.6% yielded a significantly higher IDEAL-CT index compared to the same mix at 6.6% percent air voids (Mix Code 1). In fact, this high air void mix delivers the highest IDEAL-CT index. As a background note, Mix 1 was produced at two air void levels for IDEAL-CT testing to match the air voids of the slabs that were tested in the HWTD. The corresponding HWTD slabs for Mix 1 delivered 10.6% air voids and 6.7% air voids for the high and low air void contents, respectively.

One can also see the effect of the binder content on the results when comparing Mixes 1, 5, and 6. Mix 5 with the binder content of 0.5% above the optimum binder content, yields the highest IDEAL-CT among the three mixes; and Mix 6, with the binder content of 0.5% below the optimum value, yields the lowest. In fact, Mix 4 delivers the lowest index among all the tested mixes, and it did not pass the current criteria for traffic levels of >10 million. Finally, the SMA mixture (Mix 3) provides the highest index value (other than the high-void Mix 1) and is comparable with the high binder content mix (Mix 5).

Comparison of Results between HWTD Fatigue Test and IDEAL-CT Test

Among all the parameters that were investigated for their effect on the tensile strain response in the HWTD, only the mix parameters can be considered for comparison with the results from IDEAL-CT testing. These parameters include the binder content, the air void content, and inclusion of RAP. There is also the possibility of making a general comparison between the 9.5-mm dense-graded Superpave mix and the SMA mix.

It is well established that higher air void content for the same mix results in a higher IDEAL-CT index. This situation was also observed in this study. However, it is also well known that high void content makes the mix more prone to fatigue damage and reduced service life. The HWTD fatigue testing for this study indicated significantly higher strain levels and a higher rate of strain growth for the higher air void mix. This is expected, as a higher rate of strain increase is an indicator of higher rate of damage growth and in concord with the expected field behavior for high air-void mixes. Therefore, caution should be exercised in using the IDEAL-CT values, and the results from this test must be considered only when testing is conducted on specimens within the air voids range

established in specifications. A higher IDEAL-CT index is not necessarily an indicator of better crack resistance if the air void content is high, as clearly seen in the higher strain growth rate when testing this high-void mix in the HWTD.

Lowering the binder content in this study indicated reduction of the IDEAL-CT index and an increase in the rate of strain amplitude growth in the asphalt mix. In this respect, the results from both the IDEAL-CT test and the HWTD agree and indicate increased potential of the mix to fatigue crack when the binder content is reduced.

The last two comparisons relate to the RAP in the mix and behavior of the SMA mix. Comparing the mix with no RAP with PG 64S-22 binder and the mix with 35% RAP with PG 58S-28 binder indicates the mix with RAP in HWTD produced not only lower strain levels but also a lower magnitude in the rate of growth for the strain amplitude. However, the IDEAL-CT index for the mix containing RAP was to some extent lower than that of the mix with no RAP (118.6 versus 134.1). This observation indicates that, at least for the loading condition applied in the HWTD for this research, the RAP mix did exhibit potential for cracking. The IDEAL-CT index, even though lower than that of the mix with no RAP, is also high enough to indicate fatigue resistance of the mix.

CHAPTER 5

Summary, Conclusions, and Recommendations

A Summary of Accomplished Work

This research study was sponsored by PennDOT and U.S. Department of Transportation's University Transportation Centers Program to evaluate the potential of the Hamburg wheel tracking device (HWTD) in determining the mix quality in terms of fatigue cracking resistance. The tests used for the purpose of asphalt mixture fatigue resistance evaluation are, in general, classified as either single-cycle (monotonic) tests or repeated load (cyclic load) tests. Two of the tests of the former type are the semi-circular bend test and the IDEAL-CT test. Both are under consideration or in use by several state highway agencies. In the case of cyclic loading, one can name the tension-compression test and Texas overlay test as examples of those under consideration by some state highway agencies.

This research was conducted to develop a repeated loading test protocol using the HWTD to capture fatigue resistance characteristics of asphalt mixtures. The following tasks were followed to achieve this goal.

- Apply changes to HWTD
- Establish the test setup
- Develop experimental plan
- Conduct the required tests
- Conduct data analysis
- Develop the test protocol

Beyond a review of current test protocols, the efforts were first focused on the complete evaluation of HWTD and determining the setup needed with the equipment and specimen assembly to make the required testing feasible. HWTD is primarily used for evaluation of moisture damage and rutting potential of asphalt mixtures. To achieve the objectives of this research, it was important to determine the changes needed to the equipment and the specimen type and assembly. As testing was to be

conducted under dry conditions, a special hood was purchased from the equipment manufacturer and installed on the existing HWTD to give the researchers the ability to control the temperature during the test. Several factors had to be considered and addressed before testing specimens in HWTD:

- Dimensions of the rectangular asphalt concrete slabs to be tested
- Technique of preparing the slabs
- Type of underlying support for the asphalt concrete slabs
- Bond between the underlying support and the asphalt concrete slabs
- Technique of establishing the bond in cases when bonding between the layers was needed
- Type of sensors needed for data collection
- Technique of installing the sensors on the slabs
- Data collection system
- Times for data collection and the rate of data sampling (number of data points per second)
- Technique of assembling the slabs inside the equipment
- Number of wheel tracking passes needed to achieve meaningful results
- Response parameters for analysis

To establish the slab dimensions, numerical analysis was conducted using both the Abaqus finite element analysis application program and a layered-elastic analysis software (Kenlayer). The idea was to determine the magnitude of tensile strains developed at the bottom of the asphalt concrete slab as well as the width of the slab needed to minimize the effect of the confinement. Based on the computational work, it was found that as the width increased beyond approximately 6 inches, there was not a considerable change in the strain response of the slab. Therefore, the slab width for the first experiment was selected to be 6 inches. To determine the sensitivity of the test results in HWTD to the slab geometry, 4-inch-wide slabs were also fabricated and tested. Similarly, the 1.5-inch thickness was selected as the main thickness, but slabs at 1-inch and 2-inch thickness were also made and tested.

Several techniques were tried to compact the asphalt concrete slabs, but they were mostly unsuccessful in delivering a reasonable level of air void content, as the achieved air voids were most often exceeding 10 percent. Since it seemed difficult to produce testing slabs of asphalt concrete at the desired air void content using the existing compaction equipment at Penn State, assistance was sought from the Michigan Technological University (MTU) in compacting the slabs. The asphalt laboratory at MTU is equipped with a slab compactor capable of producing the slabs at the desired air voids.

In deciding the underlying support, it was important to select a material that was uniform in properties, was feasible to use, had a reasonable magnitude of stiffness, and had known engineering properties. Based on such criteria, neoprene, a synthetic rubber with known properties, was selected. For most of the experimental work, neoprene with a shore hardness of 60A was used to represent a harder grade. A limited part of the work included a softer neoprene with Shore hardness of 40A for comparison. The grading of rubbers using the durometer fell into shore A and shore D categories, the former being for softer and more flexible rubbers and the latter for hard rubber and hard plastics.

In addition to the 60A neoprene, as the main type of support, and the 40A neoprene, an unbound aggregate base (PennDOT No. 2A aggregate) was also used for comparison. Work with the aggregate base proved to be challenging because of difficulty in maintaining a smooth, flat surface; however, it was used in part of the experiment. To bond the asphalt concrete slabs to the underlying support, a cationic slow-setting emulsified asphalt (CSS-1h) was used. As part of the experimental work, a few of the slabs were tested without any bonding.

A major part of the testing setup was determination of the displacement measuring sensors. Considering available options among the sensors, such as linear variable displacement transducers and strain gauges of various types, the foil strain gauges seemed the simplest and most practical. Further studies beyond this first experiment are needed to explore the possibility of applying other types of displacement measuring sensors. After selection of the type of gauges, the gauge configuration was determined. This configuration refers to how the gauges were to be oriented at the bottom of the slabs. Various configurations were used throughout the experiment, with the main idea being collection of the data from the gauges in the direction of tracking (i.e., the longitudinal direction) as well as in the direction perpendicular to tracking (i.e., the transverse direction).

Once the decision was made to use foil strain gauges, the next step was determination of the length of the gauge. Considering the inhomogeneity of the asphalt mixture and the nominal maximum aggregate size of the asphalt mixture, using short-length gauges (for example, a 10-mm gauge length) seemed unreliable. The best option appeared to be a gauge length of 30 mm to accommodate the size of the aggregates present in the mixture. Using 9.5-mm nominal maximum aggregate size asphalt mixture (as was the case in this research) or even a 12.5-mm nominal maximum aggregate size asphalt mixture provides a ratio of at least approximately 2.5 between the gauge length and the aggregate

size. In connection with finalizing the type and size of the strain gauge, a decision had to be made on the type of data acquisition system (DAQ). A system was selected capable of collecting data at a very rapid dynamic rate out of 8 data channels. A LabView™ program was written to establish the connection between the gauges and the DAQ as well as the rate of data collection. A data collection schedule was developed to present the times the data are to be collected during the test and the number of data points at each of these time intervals. In deciding the data collection schedule, attention was paid to two factors: (1) to have enough intervals of collection and enough sampling rate to obtain results that could be analyzed in a meaningful way and (2) to ensure the data file does not get too large, making the analysis either impossible or inefficient.

After installation of the gauges on the slab and bonding the layers, the next step was placement of the slab assembly inside the HWTD. It was important to ensure the slabs were properly secured in the machine and not to be loose to move around during the tracking of the wheels. Therefore, wherever needed, fillers were placed at the sides and at the edges of the mold to secure the slab. Once the setup of the slab in the machine was complete, and after connecting the DAQ, the slab was left to be conditioned at the test temperature before tracking began. A typical Hamburg wheel tracking test based on AASHTO T 324 consists of up to 10,000 load cycles (20,000 wheel passes). It takes over 6 hours to complete the passes for this test. However, to ensure sufficient data are collected for fatigue testing using HWTD in this research, the number of passes was extended well beyond 20,000. Almost 50,000 wheel passes were applied for most of the slabs, and even a few exceeding 100,000 wheel passes. It took over 16 hours to complete 50,000 wheel passes.

The outcome of the test was strain response from various strain gauges installed on the slab and the corresponding time (or the number of wheel passes). In the early testing, some of the strain gauges did not survive during the whole period of tracking. As further experience was gained, significantly a higher rate of survival was achieved and in many cases all gauges remained functional throughout the whole test period. In case of gauge loss during the test, the redundancy in the number of gauges used helped in obtaining the required data. In a few cases, gauge loss was significant and the amount of collected data was not sufficient, leading to repetition of making and testing slabs.

The main parameter considered once the strain response was collected was the strain amplitude and its growth during the cycling period. For most of the slabs, except the ones tested at 1-inch thickness,

no visible cracks were observed, but the growth of tensile strain amplitude was an indicator of the internal damage induced due to the wheel tracking of the slab. Various asphalt mixtures were included in the study. The mixtures were all 9.5-mm in nominal maximum aggregate size and included both dense-graded Superpave mix and gap-graded stone mastic asphalt. The study also included a sensitivity analysis based on changing the binder grade, binder content, and inclusion of reclaimed asphalt pavement (RAP). Furthermore, the effect of test temperature and the tracking speed were also investigated. The main criterion followed in this study to determine the mix quality was the number of wheel passes it takes to double the magnitude of induced strain amplitude. This is one of the approaches used in the past to determine the mixture fatigue life based on the laboratory fatigue tests.

Conclusions

This study was the first step in looking into the use of HWTD for assessing the asphalt mixture quality in terms of its fatigue cracking resistance. The study resulted in generating an extended amount of data that were subjected to a good level of analysis and interpretation.

It was mentioned that, based on the numerical analysis, a width of 6 inches was used for the majority of the slabs tested in this work. However, the experiment also included the 4-inch width for comparison. The thickness of the slab was also selected at three levels: 1, 1.5, and 2 inches, with the 1.5-inch thickness being the core thickness applied to most of the slabs. The experiment showed that as the width and the thickness become smaller, the strain amplitude and its corresponding growth rate become larger, exhibiting a higher rate of fatigue damage. Using the unbound aggregate base proved to be challenging because of difficulty in achieving a smooth, even surface. A smooth surface was required to ensure proper bond of the gauges and collection of the data. Using synthetic rubber neoprene provided a smooth base and delivered a more reliable dataset compared to the aggregate base in this study. As expected, temperature played a significant role in the experiment, as a higher increase in strain amplitude was observed at elevated test temperatures. Similarly, a higher strain and increased strain growth rate were observed at lower loading or tracking speeds.

It was mentioned that various types of asphalt mixtures were tested in the course of this research. It was found that the rate of growth in strain amplitude during the test considerably increased when the binder content in the mix was decreased. The SMA mixture demonstrated a higher rate of strain amplitude increase compared to the dense-graded mixtures. Only one SMA mixture was tested, and

it is not clear why the rate of growth was higher for this mix compared with the dense-graded Superpave mixtures. The mix with 35% RAP content and a softer binder delivered lower growth in strain amplitude compared with the mix with no RAP.

Recommendations

The results from this study were utilized in developing a test protocol that is provided as Appendix F to this report. In developing this protocol, attention was paid to selection of test parameters, slab geometry, and test temperature in a way to expedite growth of tensile strains in the specimen and reduce the required number of repeated loads in the HWTD.

This study was unique in the sense that it was the first time HWTD was investigated to this extent in terms of its use for determination of the mix fatigue characteristics. However, it is recommended that further research be conducted to build upon the experience and data obtained from this research. Improvements could be made if several areas of concern are further investigated. These areas deal with slab geometry, test temperature, loading speed, and asphalt mixture types.

Most of the slabs used in this study were made 6 inches wide and 1.5 inches thick. Developing a sufficient level of strain development under wheel tracking requires a sizable number of wheel passes, as evidenced from the data generated in this research. As the idea is to make this test a practical one, the duration of time required to complete testing becomes of concern and an important consideration. Further work is needed beyond this study to determine and validate if 4-inch-wide slabs produce a faster rate of damage and if this thinner width should replace the 6-inch-wide slabs mainly tested in this research. While the slab width can change and should be further researched, reducing the slab thickness below the 1.5-inch level is not recommended. The study indicated that when the slab is produced at 1-inch thickness, the strain amplitude and its growth increase considerably, hence expediting the fatigue damage. However, considering the fact that many of the surface course mixes include nominal maximum aggregate sizes of 9.5 mm and 12.5 mm, using 1-inch-thick slabs will not produce enough thickness to properly accommodate NMAS. In addition, the fatigue resistance of the mix is affected by the thickness of the mix, and placing the mix at one-inch thickness is generally not considered structural enhancement of the asphalt pavement.

Two other factors to consider in expediting the growth of strain amplitude and fatigue damage are the test temperature and the loading speed. The study showed that increasing the temperature and

decreasing the speed both contributed to a faster rate of damage. Further study is recommended to validate this finding and, if warranted, a test temperature as high as 30 °C and loading speed of about half of the conventional tracking speed in HWTD could be used.

Finally, there are two other areas worth investigating. One regards the types of asphalt mixtures to be studied and the other relates to the type of instrumentation and the sensors needed. Several mixtures were included in this study to the extent that the budget and time for this research allowed. In spite of the fact that the performed study provided particularly useful data regarding various types of asphalt mixtures, there is a need to include a wider range of asphalt mixtures. Only one SMA mixture was included, and it would be wise to include more mixtures of this type. Only one type of RAP was included at 35% by the weight of the mixture. A higher percentage of RAP as well as inclusion of at least two other types of RAP will provide more solid evidence of the effect of RAP on the mixture behavior in HWTD. Inclusion of poor-performing mixtures will help in deciding the criteria to be used for acceptance or rejection of the mixtures tested in HWTD.

Foil strain gauges were used in this research. Strain gauges are highly useful and accurate in measuring the magnitude of the strains when properly bonded to the material to be tested. However, two drawbacks in using strain gauges for this testing are the time and experience it takes for proper placement and bonding and the fact that the strain gauges are not reusable, and a new set has to be used for testing every new slab. It will be important to study the feasibility of alternative displacement measuring techniques such as the use of LVDTs or DIC (digital image correlation). While the use of DIC adds to the cost of the equipment and the initial setup is somewhat complicated, it could become an integrated part of the testing system once established, needing simple initiation for every new test.

References

Al-Qadi, I. L., Ozer, H., & Lambros, J. (2019). Development of the Illinois Flexibility Index Test. *Transportation Research Circular of Transportation Research Board, E-C252, Relationship Between Laboratory Cracking Tests and Field Performance of Asphalt Mixtures* . https://trid.trb.org/view/1666456

Alfalah, A., Offenbacker, D., Ali, A., Mehta, Y., Elshaer, M., & Decarlo, C. (2021). Evaluating the impact of fiber type and dosage rate on laboratory performance of Fiber-Reinforced asphalt mixtures. *Construction and Building Materials*, *310*, 125217. https://doi.org/10.1016/j.conbuildmat.2021.125217

Asphalt Institute. (2014). *Asphalt mix design methods.*

Chen, H., Zhang, Y., & Bahia, H. U. (2021). The role of binders in mixture cracking resistance measured by ideal-CT test. *International Journal of Fatigue*, *142*, 105947. https://doi.org/10.1016/j.ijfatigue.2020.105947

Chen, X., & Solaimanian, M. (2019). Effect of long-term aging on fracture properties of virgin and recycled asphalt concrete. *Advances in Civil Engineering Materials*, *8*(1), 527–543. https://doi.org/10.1520/ACEM20190092

Chong, K. P., & Kuruppu, M. D. (1984). New specimen for fracture toughness determination for rock and other materials. *International Journal of Fracture*, *26*(2), R59–R62. https://doi.org/10.1007/BF01157555

Füssl, J., Kluger-Eigl, W., & Blab, R. (2015). Mechanical performance of pavement structures with paving slabs - Part I: Full-scale accelerated tests as validation for a numerical simulation tool. *Engineering Structures*, *98*, 212–220. https://doi.org/10.1016/j.engstruct.2014.10.054

Germann, F. P., & Lytton, R. L. (1979). *METHODOLOGY FOR PREDICTING THE REFLECTION CRACKING LIFE OF ASPHALT CONCRETE OVERLAYS.*

Gu, F., Luo, X., Zhang, Y., & Lytton, R. L. (2015). Using overlay test to evaluate fracture properties of field-aged asphalt concrete. *Construction and Building Materials*, *101*(Part 1), 1059–1068. https://doi.org/10.1016/j.conbuildmat.2015.10.159

Huang, Y., Wang, L., & Xiong, H. (2017). Evaluation of pavement response and performance under different scales of APT facilities. *Road Materials and Pavement Design*, *18*, 159–169. https://doi.org/10.1080/14680629.2017.1329871

Kaseer, F., Yin, F., Arámbula-Mercado, E., Epps Martin, A., Daniel, J. S., & Salari, S. (2018). Development of an index to evaluate the cracking potential of asphalt mixtures using the semi-circular bending test. *Construction and Building Materials*, *167*, 286–298. https://doi.org/10.1016/j.conbuildmat.2018.02.014

Krans, R. L., Tolman, F., & Van De Ven, M. F. (1996). *Semi-circular bending test: a practical crack growth test using asphalt concrete cores*.

Lytton, R. L., Uzan, J., Fernando, E. G., Roque, R., Hiltunen, D., & Stoffels, S. M. (1993). Development and Validation of Performance Prediction Models and Specifications for Asphalt Binders and Paving Mixes. *Strategic Highway Research Program, National Research Council, Washington, DC*.

Ma, W., Tran, N., Taylor, A. J., & Li, X. (2014). Proposed Improvements to Overlay Test for Determining Cracking Resistance of Asphalt Mixtures. *Materials Science*.

Majidifard, H., Jahangiri, B., Rath, P., & Buttlar, W. G. (2021). Development of a balanced cracking index for asphalt mixtures tested in semi-circular bending with load-LLD measurements. *Measurement: Journal of the International Measurement Confederation*, *173*, 108658. https://doi.org/10.1016/j.measurement.2020.108658

Mogawer, W. S., Austerman, A. J., Bonaquist, R., & Roussel, M. (2011). Performance characteristics of thin-lift overlay mixtures: High reclaimed asphalt pavement content, recycled asphalt shingles, and warm-mix asphalt technology. *Transportation Research Record*, *2208*, 17–25. https://doi.org/10.3141/2208-03

Mohammad, L., Wu, Z., Prevention, M. A., Petit, E., C., undefined, Al-Qadui, undefined, & 2004, undefined. (2004). Characterization of fracture and fatigue resistance on recycled polymer-modified

asphalt pavements. *Proc., 5th RILEM Conference on Pavement Cracking, Lemoges, France*, 375–382. http://www.rilem.net/publication/publication/42?id_papier=1042

Molenaar, A. A. A., Scarpas, A., Liu, X., & Erkens, S. M. J. G. (2002). Semi-Circular Bending Test; Simple but Useful? *Association of Asphalt Paving Techno*, *71*. https://trid.trb.org/view/698764

Nemati, R., Haslett, K., Dave, E. V., & Sias, J. E. (2019). Development of a rate-dependent cumulative work and instantaneous power-based asphalt cracking performance index. *Road Materials and Pavement Design*, *20*(sup1), S315–S331. https://doi.org/10.1080/14680629.2019.1586753

Nsengiyumva, G., Haghshenas, H. F., Kim, Y. R., & Kommidi, S. R. (2020). Mechanical-Chemical Characterization of the Effects of Type, Dosage, and Treatment Methods of Rejuvenators in Aged Bituminous Materials. *Transportation Research Record*, *2674*(3), 126–138. https://doi.org/10.1177/0361198120909110

Nsengiyumva, G., & Kim, Y. R. (2019). Effect of Testing Configuration in Semi-Circular Bending Fracture of Asphalt Mixtures: Experiments and Statistical Analyses. *Transportation Research Record*, *2673*(5), 320–328. https://doi.org/10.1177/0361198119839343

Sabouri, M., & Kim, Y. R. (2014). Development of a failure criterion for asphalt mixtures under different modes of fatigue loading. *Transp. Res. Rec., 2447 (1)*, 117–125.

Solaimanian, M., Stoffels, S. M., Hunter, D. A., Morian, D., & Sadasivam, S. (2006). Superpave In-Situ/Stress Strain Investigation. *Final Report, Report No. FHWA-PA-2006-019-350R02, Pennsylvania Transportation Institute, 132pp.*

Soltani, A., & Anderson, D. A. (2005). New test protocol to measure fatigue damage in asphalt mixtures. *Road Materials and Pavement Design*, *6*(4), 485–514. https://doi.org/10.1080/14680629.2005.9690017

Soltani A, Solaimanian M, & Anderson D. (2006). An Investigation of the Endurance Limit of Hot-Mix Asphalt Concrete Using a New Uniaxial Fatigue Test Protocol. In *International Journal of Pavement Research and Technology* (Vol. 14, Issue 3). Springer. https://doi.org/10.1007/s42947-020-0024-1

Underwood, B. S., Baek, C., & Kim, Y. R. (2012). Simplified viscoelastic continuum damage model as platform for asphalt concrete fatigue analysis. *Transportation Research Record*, *2296(1)*, *3*.

Wang, Y. D., Keshavarzi, B., & Kim, Y. R. (2018). Fatigue performance analysis of pavements with rap using viscoelastic continuum damage theory. *KSCE J. Civ. Eng.*, *Eng.*, *22 (*, 2118–2125.

Wu, H., Huang, B., & Shu, X. (2012). Characterizing viscoelastic properties of asphalt mixtures utilizing loaded wheel tester (LWT). *Road Materials and Pavement Design*, *13*(SUPPL. 1), 38–55. https://doi.org/10.1080/14680629.2012.657049

Xuan Chen, Mansour Solaimanian, & Scott Milander. (2019). Rejuvenator Content Optimization Using Semi-Circular Bend Test and Balanced Mix Design. *Journal of Association of Asphalt Paving Technologists*, *88*, 401–430.

Yan, C., Zhang, Y., & Bahia, H. U. (2020). Comparison between SCB-IFIT, un-notched SCB-IFIT and IDEAL-CT for measuring cracking resistance of asphalt mixtures. *Construction and Building Materials*, *252*, 119060. https://doi.org/10.1016/j.conbuildmat.2020.119060

Zhang, Z., Kohlmeier, J., Schulze, C., & Oeser, M. (2021). Concept and development of an accelerated repeated rolling wheel load simulator (Arrows) for fatigue performance characterization of asphalt mixture. In *Materials* (Vol. 14, Issue 24). MDPI. https://doi.org/10.3390/ma14247838

Zhang, Z., Shen, S., Shi, B., & Wang, H. (2021). Characterization of the fatigue behavior of asphalt mixture under full support using a Wheel-tracking Device. *Construction and Building Materials*, *277*, 122326. https://doi.org/10.1016/j.conbuildmat.2021.122326

Zhou, F., Hu, S., Chen, D. H., & Scullion, T. (2007). Overlay tester: Simple performance test for fatigue cracking. *Transportation Research Record*, *2001*, 1–8. https://doi.org/10.3141/2001-01

Zhou, F., Im, S., Sun, L., & Scullion, T. (2017). Development of an IDEAL cracking test for asphalt mix design and QC/QA. *Asphalt Paving Technology: Association of Asphalt Paving Technologists-Proceedings of the Technical Sessions*, *86*, 549–577. https://doi.org/10.1080/14680629.2017.1389082

Zhou, F., Karki, P., Xie, S., Yuan, J. S., Sun, L., Lee, R., & Barborak, R. (2018). Toward the development of performance-related specification for bio-rejuvenators. *Construction and Building Materials*, *174*, 443–455. https://doi.org/10.1016/j.conbuildmat.2018.04.093

Appendix A

Data Collection Sampling Rates and Frequencies

Table A.1. Data collection Times and Sampling Rates for the Second Half of the Project.

Time from start of tracking, hrs	Interval for data collection, minutes[1]	Duration of sampling, minutes[2]	Sampling Freq, Hz (data points per second)	Cumulative # of wheel passes at a time from the start
0.000	2[3]	2.00[4]	40	0
0.033	2	1.00	20	104
0.083	3	2.00	10	208
0.583	30	5.00	20	1,820
0.833	15	0.25	20	2,600
1.083	15	0.25	20	3,380
1.333	15	0.25	20	4,160
1.583	15	0.25	20	4,940
1.833	15	0.25	20	5,720
2.083	15	0.25	20	6,500
2.333	15	0.25	20	7,280
2.583	15	0.25	20	8,060
2.833	15	0.25	20	8,840
3.083	15	0.25	20	9,620
3.333	15	0.25	20	10,400
3.583	15	0.25	20	11,180
3.833	15	0.25	20	11,960
4.083	15	0.25	20	12,740
4.333	15	0.25	20	13,520
4.583	15	0.25	20	14,300
4.833	15	0.25	20	15,080
5.083	15	0.25	20	15,860
5.333	15	0.25	20	16,640
5.583	15	0.25	20	17,420
5.833	15	0.25	20	18,200
6.083	15	0.25	20	18,980
6.333	15	0.25	20	19,760
6.583	15	0.25	20	20,540
6.833	15	0.25	20	21,320
7.083	15	0.25	20	22,100

(1) The time interval selected for data collection

(2) Duration of data collection within the corresponding time interval.

(3) This first 2-minute time interval was before start of tracking.

(4) This 2-minute duration of data sampling at 0 time indicates the data collected for 2 minutes before the tracking started.

Table A.1. Data collection Times and Sampling Rates for the Second Half of the Project (Continued).

Time from start of tracking, hrs	Interval for data collection, minutes	Duration of sampling, minutes	Sampling Freq, Hz (data points per second)	Cumulative # of wheel passes from the start of tracking
7.333	15	0.25	20	22,880
7.583	15	0.25	20	23,660
7.833	15	0.25	20	24,440
8.083	15	0.25	20	25,220
8.333	15	0.25	20	26,000
8.583	15	0.25	20	26,780
8.833	15	0.25	20	27,560
9.083	15	0.25	20	28,340
9.333	15	0.25	20	29,120
9.583	15	0.25	20	29,900
9.833	15	0.25	20	30,680
10.083	15	0.25	20	31,460
10.333	15	0.25	20	32,240
10.583	15	0.25	20	33,020
10.833	15	0.25	20	33,800
11.083	15	0.25	20	34,580
11.333	15	0.25	20	35,360
11.583	15	0.25	20	36,140
11.833	15	0.25	20	36,920
12.083	15	0.25	20	37,700
12.333	15	0.25	20	38,480
12.583	15	0.25	20	39,260
12.833	15	0.25	20	40,040
13.083	15	0.25	20	40,820
13.333	15	0.25	20	41,600
13.583	15	0.25	20	42,380
13.833	15	0.25	20	43,160
14.083	15	0.25	20	43,940
14.333	15	0.25	20	44,720
14.583	15	0.25	20	45,500
14.833	15	0.25	20	46,280

Table A.1. Data collection Times and Sampling Rates for the Second Half of the Project (Continued).

Time from start of tracking, hrs	Interval for data collection, minutes	Duration of sampling, minutes	Sampling Freq, Hz (data points per second)	Cumulative # of wheel passes from the start of tracking
15.083	15	0.25	20	47,060
15.333	15	0.25	20	47,840
15.583	15	0.25	20	48,620
15.833	15	0.25	20	49,400
16.083	15	0.25	20	50,180
16.333	15	0.25	20	50,960
16.583	15	0.25	20	51,740
16.833	15	0.25	20	52,520

Table A.2. Data Collection Times and Sampling Rates for Low Speed.

Time from start of tracking, hrs	Interval for data collection, minutes[1]	Duration of sampling, minutes[2]	Sampling Freq, Hz (data points per second)	Cumulative # of wheel passes from the start of tracking
0.000	2[3]	2.00[4]	40	0
0.033	2	1.00	20	40
0.083	3	2.00	10	100
0.583	30	5.00	20	700
1.083	30	0.25	20	1,300
1.583	30	0.25	20	1,900
2.083	30	0.25	20	2,500
2.583	30	0.25	20	3,100
3.083	30	0.25	20	3,700
3.583	30	0.25	20	4,300
4.083	30	0.25	20	4,900
4.583	30	0.25	20	5,500
5.083	30	0.25	20	6,100
5.583	30	0.25	20	6,700
6.083	30	0.25	20	7,300
6.583	30	0.25	20	7,900
7.083	30	0.25	20	8,500
7.583	30	0.25	20	9,100
8.083	30	0.25	20	9,700
8.583	30	0.25	20	10,300
9.083	30	0.25	20	10,900
9.583	30	0.25	20	11,500
10.083	30	0.25	20	12,100
10.583	30	0.25	20	12,700
11.083	30	0.25	20	13,300
11.583	30	0.25	20	13,900
12.083	30	0.25	20	14,500
12.583	30	0.25	20	15,100
13.083	30	0.25	20	15,700
13.583	30	0.25	20	16,300
14.083	30	0.25	20	16,900
14.583	30	0.25	20	17,500
15.083	30	0.25	20	18,100
15.583	30	0.25	20	18,700
16.083	30	0.25	20	19,300
16.583	30	0.25	20	19,900

(1) The time interval selected for data collection

(2) Duration of data collection within the corresponding time interval.

(3) This first 2-minute time interval was before start of tracking.

(4) This 2-minute duration of data sampling at 0 time indicates the data collected for 2 minutes before the tracking started.

Table A.2. Data Collection Times and Sampling Rates for Low Speed (Continued).

Time from start of tracking, hrs	Interval for data collection, minutes	Duration of sampling, minutes	Sampling Freq, Hz (data points per second)	Cumulative # of wheel passes from the start of tracking
17.083	30	0.25	20	20,500
17.583	30	0.25	20	21,100
18.083	30	0.25	20	21,700
18.583	30	0.25	20	22,300
19.083	30	0.25	20	22,900
19.583	30	0.25	20	23,500
20.083	30	0.25	20	24,100
20.583	30	0.25	20	24,700
21.083	30	0.25	20	25,300
21.583	30	0.25	20	25,900
22.083	30	0.25	20	26,500
22.583	30	0.25	20	27,100
23.083	30	0.25	20	27,700
23.583	30	0.25	20	28,300
24.083	30	0.25	20	28,900
24.583	30	0.25	20	29,500
25.083	30	0.25	20	30,100
25.583	30	0.25	20	30,700
26.083	30	0.25	20	31,300
26.583	30	0.25	20	31,900
27.083	30	0.25	20	32,500
27.583	30	0.25	20	33,100
28.083	30	0.25	20	33,700
28.583	30	0.25	20	34,300
29.083	30	0.25	20	34,900
29.583	30	0.25	20	35,500
30.083	30	0.25	20	36,100
30.583	30	0.25	20	36,700
31.083	30	0.25	20	37,300
31.583	30	0.25	20	37,900
32.083	30	0.25	20	38,500
32.583	30	0.25	20	39,100
33.083	30	0.25	20	39,700
33.583	30	0.25	20	40,300
34.083	30	0.25	20	40,900
34.583	30	0.25	20	41,500
35.083	30	0.25	20	42,100
35.583	30	0.25	20	42,700
36.083	30	0.25	20	43,300
36.583	30	0.25	20	43,900
37.083	30	0.25	20	44,500
37.583	30	0.25	20	45,100
38.083	30	0.25	20	45,700

Table A.2. Data Collection Times and Sampling Rates for Low Speed (Continued).

Time from start of tracking, hrs	Interval for data collection, minutes	Duration of sampling, minutes	Sampling Freq, Hz (data points per second)	Cumulative # of wheel passes from the start of tracking
38.583	30	0.25	20	46,300
39.083	30	0.25	20	46,900
39.583	30	0.25	20	47,500
40.083	30	0.25	20	48,100
40.583	30	0.25	20	48,700
41.083	30	0.25	20	49,300
41.583	30	0.25	20	49,900
42.083	30	0.25	20	50,500
42.583	30	0.25	20	51,100
43.083	30	0.25	20	51,700
43.583	30	0.25	20	52,300
44.083	30	0.25	20	52,900
44.583	30	0.25	20	53,500
45.083	30	0.25	20	54,100

APPENDIX B

Graphs of Strain Amplitude versus Tracking Time in HWTD

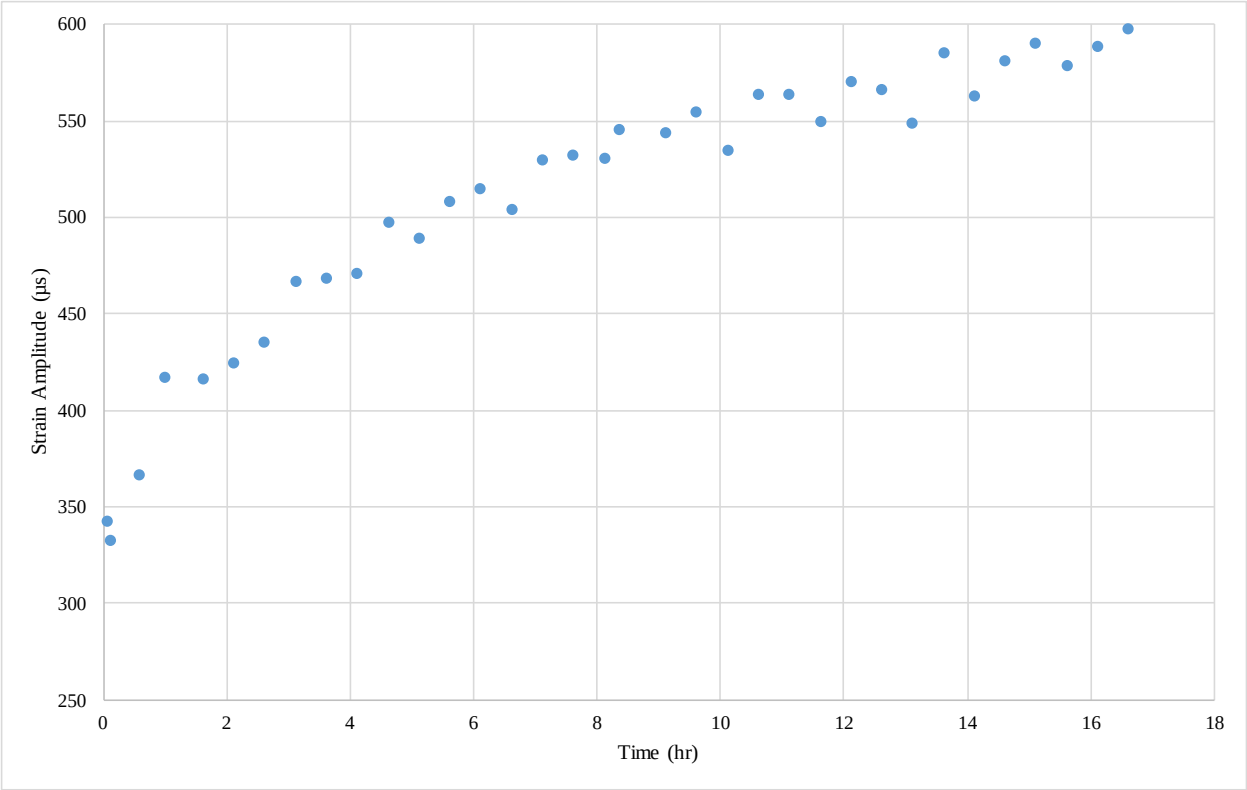

Figure B.1. The longitudinal strain amplitude for Mix #1 with the thickness of 1.5" placed on the Neoprene 60A with bonding condition.

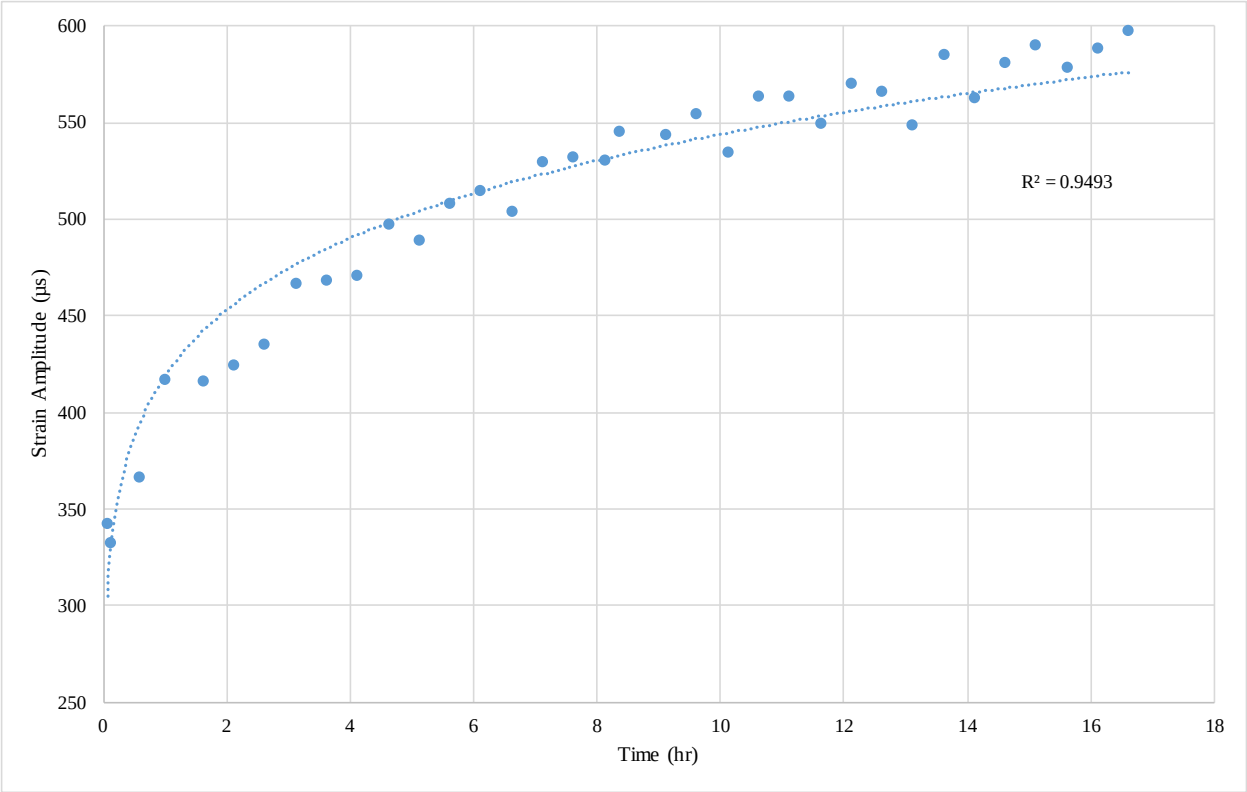

Figure B.2. The fitted power line on the longitudinal strain amplitude for Mix #1 with the thickness of 1.5" placed on the Neoprene 60A with bonding condition.

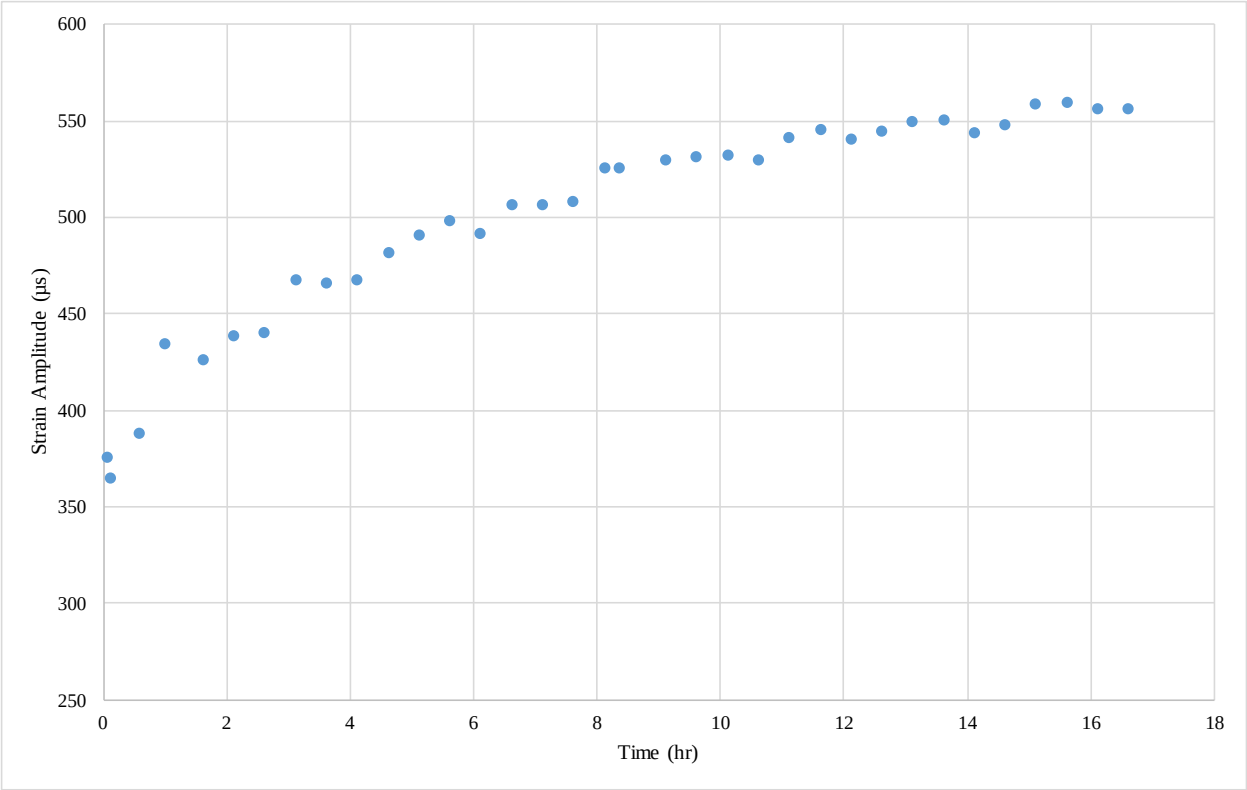

Figure B.3. The longitudinal strain amplitude for Mix #1 with the thickness of 1.5" placed on the Neoprene 60A with bonding condition (Second Slab).

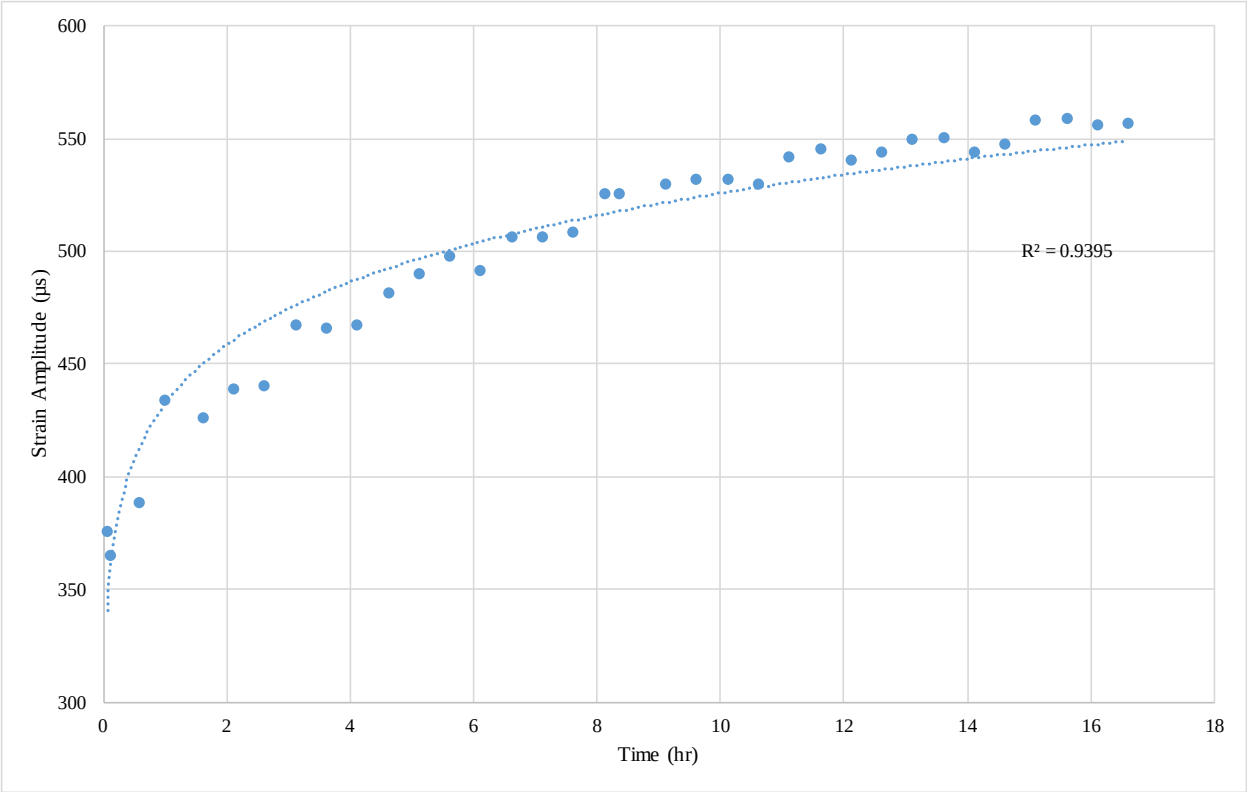

Figure B.4. The fitted power line on the longitudinal strain amplitude for Mix #1 with the thickness of 1.5" placed on the Neoprene 60A with bonding condition (Second Slab).

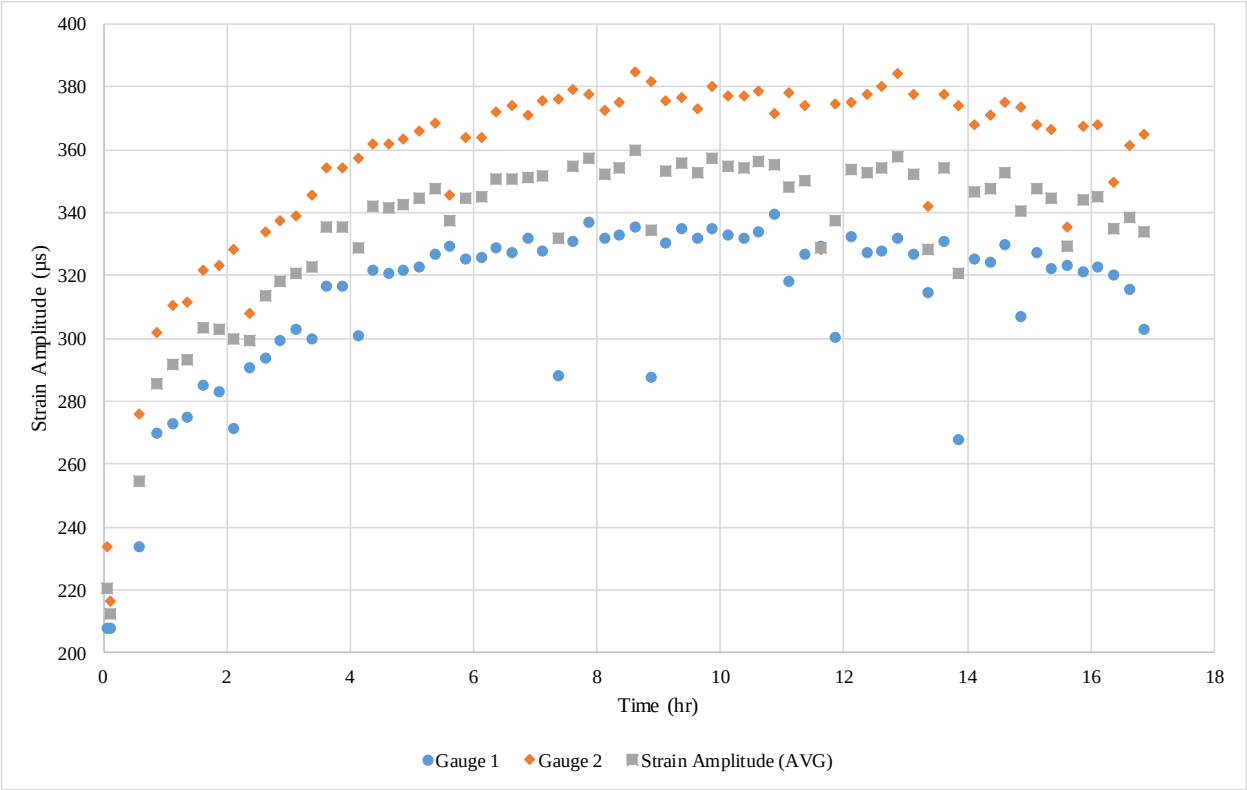

Figure B.5. The longitudinal strain amplitude for Mix #1 with the thickness of 2" placed on the Neoprene 60A with bonding condition.

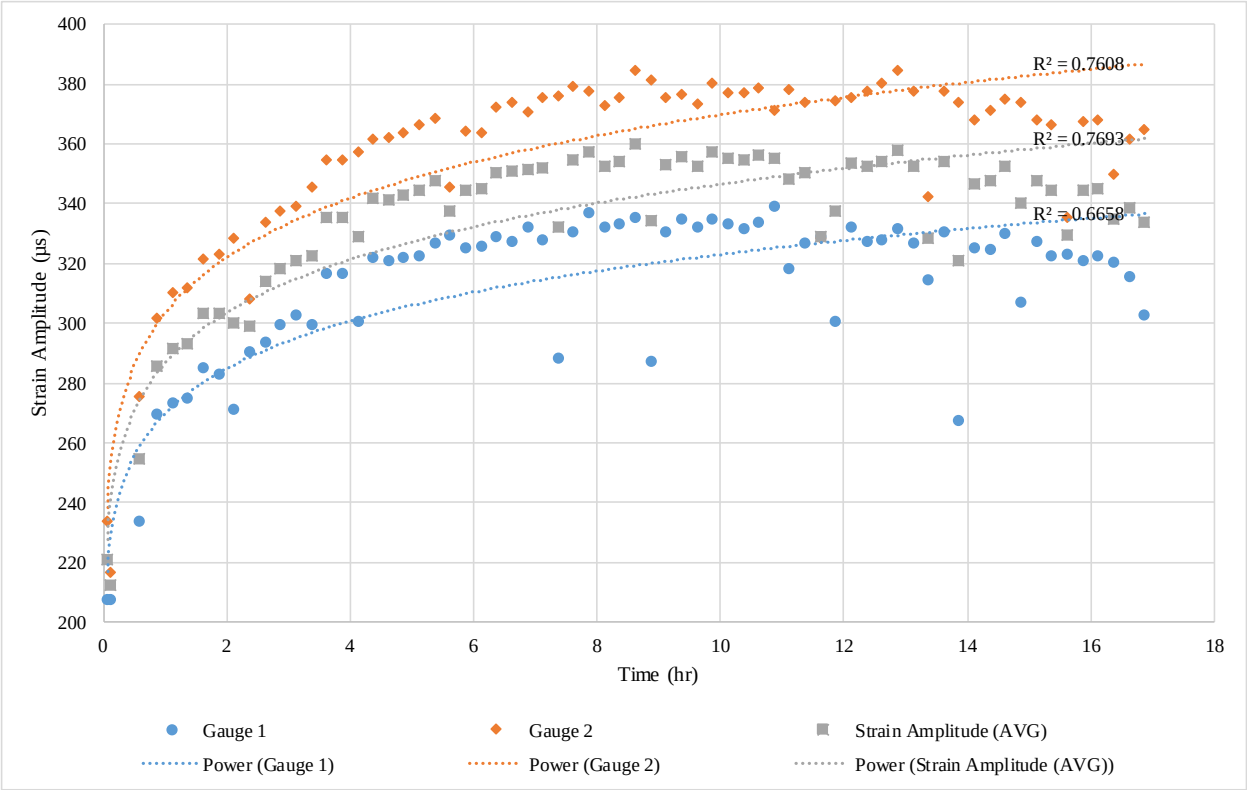

Figure B.6. The fitted power line on the longitudinal strain amplitude for Mix #1 with the thickness of 2" placed on the Neoprene 60A with bonding condition.

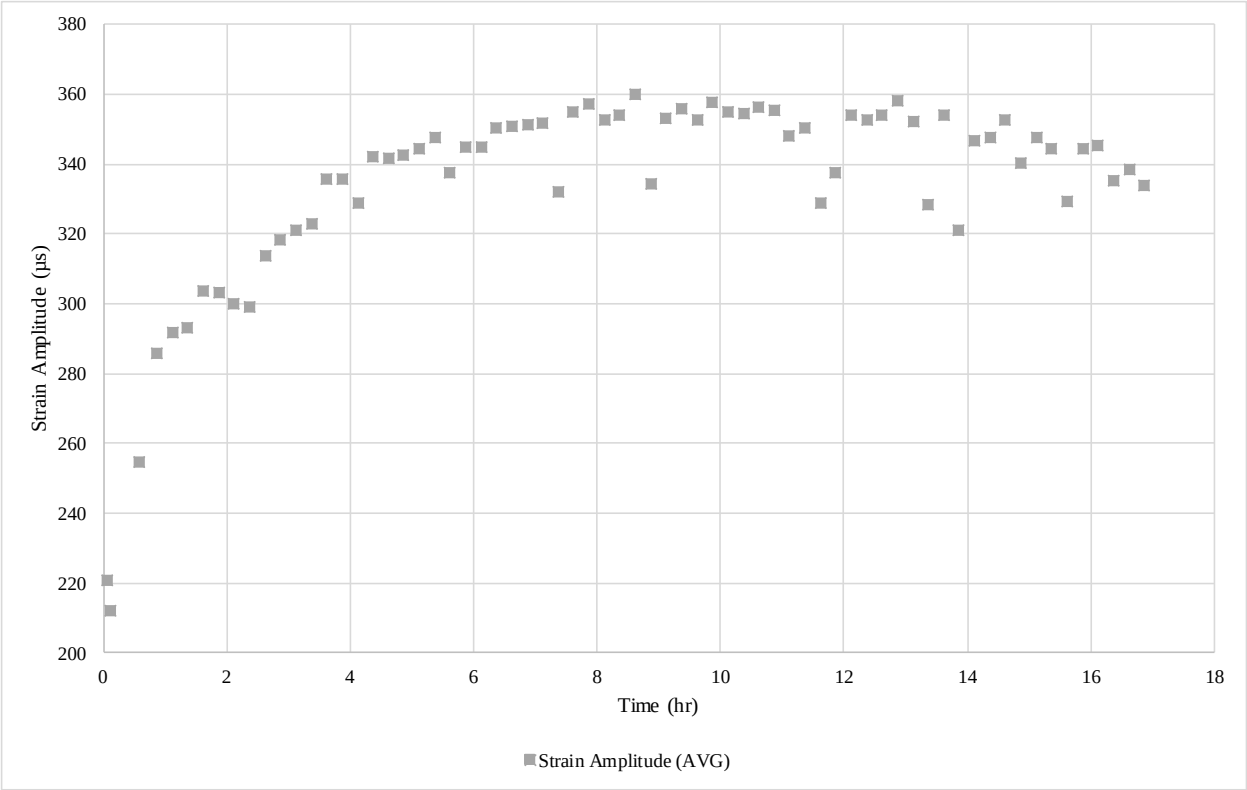

Figure B.7. The average longitudinal strain amplitude for Mix #1 with the thickness of 2" placed on the Neoprene 60A with bonding condition.

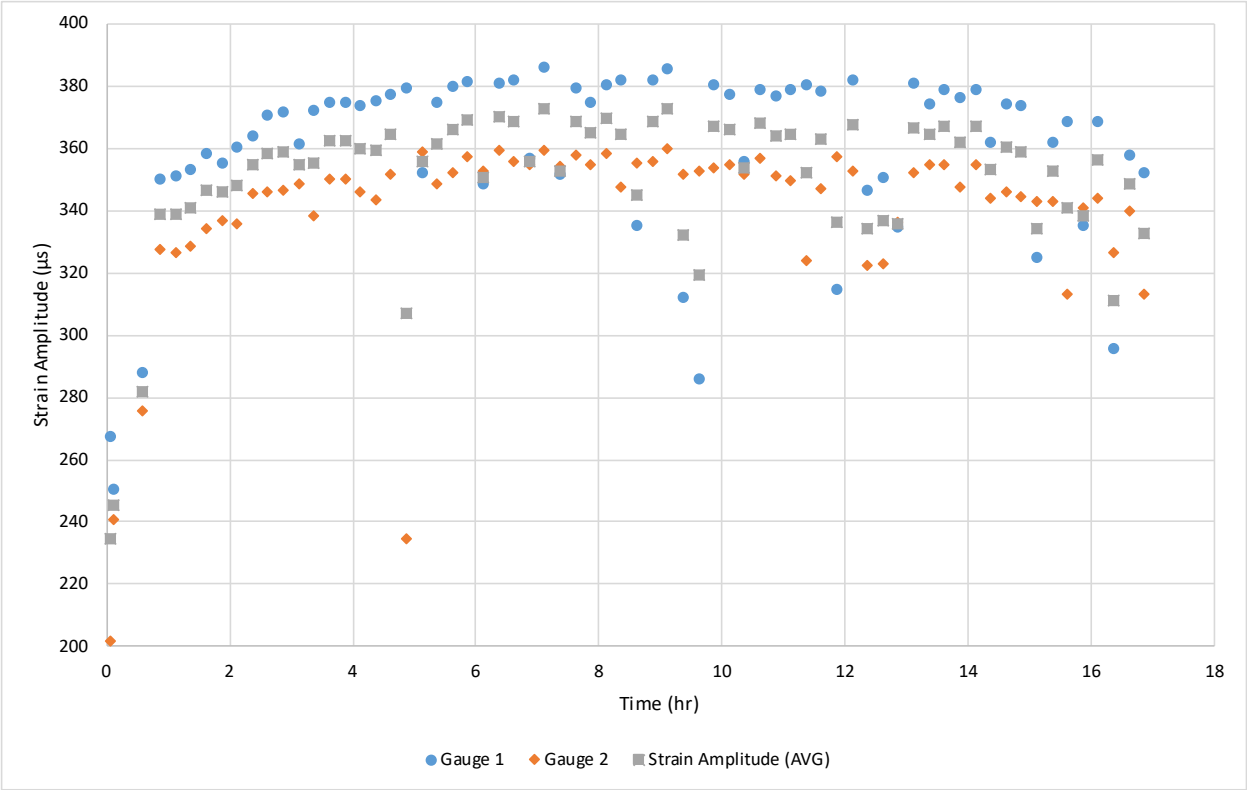

Figure B.8. The longitudinal strain amplitude for Mix #1 with the thickness of 2" placed on the Neoprene 60A with bonding condition (Second Slab).

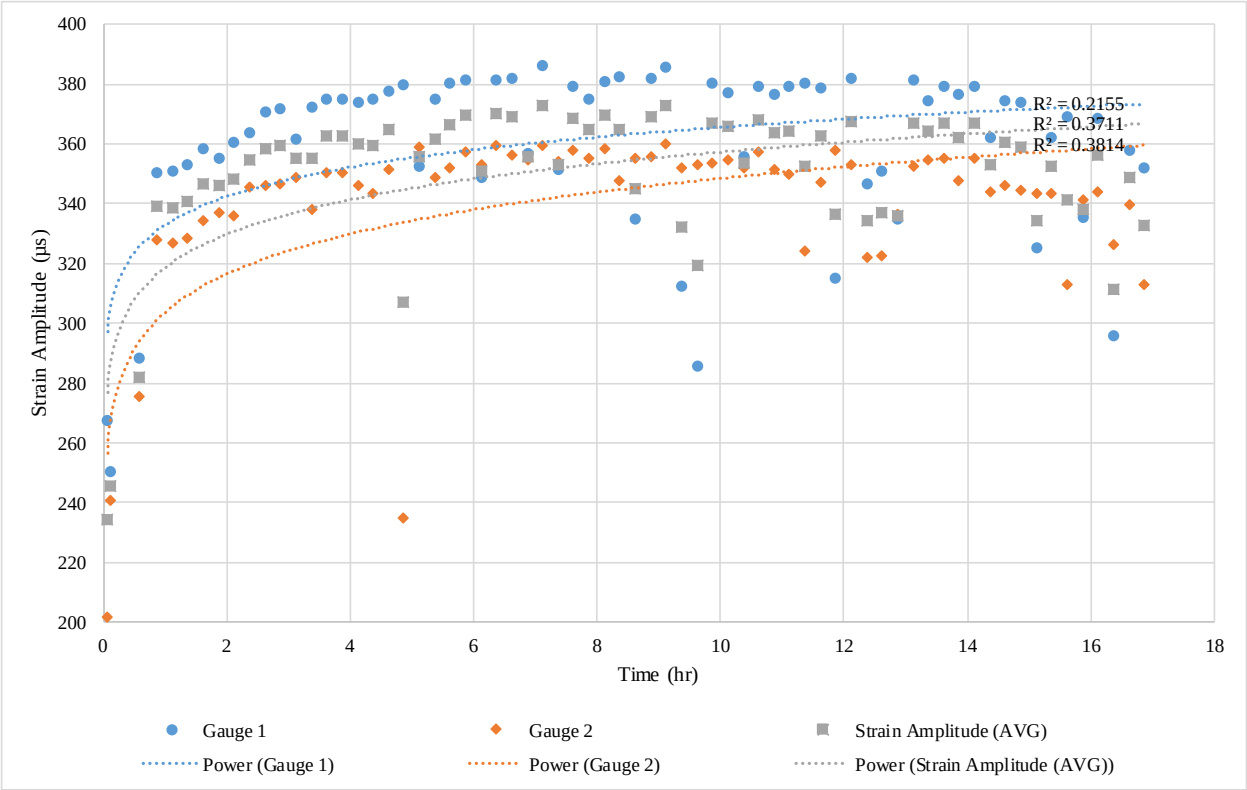

Figure B.9. The fitted power line on the longitudinal strain amplitude for Mix #1 with the thickness of 2" placed on the Neoprene 60A with bonding condition (Second Slab).

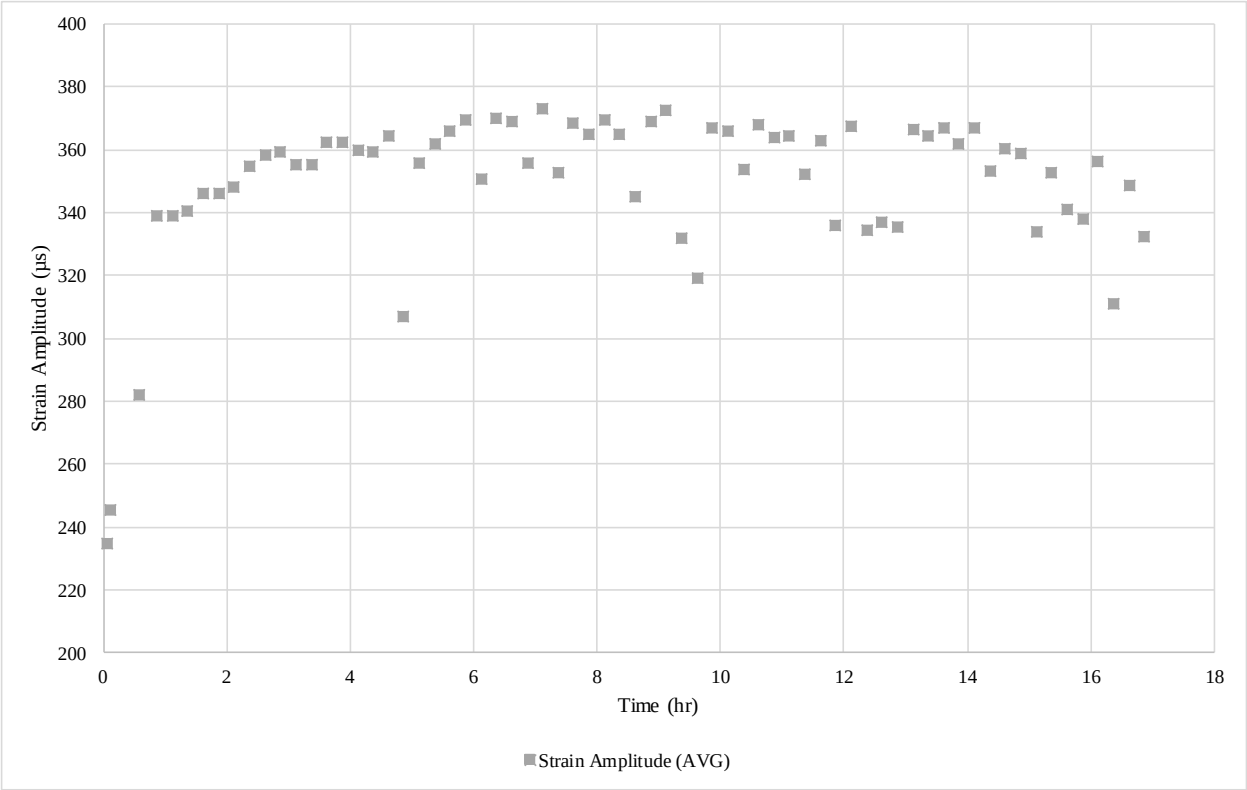

Figure B.10. The average longitudinal strain amplitude for Mix #1 with the thickness of 2" placed on the Neoprene 60A with bonding condition (Second Slab).

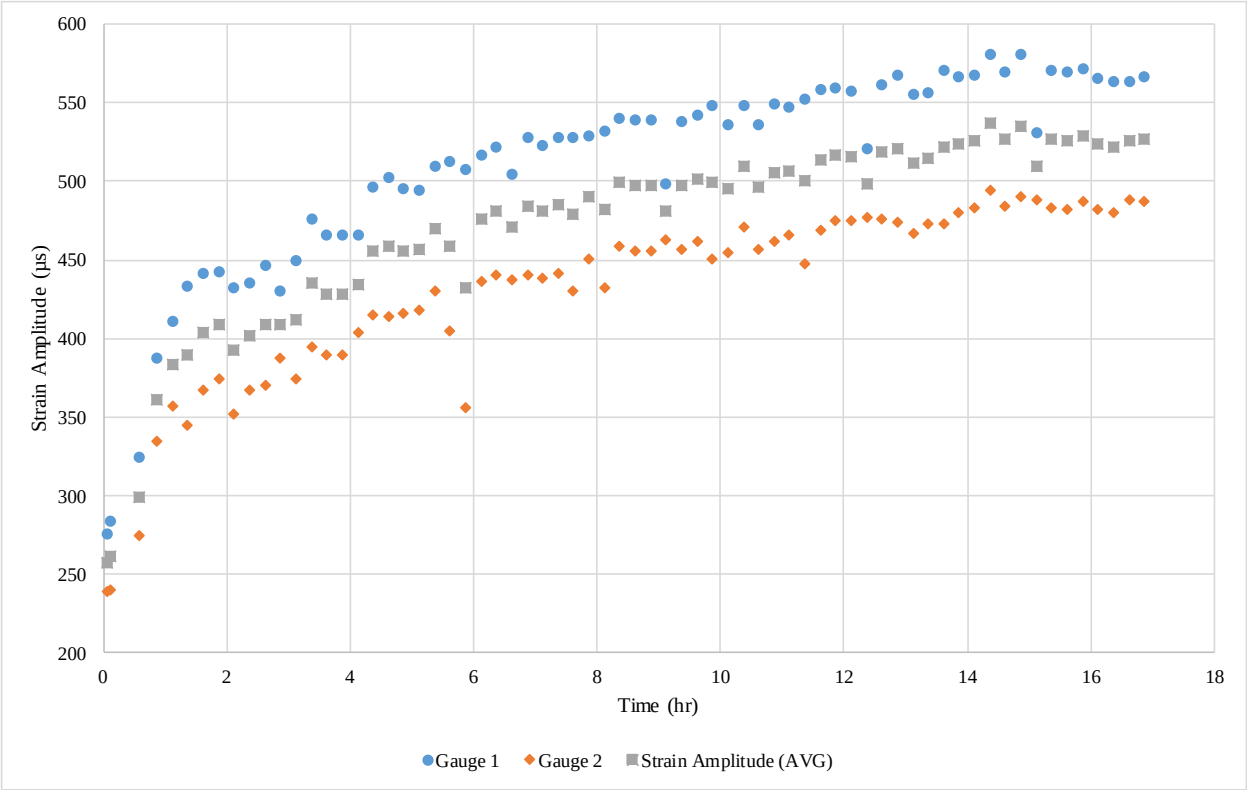

Figure B.11. The longitudinal strain amplitude for Mix #1 with the thickness of 1.5" placed on the Neoprene 40A with bonding condition.

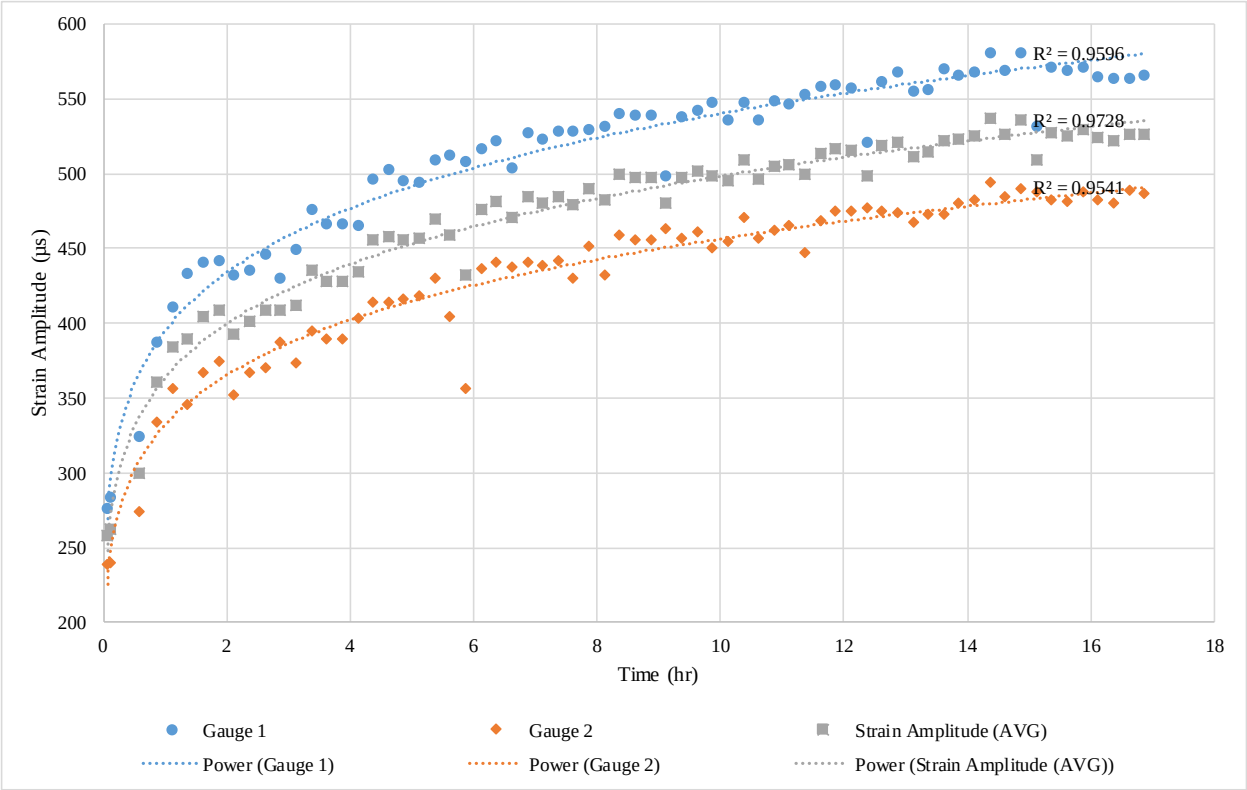

Figure B.12. The fitted power line on the longitudinal strain amplitude for Mix #1 with the thickness of 1.5" placed on the Neoprene 40A with bonding condition.

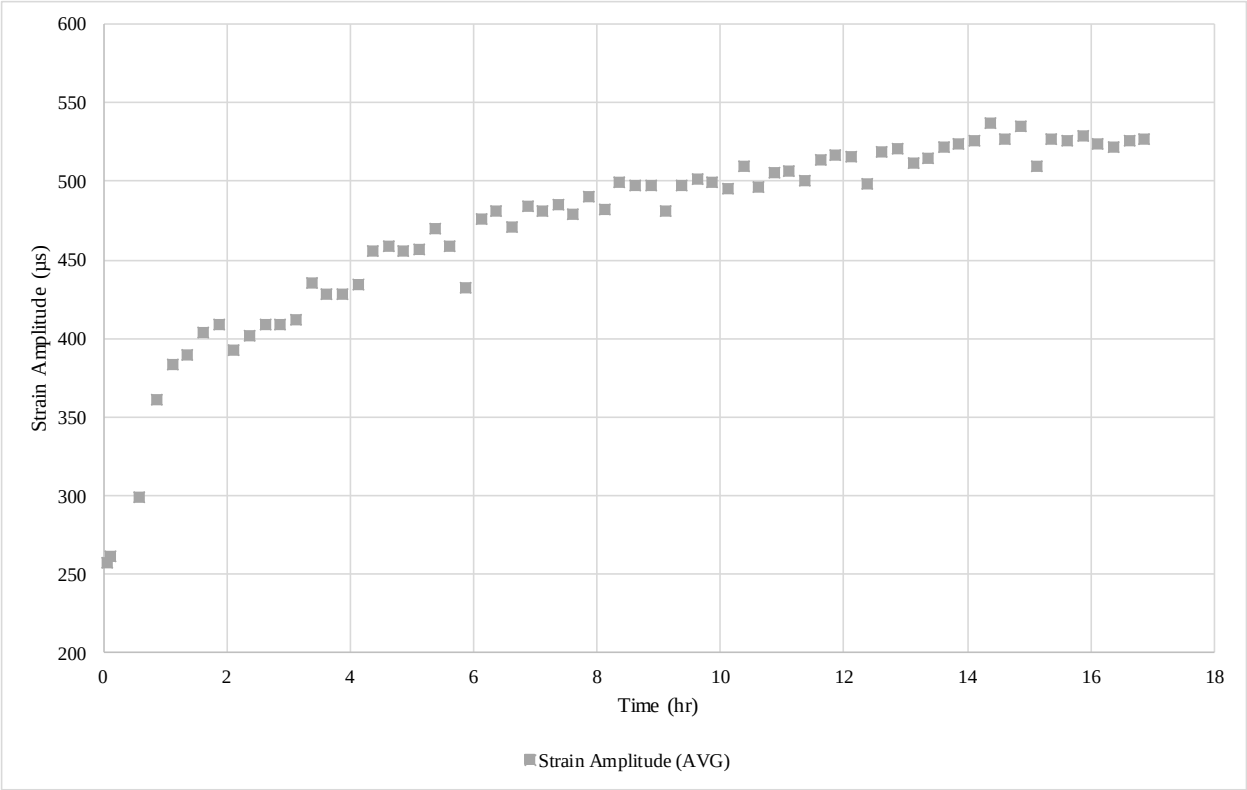

Figure B.13. The average longitudinal strain amplitude for Mix #1 with the thickness of 1.5" placed on the Neoprene 40A with bonding condition.

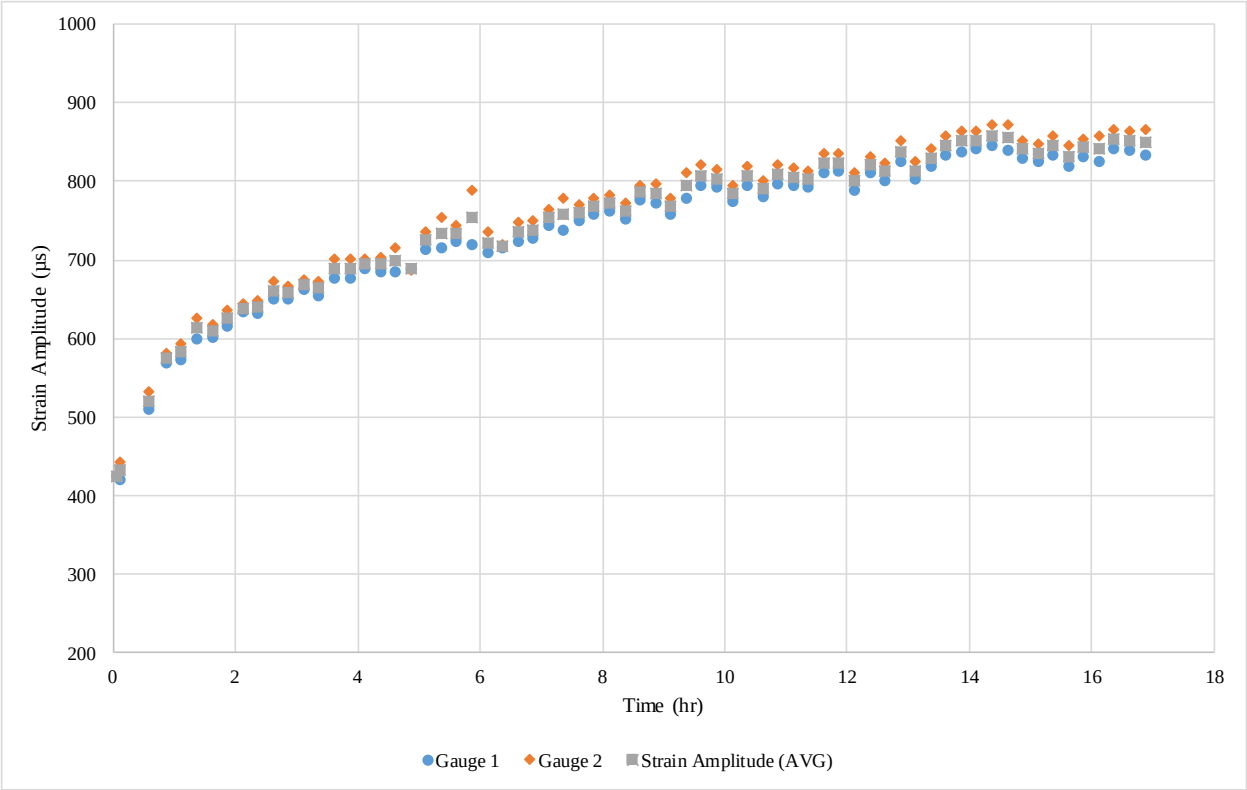

Figure B.14. The longitudinal strain amplitude for Mix #1 with the thickness of 1.5" placed on the Neoprene 40A with bonding condition (Second Slab).

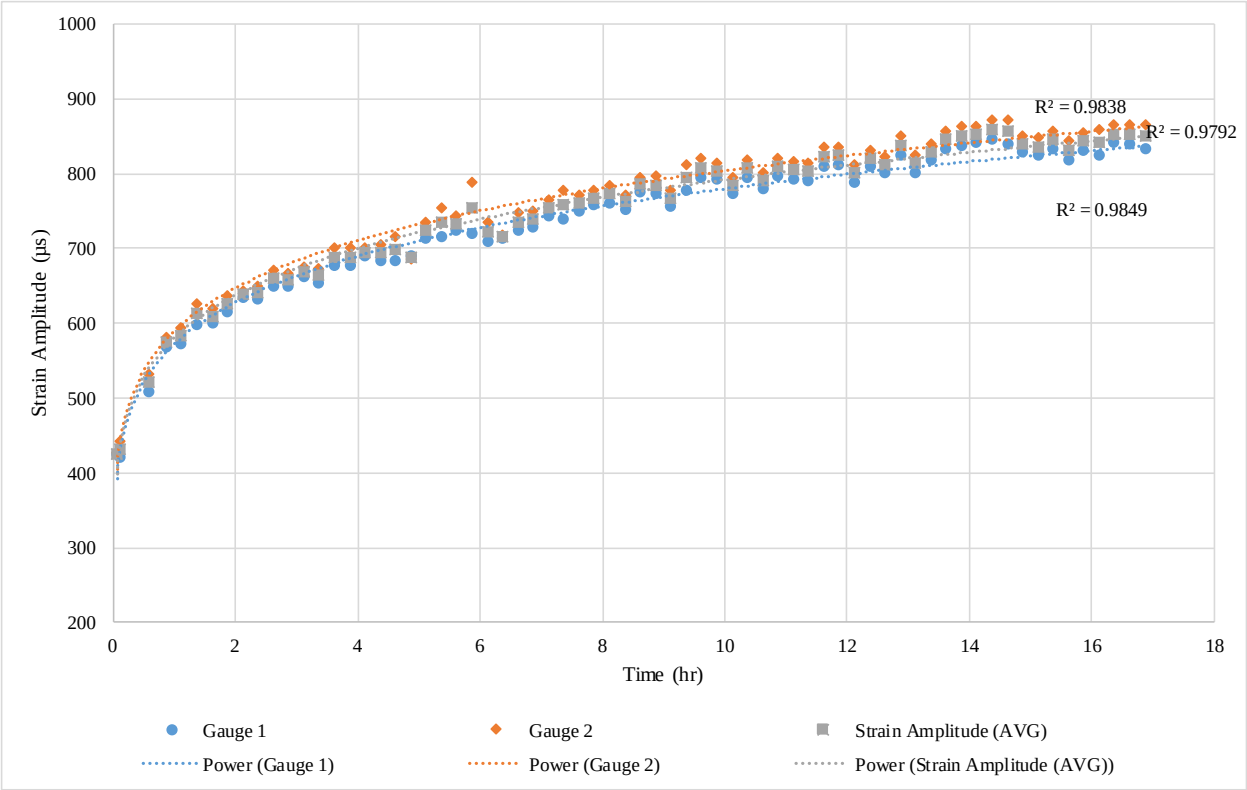

Figure B.15. The fitted power line on the longitudinal strain amplitude for Mix #1 with the thickness of 1.5" placed on the Neoprene 40A with bonding condition (Second Slab).

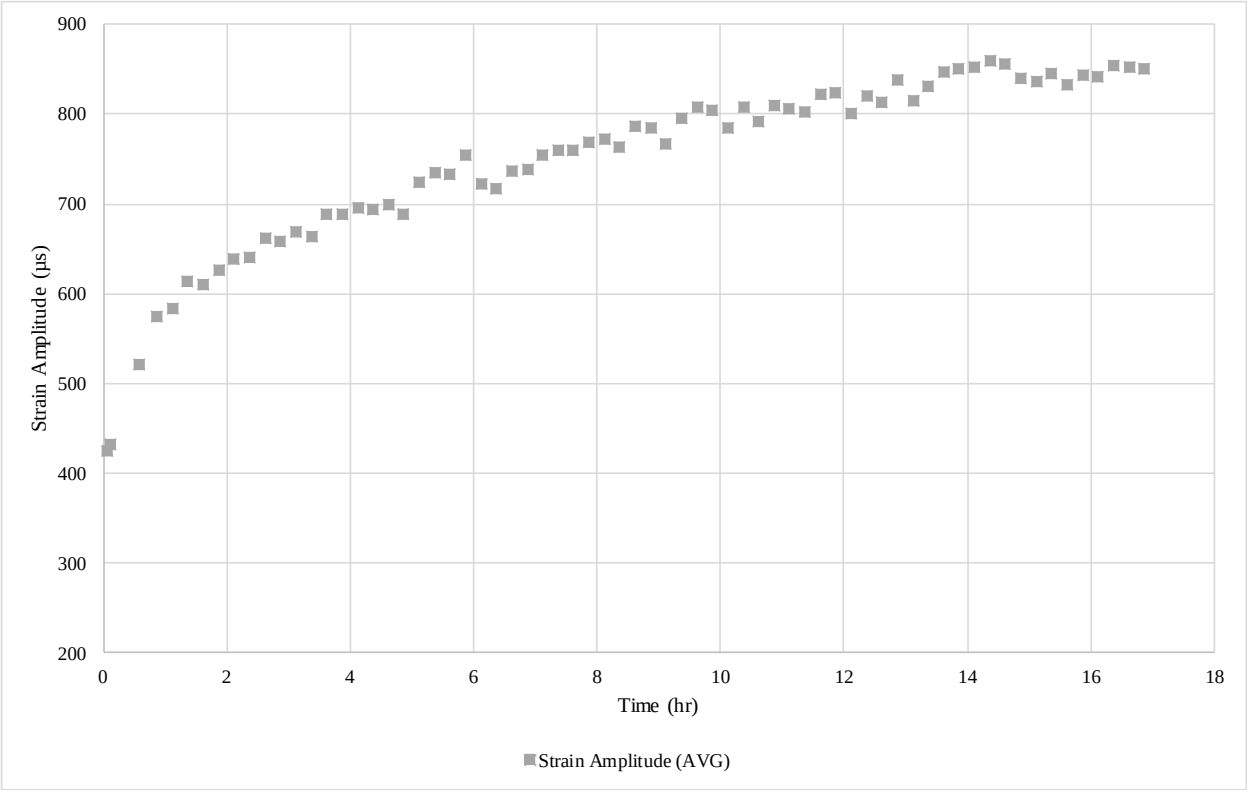

Figure B.16. The average longitudinal strain amplitude for Mix #1 with the thickness of 1.5" placed on the Neoprene 40A with bonding condition (Second Slab).

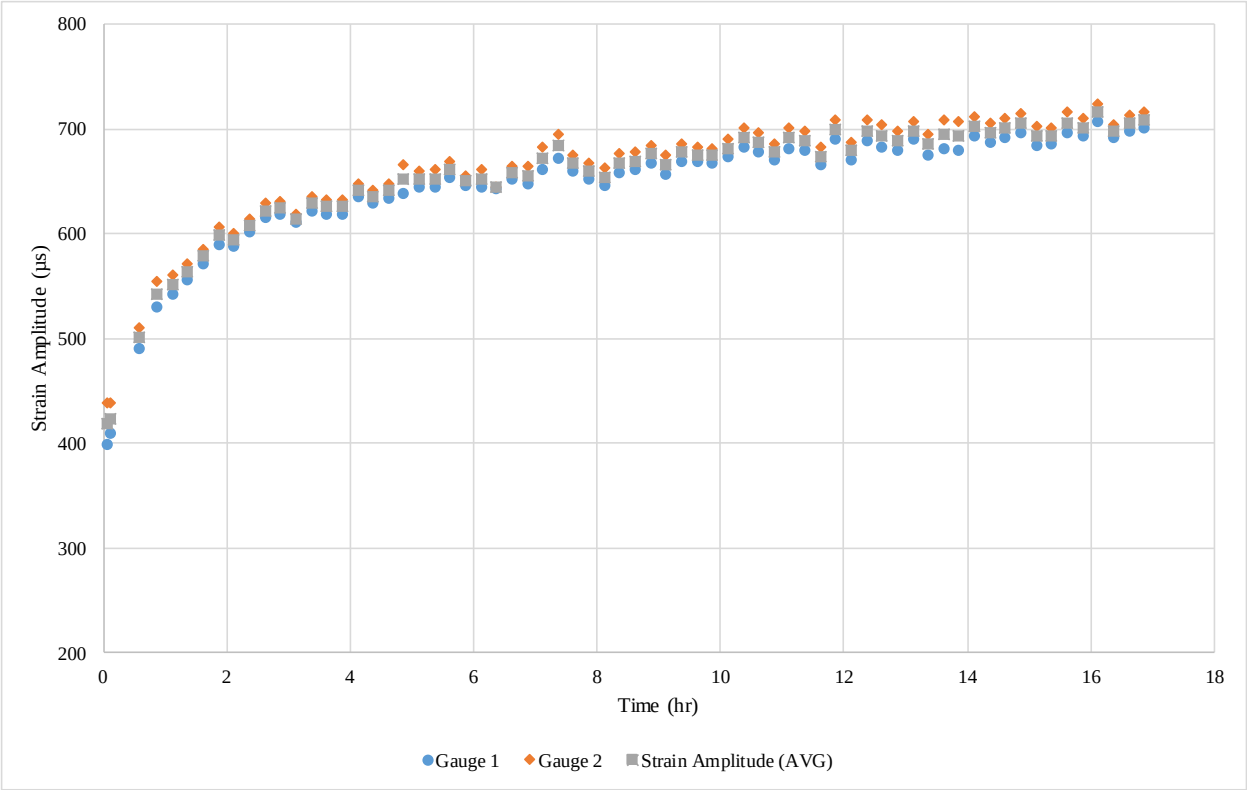

Figure B.17. The longitudinal strain amplitude for Mix #1 with the thickness of 1.5" and the width of 4" placed on the Neoprene 60A with bonding condition.

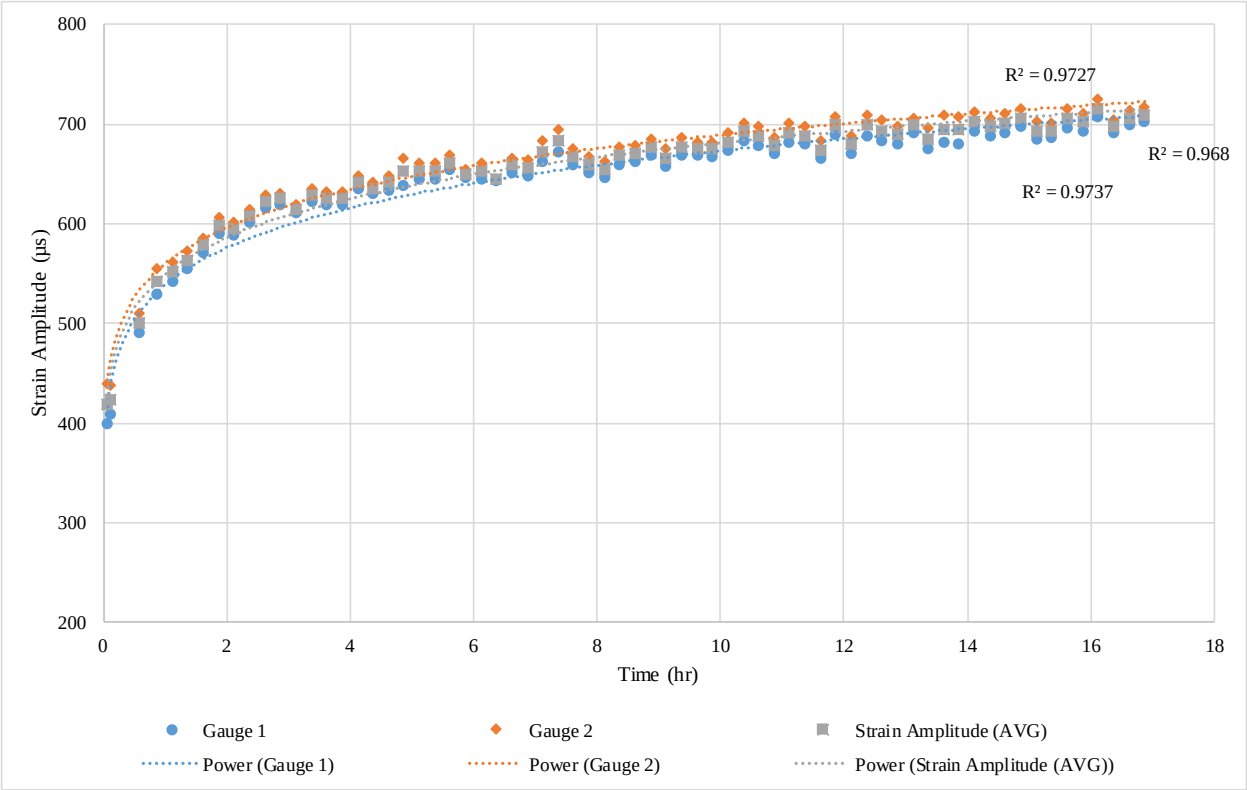

Figure B.18. The fitted power line on the longitudinal strain amplitude for Mix #1 with the thickness of 1.5" and the width of 4" placed on the Neoprene 60A with bonding condition.

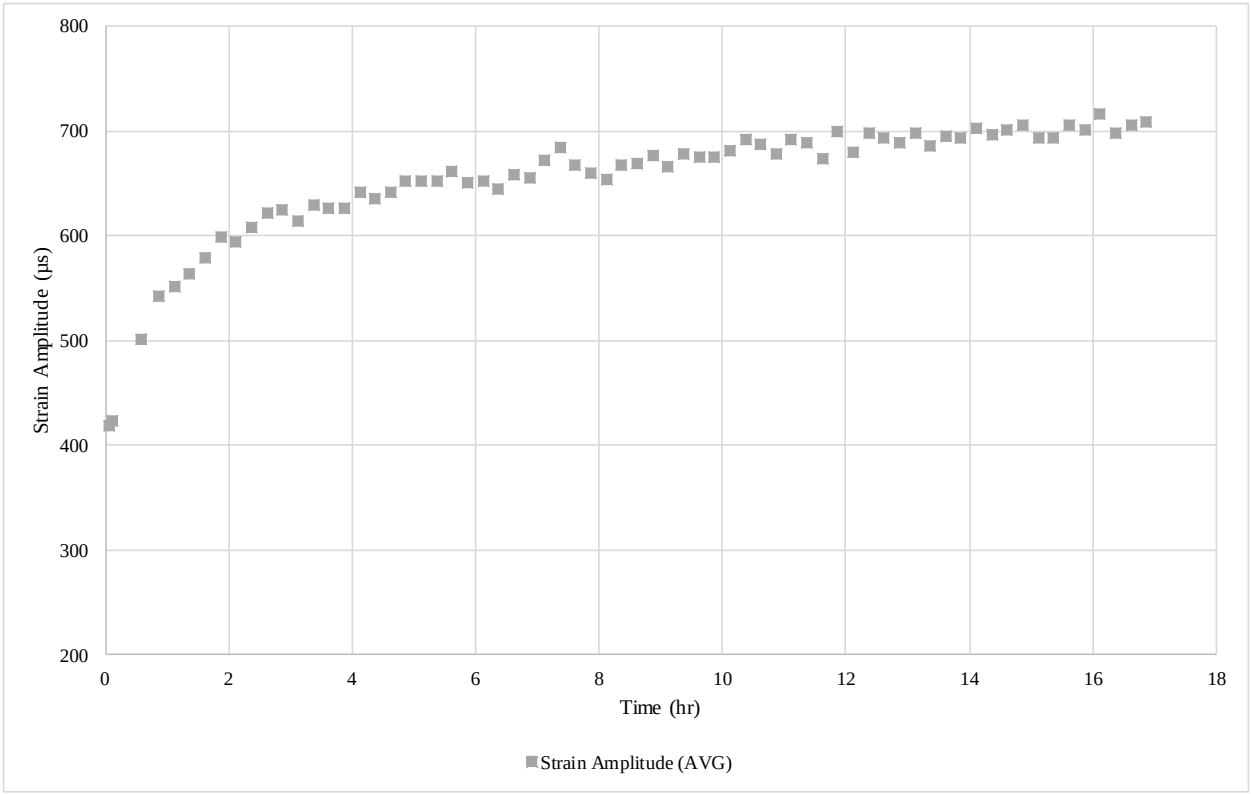

Figure B.19. The average longitudinal strain amplitude for Mix #1 with the thickness of 1.5" and width of 4" placed on the Neoprene 60A with bonding condition.

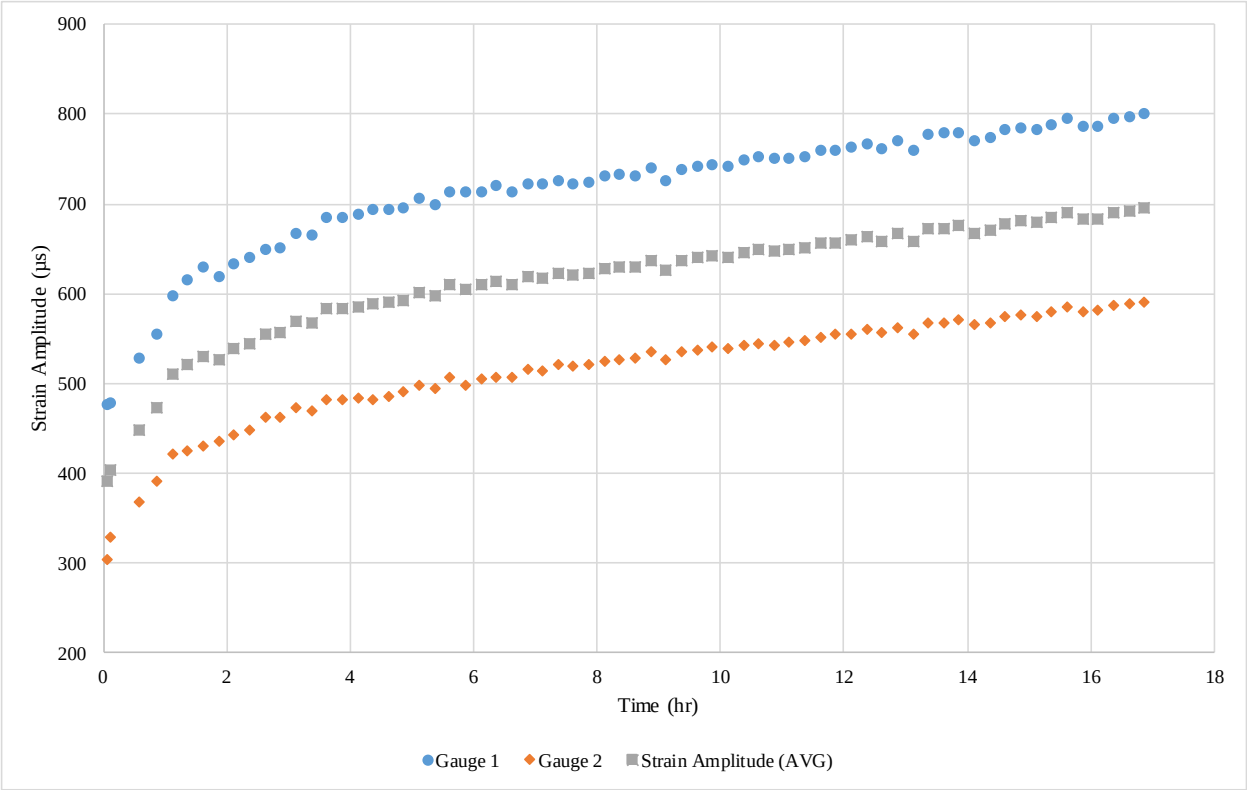

Figure B.20. The longitudinal strain amplitude for Mix #1 with the thickness of 1.5" and the width of 4" placed on the Neoprene 60A with bonding condition (Second Slab).

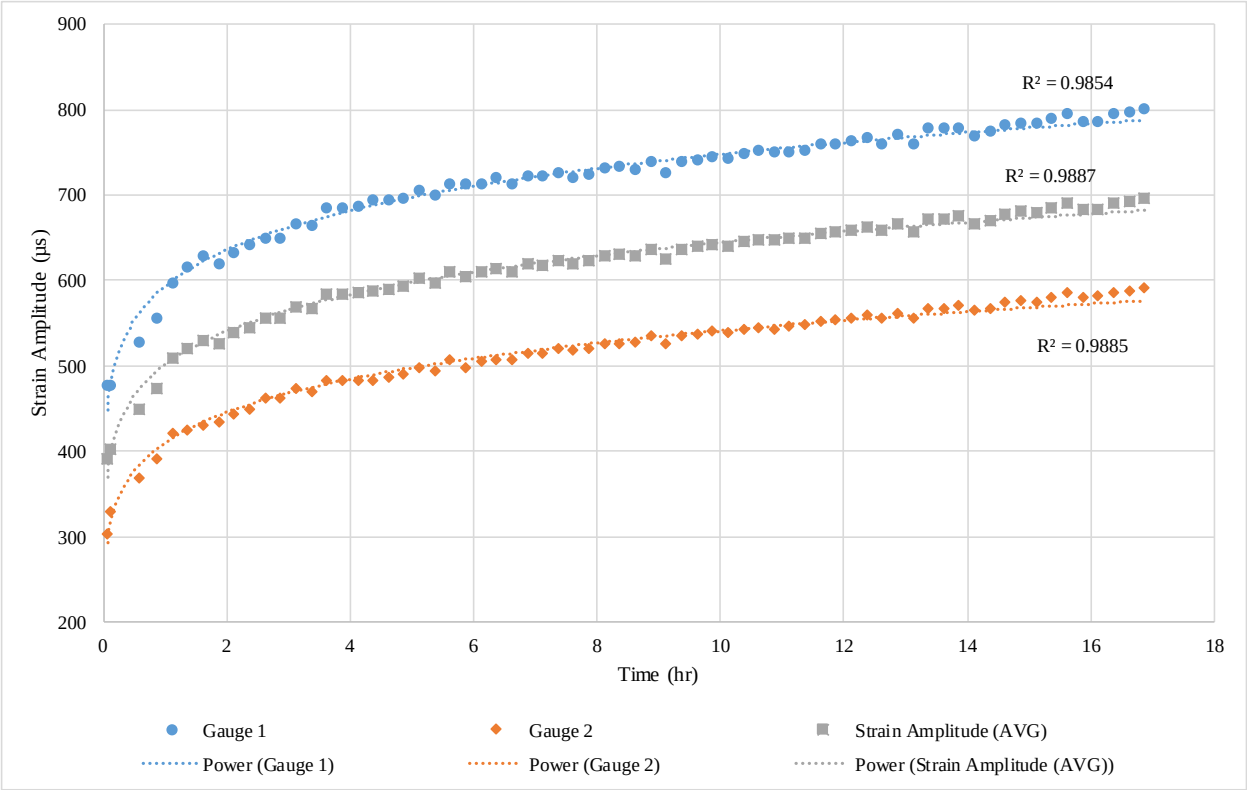

Figure B.21. The fitted power line on the longitudinal strain amplitude for Mix #1 with the thickness of 1.5" and the width of 4" placed on the Neoprene 60A with bonding condition (Second Slab).

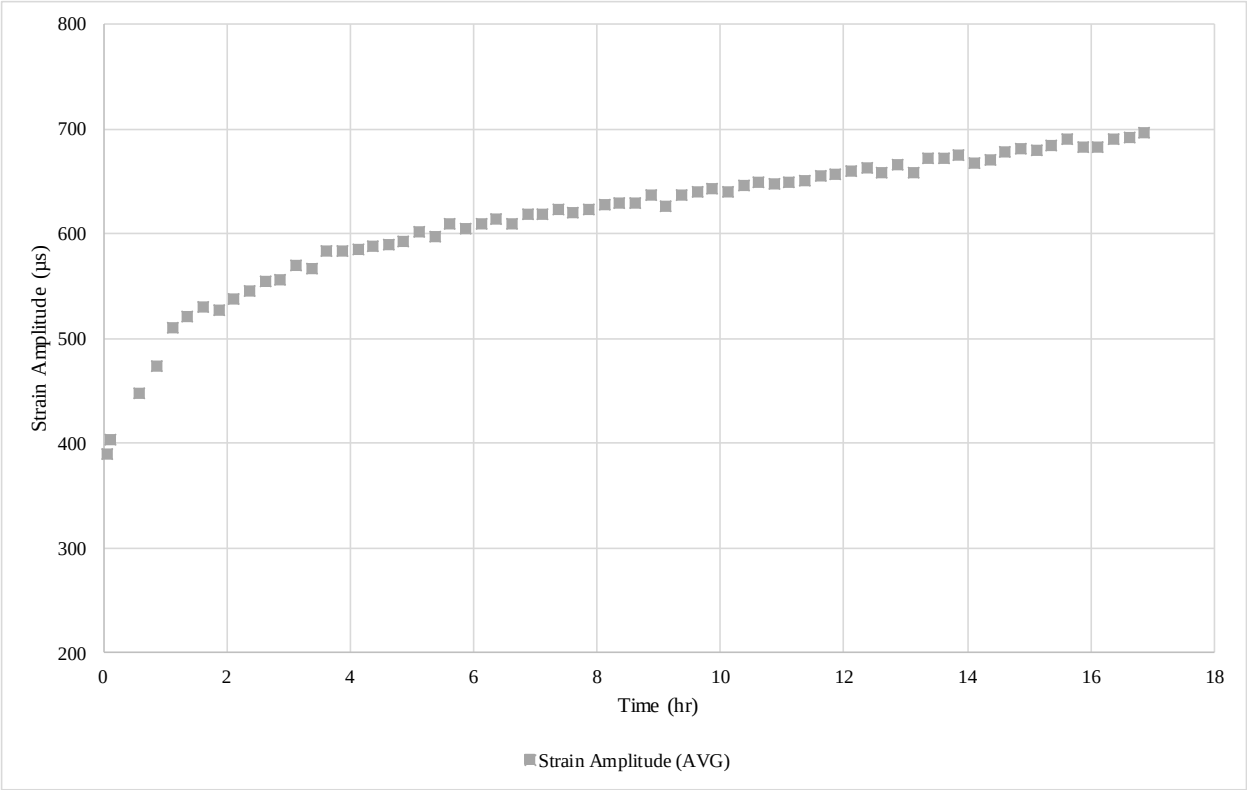

Figure B.22. The average longitudinal strain amplitude for Mix #1 with the thickness of 1.5" and width of 4" placed on the Neoprene 60A with bonding condition (Second Slab).

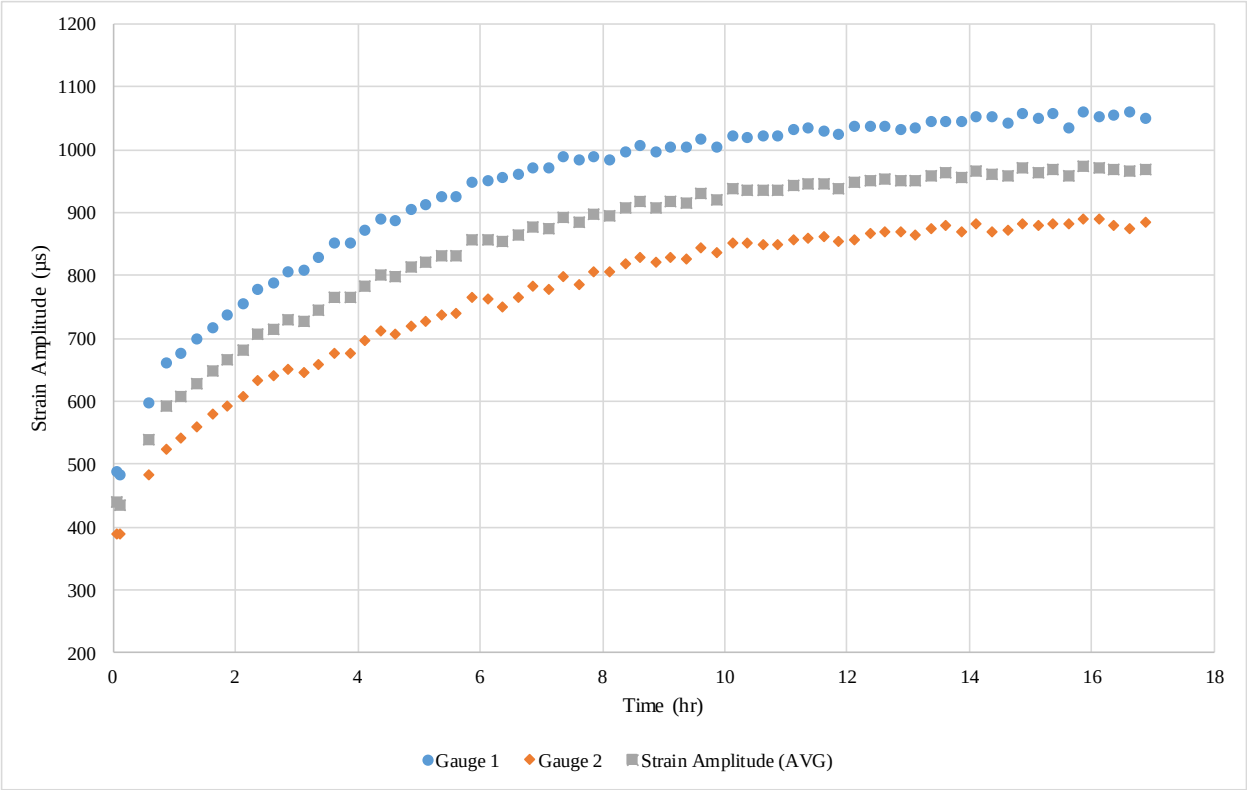

Figure B.23. The longitudinal strain amplitude for Mix #1 with the thickness of 1.5" placed on the Neoprene 60A with bonding condition tested at 30°C.

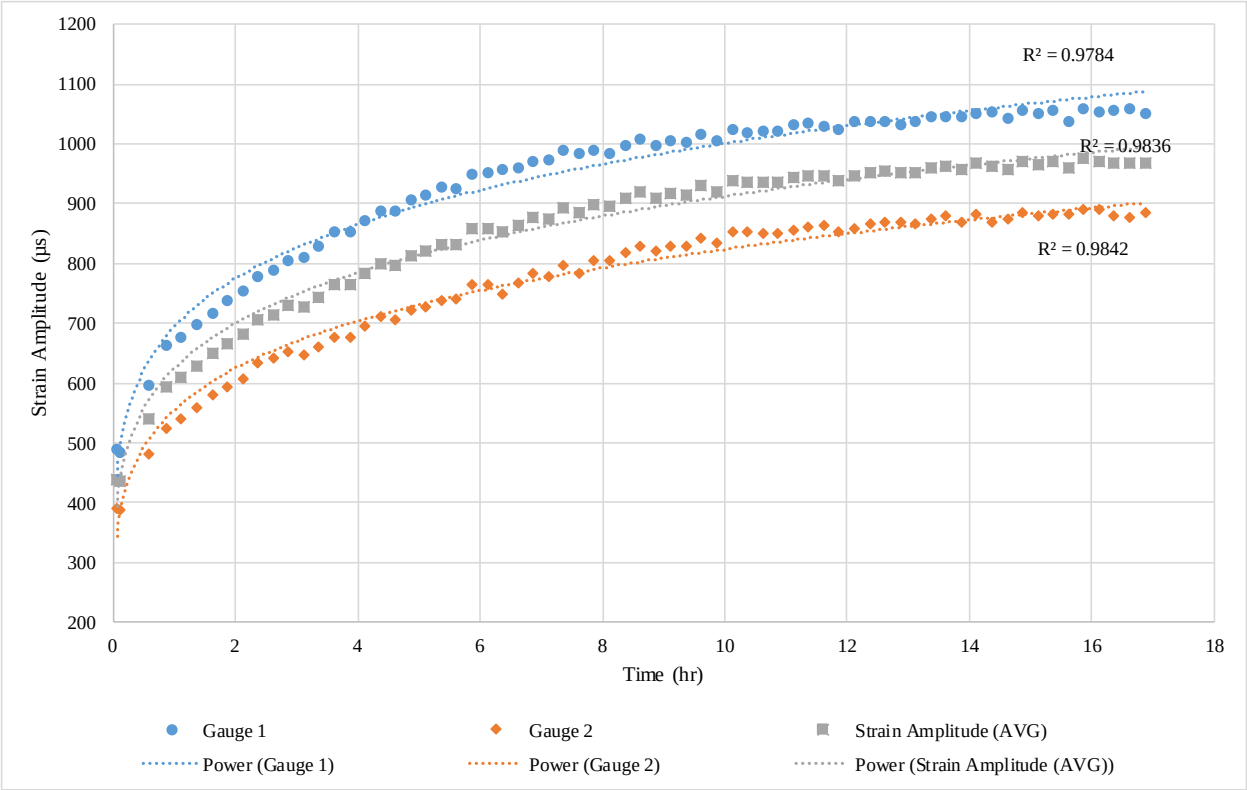

Figure B.24. The fitted power line on the longitudinal strain amplitude for Mix #1 with the thickness of 1.5" placed on the Neoprene 60A with bonding condition tested at 30°C.

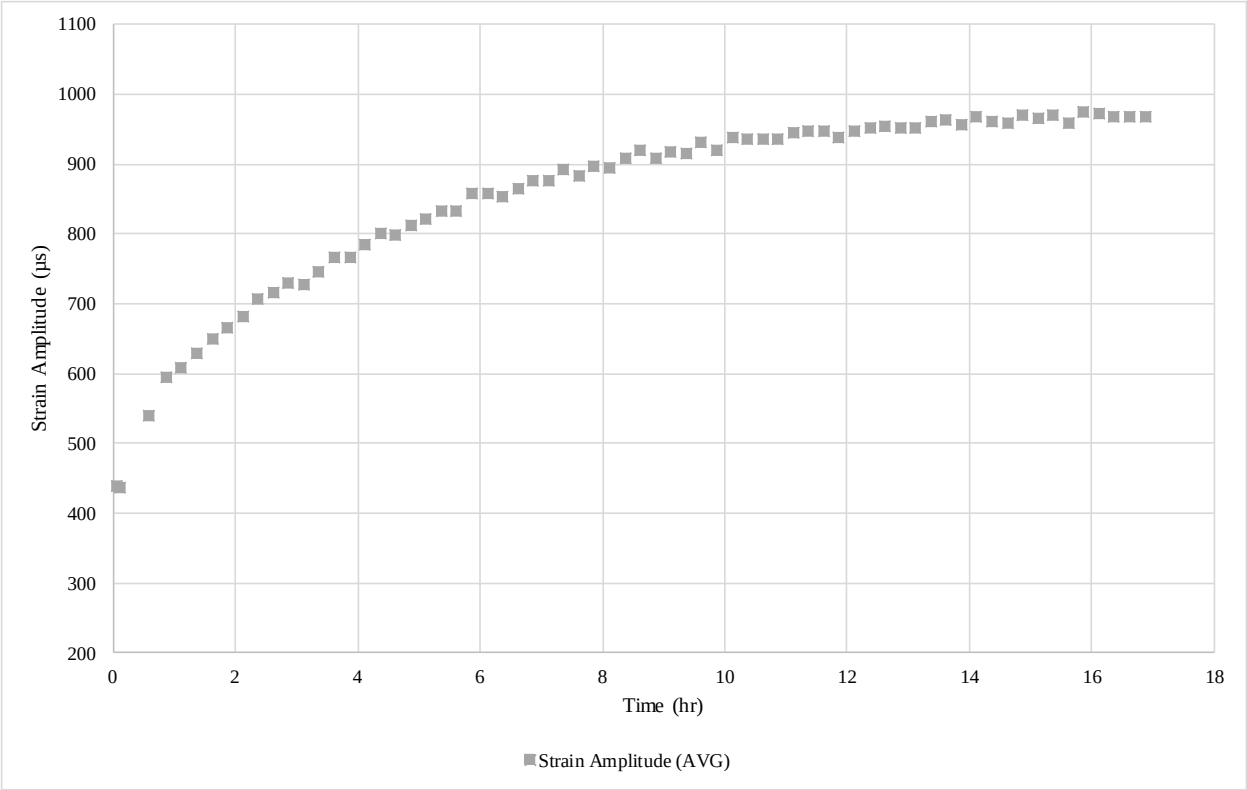

Figure B.25. The average longitudinal strain amplitude for Mix #1 with the thickness of 1.5" placed on the Neoprene 60A with bonding condition tested at 30°C.

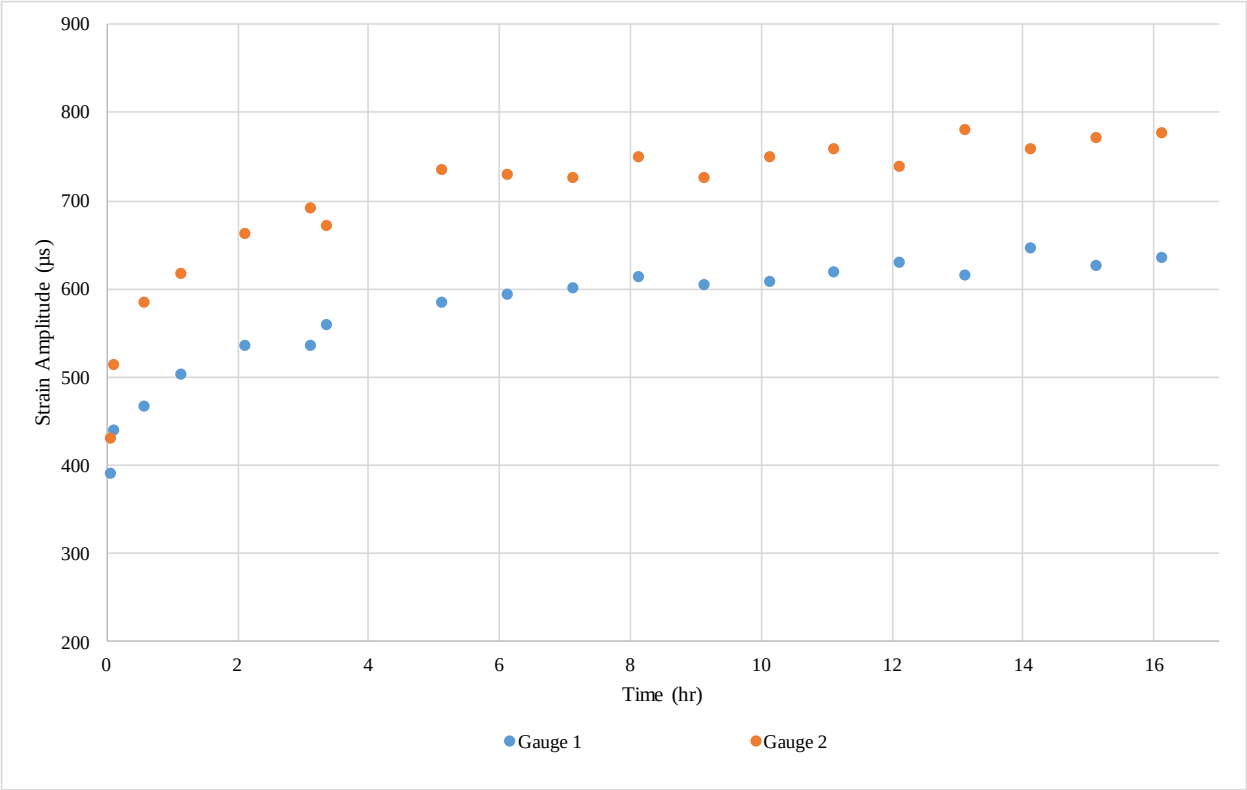

Figure B.26. The longitudinal strain amplitude for Mix #1 with the thickness of 1.5" placed on the Neoprene 60A with bonding condition and under low-speed loading condition.

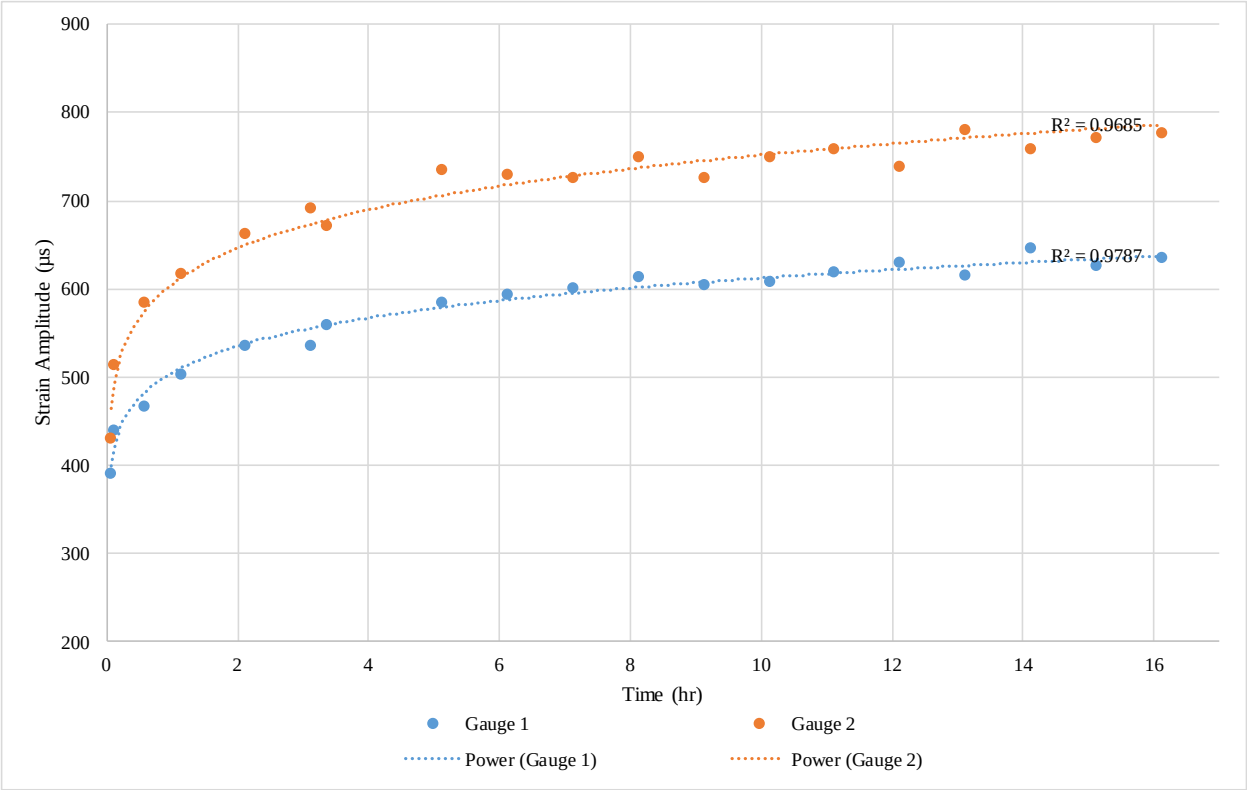

Figure B.27. The fitted power line on the longitudinal strain amplitude for Mix #1 with the thickness of 1.5" placed on the Neoprene 60A with bonding condition and under low-speed loading condition.

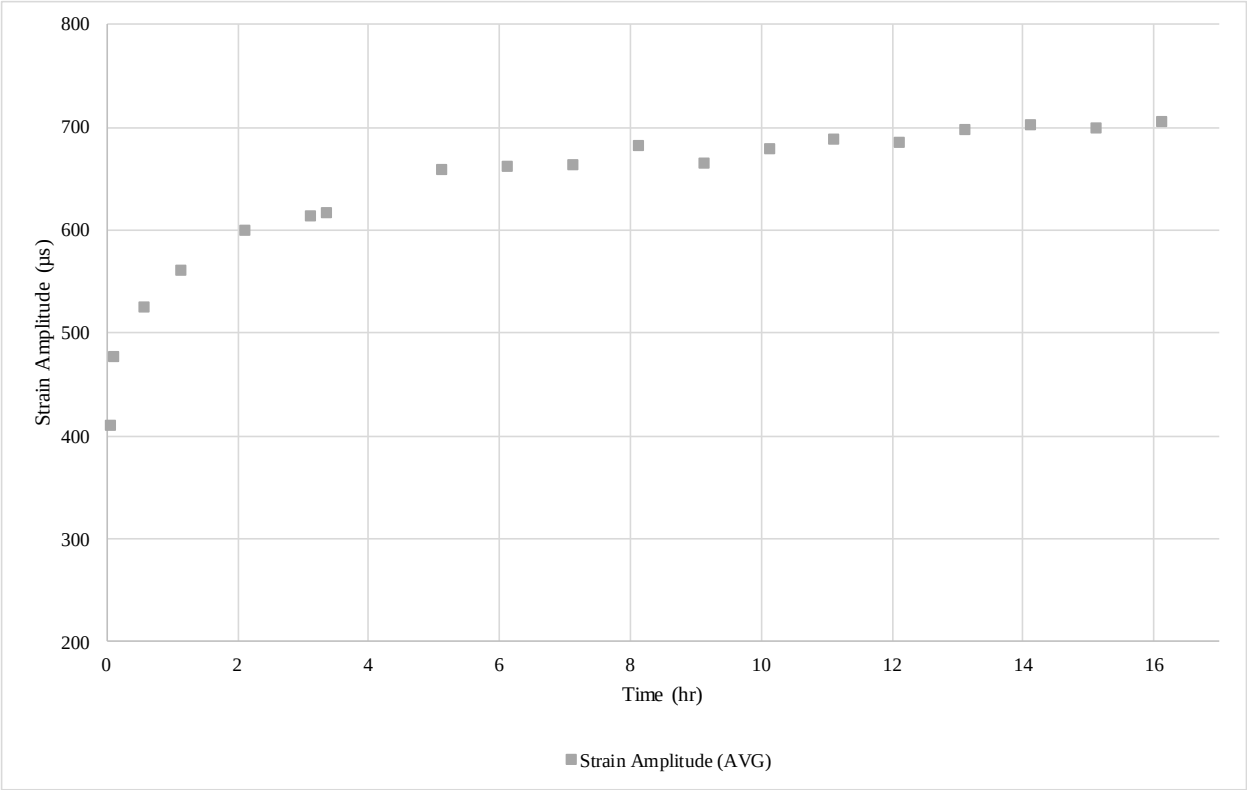

Figure B.28. The average longitudinal strain amplitude for Mix #1 with the thickness of 1.5" placed on the Neoprene 60A with bonding condition and under low-speed loading condition.

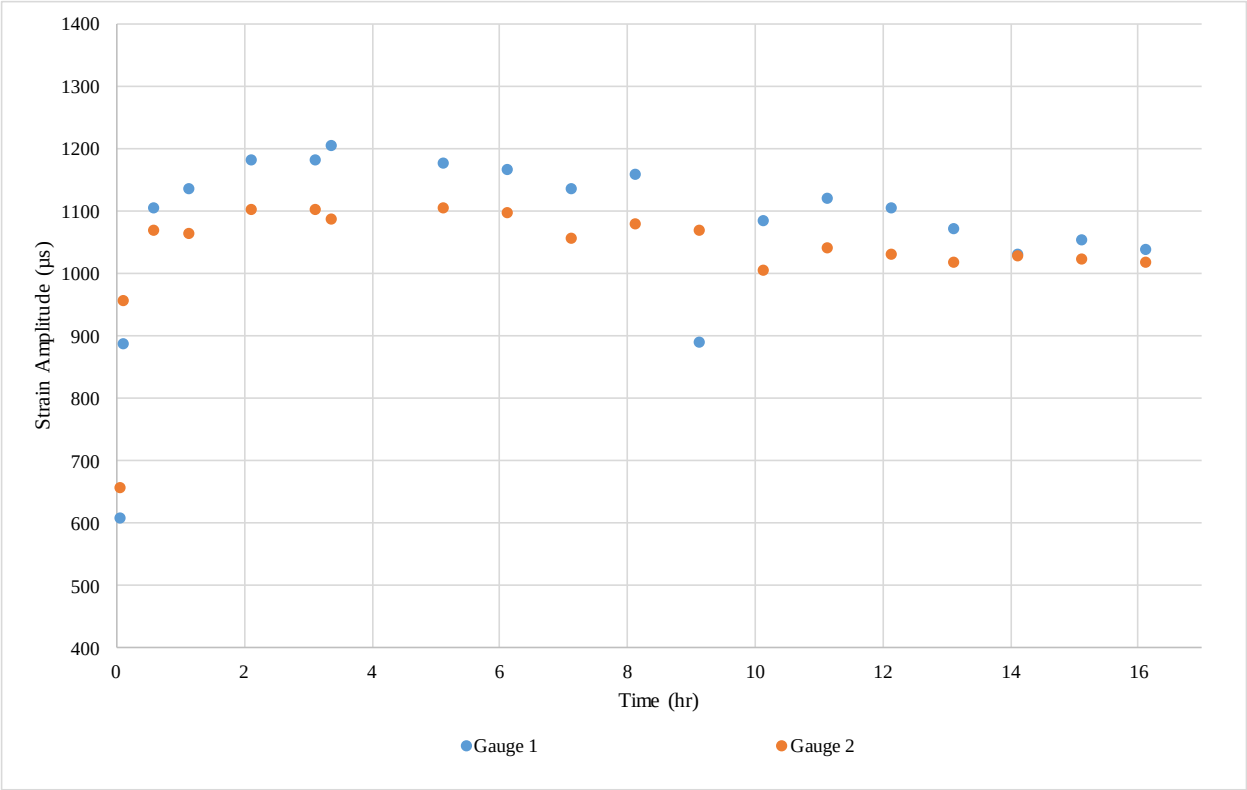

Figure B.29. The longitudinal strain amplitude for Mix #1 with the thickness of 1.5" placed on the Neoprene 60A with bonding under low-speed loading condition (Second Slab).

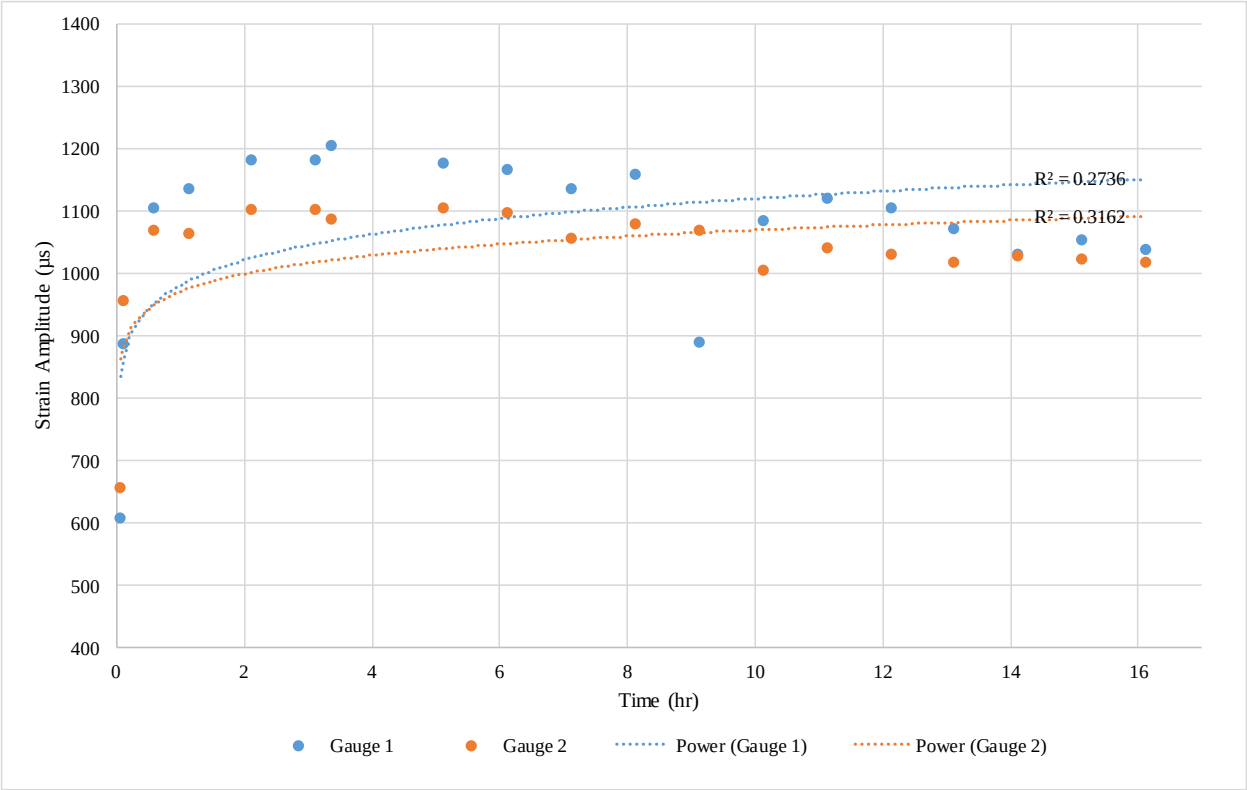

Figure B.30. The fitted power line on the longitudinal strain amplitude for Mix #1 with the thickness of 1.5" placed on the Neoprene 60A with bonding condition and under low-speed loading condition (Second Slab).

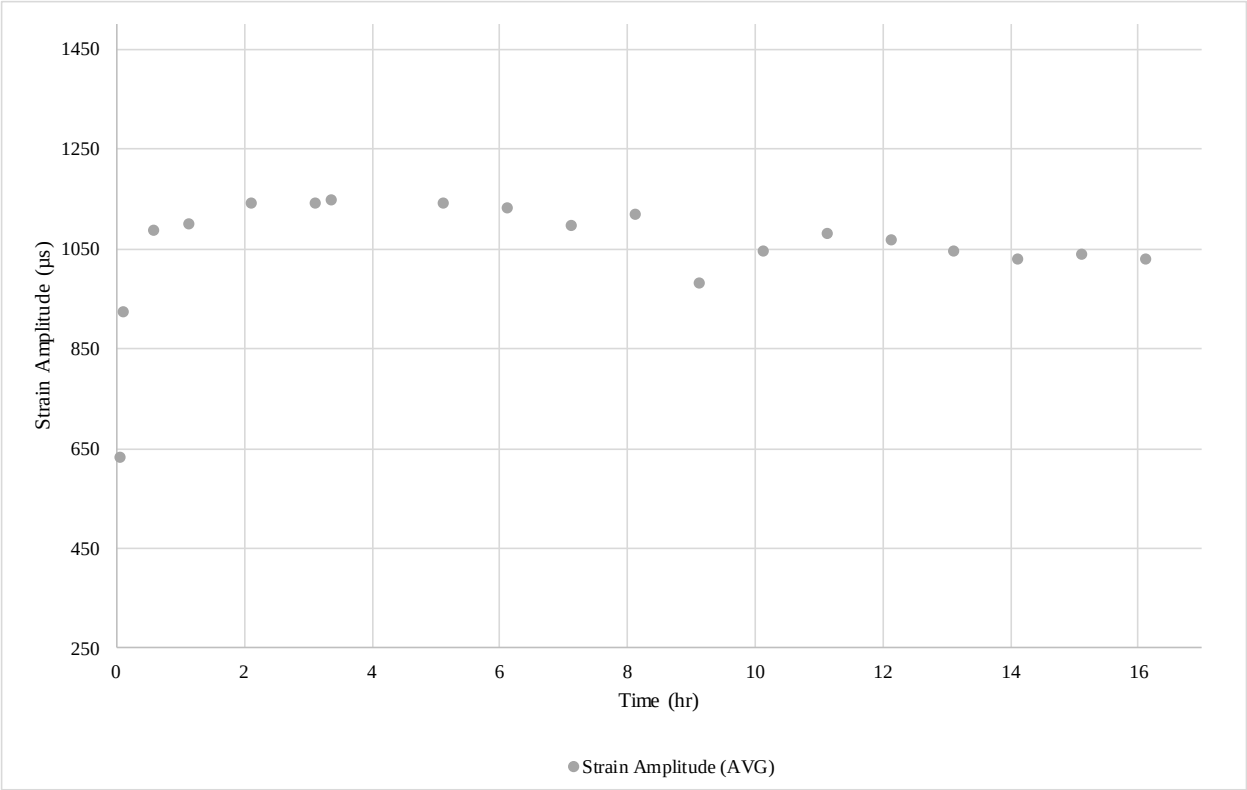

Figure B.31. The average longitudinal strain amplitude for Mix #1 with the thickness of 1.5" placed on the Neoprene 60A with bonding condition and under low-speed loading condition (Second Slab).

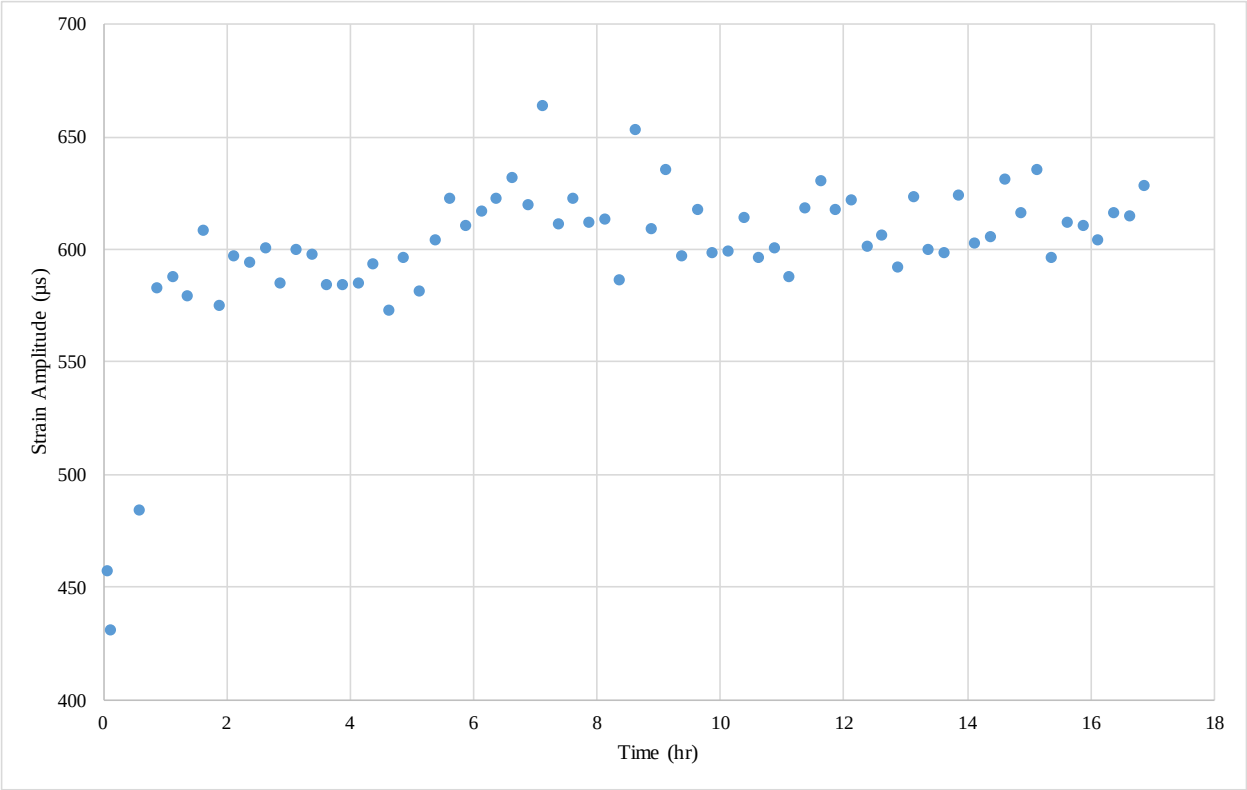

Figure B.32. The longitudinal strain amplitude for Mix #1 with the thickness of 1.5" placed on the PennDOT No. 2A aggregate base tested at 30°C.

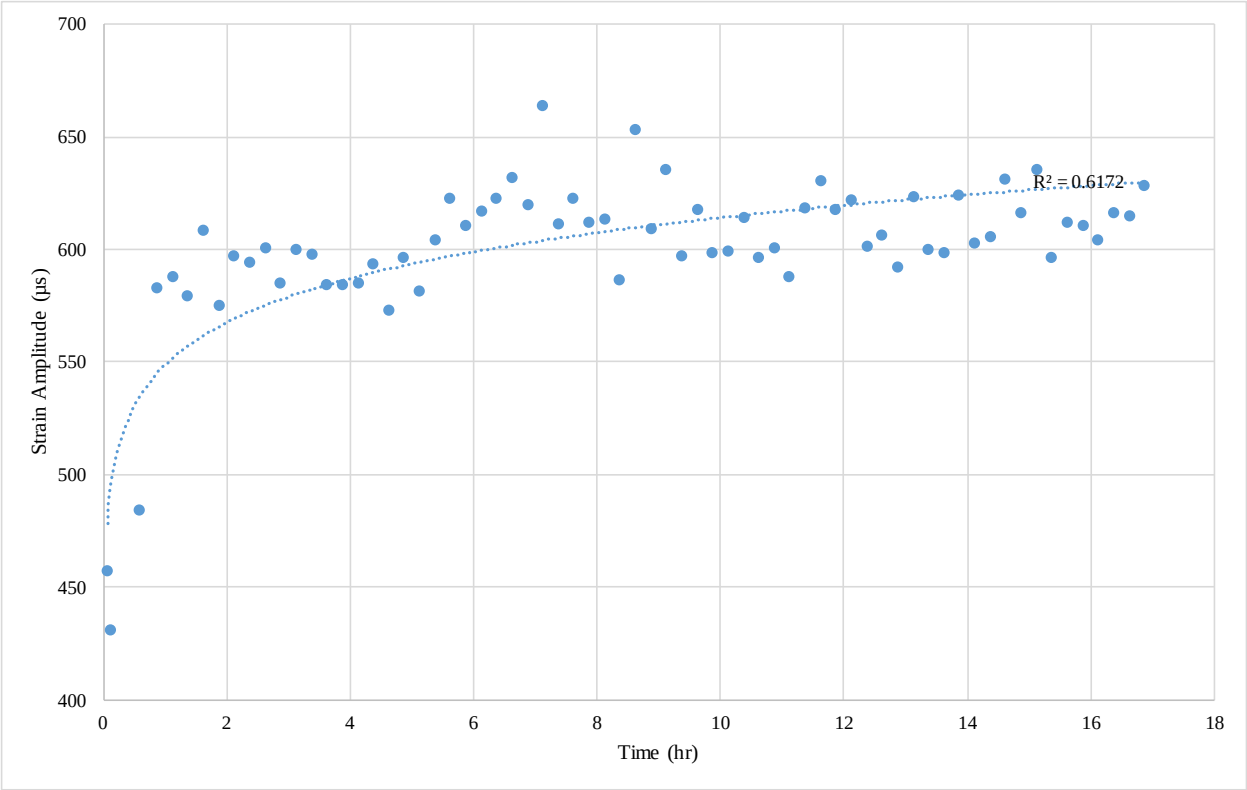

Figure B.33. The fitted power line on the longitudinal strain amplitude for Mix #1 with the thickness of 1.5" placed on the PennDOT No. 2A aggregate base tested at 30°C.

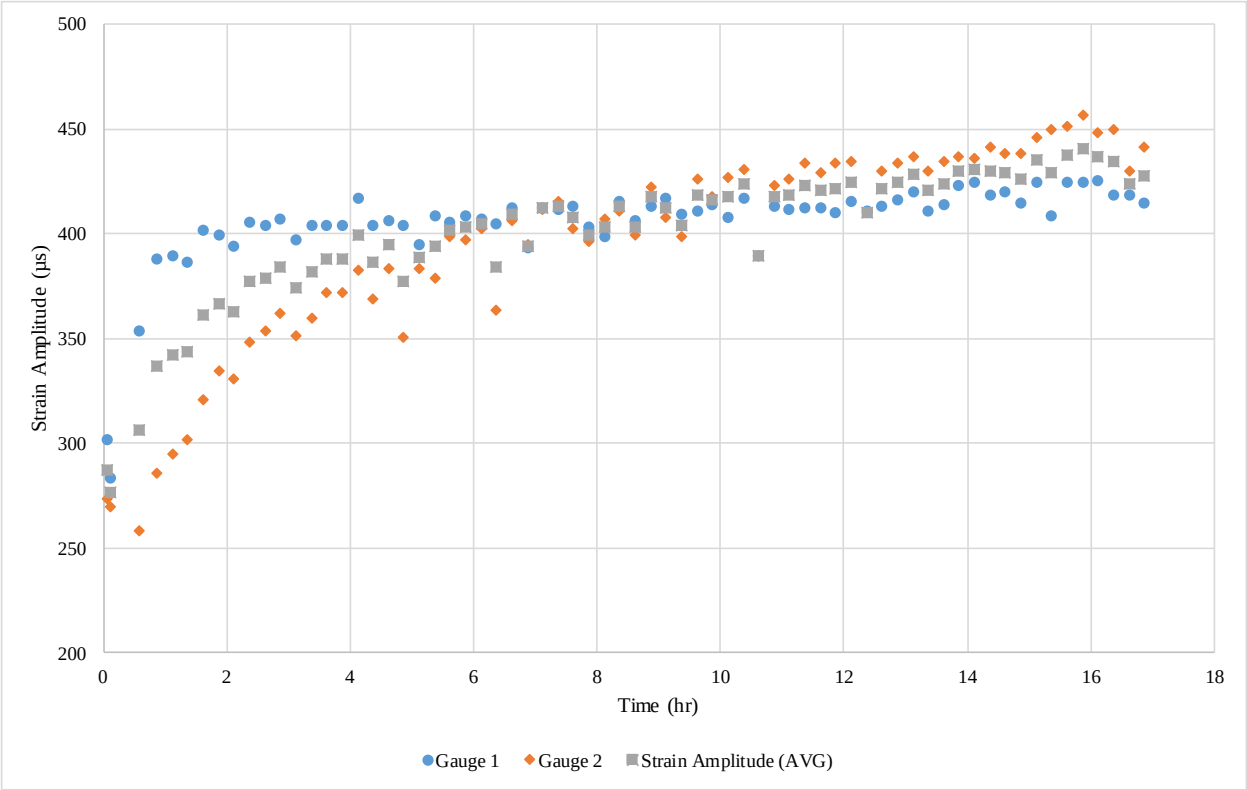

Figure B.34. The longitudinal strain amplitude for Mix #1 with the thickness of 1.5" placed on the PennDOT No. 2A aggregate base with no bonding condition.

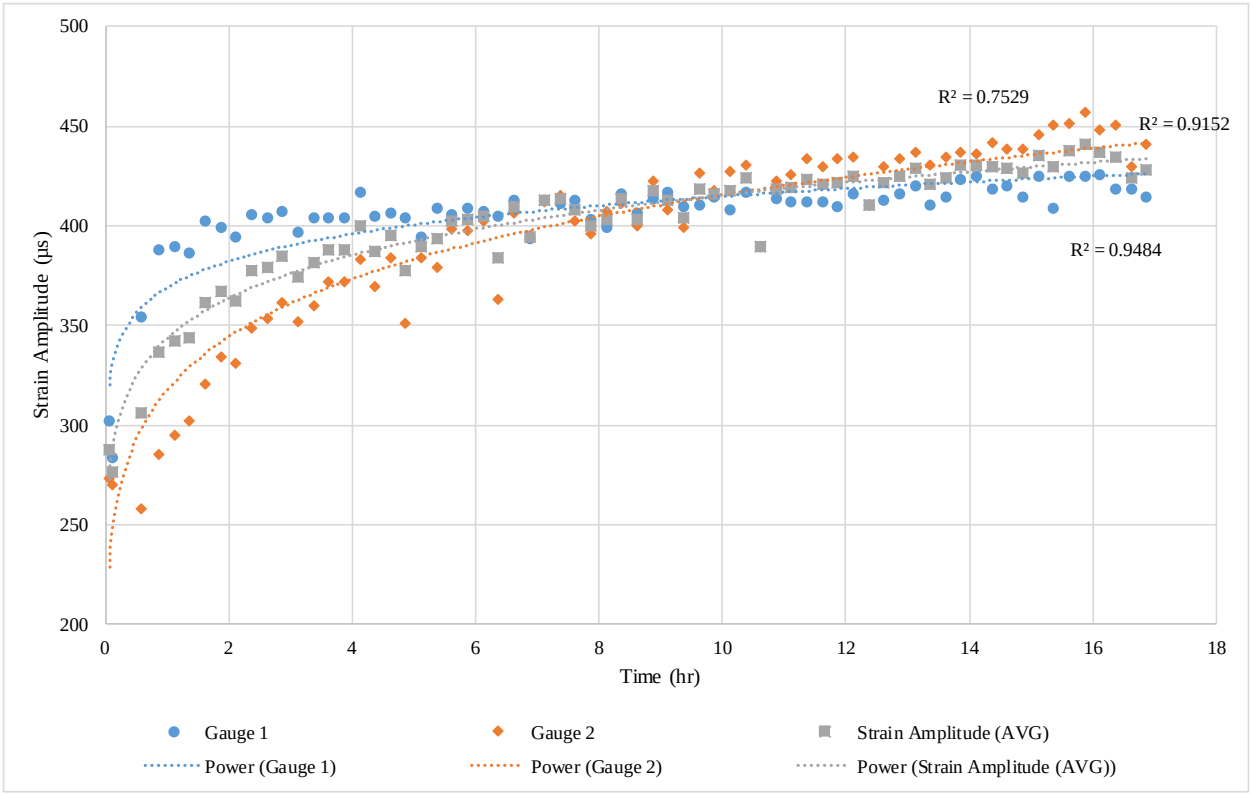

Figure B.35. The fitted power line on the longitudinal strain amplitude for Mix #1 with the thickness of 1.5" placed on the PennDOT No. 2A aggregate base with no bonding condition.

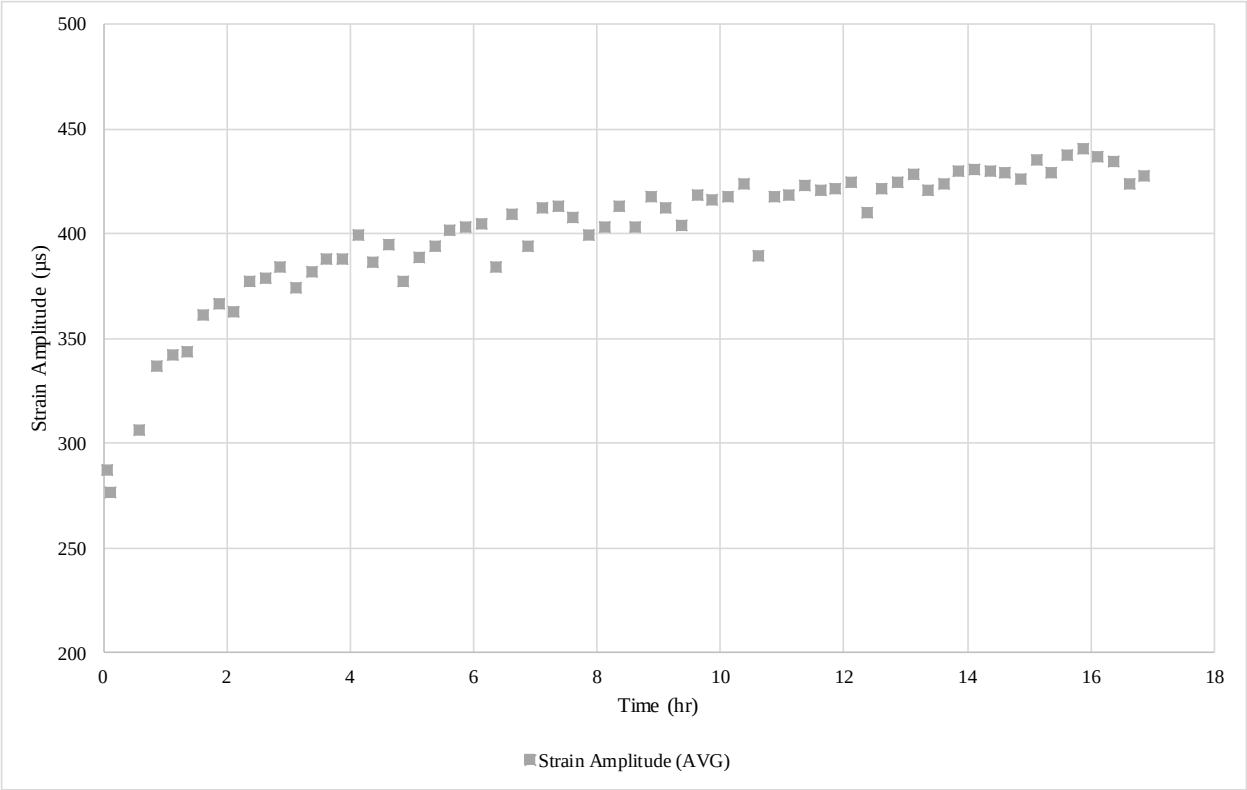

Figure B.36. The average longitudinal strain amplitude for Mix #1 with the thickness of 1.5" placed on the PennDOT No. 2A aggregate base with no bonding condition.

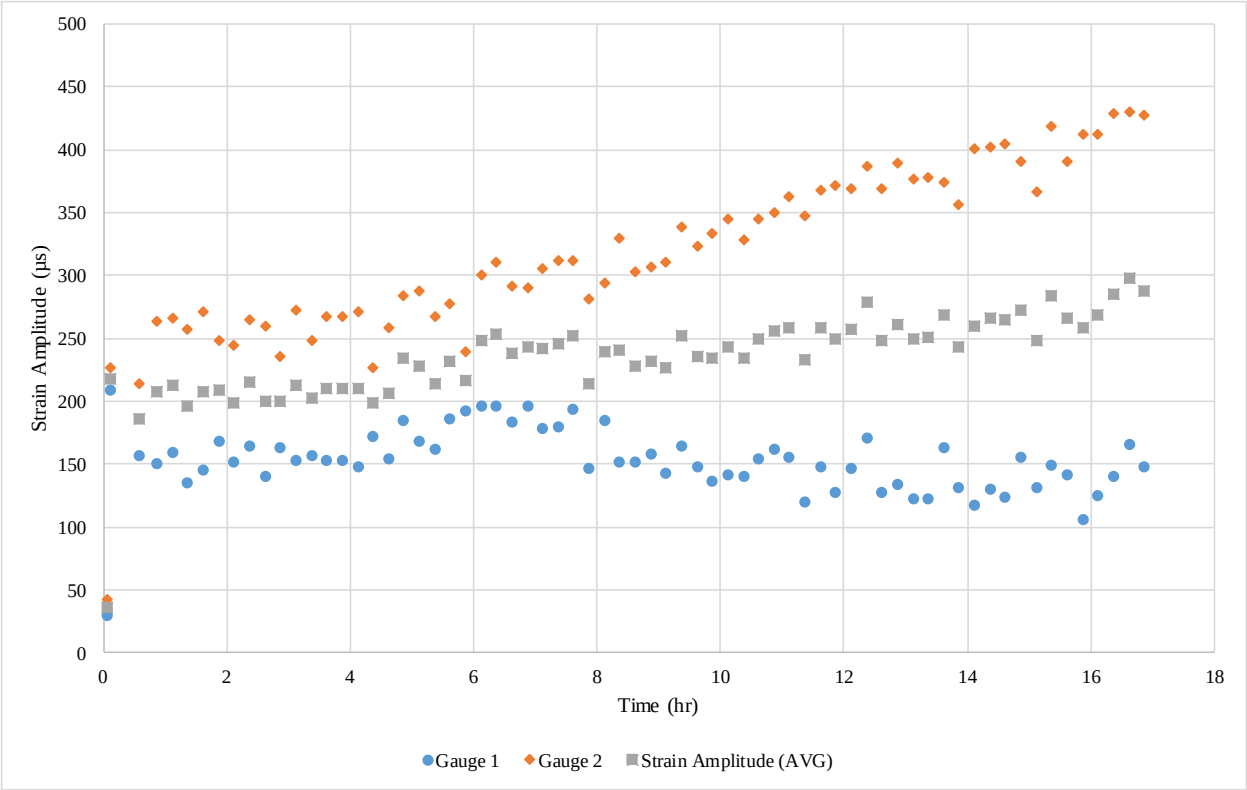

Figure B.37. The longitudinal strain amplitude for Mix #1 with the thickness of 1.5" placed on the PennDOT No. 2A aggregate base with no bonding condition (Second Slab).

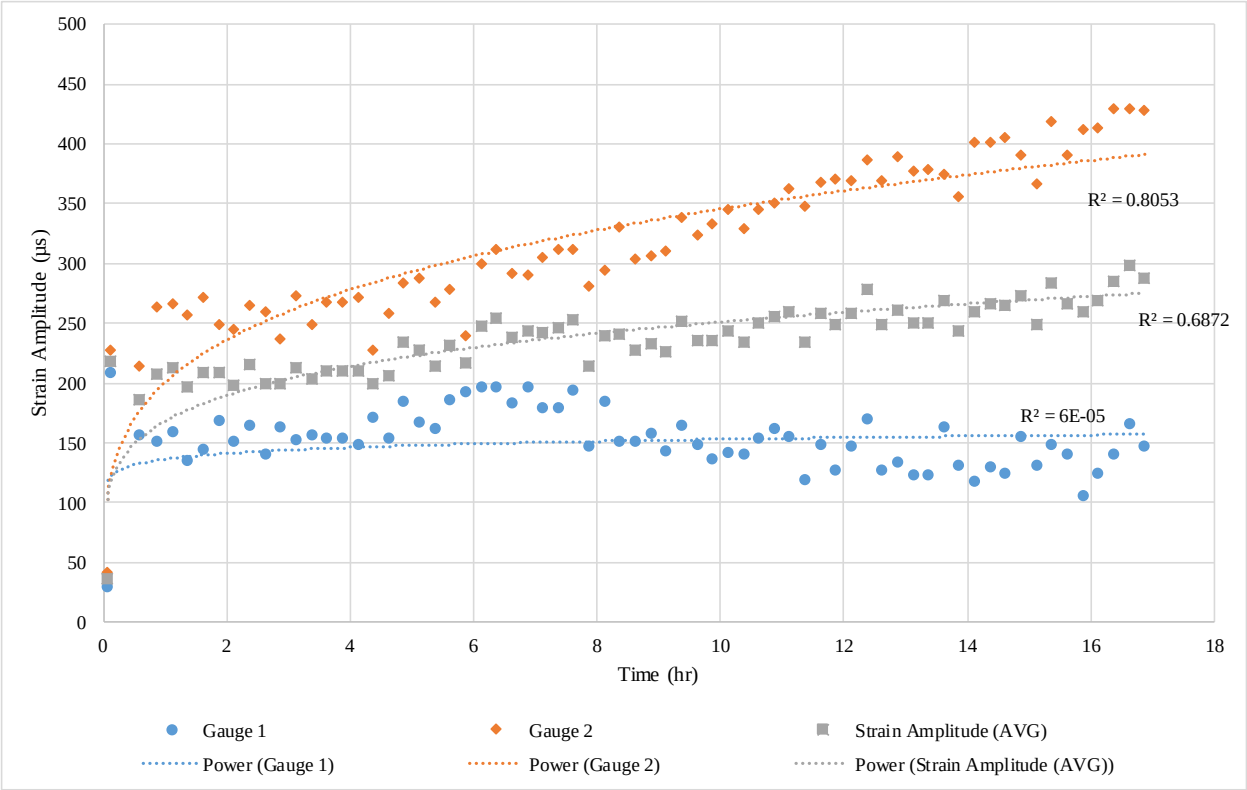

Figure B.38. The fitted power line on the longitudinal strain amplitude for Mix #1 with the thickness of 1.5" placed on the PennDOT No. 2A aggregate base with no bonding condition (Second Slab).

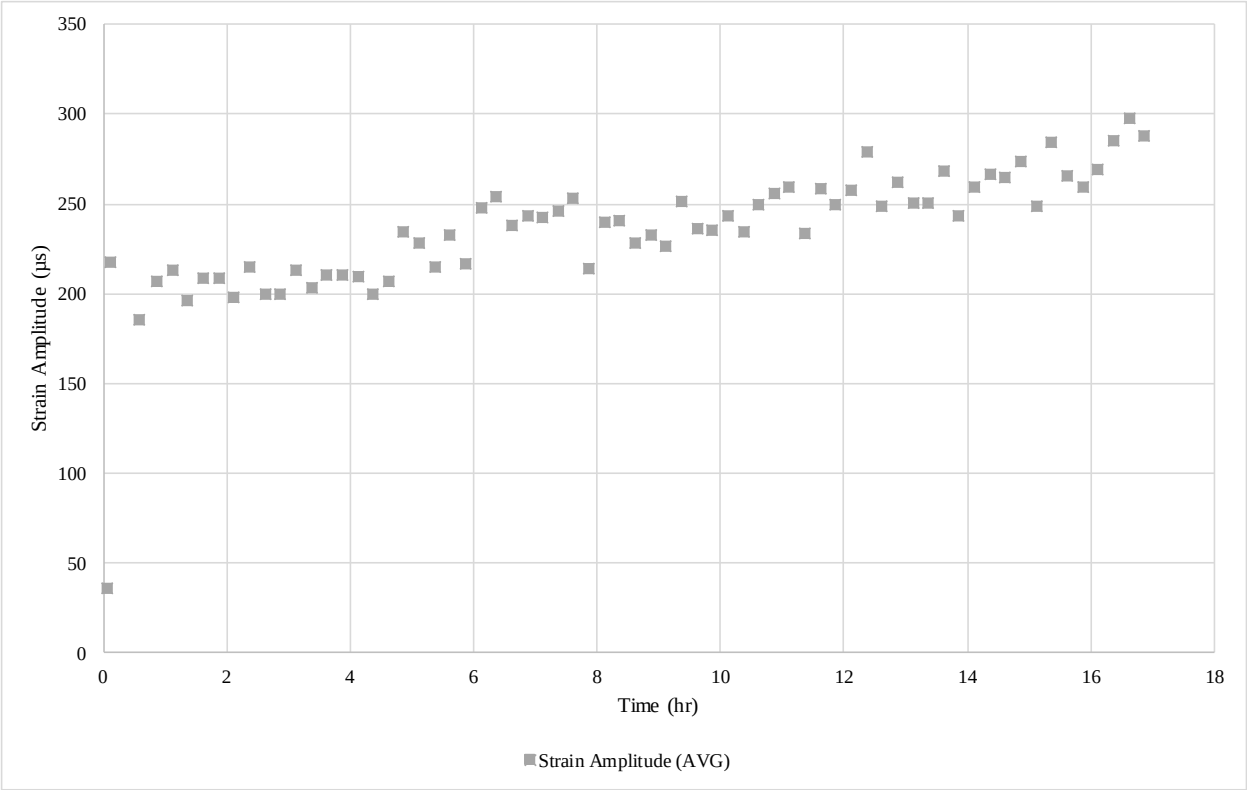

Figure B.39. The average longitudinal strain amplitude for Mix #1 with the thickness of 1.5" placed on the PennDOT No. 2A aggregate base with no bonding condition (Second Slab).

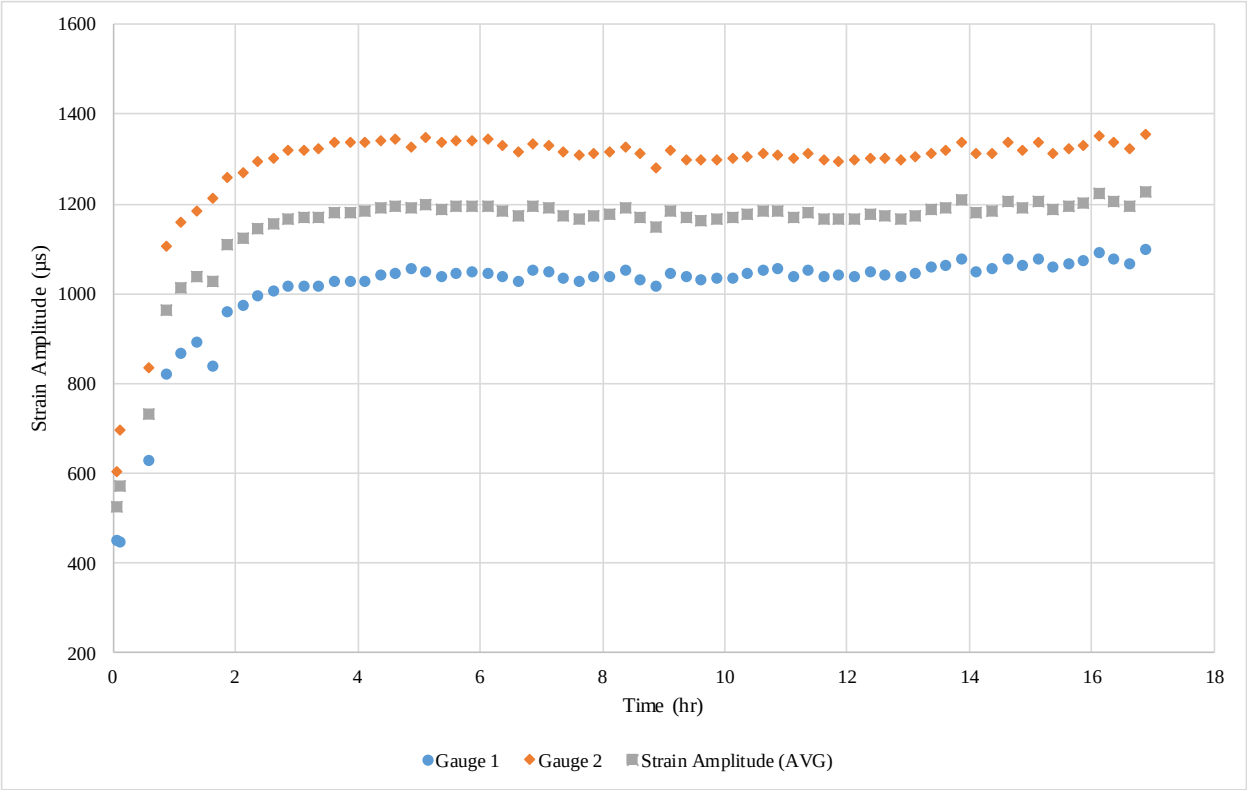

Figure B.40. The longitudinal strain amplitude for Mix #1 with the thickness of 1.5" placed on the Neoprene 60A with no bonding condition.

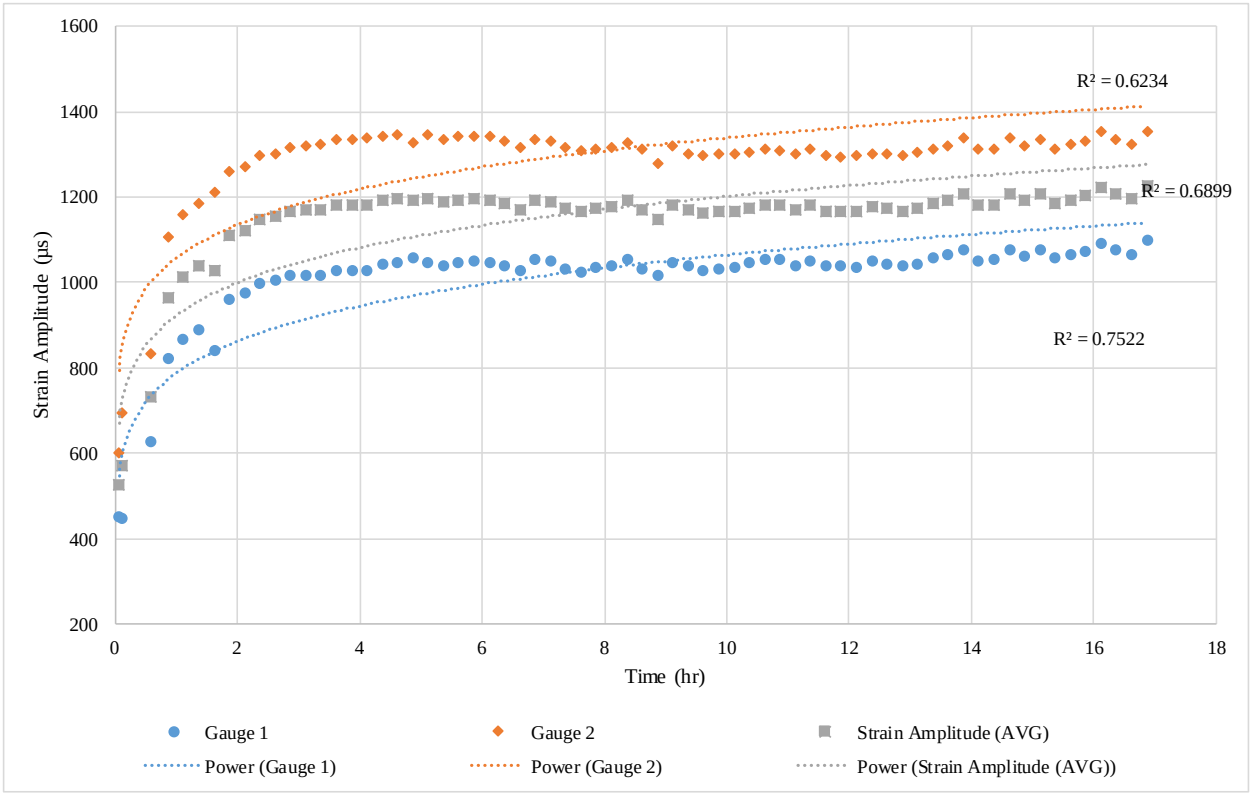

Figure B.41. The fitted power line on the longitudinal strain amplitude for Mix #1 with the thickness of 1.5" placed on the Neoprene 60A with no bonding condition.

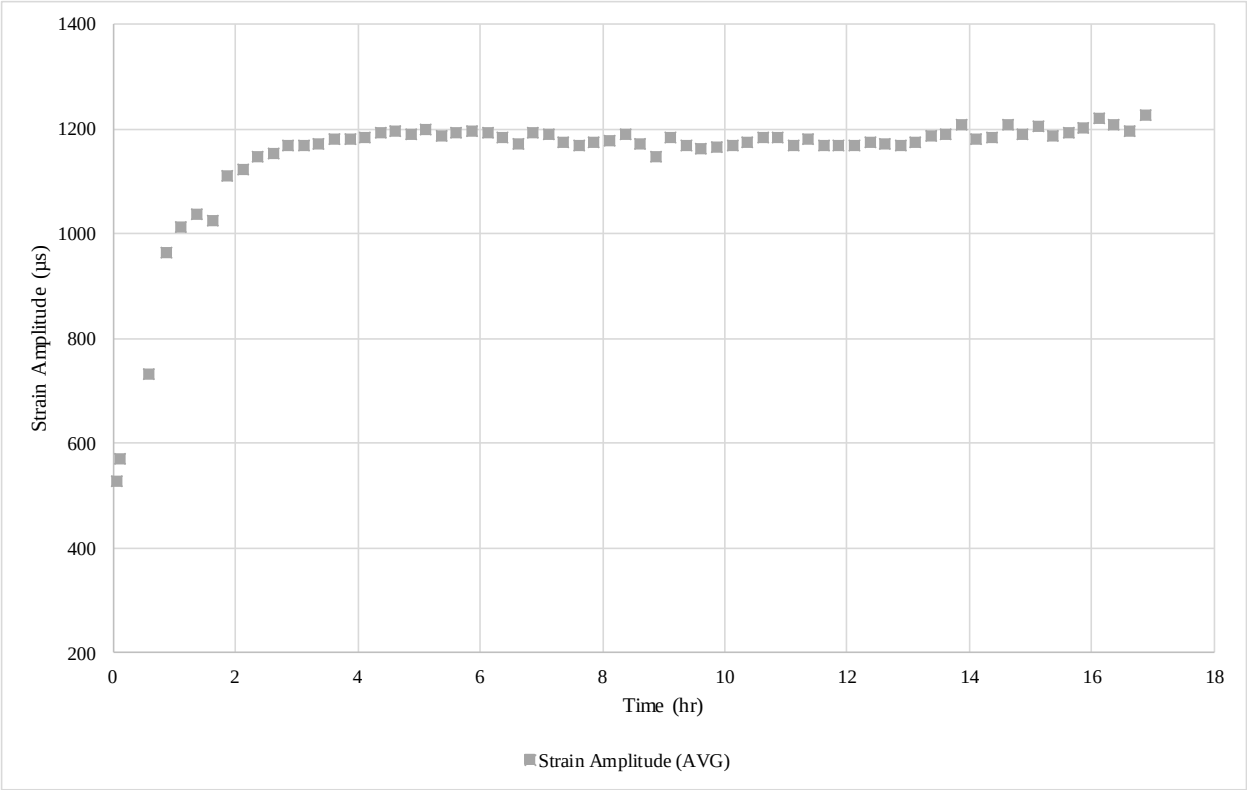

Figure B.42. The average longitudinal strain amplitude for Mix #1 with the thickness of 1.5" placed on the Neoprene 60A with no bonding condition.

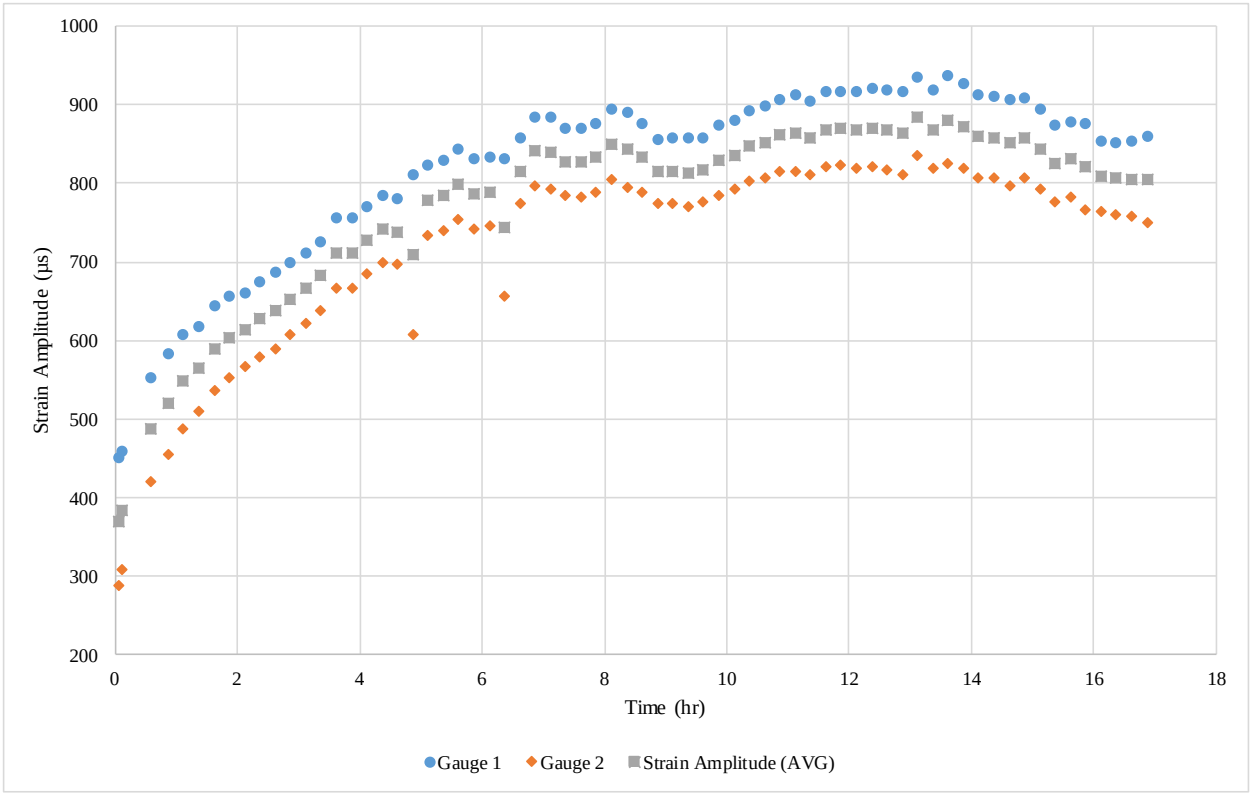

Figure B.43. The longitudinal strain amplitude for Mix #1 with the thickness of 1.5" placed on the Neoprene 60A with no bonding condition (Second Slab).

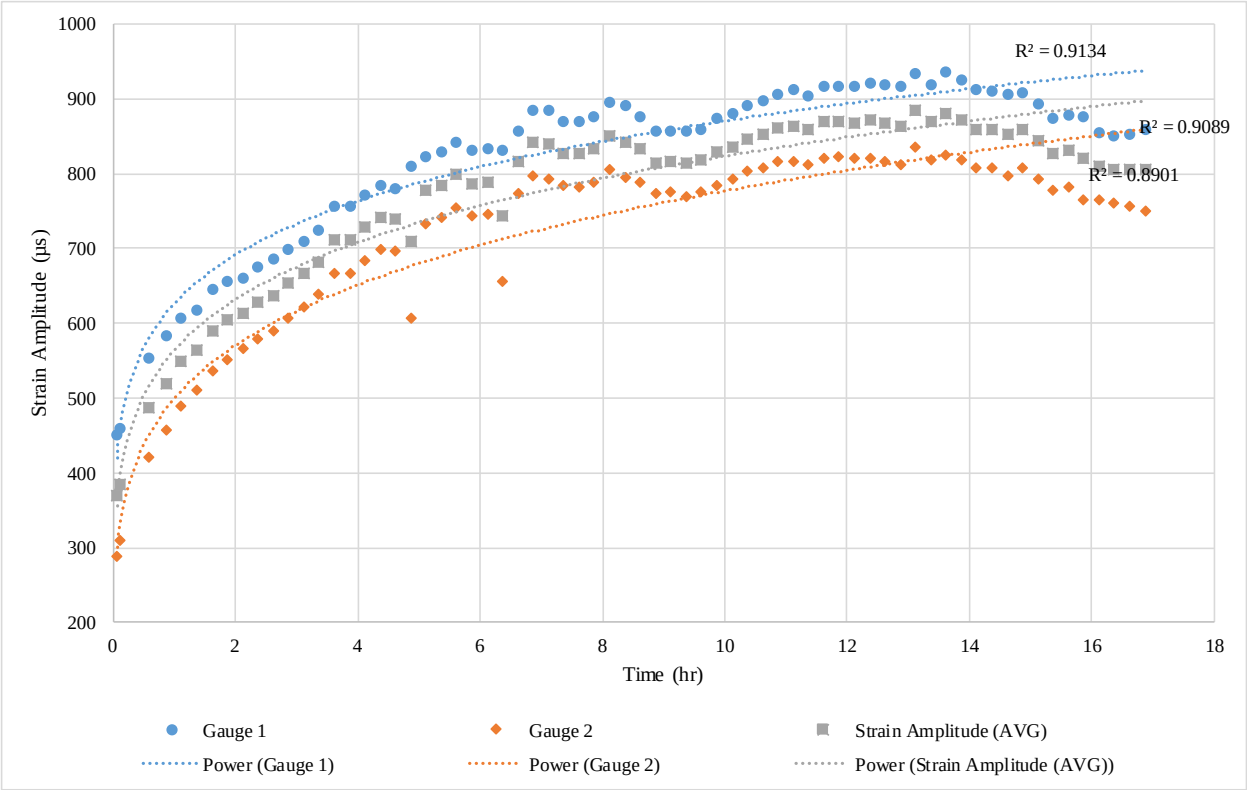

Figure B.44. The fitted power line on the longitudinal strain amplitude for Mix #1 with the thickness of 1.5" placed on the Neoprene 60A with no bonding condition (Second Slab).

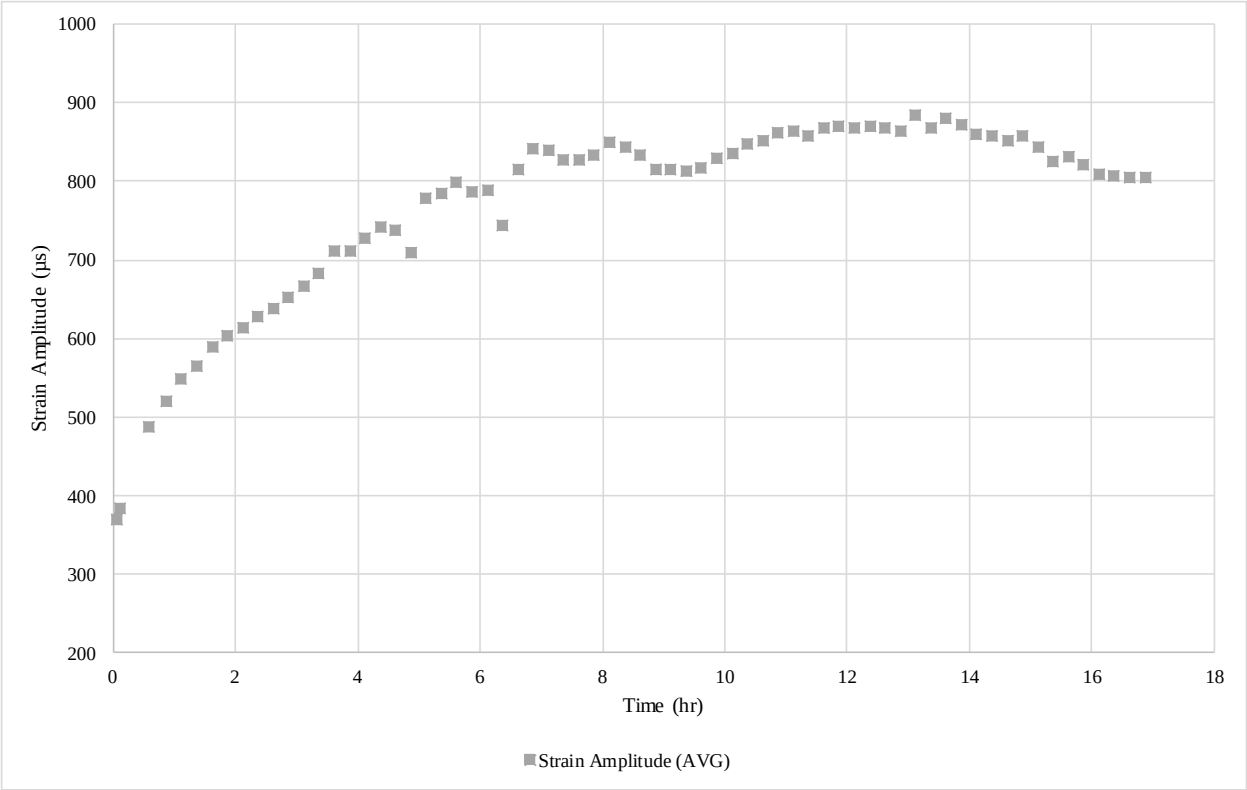

Figure B.45. The average longitudinal strain amplitude for Mix #1 with the thickness of 1.5" placed on the Neoprene 60A with no bonding condition (Second Slab).

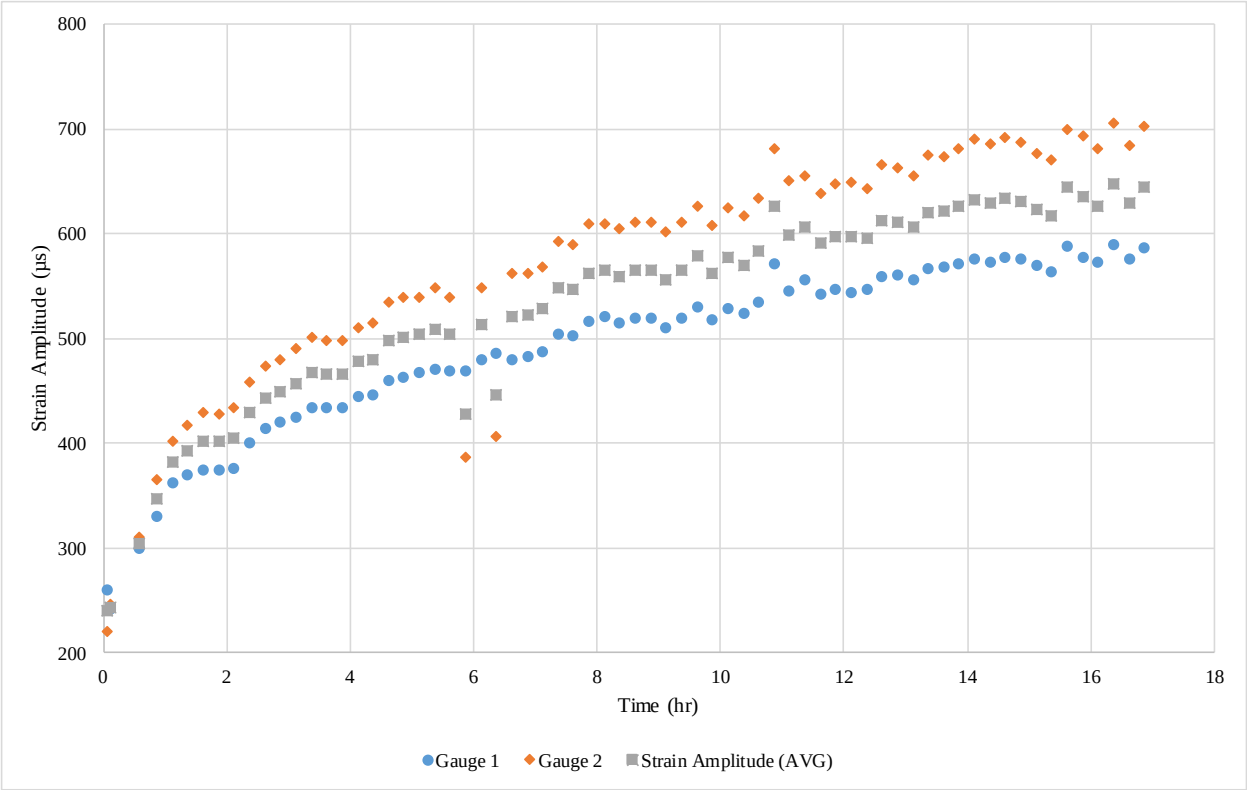

Figure B.46. The longitudinal strain amplitude for Mix #2 with the thickness of 1.5" placed on the Neoprene 60A with bonding condition.

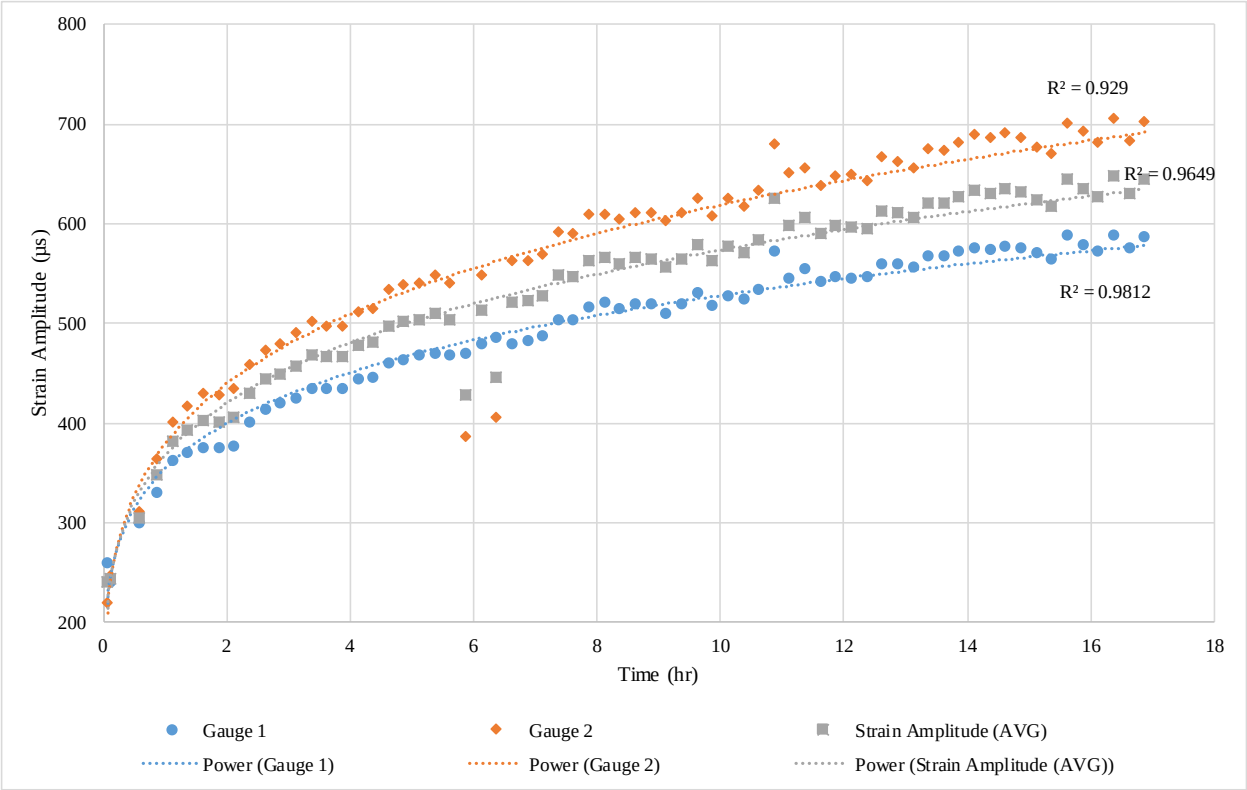

Figure B.47. The fitted power line on the longitudinal strain amplitude for Mix #2 with the thickness of 1.5" placed on the Neoprene 60A with bonding condition.

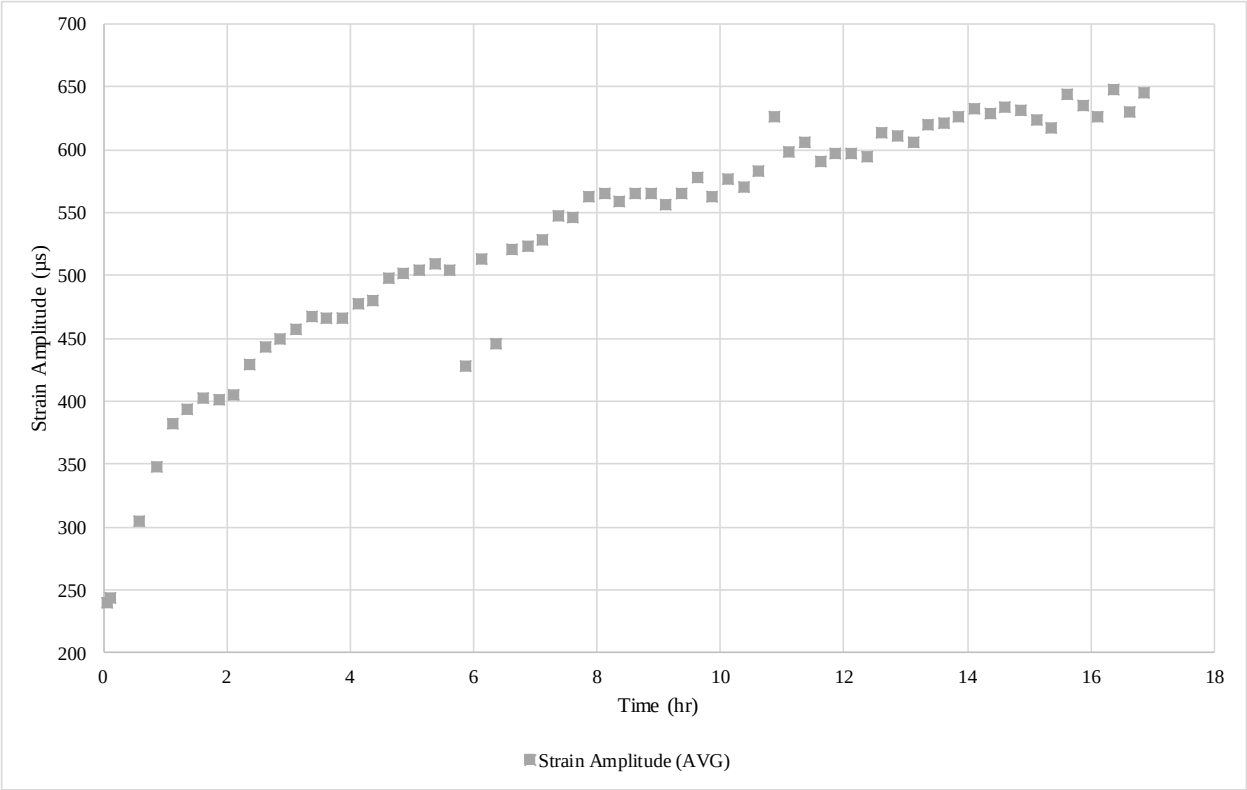

Figure B.48. The average longitudinal strain amplitude for Mix #2 with the thickness of 1.5" placed on the Neoprene 60A with bonding condition.

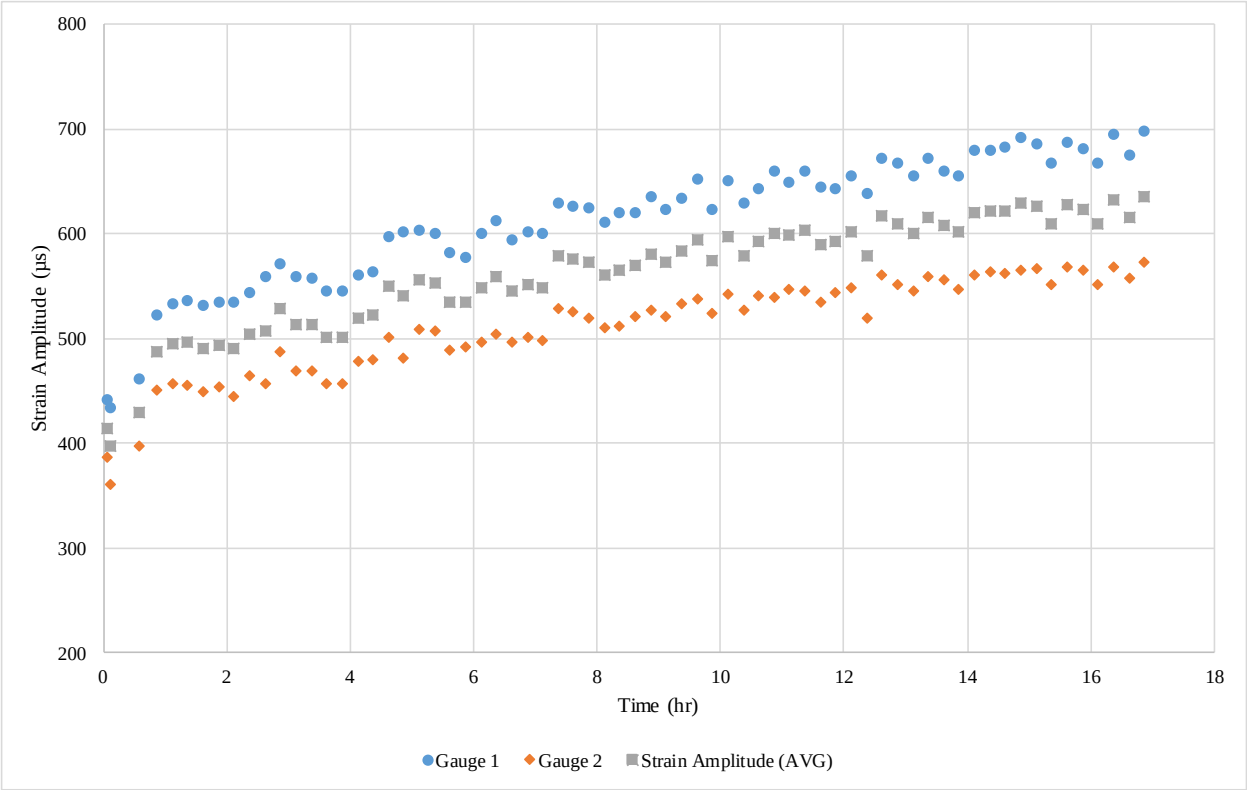

Figure B.49. The longitudinal strain amplitude for Mix #2 with the thickness of 1.5" placed on the Neoprene 60A with bonding condition (Second Slab).

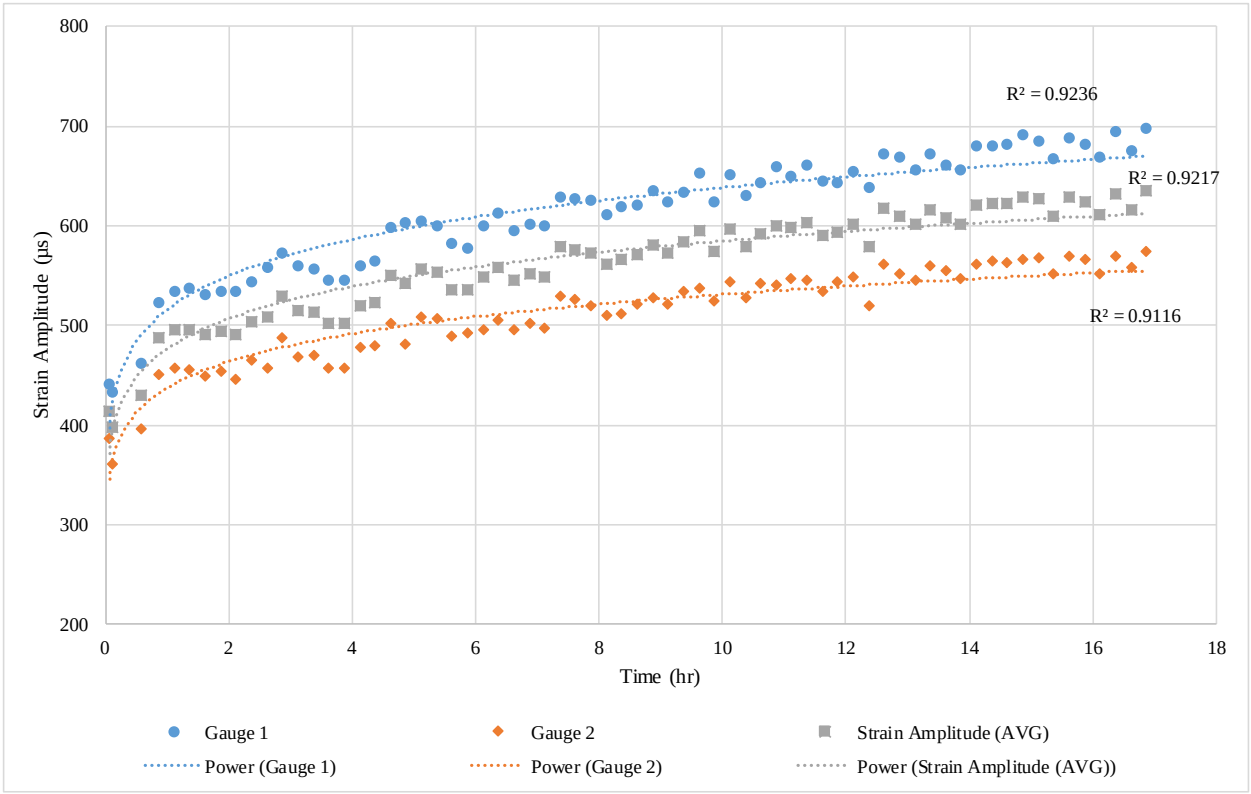

Figure B.50. The fitted power line on the longitudinal strain amplitude for Mix #2 with the thickness of 1.5" placed on the Neoprene 60A with bonding condition (Second Slab).

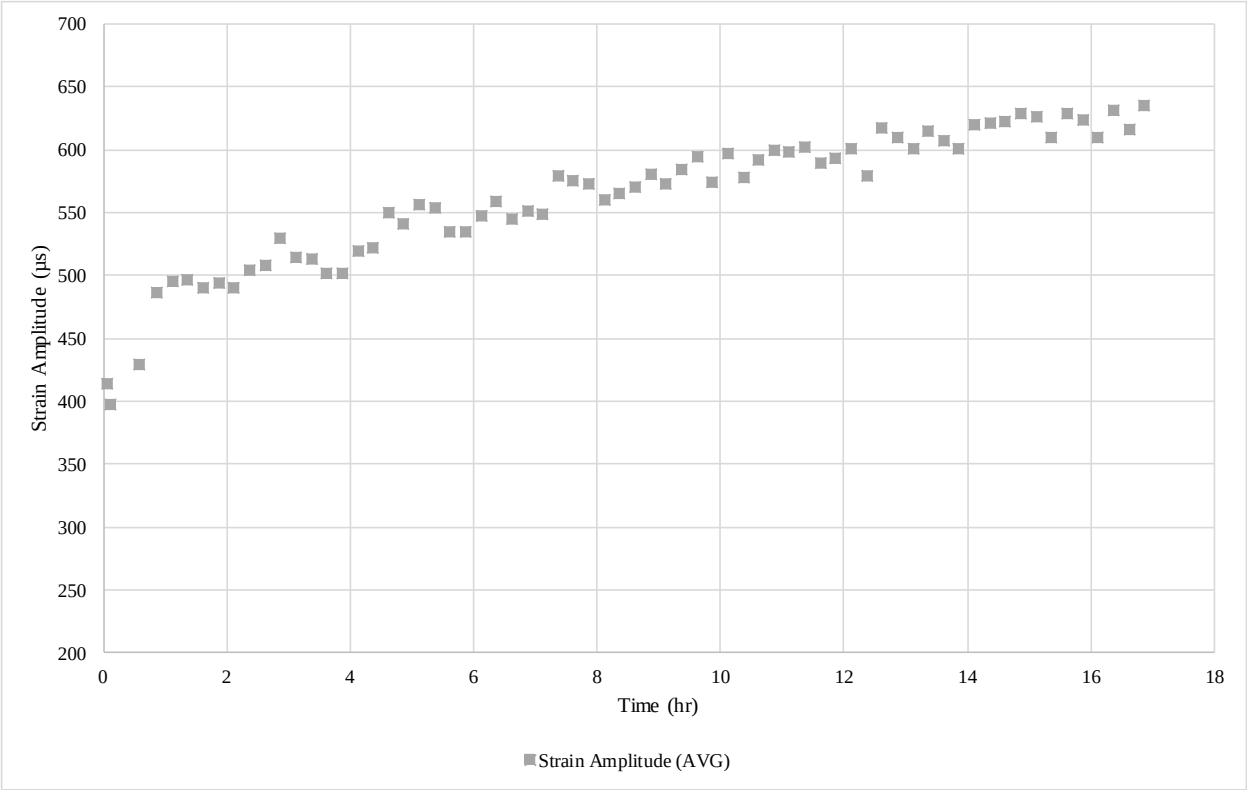

Figure B.51. The average longitudinal strain amplitude for Mix #2 with the thickness of 1.5" placed on the Neoprene 60A with bonding condition (Second Slab).

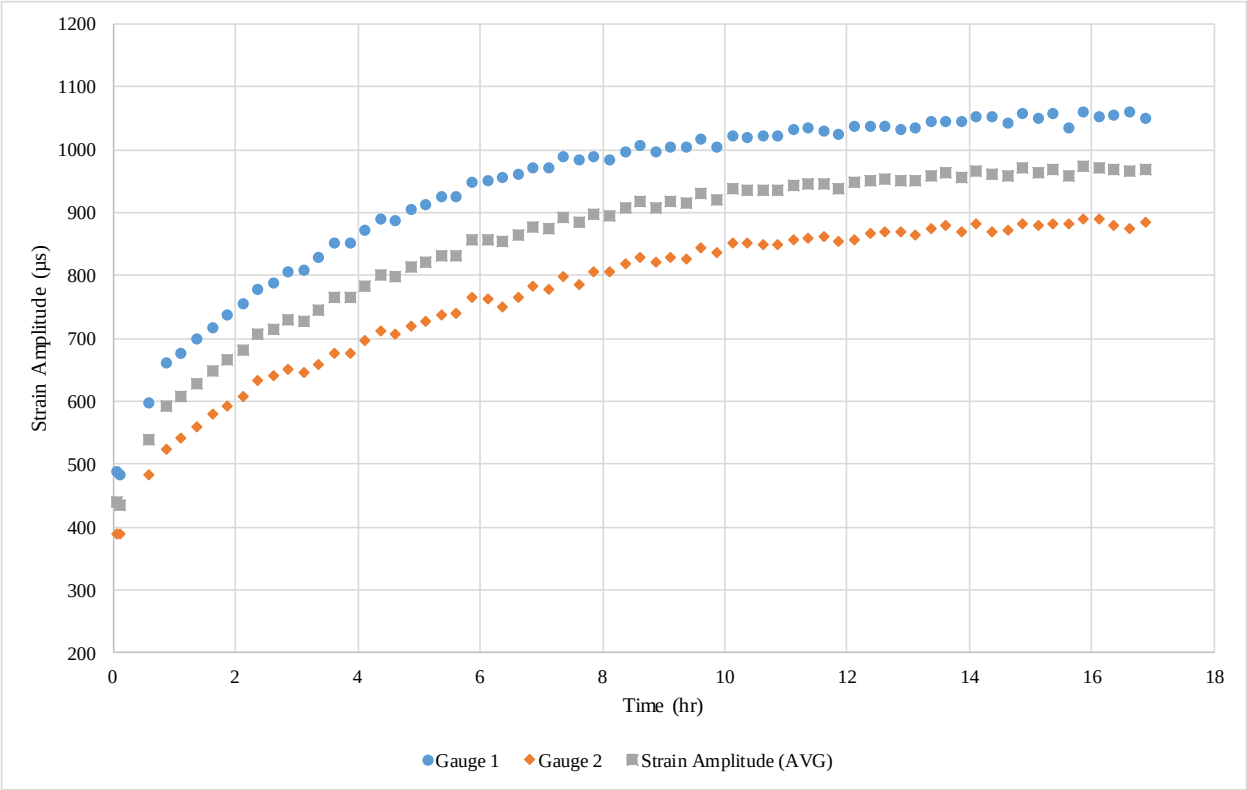

Figure B.52. The longitudinal strain amplitude for Mix #3 with the thickness of 1.5" placed on the Neoprene 60A with bonding condition.

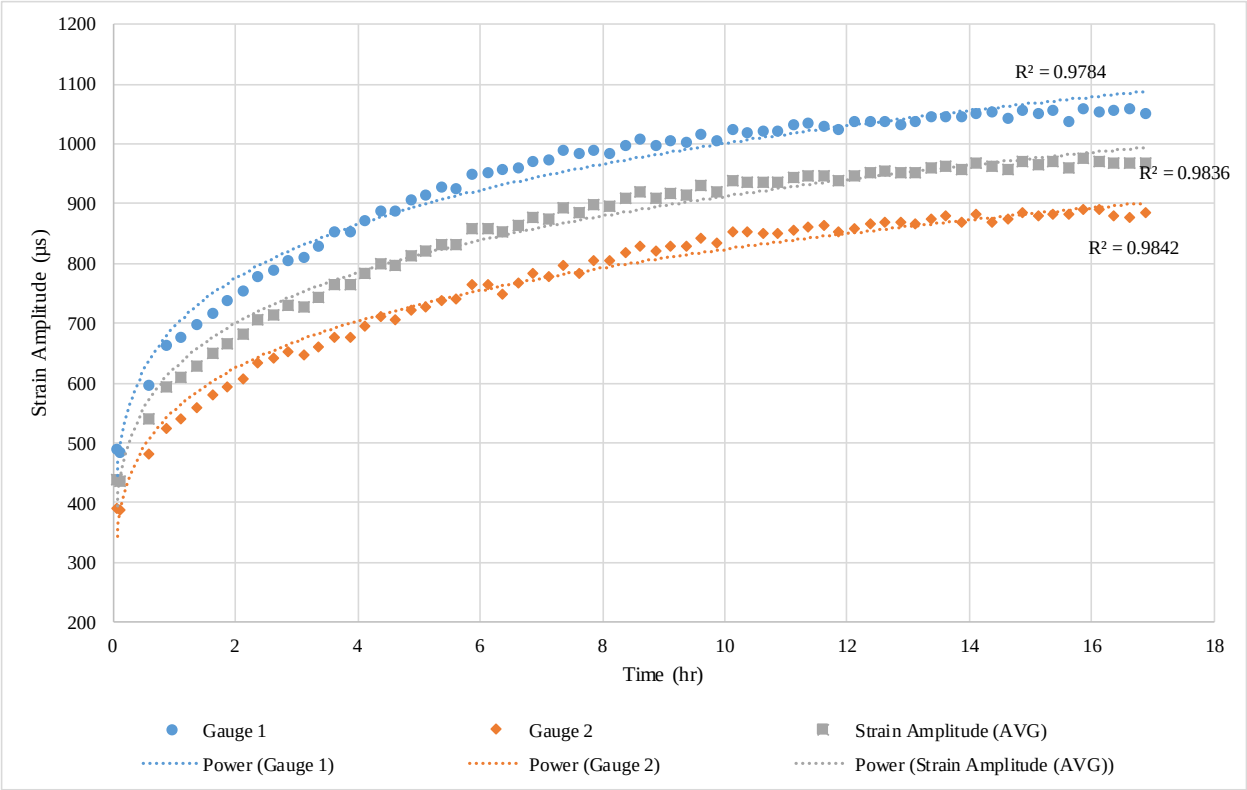

Figure B.53. The fitted power line on the longitudinal strain amplitude for Mix #3 with the thickness of 1.5" placed on the Neoprene 60A with bonding condition.

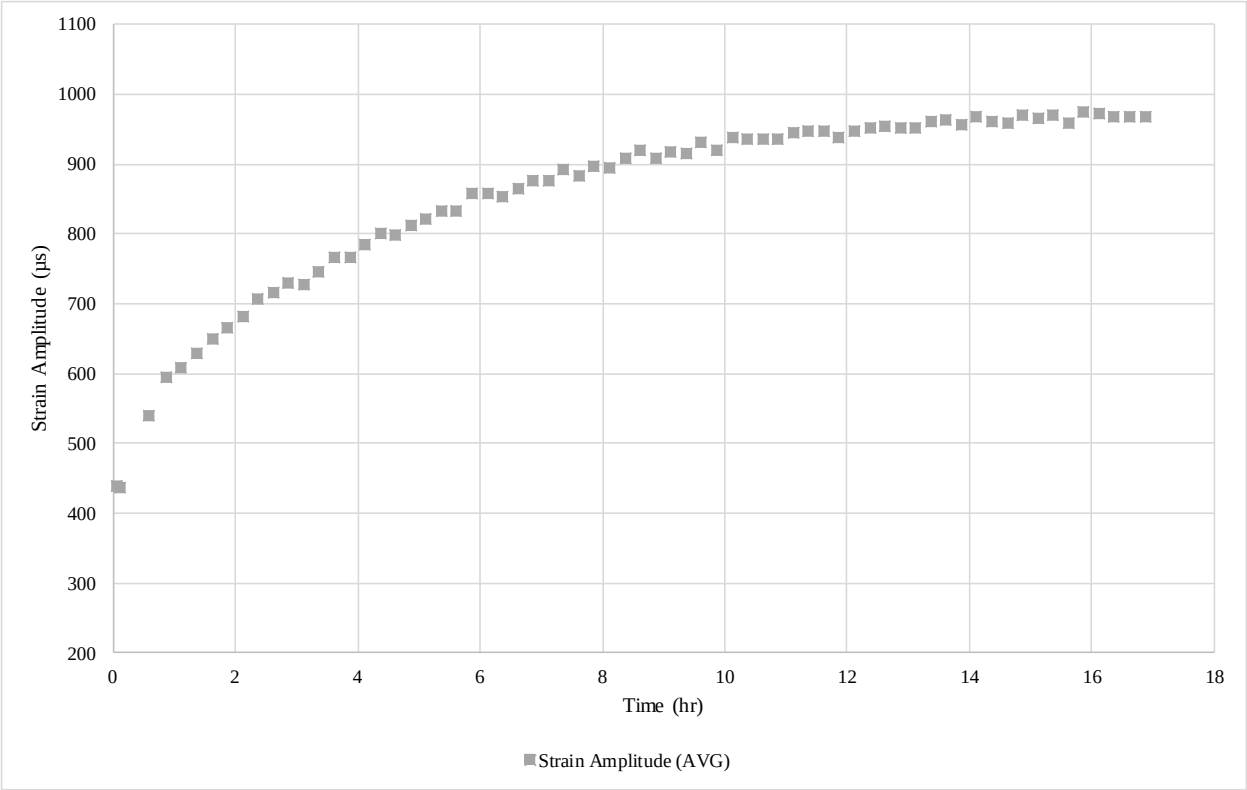

Figure B.54. The average longitudinal strain amplitude for Mix #3 with the thickness of 1.5" placed on the Neoprene 60A with bonding condition.

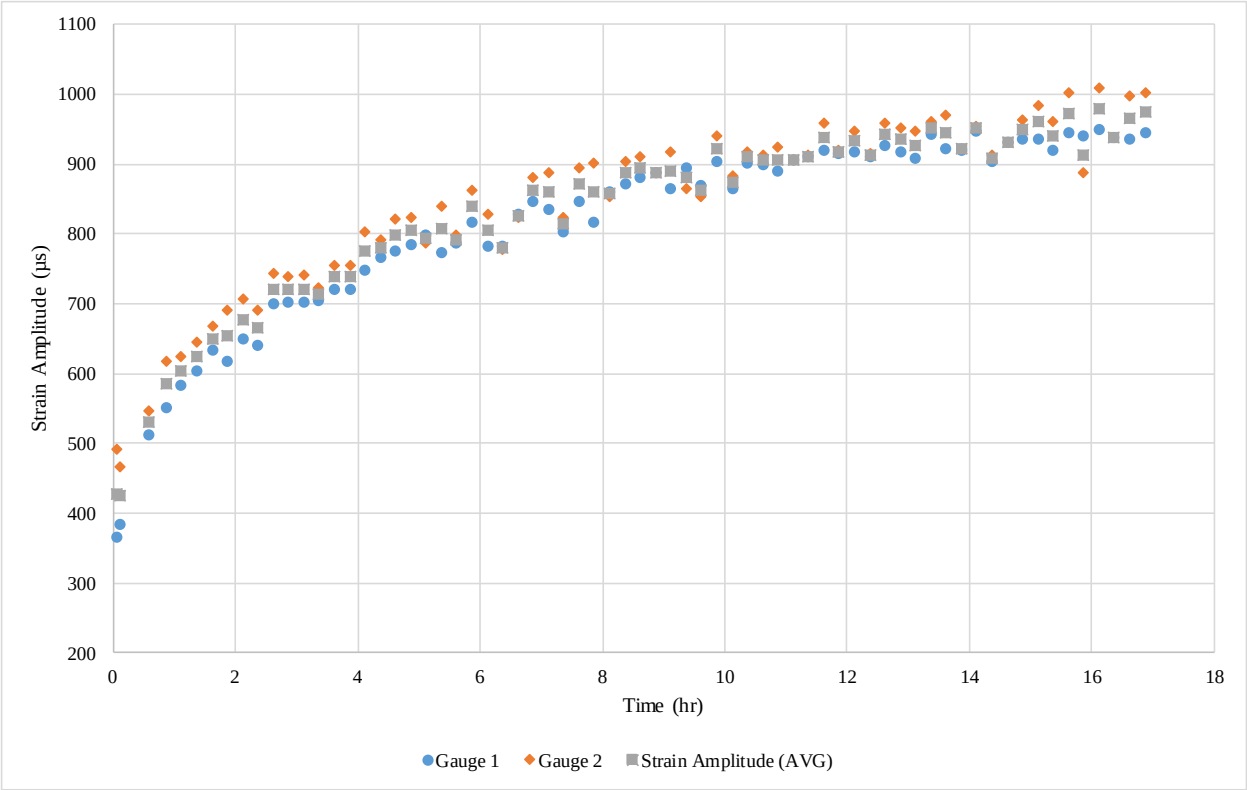

Figure B.55. The longitudinal strain amplitude for Mix #3 with the thickness of 1.5" placed on the Neoprene 60A with bonding condition (Second Slab).

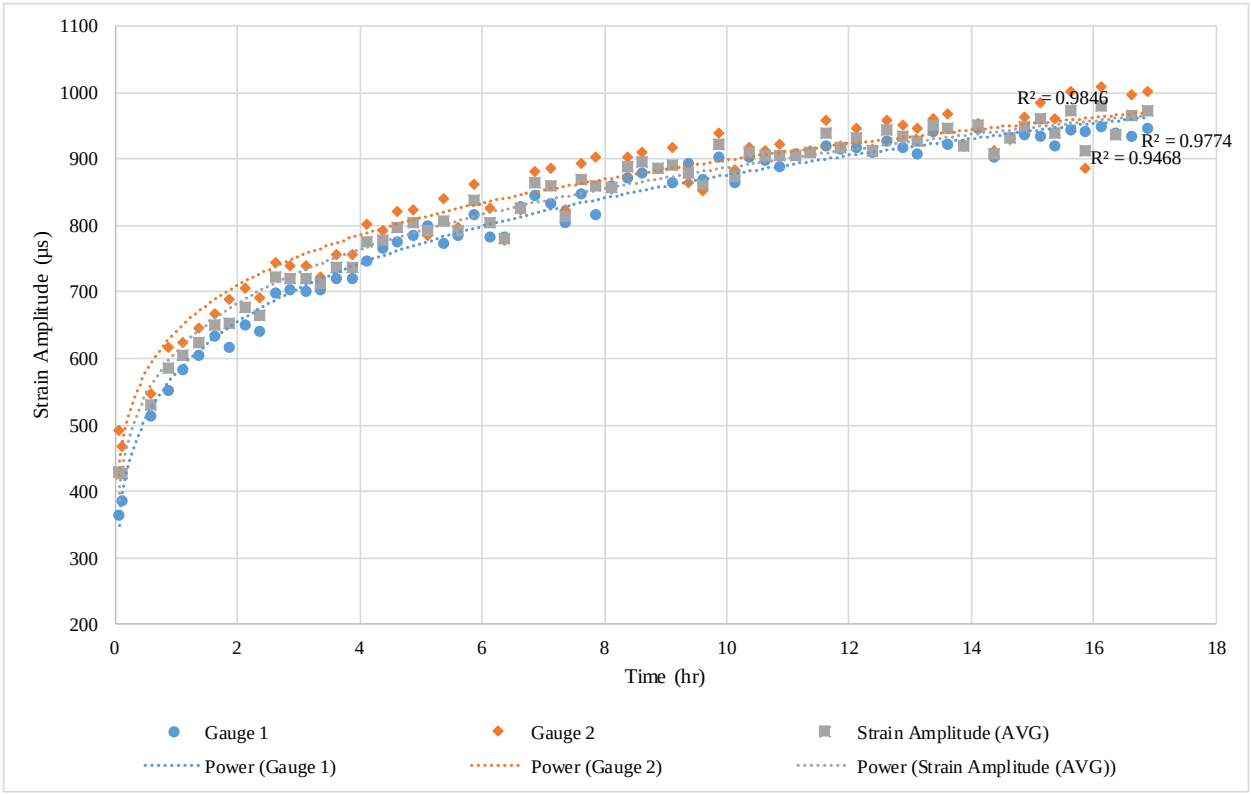

Figure B.56. The fitted power line on the longitudinal strain amplitude for Mix #3 with the thickness of 1.5" placed on the Neoprene 60A with bonding condition (Second Slab).

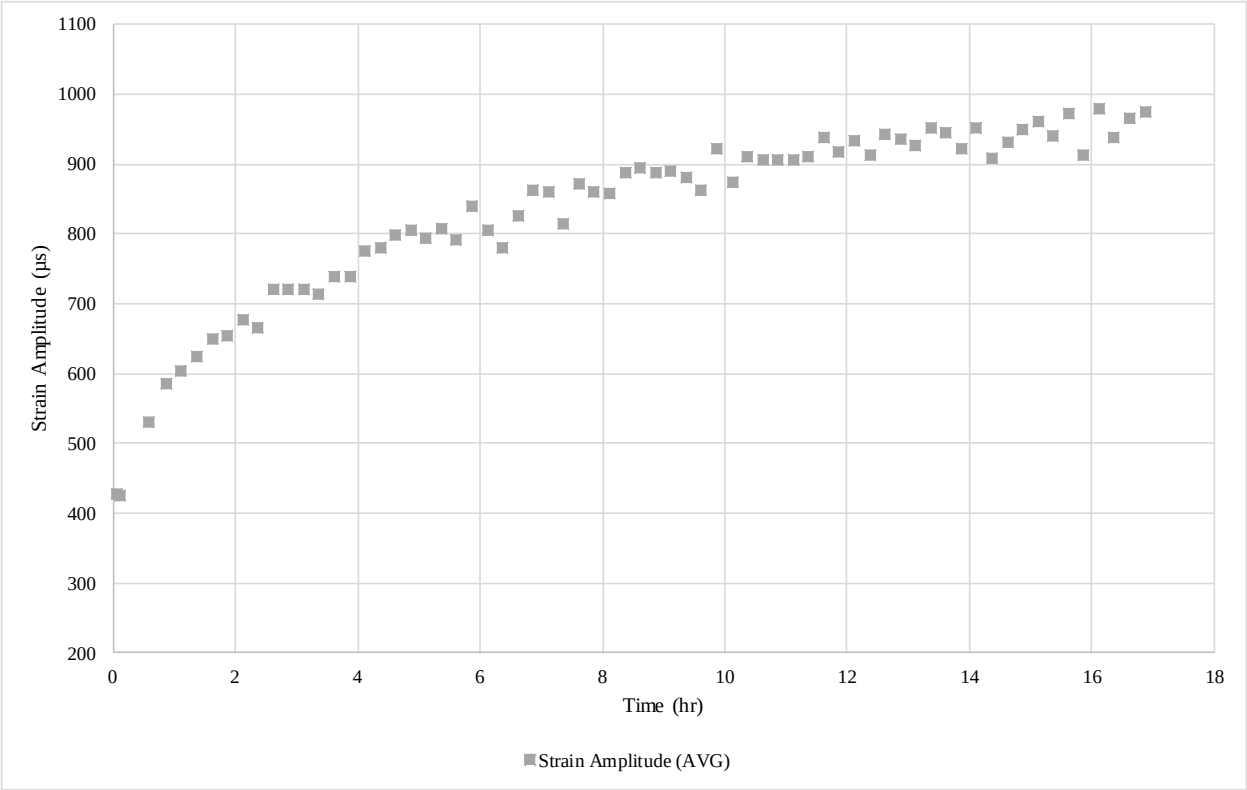

Figure B.57. The average longitudinal strain amplitude for Mix #3 with the thickness of 1.5" placed on the Neoprene 60A with bonding condition (Second Slab).

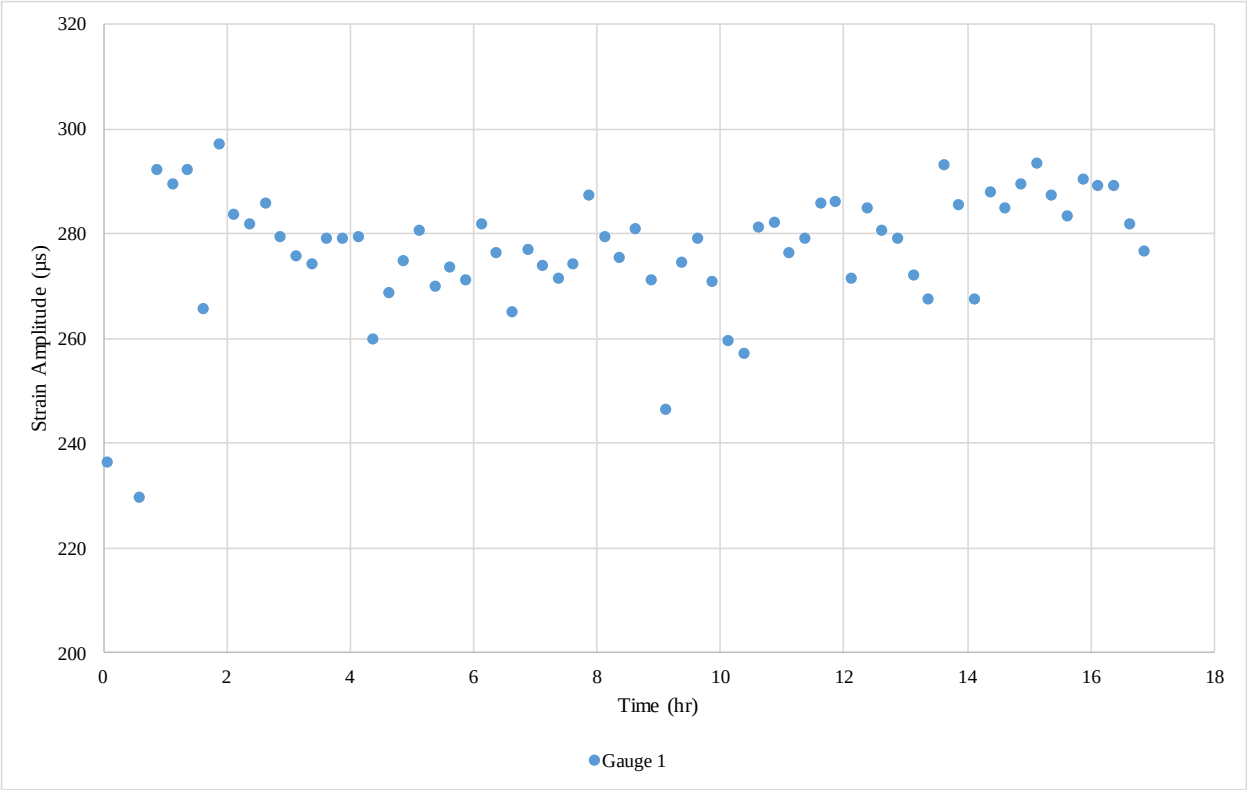

Figure B.58. The longitudinal strain amplitude for Mix #4 with the thickness of 1.5" placed on the Neoprene 60A with bonding condition.

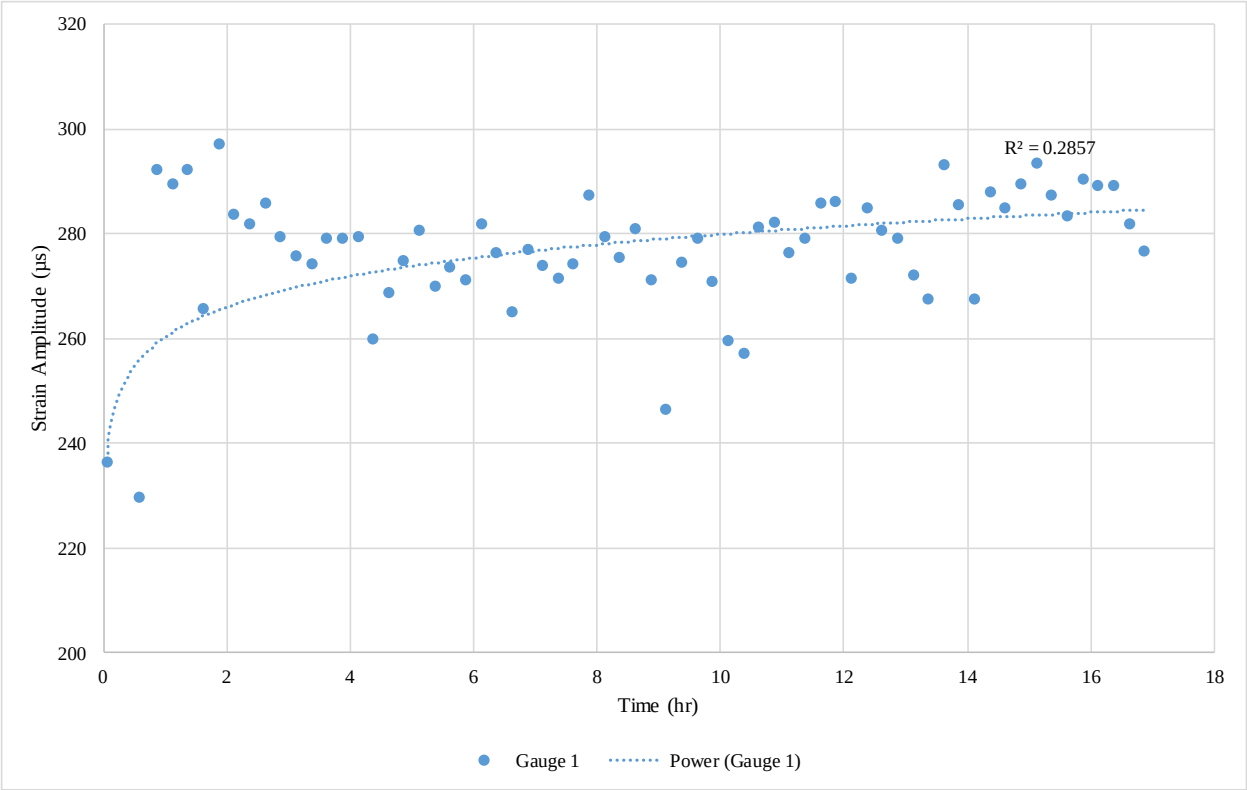

Figure B.59. The fitted power line on the longitudinal strain amplitude for Mix #4 with the thickness of 1.5" placed on the Neoprene 60A with bonding condition.

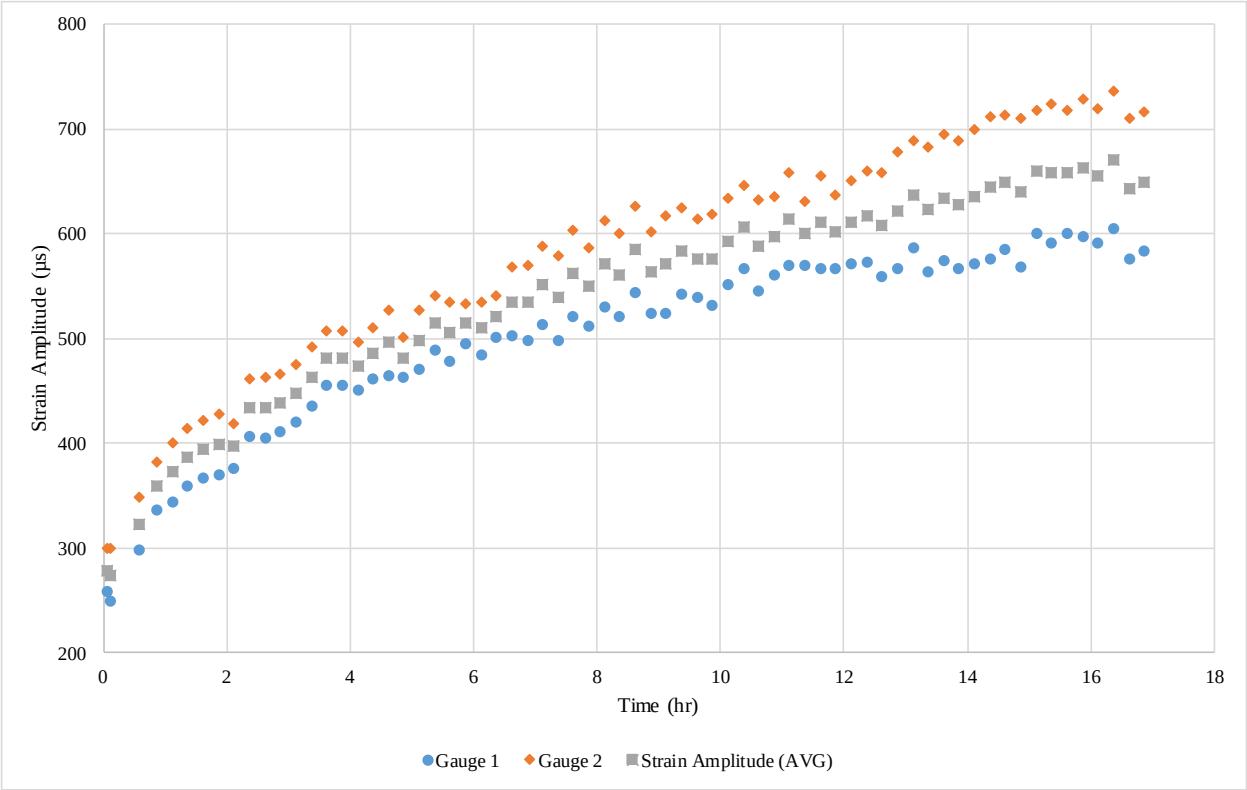

Figure B.60. The longitudinal strain amplitude for Mix #5 with the thickness of 1.5" placed on the Neoprene 60A with bonding condition.

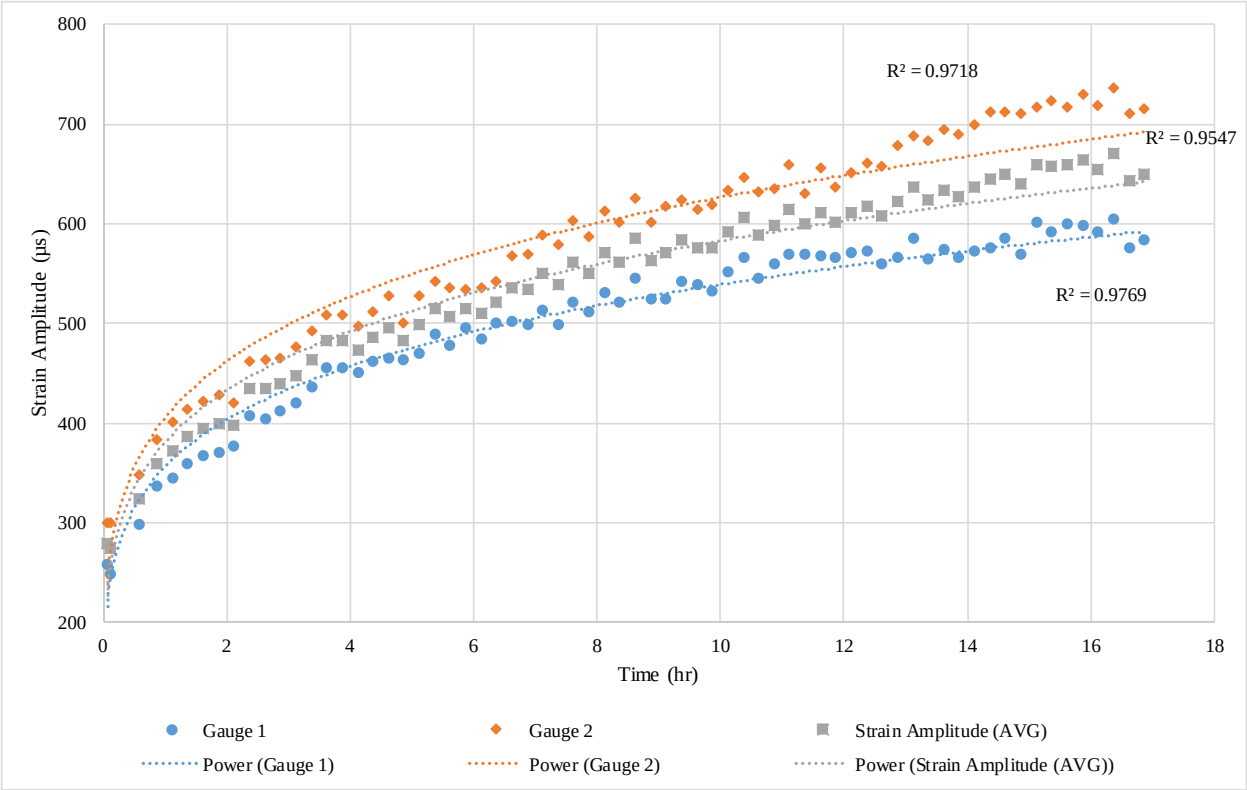

Figure B.61. The fitted power line on the longitudinal strain amplitude for Mix #5 with the thickness of 1.5" placed on the Neoprene 60A with bonding condition.

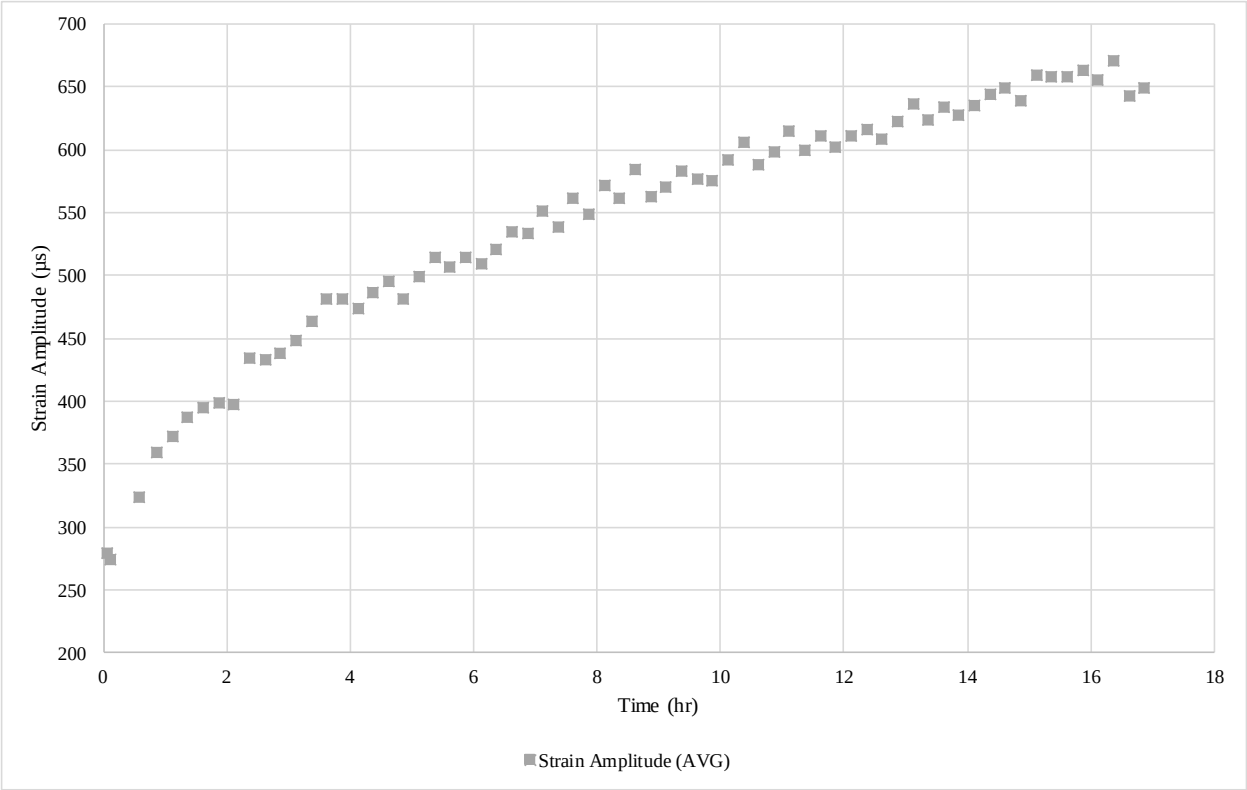

Figure B.62. The average longitudinal strain amplitude for Mix #5 with the thickness of 1.5" placed on the Neoprene 60A with bonding condition.

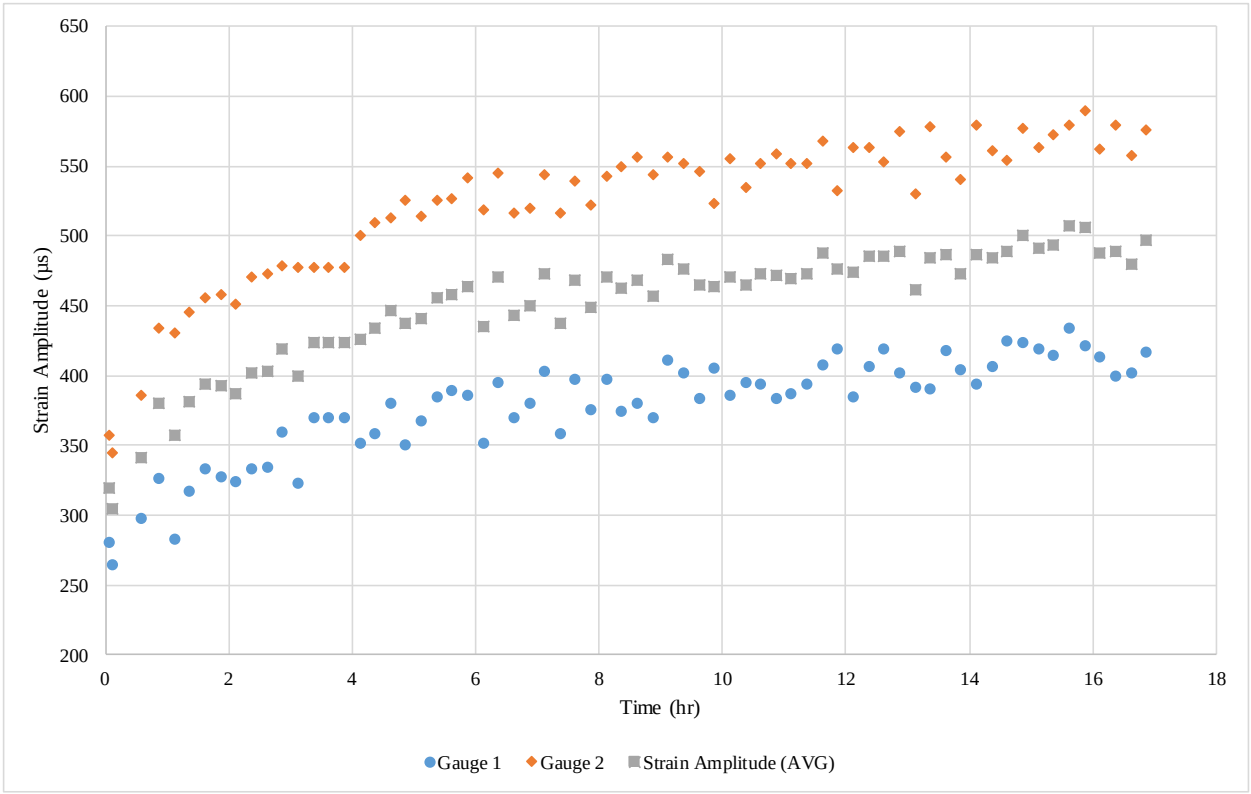

Figure B.63. The longitudinal strain amplitude for Mix #5 with the thickness of 1.5" placed on the Neoprene 60A with bonding condition (Second Slab).

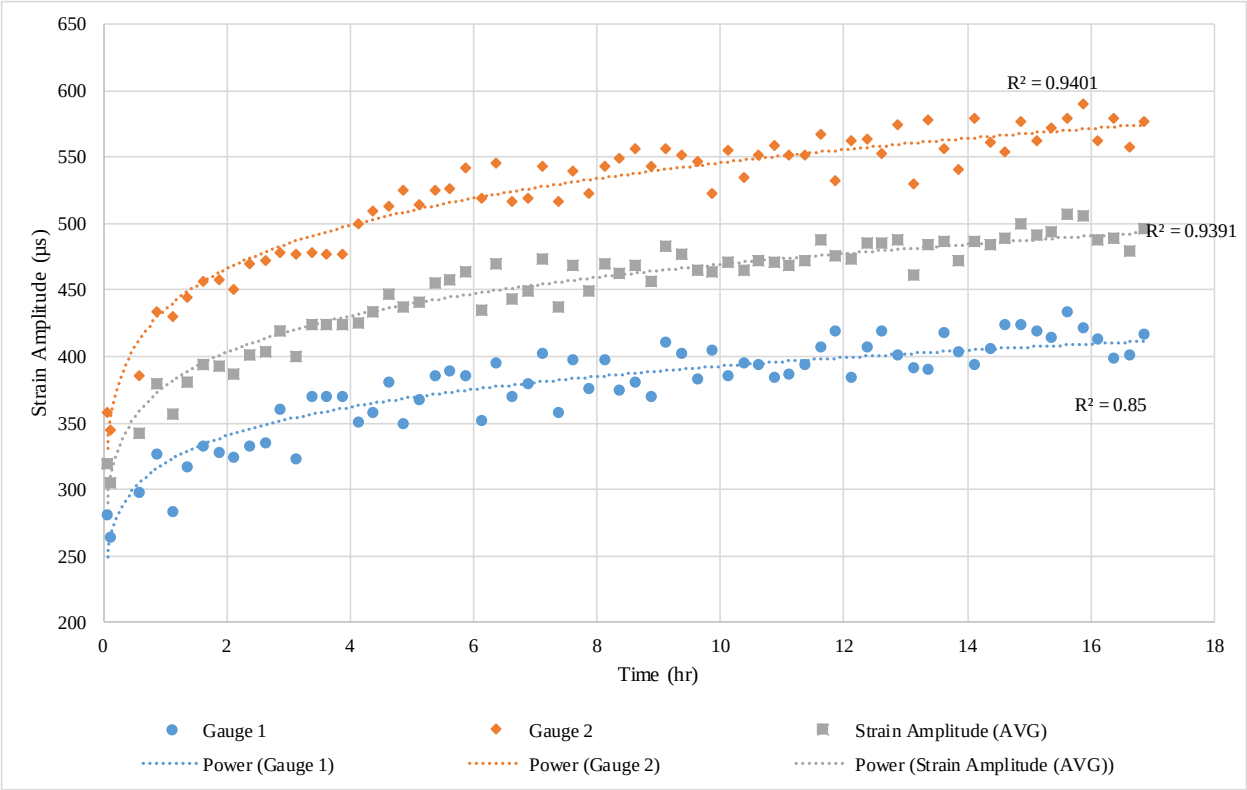

Figure B.64. The fitted power line on the longitudinal strain amplitude for Mix #5 with the thickness of 1.5" placed on the Neoprene 60A with bonding condition (Second Slab).

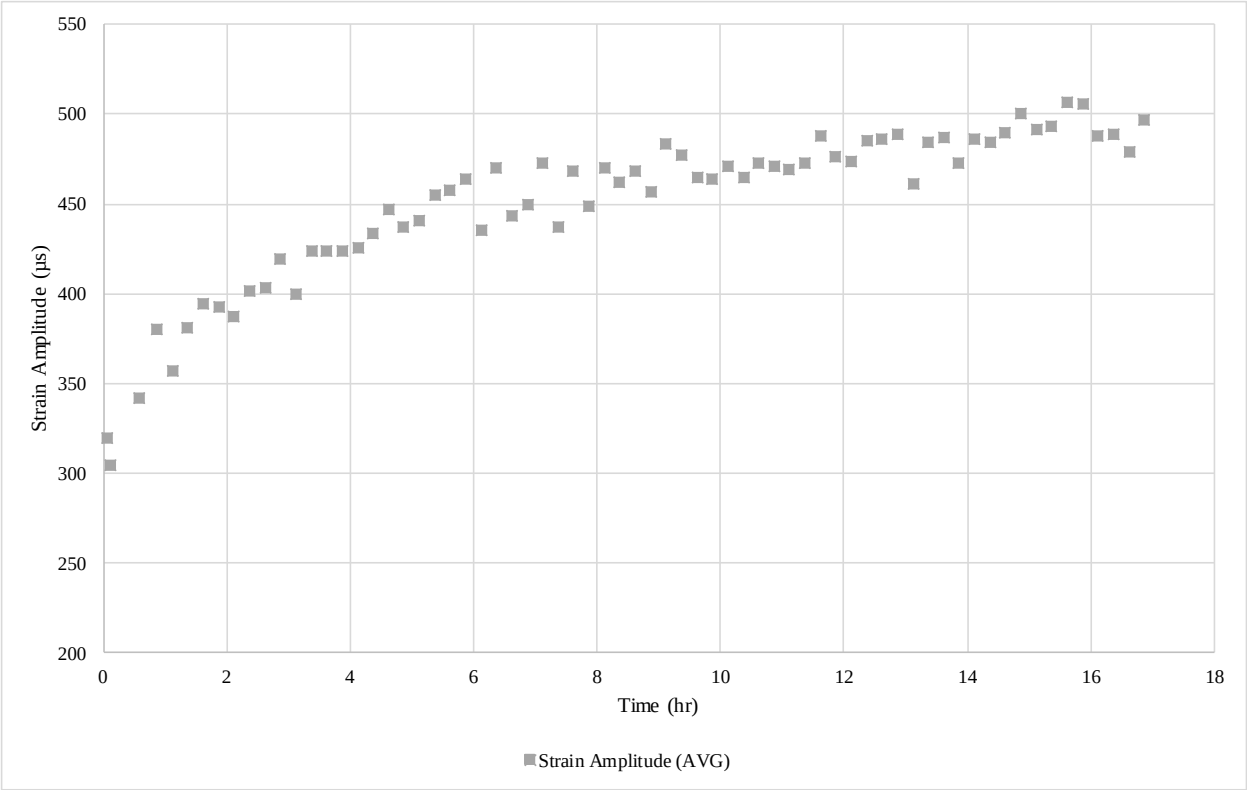

Figure B.65. The average longitudinal strain amplitude for Mix #5 with the thickness of 1.5" placed on the Neoprene 60A with bonding condition (Second Slab).

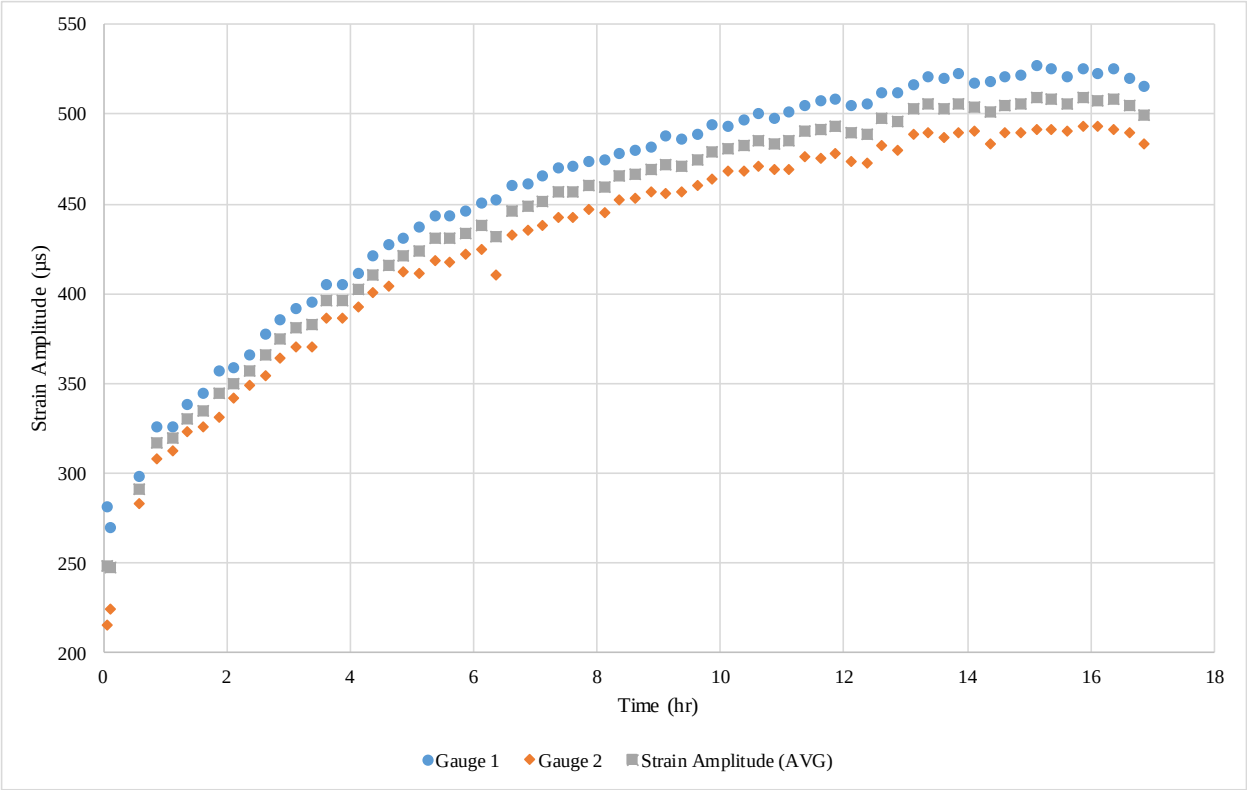

Figure B.66. The longitudinal strain amplitude for Mix #6 with the thickness of 1.5" placed on the Neoprene 60A with bonding condition.

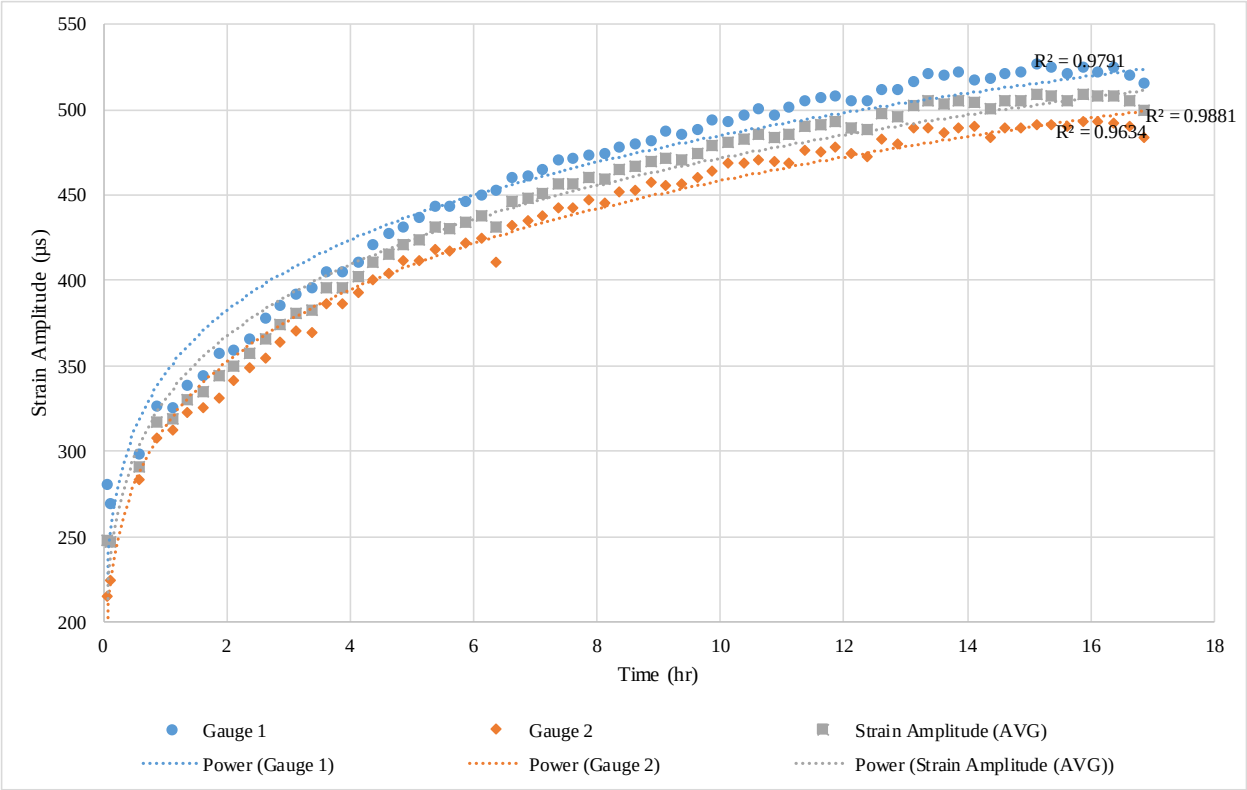

Figure B.67. The fitted power line on the longitudinal strain amplitude for Mix #6 with the thickness of 1.5" placed on the Neoprene 60A with bonding condition.

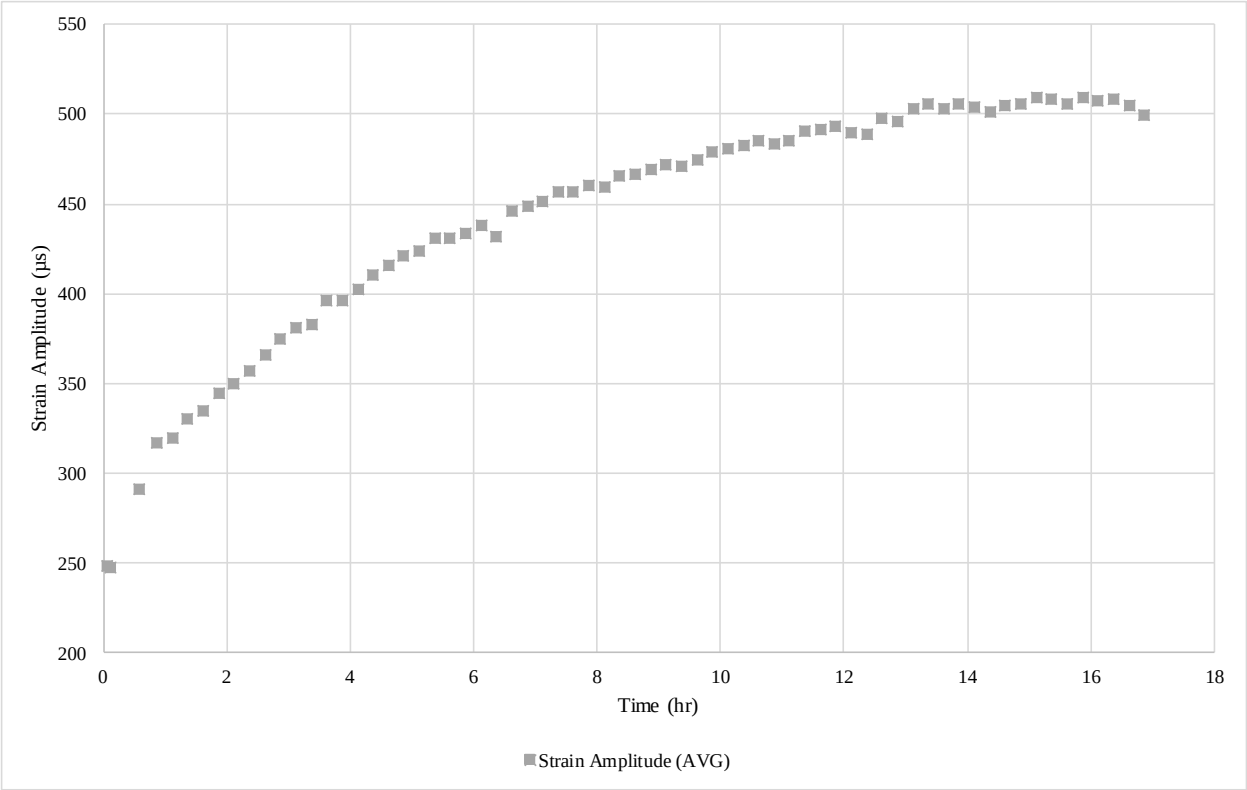

Figure B.68. The average longitudinal strain amplitude for Mix #6 with the thickness of 1.5" placed on the Neoprene 60A with bonding condition.

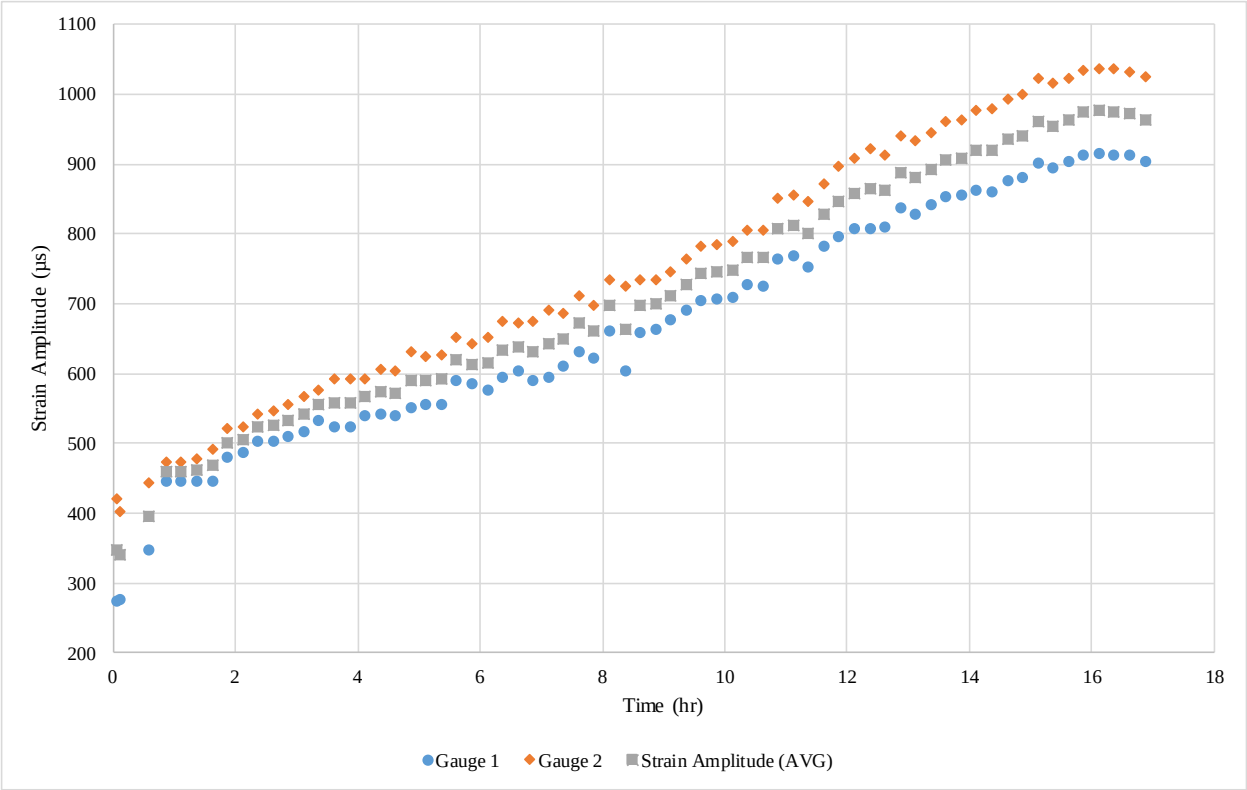

Figure B.69. The longitudinal strain amplitude for Mix #6 with the thickness of 1.5" placed on the Neoprene 60A with bonding condition (Second Slab).

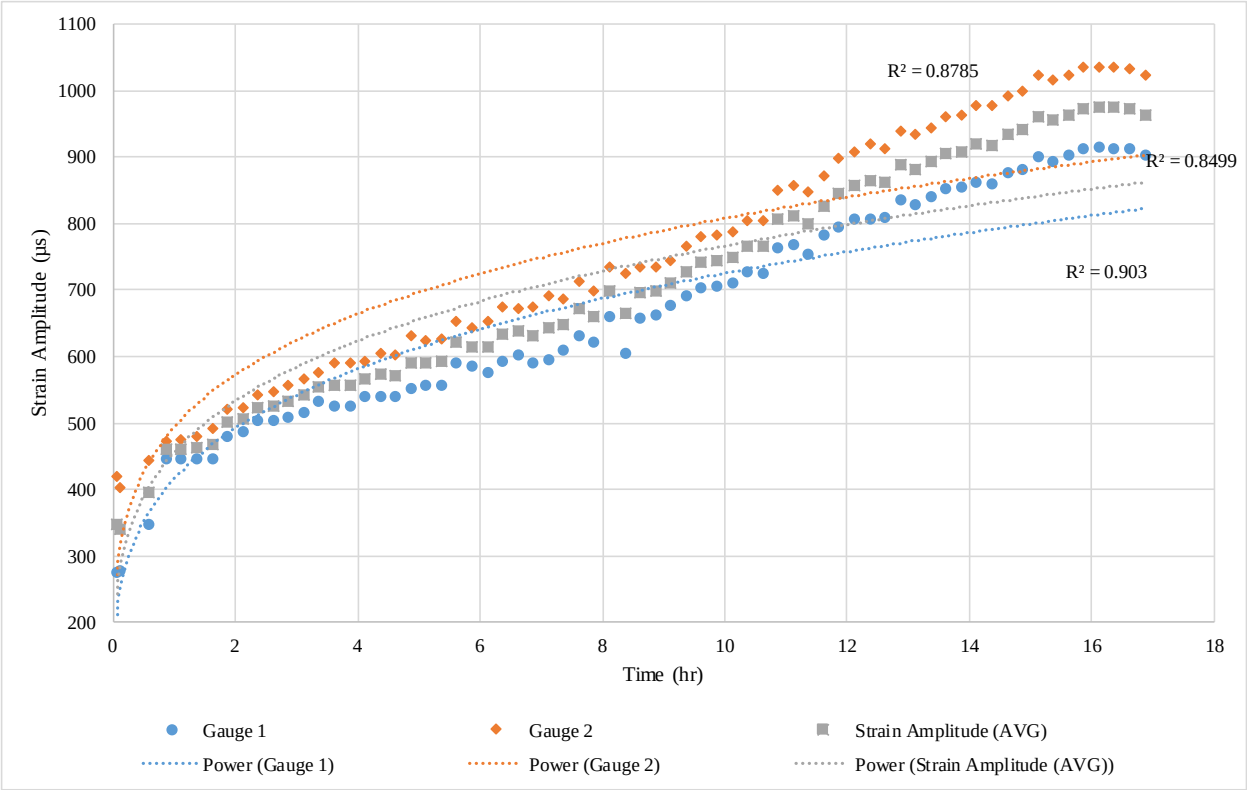

Figure B.70. The fitted power line on the longitudinal strain amplitude for Mix #6 with the thickness of 1.5" placed on the Neoprene 60A with bonding condition (Second Slab).

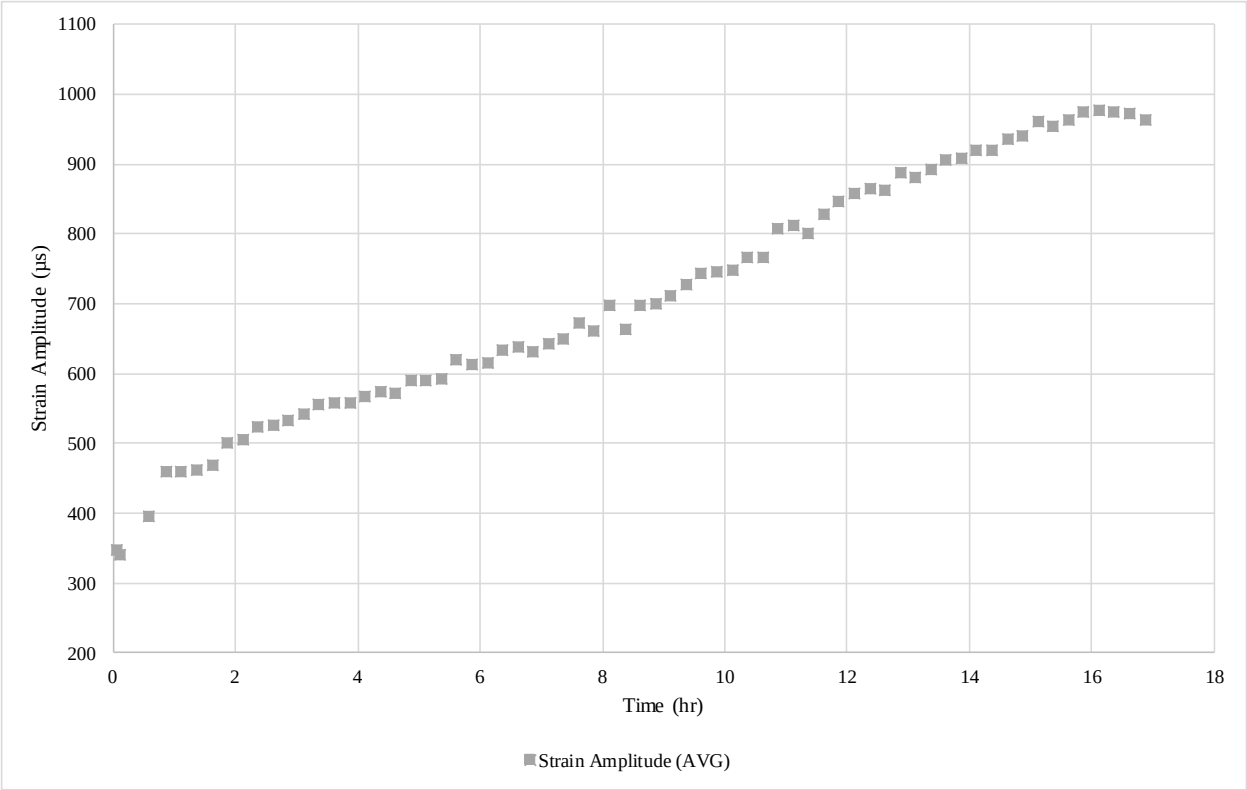

Figure B.71. The average longitudinal strain amplitude for Mix #6 with the thickness of 1.5" placed on the Neoprene 60A with bonding condition (Second Slab).

APPENDIX C

Tested Slabs and Summary of Results

Table C.1. Tested Slabs and Summary of Results (part 1).

	Dimensions in mm			Dimensions in Inches			Volumetrics and Mass				
Mix ID	Length	Width	Height	Length	Width	Height	Gmm	Target AV, %	Vol. CF	Estimated Mass, g	Gmb of compacted slab after cut
1-3	380	200	37.5	14.96	7.87	1.476	2.560	7.0	1.015	6,665	2.380
1-4	380	200	37.5	14.96	7.87	1.476	2.560	7.0	1.015	6,665	2.394
1-7	380	200	27.2	14.96	7.87	1.071	2.560	7.0	1.015	4,835	2.398
1-8	380	200	27.2	14.96	7.87	1.071	2.560	7.0	1.010	4,858	2.393
1-11	380	200	37.5	14.961	7.874	1.4764	2.560	7.0	1.015	6,665	2.366
1-12	380	200	37.5	14.961	7.874	1.4764	2.560	7.0	1.015	6,665	2.368
1-13	380	200	37.5	14.961	7.874	1.4764	2.560	7.0	1.015	6,665	2.406
1-14	380	200	37.5	14.961	7.874	1.4764	2.560	7.0	1.015	6,665	2.361
1-15	380	200	37.5	14.961	7.874	1.4764	2.560	7.0	1.015	6,665	2.366
1-16	380	200	37.5	14.961	7.874	1.4764	2.560	7.0	1.015	6,665	2.365
5-1	380	200	37.5	14.961	7.874	1.4764	2.526	7.0	1.015	6,577	2.358
5-2	380	200	37.5	14.961	7.874	1.4764	2.526	7.0	1.015	6,577	2.397
6-1	380	200	37.5	14.961	7.874	1.4764	2.562	7.0	1.015	6,670	2.381
6-2	380	200	37.5	14.961	7.874	1.4764	2.562	7.0	1.015	6,670	2.369
4-1	380	200	37.5	14.961	7.874	1.4764	2.538	7.0	1.015	6,608	2.370
4-2	380	200	37.5	14.961	7.874	1.4764	2.538	7.0	1.015	6,608	2.376
2-1	380	200	37.5	14.961	7.874	1.4764	2.527	7.0	1.015	6,579	2.329
2-2	380	200	37.5	14.961	7.874	1.4764	2.527	7.0	1.015	6,579	2.328
3-1	380	200	37.5	14.961	7.874	1.4764	2.467	7.0	1.015	6,423	2.294
3-2	380	200	37.5	14.961	7.874	1.4764	2.467	7.0	1.015	6,423	2.310
1-18	380	200	37.5	14.961	7.874	1.4764	2.56	7.0	1.015	6,665	2.379
1-20	380	200	37.5	14.961	7.874	1.4764	2.56	7.0	1.015	6,665	2.416
1-22	380	200	37.5	14.961	7.874	1.4764	2.56	7.0	1.015	6,665	2.364
1-23	380	200	50	14.961	7.874	1.9685	2.56	7.0	1.015	8,887	2.368

	Dimensions in mm			Dimensions in Inches			Volumetrics and Mass				
Mix ID	Length	Width	Height	Length	Width	Height	Gmm	Target AV, %	Vol. CF	Estimated Mass, g	Gmb of compacted slab after cut
1-24	380	200	50	14.961	7.874	1.9685	2.56	7.0	1.015	8,887	2.374
1-25	380	200	37.5	14.961	7.874	1.4764	2.560	7.0	1.015	6,665	2.381
1-26	380	200	37.5	14.961	7.874	1.4764	2.560	7.0	1.015	6,665	2.398
1-27	380	200	37.5	14.961	7.874	1.4764	2.560	7.0	1.015	6,665	2.378
1-19	380	200	37.5	14.961	7.874	1.4764	2.56	7.0	1.015	6,665	2.352
1-1	380	200	50	14.96	7.87	1.969	2.560	7.0	1.015	8,887	2.423
1-2	380	200	50	14.96	7.87	1.969	2.560	7.0	1.015	8,887	2.416
1-17	380	200	37.5	14.961	7.874	1.4764	2.56	7.0	1.015	6,665	2.360
1-5	380	200	25	14.96	7.87	0.984	2.560	7.0	1.015	4,444	2.259
1-6	380	200	25	14.96	7.87	0.984	2.560	7.0	1.015	4,444	2.262
1-9	380	200	37.5	14.961	7.874	1.4764	2.560	7.0	1.015	6,665	2.291
1-10	380	200	37.5	14.961	7.874	1.4764	2.560	7.0	1.015	6,665	2.287

Table C.2. Tested Slabs and Summary of Results (part 2).

-	Dates					Air void			
Mix ID	Prepare Loose Mix	Ship Loose Mix	Received Compacted Slab	Date, Voids Measurement Before Trim, at NECEPT	Gmb after Trimming	Before Trim, at NECEPT	After Trim, at NECEPT	Virgin AC, %	RAP, %
1-3	5/2/22	5/5/22	5/31/22	5/31/2022	6/3/22	7.5	7.0	5.7	0
1-4	5/2/22	5/5/22	5/31/22	5/31/2022	6/15/22	6.9	6.5	5.7	0
1-7	7/14/22	7/15/22	8/8/22	8/9/2022	8/11/22	6.0	6.3	5.7	0
1-8	7/14/22	7/15/2022	8/8/22	8/9/2022	8/15/22	6.4	6.5	5.7	0
1-11	9/9/22	9/13/22	9/28/22	9/30/2022	10/5/22	8.2	7.6	5.7	0
1-12	9/9/22	9/13/22	9/28/22	10/3/2022	10/10/22	7.5	7.5	5.7	0
1-13	9/12/22	9/13/22	9/28/22	10/14/2022	10/18/22	6.8	6.0	5.7	0
1-14	9/12/22	9/13/22	9/28/22	10/14/2022	10/18/22	8.2	7.8	5.7	0
1-15	9/12/22	9/13/22	9/28/22	10/14/2022	10/18/22	7.7	7.6	5.7	0
1-16	9/12/22	9/13/22	9/28/22	10/14/2022	10/18/22	7.6	7.6	5.7	0
5-1	9/26/22	10/18/22	11/2/22	11/3/2022	11/7/22	7.0	6.7	6.2	0
5-2	9/26/22	10/18/22	11/2/22	11/3/2022	11/7/22	5.6	5.1	6.2	0
6-1	9/26/22	10/18/22	11/2/22	11/3/2022	11/10/22	7.5	7.1	5.2	0
6-2	9/26/22	10/18/22	11/2/22	11/3/2022	11/10/22	7.9	7.5	5.2	0
4-1	11/4/22	11/10/22	12/2/22	12/5/2022	12/7/22	7.3	6.6	3.8	35
4-2	11/4/22	11/10/22	12/2/22	12/5/2022	12/7/22	7.3	6.4	3.8	35
2-1	11/4/22	11/10/22	12/2/22	12/5/2022	12/12/22	8.2	7.8	3.8	35
2-2	11/4/22	11/10/22	12/2/22	12/5/2022	12/12/22	8.4	7.9	3.8	35
3-1	12/13/22	12/14/22	1/3/23	1/5/2023	1/9/23	7.6	7.0	6.8	0
3-2	12/13/22	12/14/22	1/3/23	1/5/2023	1/9/23	7.1	6.4	6.8	0
1-18	12/13/22	12/14/22	1/3/23	1/5/2023	1/18/23	7.4	7.1	5.7	0
1-20	2/16/23	2/23/23	3/9/23	3/10/2023	3/13/23	6.5	5.6	5.7	0
1-22	2/16/23	2/23/23	3/9/23	3/10/2023	3/13/23	8.0	7.6	5.7	0
1-23	2/16/23	2/23/23	3/9/23	3/10/2023	3/14/23	8.2	7.5	5.7	0

	Dates					Air Void			
Mix ID	Prepare Loose Mix	Ship Loose Mix	Received Compacted Slab	Date, Voids Measurement Before Trim, at NECEPT	Gmb after Trimming	Before Trim, at NECEPT	After Trim, at NECEPT	Virgin AC, %	RAP, %
1-24	2/16/23	2/23/23	3/9/23	3/10/2023	3/14/23	7.7	7.3	5.7	0
1-25	3/14/23	3/15/23	3/29/23	3/31/23	4/6/23	7.3	7.0	5.7	0
1-26	3/14/23	3/15/23	3/29/23	3/31/23	4/6/23	6.9	6.3	5.7	0
1-27	3/14/23	3/15/23	3/29/23	3/31/23	4/18/23	7.1	7.1	5.7	1
1-19	12/13/22	12/14/22	1/3/23	1/5/2023	1/18/23	8.2	8.1	5.7	2
1-1	2/1/22	2/7/22	2/24/22	2/22/2022	2/28/22	N/A	5.3	5.7	3
1-2	2/1/22	2/7/22	2/24/22	2/23/2022	2/28/22	N/A	5.6	5.7	4
1-17	12/13/22	12/14/22	1/3/23	1/14/2022	1/12/23	8.1	7.8	5.7	5
1-5	6/21/22	6/23/22	7/7/22	7/5/2022	7/12/22	11.3	11.8	5.7	6
1-6	6/21/22	6/23/22	7/7/22	7/5/2022	7/13/22	11.0	11.7	5.7	7
1-9	8/18/22	8/19/22	9/12/22	9/5/2022	9/19/22	10.1	10.5	5.7	8
1-10	8/18/22	8/19/22	9/12/22	9/5/2022	9/27/22	10.9	10.7	5.7	9

Table C.3. Tested Slabs and Summary of Results (part 3).

Mix ID	PG	Mix	Strain amplitude at early stage	Strain amplitude at middle stage	Strain amplitude at late stage	Strain amplitude increment from early to middle stage	Strain amplitude increment from early to late stage	Strain amplitude increment from middle to late stage	Note
1-3	64S-22	Mix #1	373.50	516.11	575.79	38.18%	54.16%	11.56%	Reference mix (1.5")
1-4	64S-22	Mix #1							
1-7	64S-22	Mix #1, 1" thick	526.35	1268.73	3309.45	141.04%	528.75%	160.85%	Reference mix (1")
1-8	64S-22	Mix #1, 1" thick							
1-11	64S-22	Mix #1	461.05	565.98	598.47	22.76%	29.80%	5.74%	Reference mix (1.5") at 30°C on PennDOT No. 2A aggregate base
1-12	64S-22	Mix #1							
1-13	64S-22	Mix #1	299.73	403.50	450.46	34.62%	50.29%	11.64%	Reference mix (1.5") at 25°C on PennDOT No. 2A aggregate base
1-14	64S-22	Mix #1							
1-15	64S-22	Mix #1, 4" wide slab	421.45	638.85	680.06	51.58%	61.36%	6.45%	Reference mix (1.5"*4" width) at 25°C on Neoprene
1-16	64S-22	Mix #1, 4" wide slab							
5-1	64S-22	Mix #5, (Mix #1, Opt AC+0.5%)	320.56	495.18	516.84	54.48%	61.23%	4.37%	Reference mix (1.5") AC+0.5% binder
5-2	64S-22	Mix #5, (Mix #1, Opt AC+0.5%)							
6-1	64S-22	Mix #6, (Mix #1, Opt AC-0.5%)	320.66	572.74	729.71	78.61%	127.57%	27.41%	Reference mix (1.5") AC-0.5% binder
6-2	64S-22	Mix #6, (Mix #1, Opt AC-0.5%)							
4-1	64S-22	Mix #4	269.54	271.62	277.43	0.77%	2.93%	2.14%	RAP with PG 64-22
4-2	64S-22	Mix #4							
2-1	58S-28	Mix #2	374.64	566.92	624.93	51.32%	66.81%	10.23%	RAP with PG 58-22
2-2	58S-28	Mix #2							
3-1	64E-22	Mix #3 SMA	472.72	876.59	966.51	85.44%	104.46%	10.26%	SMA
3-2	64E-22	Mix #3 SMA							
1-18	64S-22	Mix #1	469.75	968.82	1059.72	106.24%	125.59%	9.38%	Reference mix (1.5") at 30°C on Neoprene

Mix ID	PG	Mix	Strain amplitude at early stage	Strain amplitude at middle stage	Strain amplitude at late stage	Strain amplitude increment from early to middle stage	Strain amplitude increment from early to late stage	Strain amplitude increment from middle to late stage	Note
1-20	64S-22	Mix #1	387.01	635.40	681.30	64.18%	76.04%	7.22%	Reference mix (1.5") on Neoprene 40A
1-22	64S-22	Mix #1							
1-23	64S-22	Mix #1, 2" thick	245.61	322.51	308.76	31.31%	25.71%	-4.26%	Reference mix (2")
1-24	64S-22	Mix #1, 2" thick							
1-25	64S-22	Mix #1	448.60	1012.90	990.26	125.79%	120.74%	-2.24%	Reference mix (1.5"), No bonding
1-26	64S-22	Mix #1							
1-27	64S-22	Mix #1	522.12	900.76	867.14	72.52%	66.08%	-3.73%	Low speed
1-19	64S-22	Mix #1							
1-1	64S-22	Mix #1, 2" thick	_	_	_	_	_	-	strain gauges did not survive to take any stage readings
1-2	64S-22	Mix #1, 2" thick	_	_	_	_	_	-	
1-17	64S-22	Mix #1	_	_	_	_	_	-	
1-5	64S-22	Mix #1, 1" thick	_	_	_	_	_	-	High air voids (1"), the strain gauges died at an early stage
1-6	64S-22	Mix #1, 1" thick	_	_	_	_	_	-	
1-9	64S-22	Mix #1	375.8	508.3	514.3	35.26%	36.85%	1.18%	High air voids placed on Neoprene 60A
1-10	64S-22	Mix #1	426.7	767.8	797.9	79.94%	86.99%	3.92%	High air voids placed on PennDOT No. 2A aggregate base

APPENDIX D

Response from Transverse Strains

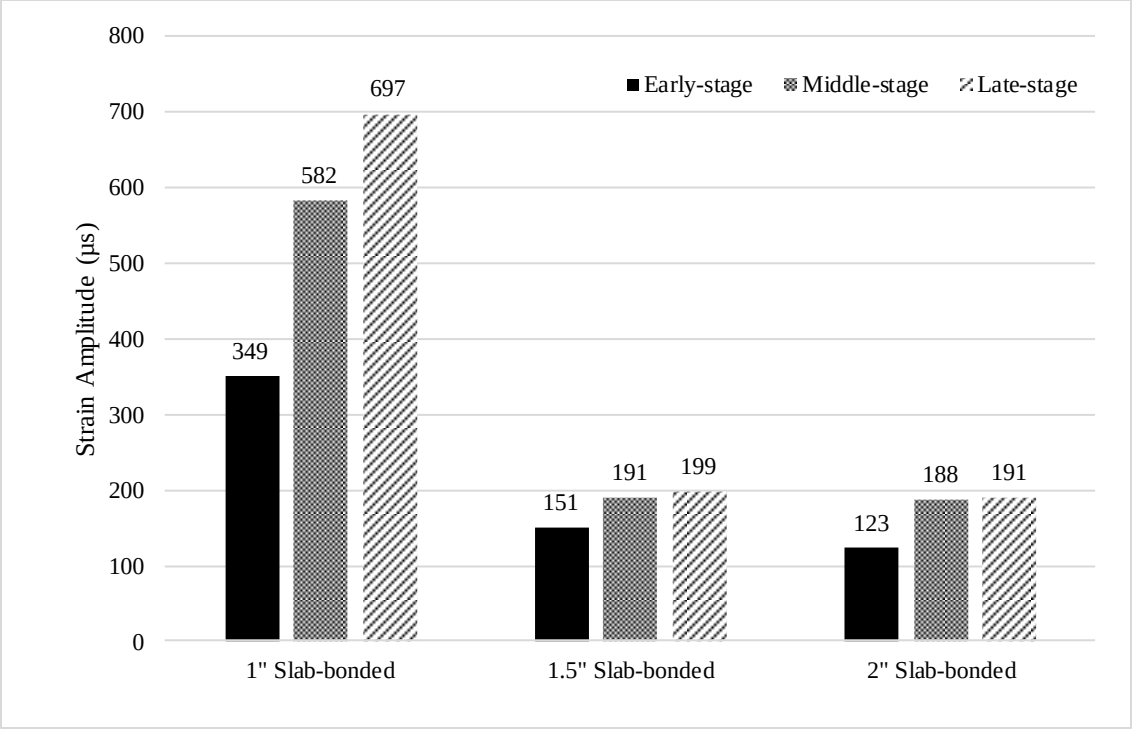

Figure D.1. The transverse strain amplitude at the bottom of the slab with different thicknesses.

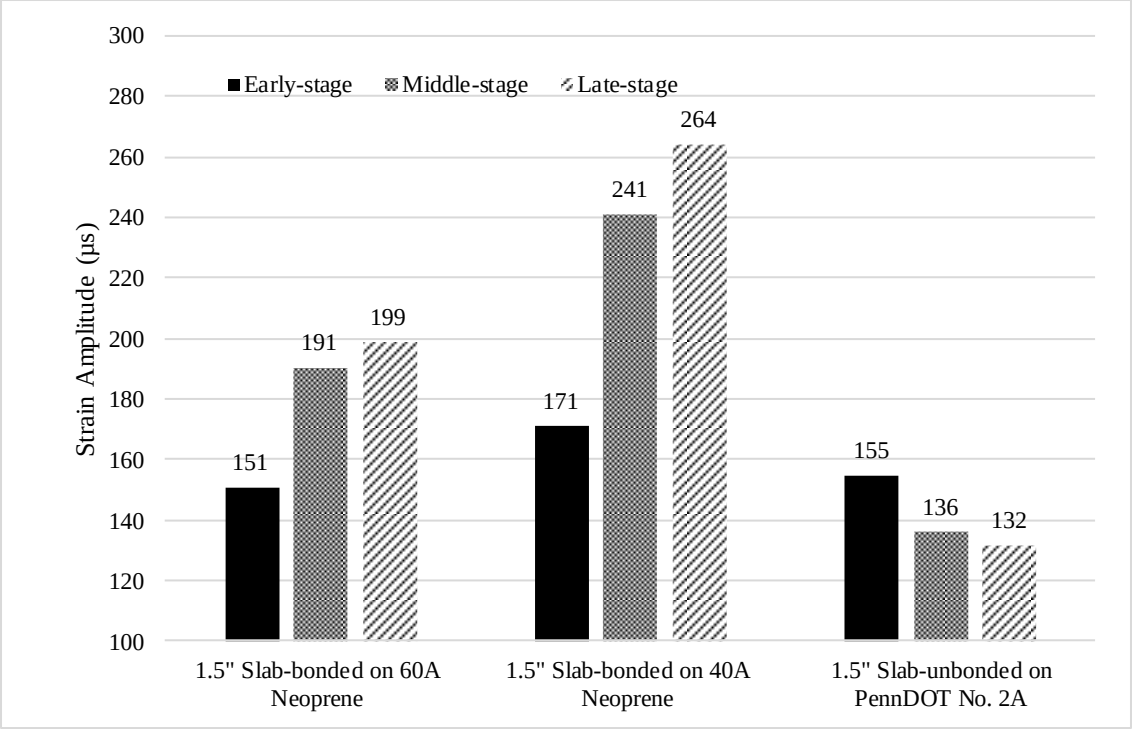

Figure D.2. The transverse strain amplitude at the bottom of the slab placed on the Neoprene (60A and 40A) and PennDOT No. 2A.

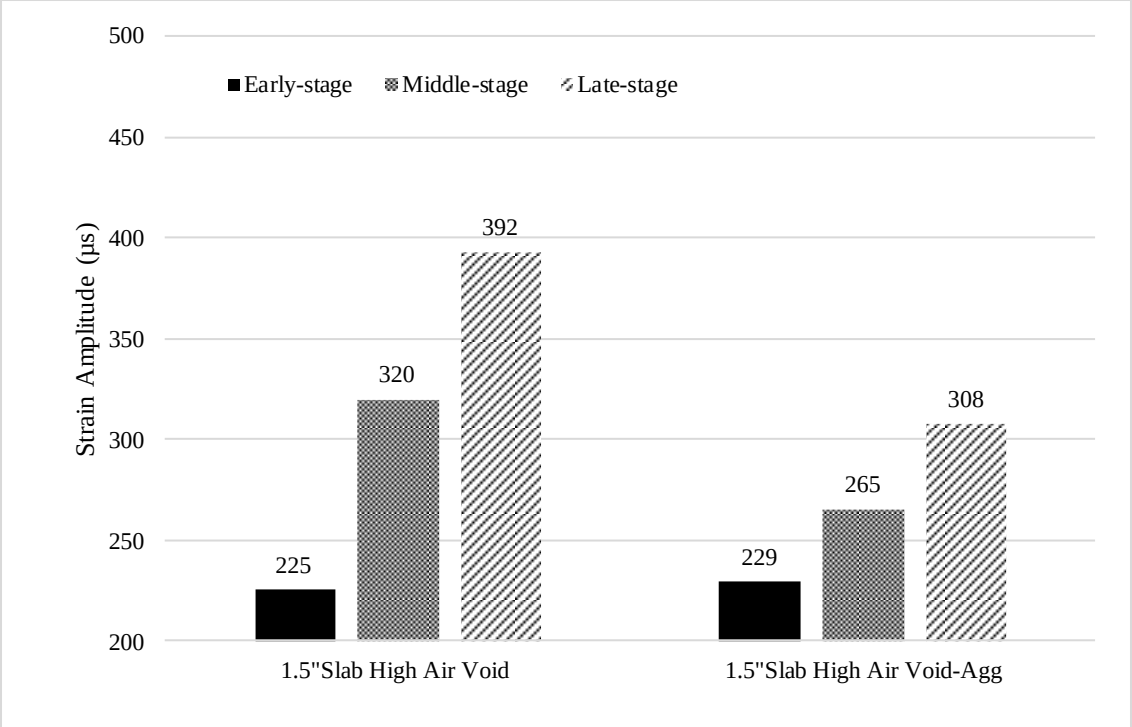

Figure D.3. The transverse strain amplitude at the bottom of the high air void slabs placed on the Neoprene (60A) and PennDOT No. 2A.

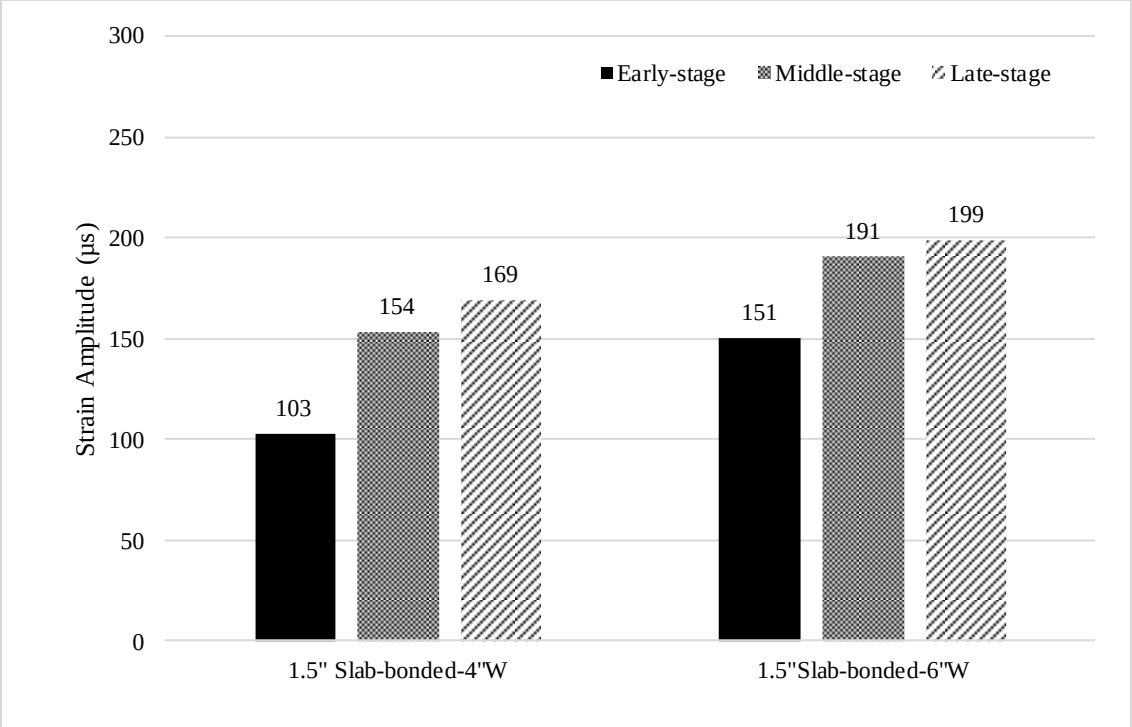

Figure D.4. The transverse Strain amplitude for the samples with the width of 4 and 6 inches at three different stages.

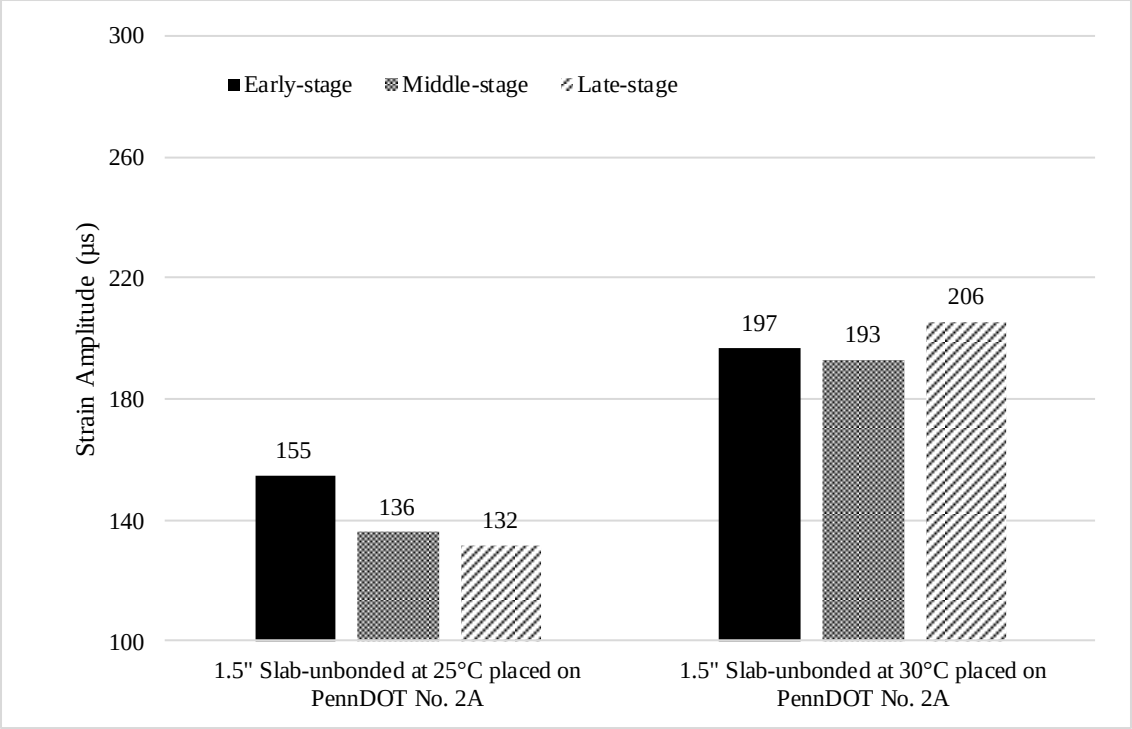

Figure D.5. The transverse strain amplitude at two different temperatures for the sample placed on PennDOT No. 2A aggregate.

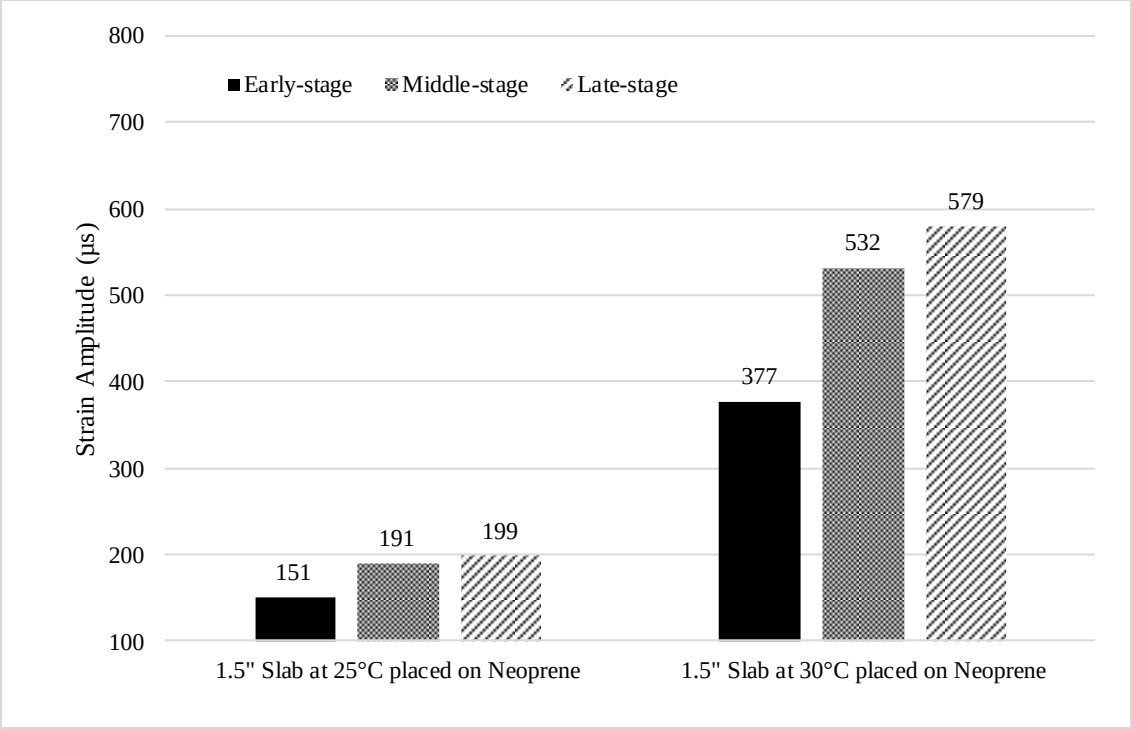

Figure D.6. The transverse strain amplitude at two different temperatures for the sample placed on Neoprene 60A.

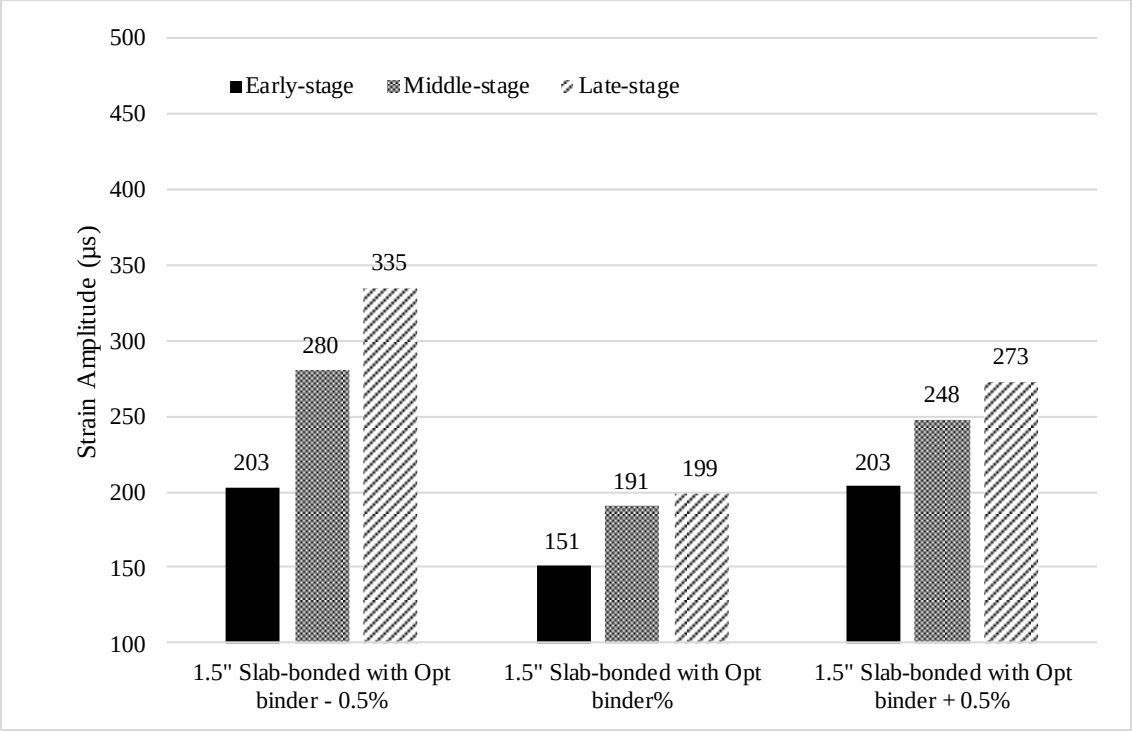

Figure D.7. The transverse strain amplitude for high and low binder mixes.

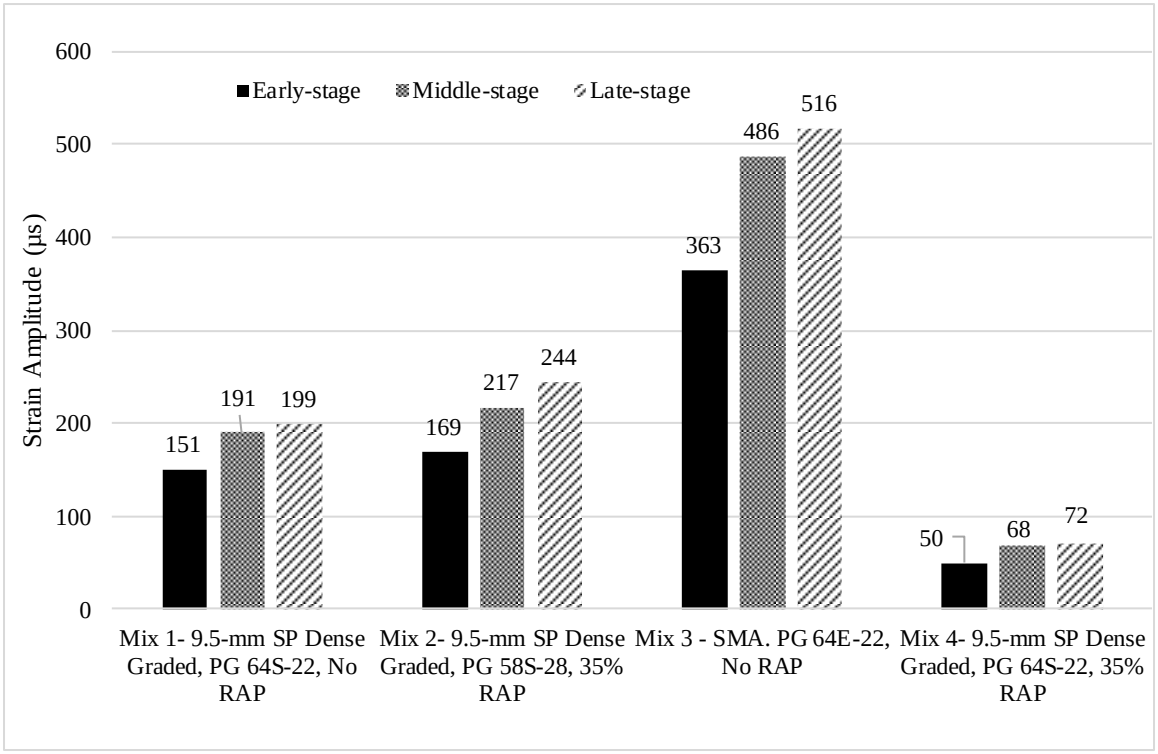

Figure D.8. The transverse strain amplitude for different mixes.

Appendix E

Load-Displacement Graphs

from IDEAL-CT Tests

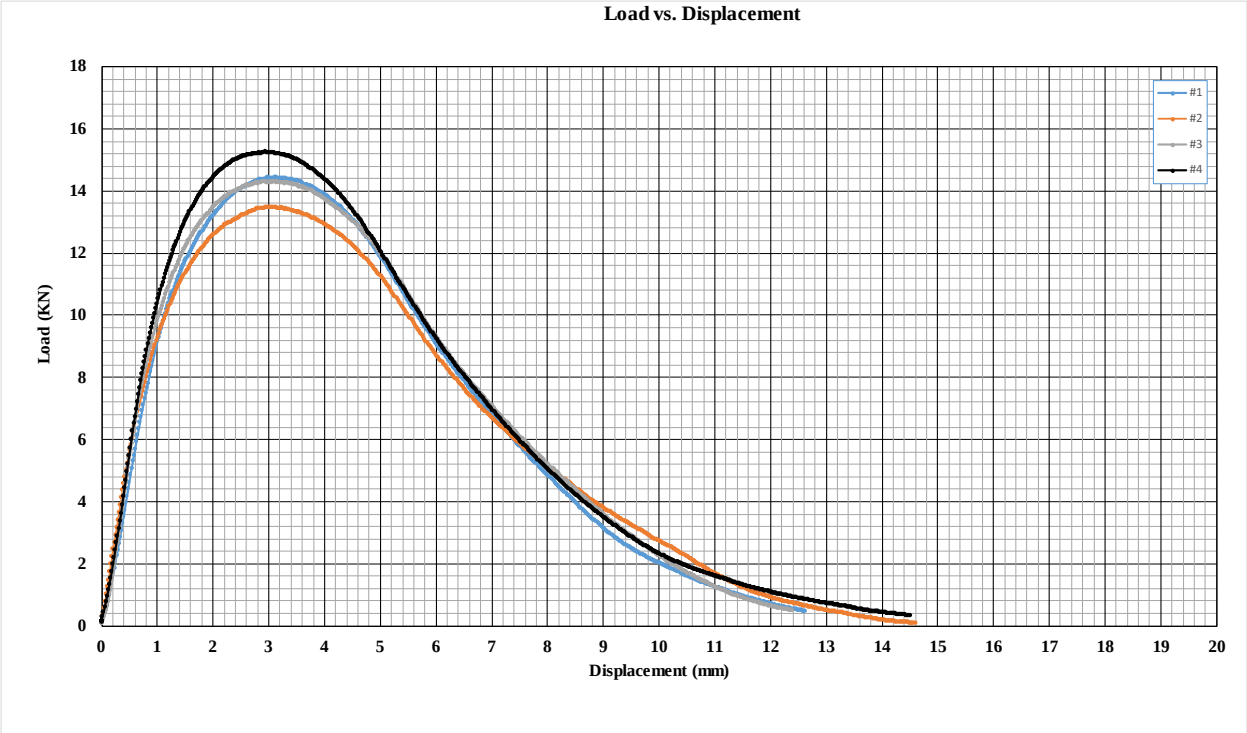

Figure E.1. The load-displacement curve for Mix 1 (9.5-mm SP Dense Graded, PG 64S-22, No RAP).

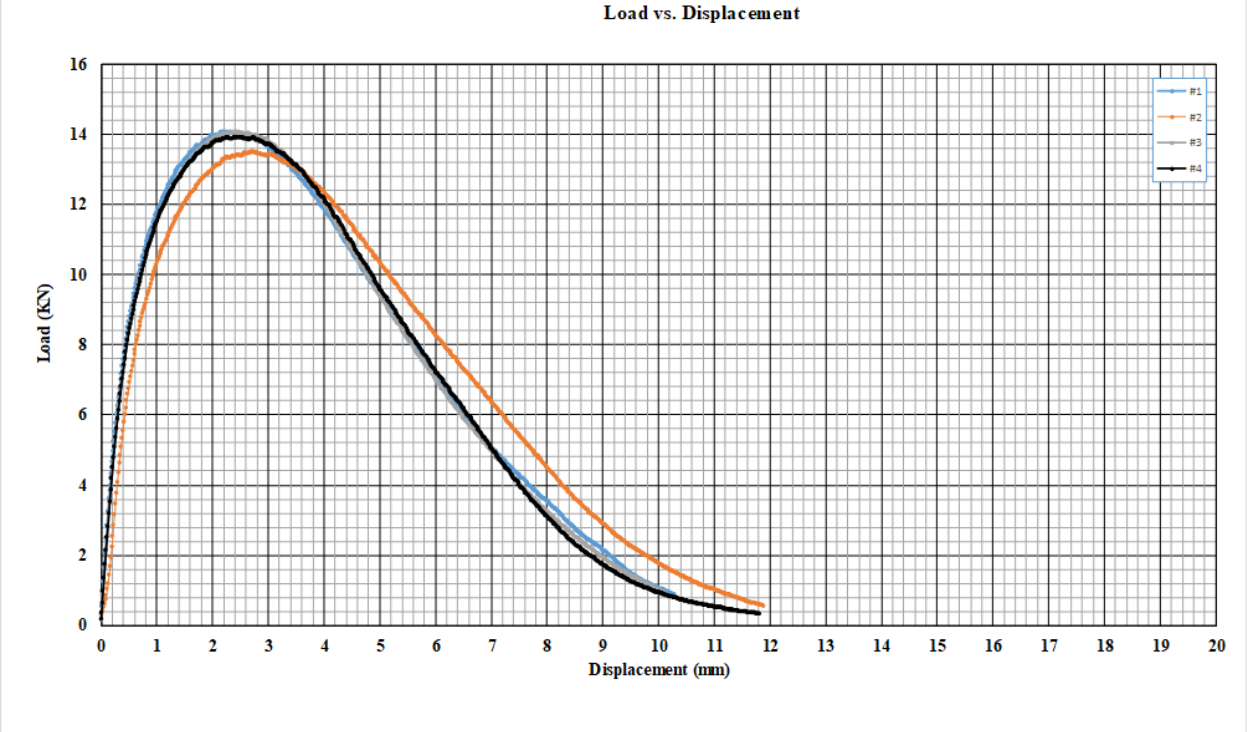

Figure E.2. The load-displacement curve for Mix 2 (9.5-mm SP Dense Graded, PG 58S-28, 35% RAP).

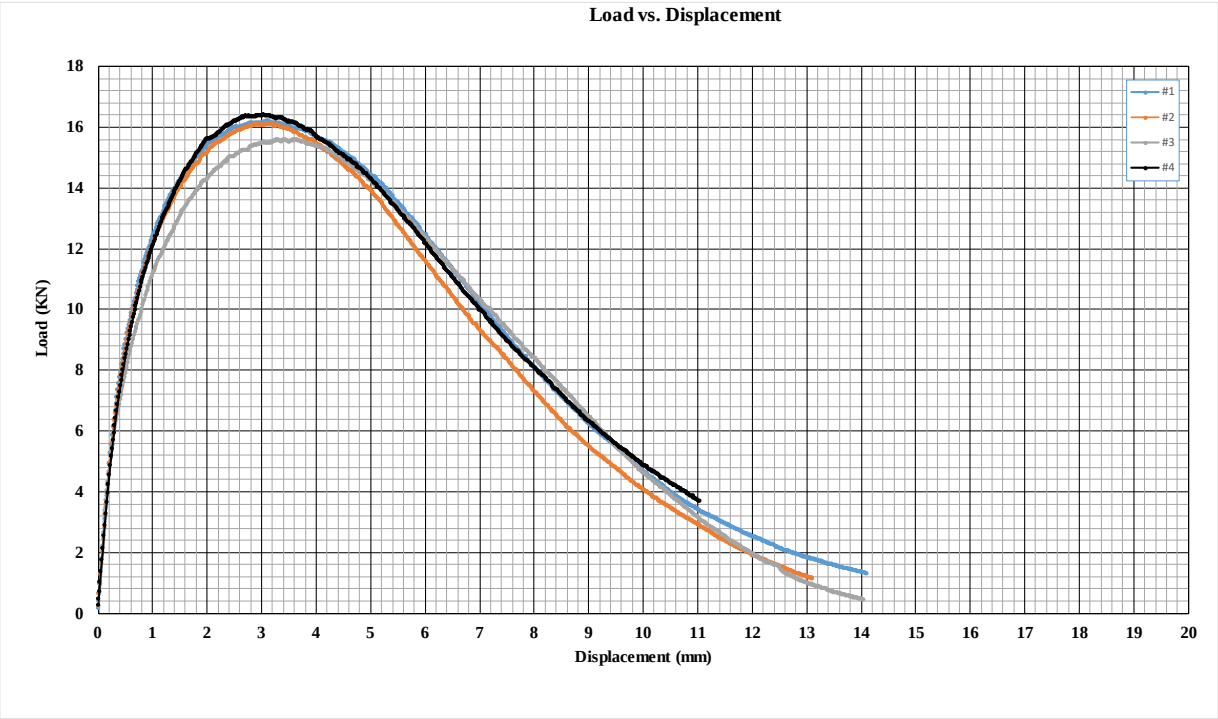

Figure E.3. The load-displacement curve for Mix 3 (SMA, PG 64E-22, No RAP).

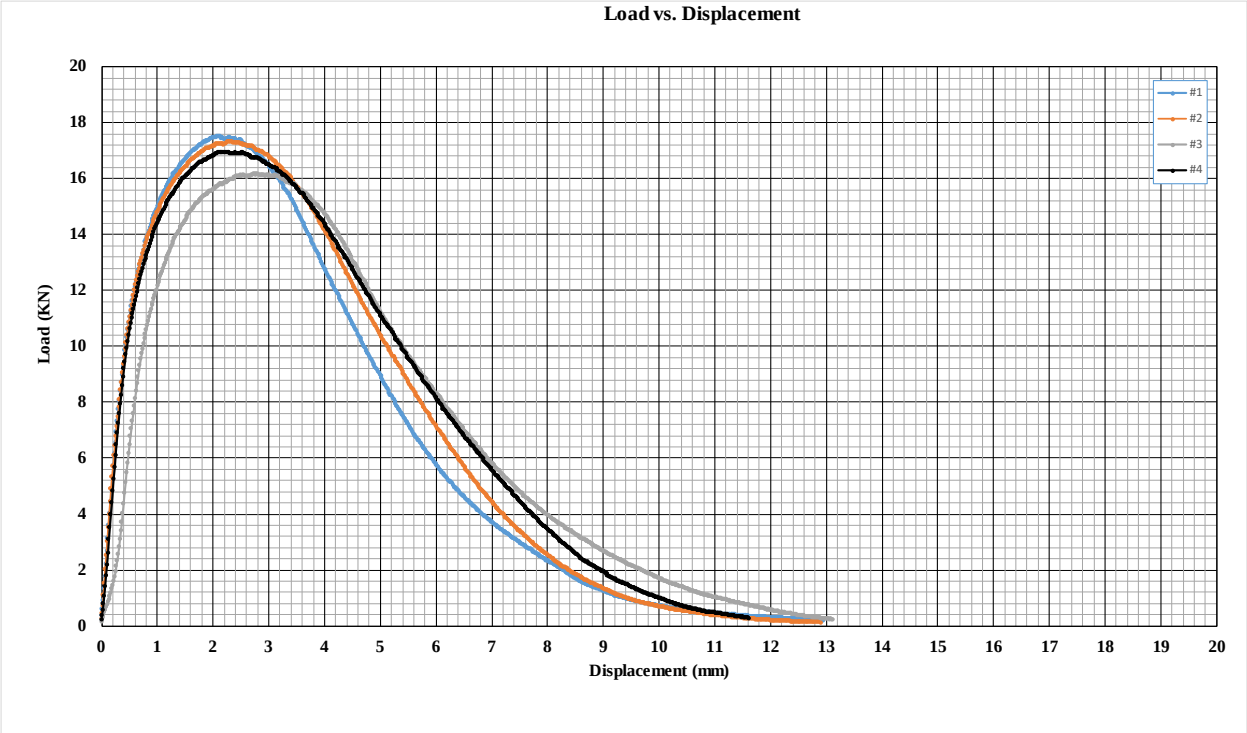

Figure E.4. The load-displacement curve for Mix 4 (9.5-mm SP Dense Graded, PG 64S-22, 35% RAP).

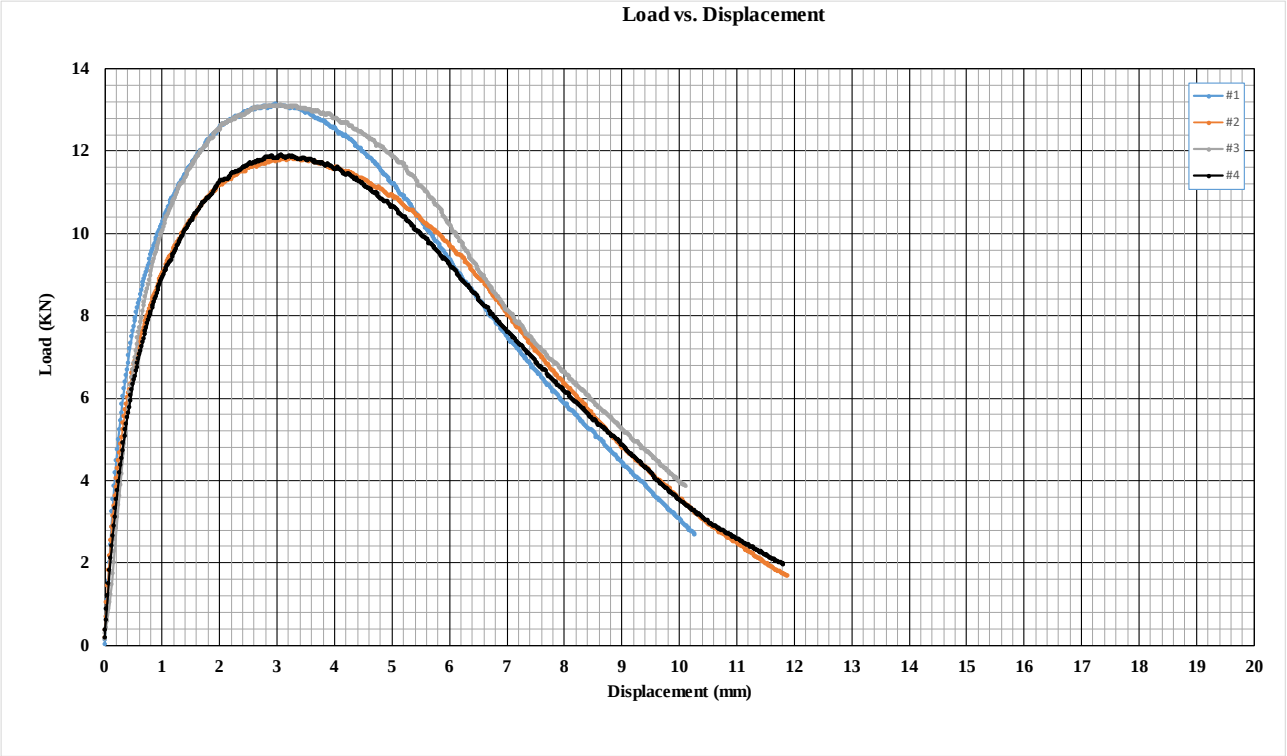

Figure E.5. The load-displacement curve for Mix 5 (Mix 1 + 0.5% binder, PG 64S-22, No RAP).

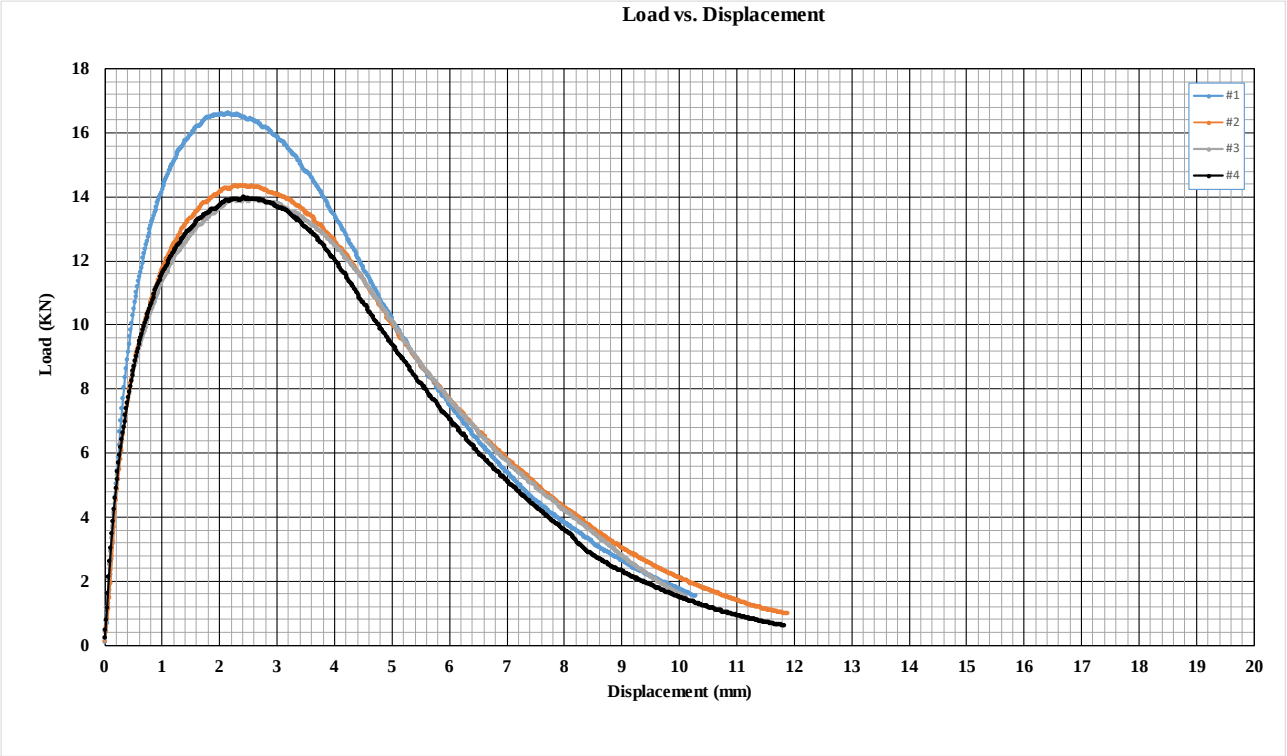

Figure E.6. The load-displacement curve for Mix 6 (Mix 1 - 0.5% binder, PG 64S-22, No RAP).

APPENDIX F

Proposed Test Protocol

Method of Test for Capturing Fatigue Resistance of Asphalt Concrete Using Hamburg Wheel Tracking Device

1.0 Scope

1.1. This test method is used to determine the fatigue cracking resistance of asphalt mixture under repeated loading using the Hamburg Wheel Tracking Device (HWTD). The test is conducted on rectangular asphalt concrete slabs of specified dimensions over a supporting neoprene layer with known properties.

1.2 The fundamental principle behind this test involves applying a moving load to the specimen's surface and measuring the induced tensile strain at the bottom of the asphalt mixture specimens.

1.3 The values stated in SI units are to be regarded as the standard. Values in parenthesis are provided for information only.

2.0 Referenced Documents

2.1. Pennsylvania Test Methods (PTMs)

- 715 - Determination of Bulk Specific Gravity of Compacted Bituminous Mixtures

2.2. AASHTO Standards

- R 30 - Laboratory Conditioning of Asphalt Mixtures
- T 166 - Bulk Specific Gravity (Gmb) of Compacted Asphalt Mixtures Using Saturated Surface-Dry Specimens
- T 209 - Theoretical Maximum Specific Gravity (Gmm) and Density of Hot Mix Asphalt (HMA)
- T 269 - Percent Air Voids in Compacted Dense and Open Asphalt Mixtures
- T 324 - Hamburg Wheel Track Testing of Compacted Asphalt Mixtures

3.0 Significance and Use

3.1 This test is utilized to measure the fatigue resistance of compacted asphalt mixtures with a maximum nominal aggregate size not exceeding 12.5 mm.

4.0 Apparatus

4.1. Hamburg Wheel-Tracking Device - AASHTO T 324, Section 5.1.

4.2. Temperature Control System: A dry hood attachment to the HWTD is needed, if not equipped, capable of maintaining the air temperature inside the equipment to the specified test temperature within ± 1ºC during testing.

4.3. Linear Kneading Compactor: This is a device that operates on hydraulic power, designed to compact asphalt mixtures into uniform, flat slabs. It accomplishes this through the action of a vertically aligned set of steel plates. The outcome is a slab with a predetermined thickness and density.

4.4. Balance: A device capable of supporting up to 12,000 grams, with precision down to 0.1 grams.

4.5. Ovens: These are used to heat aggregate and asphalt binders to the required mixing temperatures. The ovens shall be properly standardized and capable of achieving a temperature range of 100 to 175°C (212 to 347°F), with a precision of ± 5°C (± 9°F). Multiple ovens can be utilized as long as each operates within its appropriate temperature range. The thermometer used to measure material temperatures shall comply with the specifications of AASHTO M 339M/M 339, featuring a temperature range of 140 to 175°C (284 to 347°F), and an accuracy of ± 1.25°C (± 2.25°F).

4.6. Foil Strain Gauge: A sensor used to measure strain induced to an object. In the laboratory setting, foil strain gauges are commonly utilized to record deformations and displacements in conjunction with other devices such as linear variable displacement transducers (LVDT) and extensometers. Foil strain gauges are particularly effective in measuring tensile and compressive strains in asphalt concrete slabs subjected to the wheel loading of a Hamburg Wheel Tracking Device. Use foil strain gauges with gauge length of 30 mm (1.2 inches).

4.7. Data Acquisition System (DAQ): This system comprises a specialized hardware setup integral to the process of sampling electrical signals, which are produced as a result of the physical behavior of a system under load. The DAQ effectively transforms these analog signals, captured from the system's sensors, into digital counterparts. The digitized data can then be processed and analyzed by specific application software installed on a computer. DAQ shall be capable of collecting data from a minimum of four channels.

Note: An example of DAQ for this purpose is the National Instruments DAQ system (NI PXIe-1078). This system is capable of amplifying the detected voltage changes from strain gauges and transforming these analog signals into a digital format. The DAQ can simultaneously collect data from up to eight channels, and this data can be archived for future analysis. Although the system accommodates quarter-, half-, and full-bridge configurations, a quarter-bridge setup is recommended for this test method.

4.8. Saw: Laboratory saw capable of cutting the asphalt specimens to the desired length and width, and can be either a wet or dry saw.

4.9. Water Bath: A water bath capable of maintaining a constant temperature between 20 and 30°C.

4.10. Thermometer: A liquid-in-glass thermometer or other thermometric device, accurate to 0.5°C shall be used to measure the temperature of the water bath. The thermometer shall be standardized at least every 12 months.

4.11. Vacuum Pump: Capable of evacuating the air from the vacuum container to the desired residual pressure.

4.12. Vacuum Measurement Device: A residual pressure manometer or vacuum gauge to be connected directly to the vacuum container and capable of measuring residual pressure down to 4.0 kPa or less.

4.13. Vacuum Container: A vacuum container must be capable of withstanding the full vacuum applied and must be equipped with the fittings and other necessary accessories required by the test procedure being employed. The container may be a metal bowl equipped with a transparent cover or a thick-walled glass flask.

5.0 Summary of Procedure

5.1. The procedure for testing resistance of asphalt mixtures to fatigue damage using the Hamburg Wheel Tracking Device (HWTD) can be outlined as follows:

5.1.1 Base Layer: Utilize a neoprene rubber elastomer, known for its excellent resiliency, as the load-bearing base for the test. Neoprene sheets with a Shore hardness of 40A and 60A are recommended.

5.1.2. Preparation of the Asphalt Concrete Slab: prepare asphalt concrete slab specimens with dimensions of approximately 380 mm (15 inches) in length, 203 mm (8 inches) in width, and 38 mm (1.5 inches) in thickness. Trim these slabs 318 mm (12.5 inches) in length and 152 or 102 mm (6 or 4 inches) in width. The 102 mm (4-inch) width is recommended to expedite the test procedure. The slabs are 38 mm (1.5 inches) thick as prepared in the linear kneading compactor. The air voids shall be between 6 to 8%. Affix two longitudinal strain gauges to the center of the slab using a strong adhesive, such as Gorilla™ superglue. More details are provided in Section 6.

5.1.3. Assembly and Testing: Apply an emulsified asphalt as a tack coat to the surface of the neoprene at a rate of 0.20 liters per square meter (0.045 gallons per square yard) to create a bonding condition between the slab and base layer. A cationic slow setting emulsified asphalt such as CSS-1h is recommended. After allowing the tack coat to set, place the asphalt mixture slab on top of the treated neoprene. Position the slab, with an underlying layer inside the standard HWTD mold, which should have internal dimensions of 318 mm (12.5 inches) in length and 264 mm (10.4 inches) in width. Ensure the slab is secured within the mold using wood blocks to fill any gaps. Once the assembly is complete, place the sample inside the testing machine. Maintain a consistent test temperature of 25 ± 1ºC throughout the test duration.

6.0 Specimen and Testing Environment Preparation

6.1. Prepare the mixture according to the specified job mix formula.

6.2. Set the mixing temperature based on the minimum and maximum temperature of mixture and the binder performance grade or class of material specified in Publication 408, Section 413, Table A.

6.3. Initiate the process by dry mixing the aggregates and mineral admixture, if any. Subsequently, incorporate the appropriate proportion of asphalt binder, ensuring thorough coating of all aggregate components.

6.4. Subject the asphalt mixture to short-term conditioning at the proper compaction temperature according AASHTO R 30.

6.5. Use the compaction temperature based on the minimum and maximum temperature of mixture and the binder performance grade or class of material specified in Publication 408, Section 413, Table A.

6.6. Use a Linear Kneading Compactor to compact slab specimens to a thickness of 38 ± 2.5 mm (1.5 ± 0.1 inches). Preheat molds and tools to the compaction temperature and compact slab specimens that are 318 mm (12.5 inches) long and 264 mm (10.4 inches) wide. Ensure the specimen thickness is at least triple the nominal maximum aggregate size of the asphalt mixture. After compaction, allow the slab specimens to cool at room temperature on a clean, flat surface for 24 hours.

6.7. Trim the slab specimen to the required dimensions: 152 or 102 mm (6 or 4 inches) in width and 318 mm (12.5 inches) in length. This is performed by using a wet or dry saw. The slab is trimmed from its original size to test size of 152 mm (6 inches) in width and 318 mm (12.5 inches) in length.

6.8. Determine the air void content of the trimmed specimen according to Section 7.

6.9. Utilize sandpaper to smoothen the bottom of the slab. Following this step, clean the bottom of the slab thoroughly to ensure no dust or debris remains.

6.10. Apply superglue to secure the strain gauges at the bottom of the slab. Position the strain gauges no more than 10 mm (0.4 inches) from the middle longitudinal axis. Schematics of strain gauge installation are presented in Figure 1.

6.11. Once the strain gauges are glued, allow the slab specimen to rest overnight. This ensures the glue has dried thoroughly and the strain gauges are securely affixed.

6.12. Prepare the neoprene layer by applying an emulsified asphalt tack coat at a rate of 0.20 liters per square meter (0.045 gallons per square yard). This creates a bonding condition between the slab and the neoprene layer. Allow the tack coat to set before placing the asphalt mixture slab on top of the neoprene.

6.13. Position the two-layer system (comprising the slab and neoprene) inside the test mold. Secure the system using prepared wooden beams, ensuring the slab is tightly fitted within the mold and exhibits no movement in any direction.

6.14. Set the testing environment at a temperature of 25 ± 1°C using a hood and a fan.

6.15. Position the prepared sample inside the testing machine and let it set for two hours prior to commencing the test. Maintain the testing environment at a temperature of 25 ± 1°C throughout the test duration.

6.16. Connect the strain gauges to the DAQ and ensure that the wires cannot be damaged by the wheel. If necessary, use clear tape to keep the wires in a suitable location.

6.17. Set the speed of the track using the computer connected to the HWTD. Set the speed of track for 26 cycles per minute unless the goal of the study is to examine the effect of different speeds. One cycle includes a forward pass and a backward pass of the wheel.

6.18 Start the wheel tracking and collect strain data based at preset time intervals and preset sampling rate. The time intervals and the sampling rate are presented in Table 1.

6.19 At the completion of the test, observe the slab for any visual damage and report any visible damage or cracks. Note that not observing damage or cracks is not an indication of no damage (See Section 8).

7.0 Determining Air Void Content

7.1 Determine the bulk specific gravity (Gmb) of the specimens according to the standard test method PTM No. 715 or AASHTO T 166.

7.1 Determine the theoretical maximum specific gravity (Gmm) of the mixture according to the standard test method AASHTO T 209.

7.3 Calculate the air void content of the specimens according to AASHTO T 269. The target air void content shall be within 7.0 ± 1.0 percent for the lab-compacted slab specimens.

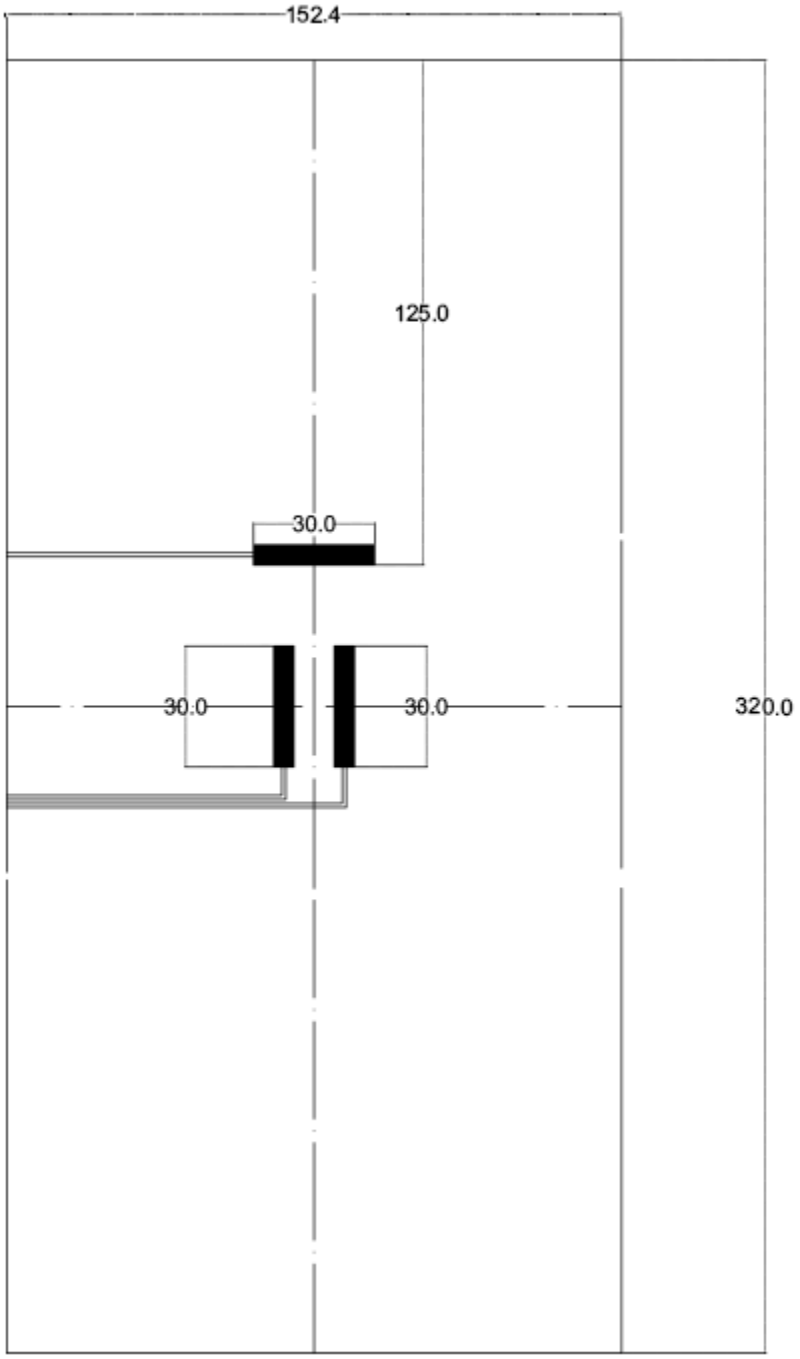

Figure 1. Configuration of strain gauges (all units in mm).

Table 1. Data Collection Times and Sampling Rates.

Time from start of tracking, hrs.	Interval for data collection, minutes[1]	Duration of sampling, minutes[2]	Sampling Freq, Hz (data points per second)	Cumulative # of wheel passes from the start of tracking
0.000	2[3]	2.00[4]	40	0
0.033	2	1.00	20	104
0.083	3	2.00	10	260
0.583	30	5.00	20	1,820
1.083	30	0.50	20	3,380
1.583	30	0.50	20	4,940
2.083	30	0.50	20	6,500
2.583	30	0.50	20	8,060
3.083	30	0.50	20	9,620
3.583	30	0.50	20	11,180
4.083	30	0.50	20	12,740
4.583	30	0.50	20	14,300
5.083	30	0.50	20	15,860
5.583	30	0.50	20	17,420
6.083	30	0.50	20	18,980
6.583	30	0.50	20	20,540
7.083	30	0.50	20	22,100
7.583	30	0.50	20	23,660
8.083	30	0.50	20	25,220
8.583	30	0.50	20	26,780
9.083	30	0.50	20	28,340
9.583	30	0.50	20	29,900
10.083	30	0.50	20	31,460
10.583	30	0.50	20	33,020
11.083	30	0.50	20	34,580
11.583	30	0.50	20	36,140
12.083	30	0.50	20	37,700
12.583	30	0.50	20	39,260
13.083	30	0.50	20	40,820
13.583	30	0.50	20	42,380
14.083	30	0.50	20	43,940
14.583	30	0.50	20	45,500

(1) The time interval selected for data collection.

(2) Duration of data collection within the corresponding time interval.

(3) This first 2-minute time interval was before the start of tracking.

(4) This 2-minute duration of data sampling at 0 time indicates the data collected for 2 minutes before the tracking started.

Table 1. Data collection Times and Sampling Rates (Continued).

Time from start of tracking, hrs.	Interval for data collection, minutes	Duration of sampling, minutes	Sampling Freq, Hz (data points per second)	Cumulative # of wheel passes from the start of tracking
15.083	30	0.50	20	47,060
15.583	30	0.50	20	48,620
16.083	30	0.50	20	50,180
16.583	30	0.50	20	51,740

8.0. Calculation

8.1. The underlying principle to assessing the fatigue damage is that as a result of repeated passes of the wheel on the slab, the strain amplitude grows within the specimen. The higher rate of stain growth is an indication of higher level of fatigue damage. A material displaying a larger strain growth under identical loading conditions is deemed more susceptible to fatigue cracking.

8.2. Identify three distinct stages during the test for easier assessment of the strain growth rate:

8.2.1. Early Stage: 3 minutes after the test initiation.

8.2.2. Middle Stage: approximately 8 hours after the test initiation.

8.2.3. Late Stage: approximately 16.5 hours after the test initiation.

8.3. Measure the average strain amplitude at the specified times corresponding to the early, middle, and late stages of the test.

8.4. Evaluate the rate of increase in strain amplitude from the early to middle stage and from the early to the late stage. A higher rate of increase in strain amplitude corresponds to lower fatigue resistance performance.

The following is an example of the calculation process for strain amplitude during different stages of the testing procedure. For each stage, the representative value is obtained by computing the average of the four highest strain amplitude cycles. Figure 2 shows the strain cycles as a result of the moving load; the difference between the peak and valley is strain amplitude.

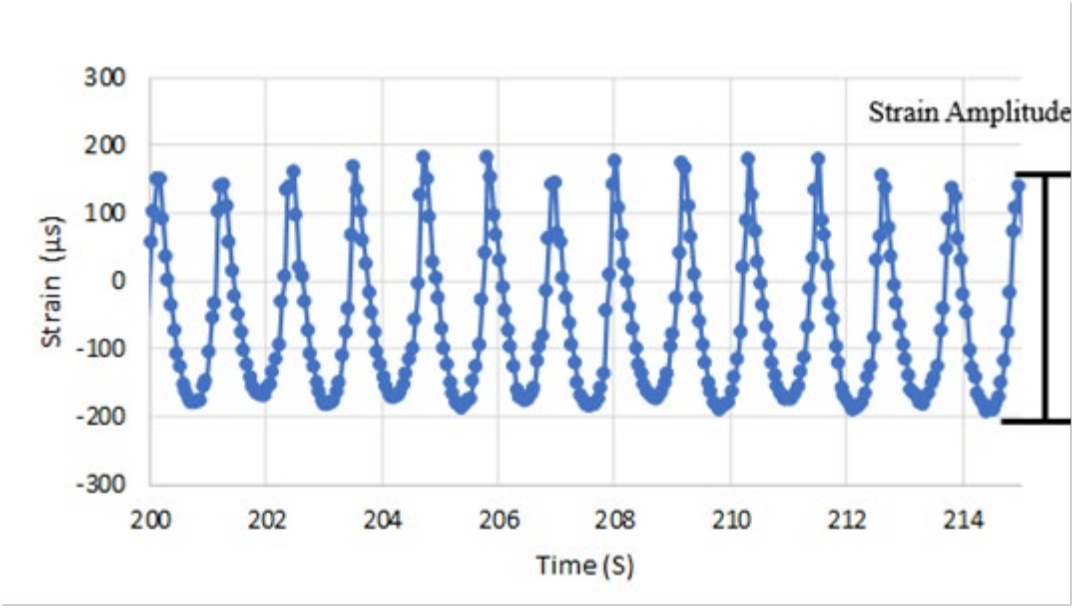

Figure 2. The strain cycles as a result of the moving load.

For the initial stage of the test, approximately three minutes post commencement: We presume the four highest strain amplitude readings to be 369, 367, 365, and 368. As such, the representative value, or the average of these four highest strain amplitudes, equals 367.25.

Proceeding to the middle stages of the test, approximately eight hours into the process: For this stage, the four highest recorded strain amplitudes are assumed to be 551, 555, 554, and 557. Hence, the average of these four highest strain amplitudes, serving as the representative value for this stage, comes out to be 554.25.

Moving towards the late stages of the test, approximately 16.5 hours after the test has begun: The four highest strain amplitudes are postulated to be 601, 559, 603, and 602. Therefore, the average of these four highest strain amplitudes, our representative value for the late stage, is calculated to be 601.25.

Subsequently, the percentage increase in strain amplitude from the early to the middle and late stages can be computed as follows:

$$Increase\ in\ Strain\ Amplitude\ from\ early\ to\ middle\ stages = \left(\frac{B - A}{A}\right) \times 100$$
$$= \left(\frac{554.25 - 367.25}{367.25}\right) \times 100 = 50.9\%$$

$$Increase\ in\ Strain\ Amplitude\ from\ early\ to\ late\ stages = (\frac{C - A}{A}) \times 100$$
$$= (\frac{601.25 - 367.25}{367.25}) \times 100 = 63.7\%$$

Where:

A = the average strain amplitude at the early stage,

B = the average strain amplitude at the middle stage,

C = the average strain amplitude at the late stage.

9.0 Report

9.1. Report the following information in the Report.

9.1.1 Sample Identification

9.1.2 Date of the Test

9.1.3 Operator's name or initials

9.1.4 Mix Identification Code

9.1.5. Specimen Binder Content, nearest 0.1 percent

9.1.6. Specimen Air Void, nearest 0.1 percent

9.1.7. Dimensions (length, width, height) of the specimen, nearest 0.1 mm

9.1.8. Type and configuration of strain gauges, if other than the type and configuration specified in Section 4.6 and Figure 1.

9.1.9. Test temperature, if other than test temperature specified in Section 6.14 and Section 6.15.

9.1.10. Speed of tracking, if other than the speed of track specified in Section 6.17.

9.1.11. Total number of wheel passes at each test temperature

9.1.12. Number of replicate specimens tested

9.1.13. Strain amplitude at early, late, and middle stages

9.1.14. Percent increase in strain amplitude (damage growth) from early to middle stage and from early to late stage.

10.0 Keywords

Asphalt Mixture, Fatigue Cracking Resistance, Hamburg Wheel Tracking Device (HWTD), Moving Load, Strain Measurement, Linear Kneading Compactor, Foil Strain Gauge, Data Acquisition System (DAQ), Fatigue Resistance Performance